DYNAMIC ANALYSIS OF CNT AND GRAPHENE REINFORCED COMPOSITE SANDWICH CONICAL SHELLS IN THERMAL ENVIRONMENT – A FINITE ELEMENT APPROACH

Thesis submitted by

TRIPURESH DEB SINGHA

Doctor of Philosophy
(Engineering)

Department of Mechanical Engineering
Faculty Council of Engineering & Technology
Jadavpur University
Kolkata, India

2022

JADAVPUR UNIVERSITY
KOLKATA – 700 032, INDIA

INDEX NO.: 232/18/E

1. Title of the thesis:

Dynamic Analysis of CNT and Graphene Reinforced Composite Sandwich Conical Shells in Thermal Environment- A Finite Element Approach.

2. Name, Designation & Institution of the Supervisors:

Dr. Amit Karmakar,
Professor & Head,
Department of Mechanical Engineering,
Jadavpur University, Kolkata -700032.

&

Dr. Tanmoy Bandyopadhyay,
Assistant Professor,
Department of Mechanical Engineering,
Jadavpur University, Kolkata -700032.

3. List of Publication:

I. Singha, T.D., Bandyopadhyay, T., and Karmakar, A. (2022), Transient Response of Pre-twisted FG-GRC Sandwich Conical Shell Subjected to Low-Velocity Impact in Thermal Environment, Proceedings of the IMechE, Part C: Journal of Mechanical Engineering Science, (under review).

II. Singha, T.D., Bandyopadhyay, T., and Karmakar, A. (2021), Dynamic Behavior of Temperature-dependent FG-CNTRC Sandwich Conical Shell under Low-velocity Impact, Mechanics of Advanced Materials and Structures. DOI: https://doi.org/10.1080/15376494.2021.1980930.

III. Singha, T.D., Bandyopadhyay, T., and Karmakar, A. (2021), Thermoelastic Free Vibration of Rotating Pretwisted Sandwich Conical Shell Panels with Functionally Graded Carbon Nanotube-Reinforced Composite Face Sheets using Higher-Order Shear Deformation Theory, Proceedings of the IMechE, Part L: Journal of Materials: Design and Applications, Vol. 235, No.10, pp. 2227-2253.

IV. Singha, T.D., Rout, M., Bandyopadhyay, T., and Karmakar, A. (2021), Free Vibration of Rotating Pretwisted FG-GRC Sandwich Conical Shells in Thermal Environment using HSDT, Composite Structures, Vol. 257, 113144.

V. Singha, T.D., Rout, M., Bandyopadhyay, T., and Karmakar, A. (2020), Free Vibration Analysis of Rotating Pretwisted Composite Sandwich Conical Shells with Multiple Debonding in Hygrothermal Environment, Engineering Structures, Vol. 204, 110058.

4. List of Patents: NIL.

5. List of Presentations in National/International/Conferences/Workshops:

I. Singha, T. D., Bandyopadhyay, T., and Karmakar, A. (2021), Low-velocity Oblique Impact Response of pre-Twisted Sandwich Conical Shell with CNTRC Facings, 8th International Conference on Theoretical Applied Computational and Experimental Mechanics (ICTACEM), IIT Kharagpur, India, December, 20-22.

II. Singha, T.D., Bandyopadhyay, T., and Karmakar, A. (2021), Low-velocity impact analysis of pre-twisted composite sandwich shallow conical shells in hygrothermal environment, International Conference on Thermal Engineering and Management Advances (ICTEMA), Jalpaiguri Govt. Engg. College, Jalpaiguri, India, December, 19-20.

III. Singha, T.D., Bandyopadhyay, T., and Karmakar, A. (2020), Predicting Vibration Behavior of Rotating Sandwich Blades with GRC Facings, Online International Conference on Advances in Mechanical & Industrial Engineering (ICAMIE), Kalinga Institute of Industrial Technology, Bhubaneswar, India, December, 11-13.

"Statement of Originality"

I, **TRIPURESH DEB SINGHA** registered on **17.04.2018** do hereby declare that this thesis entitled **"Dynamic Analysis of CNT and Graphene Reinforced Composite Sandwich Conical Shells in Thermal Environment - A Finite Element Approach"** contains literature survey and original research work done by the undersigned candidate as part of Doctoral studies.

All information in this thesis have been obtained and presented in accordance with existing academic rules and ethical conduct. I declare that, as required by these rules and conduct, I have fully cited and referred all materials and results that are not original to this work.

I also declare that I have checked this thesis as per the "Policy on Anti Plagiarism, Jadavpur University, 2019", and the level of similarity as checked by iThenticate software is **6** %.

Signature of Candidate: Tripuresh Deb Singha

Date: 16/02/2023

Certified by Supervisor (s):

(Signature with date, seal)

1. Amit Karmakar 16/02/2023

Professor
Dept. of Mechanical Engineering
Jadavpur University, Kolkata-32

2. Tanmoy Bandyopadhyay 16/02/2023

Assistant Professor
Dept. of Mechanical Engineering
Jadavpur University, Kolkata-32

CERTIFICATE FROM THE SUPERVISORS

This is to certify that the thesis entitled **"Dynamic Analysis of CNT and Graphene Reinforced Composite Sandwich Conical Shells in Thermal Environment - A Finite Element Approach"** submitted by **Shri Tripuresh Deb Singha**, who got his name registered on **17.04.2018** for the award of the Ph. D. (Engg.) degree of Jadavpur University is absolutely based upon his own work under the supervisions of **Dr. Amit Karmakar, Professor & Head, Department of Mechanical Engineering, Jadavpur University, Kolkata-700032** & **Dr. Tanmoy Bandyopadhyay, Assistant Professor, Department of Mechanical Engineering, Jadavpur University, Kolkata-700032** and that neither his thesis nor any part of the thesis has been submitted for any degree/diploma or any other academic award anywhere before.

1. Amit Karmakar 16/02/2023

Signature of the Supervisor
and date with Office Seal

Professor
Dept. of Mechanical Engineering
Jadavpur University, Kolkata-32

2. Tanmoy Bandyopadhyay 16/02/2023

Signature of the Supervisor
and date with Office Seal

Assistant Professor
Dept. of Mechanical Engineering
Jadavpur University, Kolkata-32

Dedicated

to

My Parents and Family

ACKNOWLEDGEMENT

The author expresses his deep sense of gratitude to Prof. (Dr.) Amit Karmakar and Dr. Tanmoy Bandyopadhyay for their keen interest, valuable guidance and constant encouragement during the course of the present research work. The author is greatly indebted to them for their valuable time and methodical guidance in the course of this work. Above all, without their moral support the author would not have completed the present research work.

The author is thankful to Prof. (Dr.) Sumanta Neogi, Prof. (Dr.) Arghya Nandi, Prof. (Dr.) Nipu Modak, Prof. (Dr.) Sudip Simlandi, and Prof. (Dr.) Anirvan DasGupta (IIT Kgp) for their encouragement and advice. The author would also like to thank all the faculty members of the Mechanical Engineering Department, Jadavpur University, for their constant support and encouragement.

The author expresses his heartiest thanks to all the research scholars of the 'Applied Mechanics Laboratory', Department of Mechanical Engineering, Jadavpur University, for their support and encouragement. The author is also very much thankful to many friends and fellow researchers, Dr. Mrutyunjay Rout, Dr. Apurba Das, and Dr. Ankuran Saha, Mr. Suman Karmakar, Mr. Pabitra Maji, Mr. Partha Halder who helped with their valuable suggestions from time to time to overcome many difficulties during this research work.

The author is grateful to the Govt. College of Engineering and Textile Technology, Serampore, Hooghly, and Higher Education Department, Govt. of West Bengal for granting the necessary permission to do this research work. The authors owes his gratitude to all faculty members and staffs of the parent institute, especially, Prof. (Dr.) Syed Kamruddin Ahamed, Dr. Tapan Mandal, Dr. Prabir Kumar Mukherjee, Dr. Priyajit Mukherjee, Mr. Prasanta Mandal for their constant encouragement and moral support to complete this research work.

The author extends sincerest gratitude to his parents for their blessings and his brothers and sisters for standing by him with lots of encouragement. The author is incredibly grateful to his wife, Mrs. Rubani Deb Singha (Roy), for her constant support and guiding him as a person and for accompanying him in the challenging situations. The author is gratified to his beloved daughter Miss Aditri Deb Singha for giving him time from his account to make this work possible.

The author is also thankful to the libraries of Jadavpur University for making available related books and research journals in the context of the present research.

Finally, but most importantly, the author thanks Almighty God for giving him the willpower and strength to make it this far.

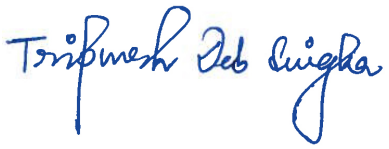

(Tripuresh Deb Singha)

LIST OF PUBLICATIONS

The following research publications are based on the present research work:

I. Singha, T.D., Bandyopadhyay, T., and Karmakar, A. (2022), Transient Response of Pre-twisted FG-GRC Sandwich Conical Shell Subjected to Low-Velocity Impact in Thermal Environment, Proceedings of the IMechE, Part C: Journal of Mechanical Engineering Science, (under review).

II. Singha, T.D., Bandyopadhyay, T., and Karmakar, A. (2021), Dynamic Behavior of Temperature-dependent FG-CNTRC Sandwich Conical Shell under Low-velocity Impact, Mechanics of Advanced Materials and Structures. DOI: https://doi.org/10.1080/15376494.2021.1980930.

III. Singha, T.D., Bandyopadhyay, T., and Karmakar, A. (2021), Thermoelastic Free Vibration of Rotating Pretwisted Sandwich Conical Shell Panels with Functionally Graded Carbon Nanotube-Reinforced Composite Face Sheets using Higher-Order Shear Deformation Theory, Proceedings of the IMechE, Part L: Journal of Materials: Design and Applications, Vol. 235, No.10, pp. 2227-2253.

IV. Singha, T.D., Rout, M., Bandyopadhyay, T., and Karmakar, A. (2021), Free Vibration of Rotating Pretwisted FG-GRC Sandwich Conical Shells in Thermal Environment using HSDT, Composite Structures, Vol. 257, 113144.

V. Singha, T.D., Rout, M., Bandyopadhyay, T., and Karmakar, A. (2020), Free Vibration Analysis of Rotating Pretwisted Composite Sandwich Conical Shells with Multiple Debonding in Hygrothermal Environment, Engineering Structures, Vol. 204, 110058.

ABSTRACT

The use of sandwich structures with advanced composite face sheets and homogeneous core is increasing progressively in various engineering applications such as aerospace, marine, automobile due to its high strength/stiffness-to-weight ratio and other preferred properties. The introduction of carbon nanofillers such as carbon nanotubes (CNTs) and graphene for reinforcing the composite face sheets can enhance the strength/stiffness, impact resistance, corrosion resistance and thermal stability of the sandwich structures extraordinarily. These features are extremely important in selecting the materials for turbomachinery blades which work in complex environments. The turbomachinery blades with low aspect ratio can be idealized as a pretwisted conical shallow shell due to its special geometrical feature. In order to reduce the weight of the turbomachinery blades, it can be made up of sandwich construction with nanocomposite face sheets and homogeneous core. However, the performance and safety of the sandwich blades are critically influenced by their vibration characteristics and dynamic response under impact load, especially when the blades work in hot environments. Therefore, the prior knowledge of the free vibration characteristics and impact behavior of the sandwich blades considering the thermal effect is needed for reliable design and performance.

In the present study, the CNTs-reinforced composite (CNTRC) face sheets and graphene reinforced composite (GRC) face sheets in the sandwich conical shell are considered separately. The CNTs or graphene sheets considered to be aligned with the span length and distributed either uniformly or functionally graded (FG) along the thickness of the sandwich conical shell panel. The temperature-dependent elastic properties of the CNTRC face sheets are estimated using rule of mixtures, while the temperature-dependent effective elastic properties of the GRC face sheets are evaluated using extended Halpin-Tsai model. The present numerical study is carried out using the finite element method in conjunction with the higher-order shear deformation theory (HSDT). An eight-noded isoparametric shell element is employed to develop the finite element formulation. The effects of nonlinearity arising out of the initial stresses due to thermal and centrifugal loads are incorporated via geometric stiffness based on Green-Lagrange's strains. The governing equation for sandwich conical shell panels are derived using Lagrange's equation of motion at moderate rotational speeds thereby neglecting the Coriolis effect. The contact force induced between the impactor and target sandwich shell is

computed using the modified Hertzian contact law. Newmark's constant acceleration time integration scheme is employed to obtain the solutions of the resulting equations of motion of the sandwich conical shell and the impactor.

In-house computer codes based on the present formulation are developed to obtain the numerical results for free vibration and dynamic analysis of the cantilevered sandwich conical shell with CNTRC face sheets and GRC face sheets and homogenous core. The convergence and comparison studies are performed to ensure the stability and accuracy of the present formulation. Finally, a detailed parametric study is carried out to scrutinize the effects of some important parameters like grading pattern of CNTs and graphene, CNTs volume fraction, core-to-face sheet thickness ratio, pretwist angle, cone length-to-thickness ratio, temperature of the environment, rotational speed and hub radius ratio on the natural frequencies of the sandwich conical shells with CNTRC and GRC face sheets. Also, some representative mode shapes for both CNTRC and GRC sandwich conical shells are depicted to visualize the vibration pattern at different thermal conditions and rotational speeds. Moreover, the numerical results are presented to investigate the influence the grading pattern of CNTs and graphene, CNTs volume fraction, core-to-face sheet thickness ratio, pretwist angle, temperature of the environment, size and initial velocity of the impactor on the contact force, central shell displacement, indentation and impactor velocity.

CONTENTS

				Page No.
			Statement of Originality	i
			Certificate	ii
			Dedication	iii
			Acknowledgement	iv
			List of Publications	vi
			Abstract	vii
			Nomenclature	xiii
			List of Tables	xvi
			List of Figures	xviii
Chapter 1			**INTRODUCTION**	**1-37**
1.1			Overview	1
1.2			Motivation of the Present Work	5
1.3			Literature Review	6
	1.3.1		Nanocomposite Sandwich Plates and Shells	7
		1.3.1.1	FG-CNTRC Sandwich Plates and Shells	8
		1.3.1.2	FG-GRC Sandwich Plates and Shells	10
	1.3.2		Modeling of Turbo-machinery Blades	12
	1.3.3		Review on Plates/Shells Theories	15
		1.3.3.1	Classical Plate Theory	16
		1.3.3.2	First-order Shear Deformation Theory	16
		1.3.3.3	Higher-order Shear Deformation Theory	17
		1.3.3.4	Layer-wise Theory	18
	1.3.4		Review of Shell Geometry	18
		1.3.4.1	Cylindrical Shells	18
		1.3.4.2	Conical Shells	20
		1.3.4.3	Spherical Shells	21
		1.3.4.4	Shallow Shells	21
		1.3.4.5	Other Shells	22

	1.3.5		Finite Element Modeling of Laminated Composites and Sandwich Structures	23
	1.3.6		Thermal Effects on Nanocomposite Sandwich Plates and Shells	24
	1.3.7		Dynamic Analyses of Nanocomposite Sandwich Plates and Shells	25
		1.3.7.1	Free Vibration Analysis	26
		1.3.7.2	Low-Velocity Impact Analysis	27
1.4			Research Gaps Identified	33
1.5			Objectives and Scope of the Present Work	34
1.6			Organization of the Thesis	35
Chapter 2			**THEORETICAL FORMULATION**	**38-67**
2.1			Introduction	38
2.2			Basic Equations	38
	2.2.1		Sandwich Shallow Conical Shell Model	38
	2.2.2		Nanocomposite Face Sheet Layers	40
		2.2.2.1	CNTRC Face Sheets	40
		2.2.2.2	GRC Face Sheets	43
	2.2.3		Displacement Field and Strains	45
	2.2.4		Stress-Strain Relationship	47
2.3			Finite Element Formulation	52
2.4			General Dynamic Equilibrium Equation	55
	2.4.1		Kinetic Energy of Rotating Sandwich Conical Shell	55
	2.4.2		Strain Energy of Rotating Sandwich Conical Shell	59
	2.4.3		Governing Equation of Motion	61
2.5			Solution Procedure	63
	2.5.1		Boundary Conditions	63
	2.5.2		Formulating Free Vibration Problem	63
	2.5.3		Formulating Low-Velocity Impact Problem	64
Chapter 3			**THERMOELASTIC FREE VIBRATION ANALYSIS OF ROTATING PRETWISTED FG-CNTRC SANDWICH CONICAL SHELLS**	**68-91**
3.1			Introduction	68
3.2			Numerical Results and Discussions	68

3.3		Convergence Study	69
3.4		Comparison Study	70
3.5		Parametric Study	73
	3.5.1	Effect of Core-to-Face Sheets Thickness Ratio	74
	3.5.2	Effect of Temperature	77
	3.5.3	Effect of Cone Length-to-Thickness Ratio	81
	3.5.4	Effect of Rotational Speed	83
3.6		Mode Shapes	89
Chapter 4		**FREE VIBRATION ANALYSIS OF ROTATING PRETWISTED FG-GRC SANDWICH CONICAL SHELLS IN THERMAL ENVIRONMENTS**	**92-111**
4.1		Introduction	92
4.2		Numerical Results and Discussions	92
4.3		Convergence Study	94
4.4		Comparison Study	94
4.5		Parametric Study	96
	4.5.1	Effect of Pretwist Angle	96
	4.5.2	Effect of Cone Length-to-Thickness Ratio	98
	4.5.3	Effect of Core-to-Face Sheets Thickness Ratio	100
	4.5.4	Effect of Temperature	102
	4.5.5	Effect of Rotational Speed	106
4.6		Mode Shapes	109
Chapter 5		**DYNAMIC BEHAVIOR OF TEMPERATURE DEPENDENT FG-CNTRC SANDWICH CONICAL SHELLS UNDER LOW-VELOCITY IMPACT**	**112-126**
5.1		Introduction	112
5.2		Numerical Results and Discussions	112
5.3		Convergence Study	113
5.4		Comparison Study	114
5.5		Parametric Study	115
	5.5.1	Influence of CNTs Grading Pattern	116
	5.5.2	Influence of CNTs Volume Fraction	117
	5.5.3	Influence of Thermal Environment	118
	5.5.4	Influence of Pretwist Angle	120

	5.5.5	Influence of Core-to-Face Sheets Thickness Ratio	121
	5.5.6	Influence of Cone Length-to-Thickness Ratio	122
	5.5.7	Influence of Initial Velocity of the Impactor	123
	5.5.8	Influence of Size of Impactor	125
Chapter 6		**TRANSIENT RESPONSE OF FG-GRC SANDWICH CONICAL SHELL UNDER LOW-VELOCITY IMPACT IN THERMAL ENVIRONMENTS**	**127-138**
6.1		Introduction	127
6.2		Numerical Results and Discussions	127
6.3		Convergence Study	128
6.4		Parametric Study	128
	6.4.1	Effect of Graphene Grading Pattern	129
	6.4.2	Effect of Temperature	130
	6.4.3	Effect of Pretwist Angle	132
	6.4.4	Effect of Core-to-Face Sheets Thickness Ratio	133
	6.4.5	Effect of Span-to-Cone Length Ratio	134
	6.4.6	Effect of Initial Velocity of Impactor	136
	6.4.7	Effect of Size of Impactor	137
Chapter 7		**CONCLUSIONS**	**139-144**
7.1		Introduction	139
7.2		Concluding Remarks	139
	7.2.1	Free Vibration Analysis of FG-CNTRC Sandwich Conical Shells	139
	7.2.2	Free Vibration Analysis of FG-GRC Sandwich Conical Shells	141
	7.2.3	Dynamic Behavior of FG-CNTRC Sandwich Conical Shells under Low-Velocity Impact	141
	7.2.4	Dynamic Behavior of FG-GRC Sandwich Conical Shells due to Low-Velocity Impact	142
7.3		Significant Contributions of the Thesis	143
7.4		Scope of the Future Work	144
		REFERENCES	**145**
		APPENDIX	**174**

NOMENCLATURE

s, L	Cone length and span length of the conical shell
ϕ_v, ϕ_0	Vertex angle and base subtended angle
p_0, q_0	Minor and major radii of the reference elliptical cross-section
p, q	Minor and major radii of any elliptical cross-section
ψ	Pretwist angle
b_0	Reference width
r_{xy}	Pretwist radius
r_x, r_y	Curvature radii in *x* and *y*-directions
Ω, Ω^{ND}	Actual rotational speed and non-dimensional rotational speed
$\Omega_x, \Omega_y, \Omega_z$	Components of angular velocity in the shell coordinate system
ω_n	Natural frequency
h_c, h_f, h	Core thickness, face sheets thickness, and total thickness
X,Y,Z	Global coordinate axes
x, y, z	Local coordinate axes
X_0, Y_0, Z_0	Translational offsets
$\mathbf{i}_X, \mathbf{i}_Y, \mathbf{i}_Z$	Unit vectors in inertial Cartesian coordinate systems
$\mathbf{i}_x, \mathbf{i}_y, \mathbf{i}_z$	Unit vectors in shell Cartesian coordinate systems
u, v, w	Displacement variables along x, y, and z directions
u_0, v_0, w_0	Mid-surface displacement variables along x, y, and z directions
β_x, β_y	Rotations of the normal to the mid-surface about y- and x-axes
$u_0^*, v_0^*, \beta_x^*, \beta_y^*$	Higher-order displacement variables
$\{\Delta\}$	Generalized displacement parameter vector
$\{\varepsilon_l\}, \{\varepsilon_{nl}\}$	Linear and nonlinear strain components
$\{\varepsilon^0\}$	Mid-plane strain vector
Q_{ij}	On-axis reduced elastic constants
$\bar{Q}_{ij}$	Off-axis reduced elastic constants
E_{11}, E_{22}	Young's moduli in material coordinates 1 (longitudinal) and 2 (transverse)
G_{12}, G_{23}, G_{13}	Shear moduli of a lamina in the 1-2, 2-3 and 1-3 planes
ν_{12}, ν_{21}	Poison's ratios

ρ	Mass density
α_{11}, α_{22}	Coefficients of thermal expansions in longitudinal and transverse directions
T, T_0	Elevated and reference temperatures
θ	Lamination angle
$\{N\}$	Stress resultant vector
$\{M\}$	Moment resultant vector
$\{M^*\}$	Higher-order moment resultant vector
$\{Q\}, \{R\}$	Transverse shear stress resultant vector
$\{Q^*\}, \{R^*\}$	Higher-order transverse shear stress resultant vector
$\{F\}$	Stress resultant vector
$\{F^{TH}\}$	Thermal stress resultant vector
$[D]$	Elasticity matrix
$[B]$	Strain-displacement matrix
ξ, η	Natural coordinates
N_i	Shape function at i^{th} node
$[J]$	Jacobian matrix
$\{\delta_e\}$	Nodal displacement parameter vector
θ_x, θ_y	Skew and precone angles
$[m_I]$	Matrix of inertia per unit area
$[M_e]$	Elemental mass matrix
$[C_e]$	Elemental coriolis matrix
$[K_{Re}]$	Elemental rotational stiffness matrix
$\{F_{\Omega e}\}$	Elemental centrifugal force vector
$[K_e]$	Elemental elastic stiffness matrix
$[K_{\sigma THe}]$	Elemental geometric stiffness matrix due to thermal load
$[K_{\sigma Re}]$	Elemental geometric stiffness matrix due to rotation
$\{P_e^{TH}\}$	Elemental thermal load vector
$[M]$	Global mass matrix
$[K]$	Global elastic stiffness matrix
$[K_{\sigma TH}], [K_{\sigma R}]$	Global geometric stiffness matrices due to thermal load and rotation
$F(\Omega^2)$	Nodal equivalent centrifugal load vector

$\{F_C\}$	Contact force vector
F_m	Maximum contact force at the commencement of the unloading cycle
m_{imp}	Mass of the impactor
w_{imp}	Displacement of the impactor
r_{imp} , d_{imp}	Radius and diameter of the impactor
E_{imp}	Young's modulus of the impactor
ν_{imp}	Poisson's ratio of the impactor
k_c	Modified contact stiffness
η_1, η_2, η_3	Efficiency parameters of the CNTs/polymer matrix
L_G, b_G, h_G	Length, breadth, and effective thickness of the graphene sheet
λ_{ij}	Required supplementary parameters for graphene/polymer matrix
α	Local indentation
α_0	Permanent indentation
α_{cr}	Critical indentation beyond which permanent indentation occurs
α_{m}	Maximum local indentation

LIST OF TABLES

Table Number	Caption	Page Number
2.1	Volume fractions of CNTs for different distribution patterns	42
3.1	Material properties of SWCNTs (10, 10) at different levels of temperature **[** L= 9.26 nm, R = 0.68 nm, h = 0.067 nm, ν_{12}^{CNT} = 0.175, ρ_{CNT} = 1400 kg/m^3] (Mehar and Panda, 2018)	69
3.2	Effectiveness parameters of the SWCNTs (Mehar and Panda, 2018)	69
3.3	Non-dimensional fundamental frequencies $\left(\varpi = \omega_n {b_0}^2\sqrt{\rho h/D}\right)$ of pretwisted shallow conical shells with different pretwist angles [$s/h = 1000$, ϕ_v =15°, ϕ_0=30°, $\nu = 0.3$, $D = Eh^3/12(1-\nu^2)$].	71
3.4	Non-dimensional natural frequencies $\left(\varpi = \omega_n L^2/h\sqrt{\rho_0/E_0}\right)$ of CNTRC plates with different CNTs grading patterns in thermal environments [$V_{CNT}^* = 0.12$, L/b =1, b/h =10, $\eta_1 = 0.137$, η_2 =1.002, $\eta_3 = 0.7$].	71
3.5	Non-dimensional natural frequencies $\left(\varpi = \omega_n L^2/h\sqrt{\rho_{c0}/E_{c0}}\right)$ of FG-CNTRC sandwich plates at reference temperature T_0 = 300 K [L/b =1, $b/h = 20$, h_f = 1 mm]	72
3.6	Natural frequencies (Hz) of cantilevered MWCNT-reinforced composite sandwich plates with different aspect ratios [Weight fraction of MWCNT= 0.3%, $h = 0.0048$ m, $b = 0.15$ m].	72
3.7	Non-dimensional fundamental frequencies $\left(\varpi = \omega_n L^2\sqrt{\rho h^2/D}\right)$ of cantilevered isotropic plate rotating at different rotational speeds [L/b =1, $h/L = 0.12$, $D = Eh^3/12(1-\nu^2)$, $\nu = 0.3$].	73
3.8	Mode shapes of FG-CNTRC sandwich conical shells with three types of CNTs distribution patterns and two values of pretwist angles at reference temperature T = 300 K [s = 0.4 m, L/s = 0.7, $\phi_0 = \phi_v$ = 20°, s/h =1000, $r/L = 1$, $h_c/h_f = 0.5$, $V_{CNT}^* = 0.12$, $\Omega^{ND} = 0.0$]	89
3.9	Mode shapes of FG-VΛ CNTRC sandwich conical shells for three values of rotational speeds and two values of pretwist angles at elevated temperature T = 700 K [s = 0.4 m, L/s = 0.7, $\phi_0 = \phi_v$ = 20°, s/h =1000, $r/L = 1$, $h_c/h_f = 0.5$, $V_{CNT}^* = 0.12$]	91
4.1	Temperature-dependent material properties for monolayer graphene **[** L_G =14.76 nm, b_G =14.77 nm, h_G = 0.188 nm, ν_{12}^G = 0.177, ρ_G = 4118 kg/m^3] (Lin *et al.*, 2017)	93

Table Number	Caption	Page Number
4.2	Temperature-dependent efficiency parameters for graphene/PMMA nanocomposites (Shen *et al.*, 2017)	93
4.3	Non-dimensional fundamental frequencies ($\varpi = \omega_n L^2/h\sqrt{\rho_0/E_0}$) of simply supported square GRC plate [(0º/90º/0º/90º/0º)$_s$] with different types of grading pattern at T =300 K, 400 K and 500 K [$L/b = 1,\ b/h = 10$, $h = 2$ mm]	95
4.4	Non-dimensional natural frequencies ($\varpi = \omega_n L^2/h\sqrt{\rho_{c0}/E_{c0}}$) of simply supported square sandwich plate [(0º/90º/0º/90º/0º/core/0º/90º/0º/90º/0º] with FG-GRC face sheets and Ti-6Al-4V core at reference temperature T =300 K [$L/b = 1,\ b/h = 20$, $h_f = 1$ mm.]	96
4.5	Effects of temperature and rotational speed on the mode shapes of the untwisted ($\psi = 0°$) GRC sandwich conical shells with FG-VΛ grading pattern [$s = 0.4$ m, $L/s = 0.7, \phi_0 = \phi_v = 20°,\ s/h = 1000,\ h_c/h_f = 0.5$]	110
4.6	Effects of temperature and rotational speed on the mode shapes of the pretwisted ($\psi = 30°$) GRC sandwich conical shells with FG-VΛ grading pattern [$s = 0.4$ m, $L/s = 0.7, \phi_0 = \phi_v = 20°,\ s/h = 1000,\ h_c/h_f = 0.5$]	111

LIST OF FIGURES

Figure Number	Caption	Page Number
2.1	Schematic diagram of sandwich shallow conical shell model: (a) untwisted shell and (b) pretwisted shell mounted on a rotating hub	39
2.2	Types of CNTs distribution patterns in sandwich shallow conical shell	41
2.3	Types of graphene distribution patterns in sandwich shallow conical shell	44
2.4	A typical lamina with two reference systems	47
2.5	Geometrical details of an n-layered laminate	49
2.6	Discretized trapezoidal planform of the sandwich shallow conical shell	52
2.7	(a) Eight-node element in $x-y$ plane (b) The same element mapped into $\xi-\eta$ plane	53
2.8	Rotating sandwich shallow conical shell with two reference systems and their offsets	56
2.9	Pretwisted nanocomposite sandwich shallow conical shell impacted with an impactor	64
3.1	Convergence study of FG-CNTRC sandwich conical shells with three different CNTs distribution patterns in thermal environments for two pretwist angles (a) ψ =0º and (b) ψ =30º [$s = 0.4$ m, $L/s = 0.7, \phi_0 = \phi_v = 20°, s/h = 100, h_c/h_f = 2,\ \Omega^{\mathrm{ND}} = 0.0$]	70
3.2	Variation of natural frequencies (Hz) of the pretwisted FG-CNTRC sandwich conical shells against core-to-face sheets thickness ratio for different CNTs grading patterns at temperature $T = 500$ K: (a) Mode 1, (b) Mode 2, and (c) Mode 3 [$s =$ 0.4 m, $L/s = 0.7$, $\phi_0 = \phi_v = 20°$, $s/h = 100,\ \psi = 15°, r/L = 1, V^*_{CNT} = 0.12, \Omega^{ND} = 0.0$]	75
3.3	Variation of natural frequencies (Hz) of the pretwisted FG-VΛ CNTRC sandwich conical shells against core-to-face sheets thickness ratio for different values of CNTs volume fraction at temperature $T = 500$ K: (a) Mode 1, (b) Mode 2, and (c) Mode [$s =$ 0.4 m, $L/s = 0.7, \phi_0 = \phi_v =$ $20°, s/h = 100,\ \psi = 15°, r/L = 1, \Omega^{ND} = 0.0$]	76

Figure Number	Caption	Page Number
3.4	Variation of natural frequencies (Hz) of the pretwisted FG-VΛ CNTRC sandwich conical shells against core-to-face sheets thickness ratio for different values of pretwist angle at temperature T =500 K: (a) Mode 1, (b) Mode 2, and (c) Mode [$s = 0.4$ m, $L/s = 0.7$, $\phi_0 = \phi_v = 20°$, $s/h = 100$, $r/L = 1$, $V_{CNT}^* = 0.12$, $\Omega^{ND} = 0.0$]	77
3.5	Variation of natural frequencies (Hz) of the pretwisted FG-CNTRC sandwich conical shells against temperature for different CNTs distribution patterns: (a) Mode 1, (b) Mode 2, and (c) Mode 3 [$s = 0.4$ m, $L/s = 0.7$, $\phi_0 = \phi_v = 20°$, $s/h = 100$, $\psi = 15°$, $r/L = 1$, $V_{CNT}^* = 0.12$, $\Omega^{ND} = 0.0$]	78
3.6	Variation of natural frequencies (Hz) of the pretwisted FG-VΛ CNTRC sandwich conical shells against temperature for different CNTs volume fractions: (a) Mode 1, (b) Mode 2, and (c) Mode 3 [$s = 0.4$ m, $L/s = 0.7$, $\phi_0 = \phi_v = 20°$, $s/h = 100$, $\psi = 15°$, $r/L = 1$, $V_{CNT}^* = 0.12$, $h_c/h_f = 0.5$, $\Omega^{ND} = 0.0$]	79
3.7	Variation of natural frequencies (Hz) of the pretwisted FG-VΛ CNTRC sandwich conical shells against temperature for different pretwist angles: (a) Mode 1, (b) Mode 2, and (c) Mode 3 [$s = 0.4$ m, $L/s = 0.7$, $\phi_0 = \phi_v = 20°$, $s/h = 100$, $r/L = 1$, $h_c/h_f = 0.5$, $V_{CNT}^* = 0.12$, , $\Omega^{ND} = 0.0$]	80
3.8	Variation of natural frequencies (Hz) of the pretwisted FG-VΛ CNTRC sandwich conical shell panels against temperature for different core-to-face sheets thickness ratio: (a) Mode 1, (b) Mode 2, and (c) Mode 3 [$s = 0.4$ m, $L/s = 0.7$, $\phi_0 = \phi_v = 20°$, $s/h = 100$, $r/L = 1$, $\psi = 15°$, $V_{CNT}^* = 0.12$, $\Omega^{ND} = 0.0$]	81
3.9	Variation of fundamental frequency (Hz) of the pretwisted FG-CNTRC sandwich conical shells with cone length-to-thickness ratio [$s = 0.4$ m, $L/s = 0.7$, $\phi_0 = \phi_v = 20°$, $r/L = 1$, $\Omega^{ND} = 0.0$, $T = 500$ K]	82
3.10	Variation of natural frequencies (Hz) of the pretwisted FG-CNTRC sandwich conical shells against non-dimensional rotational speed for different CNTs grading pattern at elevated temperature $T = 500$ K: (a) Mode 1, (b) Mode 2, (c) Mode 3, and (d) Mode 4 [$s = 0.4$ m, $L/s = 0.7$, $\phi_0 = \phi_v = 20°$, s/h =100, $r/L = 1$, $\psi = 30°$, $h_c/h_f = 2$, $V_{CNT}^* = 0.12$]	84
3.11	Variation of natural frequencies (Hz) of the pretwisted FG-VΛ CNTRC sandwich conical shells against non-dimensional rotational speed for different pretwist angles at elevated temperature $T = 500$ K: (a) Mode 1, (b) Mode 2, (c) Mode 3, and (d) Mode 4 [$s = 0.4$ m, $L/s = 0.7$, $\phi_0 = \phi_v = 20°$, s/h =100, $r/L = 1$, $h_c/h_f = 2$, $V_{CNT}^* = 0.12$]	85

Figure Number	Caption	Page Number
3.12	Variation of natural frequencies (Hz) of the pretwisted FG-VΛ CNTRC sandwich conical shells against non-dimensional rotational speed for different values of core-to-face sheets thickness ratios at elevated temperature $T = 500$ K: (a) Mode 1, (b) Mode 2, (c) Mode 3, and (d) Mode 4 [$s =$ 0.4 m, $L/s = 0.7$, $\phi_0 = \phi_v = 20°$, $s/h =$100, $r/L = 1$, $\psi = 30°$, $V^*_{CNT} = 0.12$]	86
3.13	Variation of natural frequencies (Hz) of the pretwisted FG-VΛ CNTRC sandwich conical shells against non-dimensional rotational speed for different levels of temperature: (a) Mode 1, (b) Mode 2, (c) Mode 3, and (d) Mode 4 [$s =$ 0.4 m, $L/s = 0.7$, $\phi_0 = \phi_v = 20°$, $s/h =$100, $r/L = 1$, $\psi = 30°$, $h_c/h_f = 2$, $V^*_{CNT} = 0.12$]	87
3.14	Variation of natural frequencies (Hz) of the pretwisted FG-VΛ CNTRC sandwich conical shells against non-dimensional rotational speed for different values of hub radius-to-length ratios at temperature $T = 500$ K: (a) Mode 1, (b) Mode 2, (c) Mode 3, and (d) Mode 4 [$s =$ 0.4 m, $L/s =$ 0.7, $\phi_0 = \phi_v = 20°$, $s/h =$100, $\psi = 30°$, $h_c/h_f = 2$, $V^*_{CNT} = 0.12$]	88
4.1	Convergence study for fundamental frequencies (Hz) of the pretwisted FG-GRC sandwich conical shells with three graphene grading patterns for two different pretwist angles: (a) $\psi = 0^o$ and (b) $\psi = 30^o$. [$s = 0.4$m, $L/s =$0.7, $\phi_0 = \phi_v = 20°$, $s/h = 100$, $h_c/h_f = 2$, $\Omega^{ND} =$ 0.0]	94
4.2	Effect of pretwist angle (ψ) on the natural frequencies (Hz) of FG-GRC sandwich conical shells with three different distribution patterns at two temperature levels: (a) $T = 300$ K, Mode 1, (b) $T = 300$ K, Mode 2, (c) $T = 500$ K, Mode 1, and (d) $T = 500$ K, Mode 2 [$s = 0.4$ m, $L/s = 0.7$, $\phi_0 = \phi_v = 20°$, $s/h =$100, $\Omega^{ND} = 0.0$]	97
4.3	Effect of cone length-to-thickness ratio (s/h) on the fundamental frequencies (Hz) of the pretwisted FG-GRC sandwich conical shells with different graphene grading patterns and temperature levels: (a) FG-UU, $T =$300 K, (b) FG-UU, $T =$500 K, (c) FG-VΛ, $T =$300 K, (d) FG-VΛ, $T =$500 K, (e) FG-ΛV, $T =$300 K, and (f) FG-ΛV, $T =$500 K. [$s = 0.4$ m, $L/s = 0.7$, $\phi_0 = \phi_v = 20°$, $\psi = 30°$, $\Omega^{ND} = 0.0$]	99
4.4	Effect of core-to-face sheets thickness ratio (h_c/h_f) on the natural frequencies (Hz) of the pretwisted FG-GRC sandwich conical shells at two temperature levels: (a) $T = 300$ K, Mode 1, (b) $T = 300$ K, Mode 2, (c) $T = 500$ K, Mode 1, and (d) $T = 500$ K, Mode 2 [$s = 0.4$ m, $L/s =$ 0.7, $\phi_0 = \phi_v = 20°$, $\psi = 30°$, $s/h = 100$, $\Omega^{ND} = 0.0$]	101

Figure Number	Caption	Page Number
4.5	Percentage decrease in natural frequencies of the pretwisted FG-GRC sandwich conical shells for two levels of temperatures: (a) $T = 300$ K, Mode 1, (b) $T = 300$ K, Mode 2, (c) $T = 500$ K, Mode 1, and (d) $T = 500$ K, Mode 2 [$s = 0.4$ m, $L/s = 0.7$, $\phi_0 = \phi_v = 20°$, $\psi = 30°$, $s/h = 100$, $\Omega^{ND} = 0.0$]	102
4.6	Effect of temperature on the natural frequencies (Hz) of pretwisted FG-GRC sandwich conical shells for three values of h_c/h_f ratios: (a) h_c/h_f =0.5, Mode 1, (b) h_c/h_f =0.5, Mode 2, (c) $h_c/h_f = 2$, Mode 1, (d) $h_c/h_f = 2$, Mode 2, (e) h_c/h_f =10, Mode 1, and (f) h_c/h_f =10, Mode 2 [$s = 0.4$ m, $L/s = 0.7$, $\phi_0 = \phi_v = 20°$, $\psi = 30°$, $s/h = 100$, $\Omega^{ND} = 0.0$]	103
4.7	Percentage decreases in natural frequencies of the pretwisted FG-GRC sandwich conical shells for three values of h_c/h_f ratios: (a) h_c/h_f =0.5, Mode 1, (b) h_c/h_f =0.5, Mode 2, (c) $h_c/h_f = 2$, Mode 1, (d) $h_c/h_f = 2$, Mode 2, (e) h_c/h_f =10, Mode 1, and (f) h_c/h_f =10, Mode 2 [$s = 0.4$ m, $L/s = 0.7$, $\phi_0 = \phi_v = 20°$, $\psi = 30°$, $s/h = 100$, $\Omega^{ND} = 0.0$]	105
4.8	Effect of non-dimensional rotational speed on the natural frequencies (Hz) of untwisted ($\psi = 0°$) FG-GRC sandwich conical shells with three different distribution patterns at T =500 K: (a) FG-UU, Mode 1, (b) FG-UU, Mode 2, (c) FG-VΛ, Mode 1, (d) FG-VΛ, Mode 2, (e) FG-ΛV, Mode 2, (f) FG-ΛV, Mode 2 [$s = 0.4$ m, $L/s = 0.7$, $\phi_0 = \phi_v = 20°$, $\psi = 30°$, $s/h = 100$]	107
4.9	Effect of non-dimensional rotational speed on the natural frequencies (Hz) of pretwisted ($\psi = 30°$) FG-GRC sandwich conical shells with three different distribution patterns at $T = 500$ K: (a) FG-UU, Mode 1, (b) FG-UU, Mode 2, (c) FG-VΛ, Mode 1, (d) FG-VΛ, Mode 2, (e) FG-ΛV, Mode 2, and (f) FG-ΛV, Mode 2 [$s = 0.4$ m, $L/s = 0.7$, $\phi_0 = \phi_v = 20°$, $\psi = 30°$, $s/h = 100$]	108
5.1	Convergence of (a) contact force and (b) central shell displacement for pretwisted FG-CNTRC sandwich conical shell at an elevated temperature $T = 500$ K	113
5.2	Temporal variations of (a) contact force and (b) central plate displacement of an SSSS graphite/epoxy composite plate due to low-velocity	114

Figure Number	Caption	Page Number
5.3	Temporal variations of (a) contact force and (b) central plate displacement of an SSSS FG-VΛ CNTRC sandwich plate under low-velocity impact at two different temperatures $T = 300$ K and 500 K	115
5.4	Influence of CNTs grading pattern on impact response of FG-CNTRC sandwich conical shell panel at the reference temperature $T = 300$ K: (a) contact force, (b) central shell displacement, (c) indentation, and (d) impactor velocity	116
5.5	Influence of CNTs volume fraction on impact response of FG-CNTRC sandwich conical shell at the reference temperature $T = 300$ K: (a) contact force, (b) central shell displacement, (c) indentation, and (d) impactor velocity	118
5.6	Influence of temperature on impact response of FG-CNTRC sandwich conical shell: (a) contact force, (b) central shell displacement, (c) indentation, and (d) impactor velocity	119
5.7	Influence of pre-twist angle on impact behavior of FG-CNTRC sandwich conical shell at an elevated temperature of $T = 500$ K: (a) contact force, (b) central shell displacement, (c) indentation, and (d) impactor velocity	120
5.8	Influence of core-to-face sheets thickness ratio on impact response of FG-CNTRC sandwich conical shell at the elevated temperature of $T = 500$ K: (a) contact force, (b) central shell displacement, (c) indentation, and (d) impactor velocity	121
5.9	Influence of cone length-to-thickness ratio on impact response of FG-CNTRC sandwich conical shell panel at an elevated temperature of $T = 500$ K: (a) contact force, (b) central shell displacement, (c) indentation, and (d) impactor velocity	123
5.10	Effect of initial velocity of impactor on impact response of FG-VΛ CNTRC sandwich conical shell at an elevated temperature of $T = 500$ K: (a) contact force, (b) central shell displacement, (c) indentation, and (d) impactor velocity	124
5.11	Effect of impactor size on impact response of FG-VΛ CNTRC sandwich conical shell at an elevated temperature of T = 500 K: (a) contact force and (b) central shell displacement, (c) indentation, and (d) impactor velocity	125

Figure Number	Caption	Page Number
6.1	Convergence study of contact force of GRC sandwich conical shell with FG-UU type graphene grading pattern at $T = 500$ K: (a) mesh convergence at constant time step, $\Delta t = 2\ \mu$ s and (b) time step convergence at constant mesh size, 8×8	128
6.2	Effect of graphene grading profile on impact behavior of FG-GRC sandwich conical shell at $T =$300 K: (a) contact force, (b) central shell displacement, (c) indentation, and (d) impactor velocity	130
6.3	Effect of temperature on impact behavior of pretwisted FG-GRC sandwich conical shells with FG-VΛ and FG-ΛV graphene grading profiles: (a) contact force, (b) central shell displacement, (c) indentation, and (d) impactor velocity	131
6.4	Effect of pre-twist angle on impact behavior of FG-GRC sandwich conical panel with FG-VΛ graphene grading profile at $T = 500$ K: (a) contact force, (b) central shell displacement, (c) indentation, and (d) impactor velocity	132
6.5	Effect of core-to-face sheets thickness ratio on impact behavior of FG-GRC sandwich conical shell with FG-VΛ graphene grading profile at elevated temperature $T = 500$ K: (a) contact force, (b) central shell displacement, (c) indentation, and (d) impactor velocity	134
6.6	Effect of span-to-cone length ratio (L/s) on impact behavior of FG-GRC sandwich conical shell with FG-VΛ graphene grading profile at the elevated temperature $T = 500$ K: (a) contact force, (b) central shell displacement, (c) indentation, and (d) impactor velocity	135
6.7	Effect of initial velocity of impactor on impact behavior of FG-GRC sandwich conical shell with FG-VΛ graphene grading profile at the elevated temperature $T = 500$ K: (a) contact force, (b) central shell displacement, (c) indentation, and (d) impactor velocity	136
6.8	Effect of impactor size on impact behavior of FG-GRC sandwich conical shell with FG-VΛ graphene grading profile at the elevated temperature $T = 500$ K: (a) contact force, (b) central shell displacement, (c) indentation, (d) impactor velocity	137

CHAPTER 1

INTRODUCTION

1.1 OVERVIEW

Sandwich structures have served the growing demand for the design of the lightweight structures with high strength, stiffness, and energy absorption capacity that have potential applications in various fields of engineering such as aerospace, marine, automobile, civil, and structure. As known, sandwich structures represent a special type of multilayered composite structures that are typically formed with thin but high-strength and stiff layers (face sheets or skins) bonded to a thick homogenous layer (core). The major part of the bending loads is carried by the face sheets in the form of tensile or compressive stresses, while the shear loads are primarily carried by the core layer in the form of shear stresses. A great variety of materials are used for sandwich face sheets to achieve an excellent structural performance. These include conventional metals or alloys, laminated fiber-reinforced composites, and functionally graded ceramic-metal materials. The advancement of reinforcing materials in past few decades has made composite sandwich structures more popular, especially in aerospace and structural applications. Among the available fiber/particulate reinforcing constituents, carbon nanofillers in the form of nanotubes and nanosheets are dominating the others.

Since the discovery of carbon nanotubes (CNTs) by Ijima in 1991, it has generated huge research interest from various areas of engineering because of its extraordinary strength, stiffness, and toughness but very low density along with excellent thermal, electrical, and chemical properties. For instance, CNTs have elastic moduli in the order of ~1TPa and tensile strength over 150 GPa which are much more than those for conventional carbon fiber and metals. Moreover, CNT remains thermally stable up to 2800°C and has relatively larger specific surface area. These remarkable properties have made CNTs a potential candidate for nanoscale reinforcement into polymer matrix. From construction point of view, CNTs can be single-walled CNTs (SWCNTs) or multi-walled CNTs (MWCNTs). SWCNT is a seamless cylindrical tube which is rolled from a single sheet of graphene with ~1 nm diameter and length of order of centimeters. On the other hand, MWCNT consists of such cylindrical tubes arranged

concentrically and separated by 0.35 nm with diameters ranging from 2 nm to 100 nm and lengths of tens of microns. An addition of small amount of SWCNTs or MWCNTs to polymer matrix results in the remarkable increase in elastic moduli, strength, and hardness. Interestingly, an increase in the amount of CNTs beyond a certain limit leads to deterioration of the mechanical properties of CNTs-reinforced composites (CNTRCs) because of the lower cohesion between CNTs and matrix. The idea of functionally graded materials (FGM) can be used for the nanocomposite structures to address the issues concerned with low content CNTs in the CNTRCs. However, the type of CNTs distribution pattern is important to obtain better structural properties.

Recently, graphene which is a two-dimensional structure of carbon atoms with hexagonal crystalline structure with sp^2 bonds has emerged as a more potential candidate for reinforcement of nanocomposites owing to its extraordinarily high surface area, electron mobility, thermal conductivity, and mechanical strength since it was discovered by Geim and Novoselov in 2004. Compared with CNTs, graphene is cost-effective, has more stiffening effect in nanocomposites, and exhibits better interaction with the polymer matrix because of its extremely large surface area. Even graphene can be used at a lower volume fraction than CNTs for dramatic enhancement of the mechanical properties of polymer nanocomposites. Likewise CNTs, the excessive content of graphene in polymer nanocomposites degrades strength, stiffness, toughness, and other properties. In order to utilize the low content graphene optimally, the principle of FGM can be used in the graphene distribution along the thickness direction. One of the common types of graphene-based nanocomposites is graphene platelets-reinforced composites (GPLRCs) in which graphene platelets (GPLs) are assumed to be isotropic and temperature independent (Song *et al*., 2017). The GPLRC model which employs modified Halpin-Tsai equation to estimate the effective elastic moduli is comparatively simple. In contrast, the graphene sheets, which are assumed to have anisotropic and temperature-dependent material properties, can be aligned layer-wise into polymeric matrix to obtain graphene-reinforced composites (GRCs). The temperature-dependent elastic moduli of the GRCs are estimated using extended Halpin-Tsai model. Compared with GPLRC model, the GRC model yields more accurate results, especially when thermal effects are considered.

One of the potential applications of carbon nanofiller based composites and sandwich structures would be found as rotating blades of modern turbo-machines that are usually

considered to exhibit high level of reliability and low rates of failure. As the critical components of turbo-machineries (i.e., turbines, compressors, fans, and blowers), the blades usually work in complex environmental conditions and are subjected to high centrifugal and excitation forces. Under the working conditions of high rotational speed at elevated temperatures, the fatigue caused by the resonant vibrations is the common failure mode of turbo-machinery blades. The fatigue failure, which mostly occurs in the lower temperature stages of a turbine or an axial flow compressor, may lead to the catastrophic accident of the turbo-machines. In practice, a turbine experiences resonance vibration many times during its starting up and shutting down although it is designed to keep away from resonance at its steady running condition. Therefore, a profound knowledge of the natural frequencies of the turbo-machinery blades is indispensable to a designer in order to obtain its safe design and longer life. However, the resonance condition of the blades cannot be predicted easily due to the uncertainty of the excitation. In many works, beam models have been adopted to analyze the dynamic behavior of turbo-machinery blades since these one-dimensional models could provide accurate results for the reasonably thick blades with high aspect ratios (i.e., length-to-width ratios). However, such idealization is highly inaccurate for thin blades with low aspect ratios which are encountered in real engineering practices. In addition, the beam models are inadequate to predict the chord-wise bending and coupled chord-wise and span-wise bending modes of the blades with low aspect ratios. Hence, several attempts have been made to formulate dynamic behavior of the turbo-machinery blades with plate models. When the effect of surface curvature of the blades is considered, the shallow shell models are more preferable than the plate models. In general, the turbo-machinery blades are wider near fixed end and become narrow gradually at the free end. Thus, a cantilever pretwisted open shallow conical shell with trapezoidal planform and variable chord-wise surface curvature would be an appropriate model for the actual turbo-machinery blades.

The response of the composite sandwich structures is largely influenced by transverse shear deformation caused by the thick core layer. These effects cannot be captured adequately by classical theories (Reissner and Stavsky, 1961; Stavsky, 1961; Dong *et al.*, 1962) and thus, a shear deformation theory should be employed in order to predict the static and dynamic behavior of the structures. In this regard, first-order shear deformation theory (FSDT) (Yang *et al.,* 1966) can give consistent transverse stress distribution considering through-thickness linearly varying in-plane displacements and invariant out-of-plane displacement. Although, the first-order shear

deformation theory (FSDT) is the simplest among all shear deformation theories which assumes transverse shear stress free conditions on top and bottom surfaces, a shear correction factor must be taken into account to compensate for the error. Due to the anisotropy and other factors, the estimation of the shear correction factor of sandwich composites is very difficult. Besides, the higher-order shear deformation theories (HSDTs) take account of proper cross-sectional warping and assume realistic through-thickness variation of the transverse shear strains and stresses. For instance, the enforcement of traction-free condition on both the surfaces of the plate via through-thickness parabolic variation of transverse shear stress discards the use of shear correction factor.

The vibration of the composite sandwich structures involves complex shell geometries, internal strains and solution of boundary value problems. The finite element method (FEM) is a widely used computational tool to find the approximate solutions of complex boundary value problems involving partial differential equations. However, the applications of FEM require solutions of problems which are highly complex, computationally intensive, and involve very large matrices. The computer programming packages are however highly useful in obtaining solutions of the dynamic analysis of pretwisted sandwich conical shells in thermal environments when subjected to random impact.

The sandwich composite structures are extremely sensitive to different environmental factors such as temperature variation and moisture absorption. During processing, when the composite sandwich structures are heated to a high temperature, internal stresses are developed inside it. Moreover, these structures are exposed to very hot environmental conditions in many engineering applications such as aerospace, power plants, and nuclear reactors. With the variation of temperature, the resultant strains are developed as the thermal coefficients of the matrix and reinforcing constituents comprising the composite sandwich structures are different. The residual strains may lead to the development of micro-cracks inside the composites which result in the degradation of stiffness and strength of the structures.

It is fairly frequent for composite sandwich structures to be subjected to impacts with foreign bodies of different sizes and shapes during fabrication, operation, maintenance, and transportation. The impact with foreign bodies at low-velocity (typically less than 10 m/s) causes structural damages such as facing/core debonding, delamination in the composite facings, fiber breakage, matrix cracking, and cracking in the core, that are generally invisible and very difficult to detect. Such undetected damages not only deteriorate the stiffness, strength, and stability of

the structures but also may result in their catastrophic failure. Thus, the susceptibility of the composite sandwich structures to develop impact-induced damages is a major concern that limits their widespread usage. However, the impact resistance can be improved by using the carbon nanofillers reinforcement with functionally graded distribution. The transient response of these structures depends mostly on the presence of initial stresses arising either during manufacture or from environmental effects like thermal strains, centrifugal or aerodynamic loads.

1.2 MOTIVATION OF THE PRESENT WORK

The use of composite sandwich structures is growing steadily in various weight-sensitive engineering applications due to their high strength/stiffness-to-weight ratio. Recently, carbon nanofillers (CNTs, graphene, and their derivatives) reinforced nanocomposites have been used as the face sheets or skins of the sandwich structures to enhance their mechanical, thermal, and chemical properties remarkably without increasing weight. Interestingly, the dramatic improvement of the strength, stiffness, and impact resistance can be achieved with an addition of very small amount of carbon nanofillers in the nanocomposite media and further addition of these nanofillers results in deterioration of these mechanical properties. In order to utilize the low content nanofillers effectively, the idea of FGM can be adopted in the distribution of nanofillers. The potential applications of these FG nanocomposites and sandwich structures can be found in blades of turbo-machineries which generally work under high centrifugal force and hot environmental conditions. Since, the elevation of temperature causes degradation of overall stiffness of the rotating sandwich blades, the thermal effect on their mechanical behavior should be addressed.

The turbo-machiney blades have generally complex geometries. Accordingly, the blades are modeled as simplified structures such as cantilever beams, plates, and shells. The beam models can accurately predict the behavior of slender blades but they are not able to predict the chord-wise bending and coupled chord-wise and span-wise bending vibration modes of the short blades. In order to overcome the shortcomings of the beam models, the blades are modeled with the aid of plate and shell models. Out of these models, pretwisted shallow conical shell can be deemed as a suitable model for the real turbo-machinery blades owing to its trapezoidal planform. It is well known that resonant vibration is a critical factor for causing the blade failure. Hence, an accurate estimation of the natural frequencies and mode shapes of blades is necessary to ensure the working safety of the rotating machines. In actual practice, the turbo-machinery

blades which can be made up of composite sandwich construction are frequently subjected to low-velocity impact during fabrication, operation, maintenance, and transportation. The impact with foreign bodies may cause structural damages such as facing/core debonding, delamination in the composite facings, fiber breakage, matrix cracking, and cracking in the core, that are usually invisible. These undetected damages not only deteriorate the stiffness, strength, and stability of the structures but also may result in their catastrophic failure. However, the additions of carbon nanofillers are known to considerably enhance the impact resistance of composite face sheets in the sandwich structures. It is, therefore, indispensable to study the effects of some critical parameters on the temporal history of contact force along with the shell displacement, indentation, impactor velocity of nanocomposite sandwich structures for their reliable design and service. Computer codes are developed based on a suitably developed finite element formulation to study the influence of the critical parameters on the vibration and impact response of nanocomposite sandwich conical shells. The motivation of the present work originates from these points of view.

1.3 LITERATURE REVIEW

Over the years sandwich plates and shells have been used in several engineering applications ranging from satellites, aircraft, naval ships, wind mills, automobiles to civil infrastructures due to many advantages, introduction of new materials and the demand for high-performing but light-weight structures. The recent development of advanced composites with carbon nanofillers (CNTs and graphene) reinforcements makes the sandwich structures suitable in different multi-functional applications. For example, carbon nanofillers-based composites and sandwich structures can be considered as the future materials for turbo-machinery blades that work in complex environment. A great variety of the structural models, such as beam, plate, and shell models are employed to study the behavior of the turbo-machinery blades. However, the behaviors of the shell structures are markedly different from the beams and plates due to presence of surface curvature. The effect of surface curvature may be adequately dealt by considering shallow shell models. Literature dealing with research works on development, design, geometry, construction, and analysis of the sandwich structures considering different aspects is vast. In this section, an attempt has been made to review the CNTs and graphene reinforced composites and sandwich plates and shells with the main emphasis on the dynamic analysis of shallow conical shells in thermal environments.

The review of the literature as a background of the present research is broadly categorized into seven sub-sections given below. The first sub-section discusses the inclusion of carbon nanofillers in sandwich plates and shells. The second sub-section deals with various structural models employed for turbo-machinery blades. In third sub-section, the developments of various structural theories for laminated plates/shells are described. In fourth sub-section, various shell geometries are reviewed. The finite element modeling of laminated sandwich plates/shells, thermal effects on nanocomposites, and dynamic analysis of nanocomposite sandwich plates and shells are reviewed in the fifth, sixth, and seventh sub-sections, respectively.

1.3.1 NANOCOMPOSITE SANDWICH PLATES AND SHELLS

The concept of sandwich construction was traced back to middle of the nineteenth century, though the ideas of sandwich structure may perhaps were used before to a great extent (Noor *et al*., 1996). At the beginning of the World War-II, the principle of sandwich construction was started to use in different structural components of aircraft. The face sheets of early sandwich structures employed for aerospace applications were made of plywood and wood pulp fibers, while cork, balsa wood, and synthetic materials were selected as the core. Afterward, both face sheets and core of sandwich structures for aerospace applications were made of aluminum alloys, titanium, and stainless steel. The use of laminated composites as face sheets in the sandwich construction was extensively found in last few decades in order to take advantages of tailoring the physical and mechanical properties with proper selection of fiber orientation and staking sequence. Review articles like those by Librescu and Hause (2000), Vinson (2001), Hu *et al*. (2008), Carrera and Brischetto (2009), and Birman (2018) covered the major part of the research works carried out in last few decades. Thomsen (2009) highlighted the potential advantages and challenges of applying composite sandwich type construction in modern wind mill blades.

The development of nanolevel reinforcement of CNTs and graphene in polymeric matrix has introduced a new and attractive research arena for material scientists in recent years. These nanocomposite materials exhibit significant enhancement in properties that cannot generally be attained with the use of conventional composites or virgin polymeric and metal matrices. A considerable number of literature can be found on the carbon nanofillers reinforcement of the structures in order to improve the properties significantly; some of them are dealt with sandwich structures. In this sub-section, inclusions of two types of carbon nanofillers, namely, CNTs and graphene in the composite and sandwich structures are discussed.

1.3.1.1 FG-CNTRC Sandwich Plates and Shells

Different experimental investigations demonstrated that an inclusion of small amount of CNTs into nanocomposite media results in remarkable enhancement of mechanical, electrical, and chemical properties. Qian *et al*. (2000) found that an addition of 1 wt% MWCNTs to polystyrene resulted in 35%-42% increase in elastic modulus and about a 25% enhancement in strength, signifying considerable load transfer in the nanofiller-matrix interface. Liu *et al.* (2004) showed that elastic modulus, yield strength, and hardness of Nylon-6 matrix reinforced with only 2 wt% MWCNTs can be improved by 214%, 162%, and 83%, respectively, in compared with a pure Nylon-6. Deep and Mishra (2018) reported that the incorporation of 0.5 wt% MWCNTs in Poly (methyl methacrylate) (PMMA) matrix can lead to 16% increase in tensile strength. Laurenzi *et al.* (2013) demonstrated that impact resistance of the polymeric matrix can be increased up to 44% and 56% due to inclusion of 0.1 wt% and 0.5wt% functionalized MWCNTs, respectively. To reveal more about the mechanical properties and behavior of CNTRCs, the review articles reported by Andrews and Weisenberger (2004), Qian *et al.* (2010), Baksi *et al.* (2010), Liew *et al.* (2015, 2020), and Yengejeh *et al.* (2017) are recommended.

The estimation of effective material properties of the CNTRC structures is the basic step to study their mechanical behavior. Using experimental testing, the effective material properties of CNTRCs are obtained directly and accurately. There exist numerous experimental investigations to characterize the CNTRCs. At nanoscale, the experiments are time consuming, costly, and extremely difficult to conduct. Alternatively, theoretical formulation and numerical simulation can be treated as the efficient method to determine the properties of the CNTRCs, which may save both time and money. In many research works, the computational techniques such as molecular dynamics (MD) simulation, representative volume element (RVE) method, Mori-Tanaka (MT) scheme, and rule of mixture (ROM) were proposed to model the properties of the CNTRC media. Han and Elliot (2007) employed MD simulation to estimate the elastic moduli of the CNTRCs made by reinforcing the SWCNTs (10,10) into two different polymeric matrices. The authors found the considerable difference between the values of the elastic moduli obtained from the MD simulation and the conventional ROM. Liu and Chen (2003) determined the effective elastic properties employing 3-D nanoscale RVE based on 3D elasticity theory and solved by FEM. The simulation results were compared with the results from the extended ROM and found negligible differences between them. Seidel and Lagoudas (2007) modeled the

effective elastic properties of CNTRCs employing MT, self-consistent, and composite cylinders micromechanics methods. The randomly oriented MT results at low volume fraction of CNTs were found good agreement with the experimental results. Fidelus *et al.* (2005) conducted experimental investigation to examine the thermo-mechanical properties of randomly oriented SWCTs and MWCNTs reinforced nanocomposites at content nanofillers. The Young's modulus obtained from the experiment was found to be slightly greater than the result predicted by the extended ROM based on Krenchel's model.

Meguid and Sun (2003) demonstrated that inclusion of nanofillers beyond a certain weight fraction would lead to deteriorate the tensile and shear properties of the nanocomposite due to lower cohesion between the nanofillers and matrix. It is really a challenge to the researchers how be best utilize of low content nanofillers in CNTRCs under the current fabricating technology. The typical method of producing CNTRCs assumes that the CNTs are dispersed uniformly or randomly in such a way that resulting properties are not spatially variable at the macroscopic level. Besides, FGM belongs to a new class of composite material wherein the microstructural features are varied smoothly from one surface to another surface by distributing the reinforcing phase non-uniformly. The idea of FGMs can be used to manage the material's microstructure so that the properties of the nanocomposite can be improved. Shen (2009) first proposed a novel nanocomposite materials, namely, functionally graded CNTs reinforced composites (FG-CNTRC) in which the CNTs are distributed in the isotropic matrix according to the rule of FGMs in a specific direction to enhance the mechanical properties of the structures. The author showed that the non-linear bending characteristics of CNTRC plate are significantly improved when the CNTs volume fraction is considered to be functionally graded. This novel material FG-CNTRCs became more attractive in structural engineering applications after its successful fabrication by Kwon *et al.* (2011). Lei et al. (2013) analytically demonstrated that the distributions of CNTs reinforcement near top and bottom surfaces are more effective than those distributions near mid-plane. There exist a good number of research works on mechanical behavior of FG-CNTRC structures, some of these are reviewed by Liew *et al*. (2020).

Due to improved mechanical properties with low weight, the CNTRCs could be chosen for the face sheets of sandwich structures. For the first time, Wang and Shen (2012) proposed a sandwich plate with two symmetric CNTRC face sheets and homogeneous core (Ti-6Al-4V) to

study the effectiveness of CNTs grading pattern on its nonlinear vibration and flexural behavior. Later on, Shen and Zhu (2012) investigated the buckling and postbuckling behavior of the CNTRC sandwich plates resting on elastic foundation. The authors found that buckling load and postbuckling strength of the sandwich plate with FG-CNTRC face sheets are considerably higher than those of the same plate with UD-CNTRC face sheets. Lin *et al*. (2016) demonstrated that the mechanical properties, flexibility, and electromagnetic interference shielding effectiveness can be enhanced with sandwich structured polypropylene/MWCTs composites. Chen *et al*. (2017) demonstrated that the inclusion of MWCNTs into epoxy resin in the prepreg is an efficient way of improving the face sheets/core bonding. Patra and Mitra (2018) carried out an experimental investigation to confirm the significant improvement in fracture toughness of sandwich structures consisting of glass-fiber reinforced composite face sheets and polyvinyl-chloride foam core with an addition of MWCNTs to the epoxy resin.

1.3.1.2 FG-GRC Sandwich Plates and Shells

Graphene-based nanocomposites are expected to become more economically viable nanocomposites having unprecedented mechanical, thermal, electrical, and chemical properties at extremely low nanofiller content (Kuilla *et al*., 2010). This opens up new possibilities of extremely lightweight structures made up of graphene-based composites. Rafiee *et al*. (2009) carried out the experimental investigation to compare the mechanical properties of CNTs (both SWCNTs and MWCNTs) and graphene reinforced composite at same nanofiller weight fraction of ~ 0.1%. The authors found that at low nanofiller content, graphene is more effective than CNTs for the enhancement of tensile strength, elastic moduli, and fracture toughness. As stated by the authors, the extremely large surface area of graphene, improved adhesive bond at graphene-matrix interface and two-dimensional geometry of the graphene might be probable reasons for these incomparable enhancements. Fang *et al*. (2009) reported that reinforcement of a small weight % (0.9 wt%) of graphene sheets into polystyrene film results in 69.5% and 57.2% enhancement in tensile strength and elastic modulus, respectively. Song *et al*. (2011) demonstrated that inclusion of very small volume % (0.24 vol%) into polypropylene (PP) matrix would lead to significant increase in yield strength (~75%) and Young's modulus (~74%) of the PP. Erkliğ and Doğan (2020) reported that comprehensive improvement in tensile strength, flexural strength, and impact resistance of hybrid glass/basalt fiber composites could be obtained only with an addition of 0.1 wt% nanographene.

Apart from the experimental investigations, several theoretical and numerical efforts were conducted to model the mechanical properties of the graphene-based nanocomposites. Ji *et al.* (2010) employed the Mori-Tanaka micromechanics model to examine the stiffening effect of graphene sheets with ideal shapes and dispersions in the nanocomposite media. Rahman and Haque (2013) studied the influence of GPL wt%, aspect ratio, and dispersion on the elastic moduli and interfacial mechanical properties of GPLRCs using molecular mechanics (MM) and MD simulations. The authors found that Young's modulus predicted by MD simulation is relatively greater than those predicted by MM technique. Liu *et al*. (2015) performed MD simulations to examine the effects of graphene wrinkles, matrix type, and polymer chain length on the interfacial mechanical properties of graphene/polymer nanocomposite systems. Spanos *et al.* (2015) introduced a computational model based on the micromechanical theories using suitable RVE to estimate the elastic properties of graphene-based polymer composites.

Similar to CNTs, the graphene content in the nanocomposite media must be kept within a certain limit due to dispersion and other issues (Putz *et al*., 2010; Milani *et al*. 2013). Motivated by the work of Shen (2009) on the conception of FG-CNTRC, one type of graphene based novel composites, namely, functionally graded graphene platelets-reinforced composites (FG-GPLRC) have been proposed by Song *et al*. (2017), wherein the dispersion of square shaped GPLs are assumed to be layer-wise functionally graded in thickness direction. The effective temperature-independent elastic properties of the nanocomposite are estimated using modified Hapin-Tsai model. The authors reported that the dispersion of more GPLs near the top and bottom surfaces of the structure resulted in the increase of natural frequencies and decrease of dynamic deflection effectively. Thereafter, linear and non-linear mechanical behaviors of FG-GPLRC structures have been extensively investigated by many researchers (Yang *et al*., 2017; Song *et al*., 2017; Thai *et al*., 2019; Zhao *et al*., 2020; Ramezani *et al*., 2022). Shen *et al.* (2017) also proposed another type of novel composite material known as functionally graded graphene-reinforced composites (FG-GRCs), in which the reinforcements of aligned graphene sheets into the nanocomposite are piece-wise graded across the thickness direction. The equivalent elastic properties of this nanocomposite are assumed to be temperature-dependent and determined using extended Halpin-Tsai model. The authors found that vibration characteristics of the FG-GRC plates could be improved effectively by selecting a special type of FG pattern of graphene (FG-

X) for reinforcement. This piece of work has inspired other researchers (Kiani, 2018; Lei et al., 2018; Vu *et al*., 2021) to explore the mechanical response of FG-GRC laminated structures.

The literature dealing with mechanical behavior of graphene-reinforced sandwich structures is less in comparison to that of CNTs-reinforced sandwich structures. A sandwich plate with two symmetric FG-GRC face sheets and a homogeneous core (Ti-6Al-4V) was first introduced by Yu *et al*. (2018). It was found that the FG distribution of graphene volume fraction in the face sheets is more effective than uniform distribution to enhance the buckling and postbuckling strength of the FG-GRC sandwich plate. Following the same combination of materials for face sheets and core, Wang and Shen (2018) carried out the large deflection vibration analysis of FG-GRC sandwich plates. The authors showed that the large deflection vibration characteristics of the sandwich plate are greatly influenced by graphene grading patterns and core-to-face sheets thickness ratio.

1.3.2 MODELING OF TURBO-MACHINERY BLADES

The dynamic analysis of turbo-machinery blades has received much attention in past few decades. Rao (1973,1977, 1980, 1983) presented comprehensive review of scholarly articles about turbo-machinery blades including vital aspects of blade vibrations like determination of the natural frequencies, blade excitation forces, influence of blade aspect ratios, blade geometry, and resonant vibrations. Rafiee *et al*. (2017) carried out an extensive survey about the vibration and control of the rotating beams and blades with special focus on the analytical, semi-analytical, and numerical studies dealing with dynamical problems involving advanced materials and complicating effects and loadings.

Many researchers have idealized turbo-machinery blades as cantilevered beams since such idealization can predict the behavior of those slender blades accurately. For example, Putter and Manor (1978) treated a radial rotating beam mounted in the disc with 90° preset angle as a turbo-machinery blade. The lead-lag natural frequencies and mode shapes of the rotating blades were investigated. Using finite element technique Yokoyama (1988) analyzed the in-plane and out-of-plane free vibrations of rotating Timoshenko beams. The vibration behavior and control of rotating pretwisted thin-walled composite beams with embedded macro fiber composite (MFC) actuators and sensors were investigated by Choi *et al*. (2007) and Vadiraja and Sahasrabudhe (2009). Based on higher-order theory, Shenas *et al.* (2017) analyzed the free vibration of rotating pretwisted beams reinforced with CNTs in thermal environments. Heidari

and Arvin (2019) investigated linear and non-linear vibration of rotating FG-CNTRC Timoshenko beams. Shahedi and Mohammadimehr (2020) studied the free vibration of rotating fully-bonded and delaminated sandwich beams consisting of AL-foam flexible core and FG-CNTRC face sheets in hygrothermal environments. Zhao *et al*. (2021a, 2021b) presented a novel theoretical model to investigate free vibration response of rotating FG-GPLRC beam-hollow cylindrical hub system.

However, the beam models are not able to predict the chord-wise bending and coupled chord-wise and span-wise bending modes of the blades with low aspect ratios. In order to overcome the shortcomings of the beam models, numerous attempts have been made to grasp the dynamic behavior of the rotating blades by adopting plate models. Dokainish and Rawtani (1971) presented the free vibration analysis of cantilever plate mounted around a rotating disc considering the chord-wise bending effects. Sreenivasamurthy and Ramamurti (1981a, 1981b) employed finite element procedure to analyze the effects of Corriolis effects, aspect ratio, pretwist angle, taper, skew angle, and hub radius on the natural frequencies of rotating uniform and tapered cantilever plates. The authors found that Coriolis effects on the first and second natural frequencies of the blade rotating at moderate rotational speeds are negligible. Qatu and Leissa (1991) were the first to investigate the natural frequencies and mode shapes of pretwisted laminated fiber reinforced composite rectangular blades using the Ritz method. McGee and Chu (1994) presented three-dimensional continuum vibration analysis for rotating laminated composite blade. Karmakar and Sinha (1997, 1998, 2001) performed the dynamic and failure analyses of rotating pretwisted laminated composite cantilever plates using finite element technique. Sinha and Turner (2011) presented an analytical method in which the effect of warping of the cross section due to twist-bend coupling was incorporated to estimate natural frequencies and modes of rotating pretwisted rectangular blades. Cao *et al.* (2017) developed the pretwisted sandwich plate model to analyze free vibration of rotating turbo-machinery blades embedded with thermal barrier coatings employing FSDT, von-Karman plate theory, and Chebyshev-Ritz method. Chen and Li (2019) introduced a new dynamic model based on the shell theory to investigate the vibration response of pretwisted rectangular laminated composite blades mounted around the rotating disc. The linear and nonlinear vibration characteristics of rotating pretwisted hybrid composite blades containing CNTRC layers and cracked fiber-reinforced composite (FRC) layers using FSDT were investigated by Zhang *et al*. (2020), Pan

and Liew (2020), and Pan *et al*. (2020). The authors adopted a self-consistent model (SCM) to take into account the degradation of stiffness due to matrix cracks. Using the similar approach, Guo *et al*. (2021, 2022) analyzed the linear and non-linear vibration characteristics of rotating pretwisted FG-GPLRC rectangular blades with matrix crack in thermal environments. Cheng *et al*. (2022) established a dynamic model to study the vibration behavior of rotating pretwsited CNT-reinforced ceramic blades.

Shell type structures having different curvatures can be found as a component of turbo-machines which are key features relative to the plate models. Hence, shell models that include effect of surface curvature are preferable to the plate models for turbo-machinery blades. Leissa *et al*. (1981, 1982, 1983, 1984) performed extensive research works that help in predicting the vibration characteristics of shell type turbo-machinery blades with relatively small curvatures using shallow and thin shell theory and variational approach. Qatu and Leissa (1991) extended this work to demonstrate the effects of curvature and stacking sequence on the free vibration characteristics of laminated composite curved panels. Kee and Kim (2004) assumed the blades as pretwisted moderately thick cylindrical panels that incorporate transverse shear deformation and rotary inertia. The authors employed finite element procedure based on Reissner–Mindlin's shell theory to analyze the free vibration behavior of the rotating blades. Karmakar *et al*. (2005) and Karmakar and Kishimoto (2006) developed finite element formulation based on Mindlin's plate theory for vibration analysis of rotating pretwisted delaminated composite shallow cylindrical shells. Rout *et al.* (2019) studied vibration response of rotating pretwisted CNTRC shallow cylindrical shells under different thermal conditions using FSDT. Using Chebyshev-Ritz method in conjunction with FSDT, Niu *et al.* (2019) analyzed the natural frequencies of and mode shapes of rotating pretwisted graphene-reinforced composite cylindrical blades, while Zhang *et al.* (2020) investigated the vibration characteristics of rotating tapered cantilever cylindrical panel with graphene coating layers. Maji and Singh (2021) presented a higher-order finite element vibrational analysis of rotating pretwisted 3D braided composite cylindrical panels.

One major shortcoming of the cylindrical shallow shell model is the constant chord-wise curvature. An actual turbo-mechinery blade attributes a cantilevered shallow shell with trapezoidal planform, pretwist, and variable chordwise surface curvature. Thus, a more suitable model for turbo-machinery blades would be a shallow conical shell. The vibration analysis of cantilevered pretwisted thin shallow conical shells was first performed by Liew *et al*.

(1994). The authors used Ritz procedure to investigate the effect of pretwist angle on the natural frequency and mode shape of the isotropic structure. In another study, Liew *et al.* (1995) investigated the influences of pretwist and thickness variation on the vibration characteristics of isotropic pretwisted shallow conical shell with varying thickness. These works were extended by Lim *et al*. (1997) to cantilevered laminated fiber-reinforced composite shallow conical shells with and without pretwist in investigating the effects of fiber orientation on the free vibration. Hu *et al.* (2002) presented an efficient formulation for vibration analysis of rotating pretwisted laminated composite deep open conical shells using the Rayleigh-Ritz method. Bandyopadhyay *et al.* (2014) and Bandyopadhyay and Karmakar (2015) developed finite element based on Mindlin's plate theory to investigate the free vibration and bending characteristics of rotating pretwisted delaminated composite conical shells in hygrothermal environments. Maji *et al*. (2020) analyzed the effects of pretwist angle, temperature, aspect ratio, and rotational speed on the free vibration characteristics of CNTs-reinforced rotating pretwisted conical shallow shells in thermal environments using finite element technique in conjunction with FSDT. Xiang *et al*. (2020) investigated the vibration characteristics and staking sequence optimization of rotating pretwisted FG-CNTRC shallow conical shells employing the meshless kp-Ritz procedure in conjunction with FSDT.

1.3.3 REVIEW ON PLATES/SHELLS THEORIES

In engineering, majority of the problems are involved with complex geometry that requires being solved employing plate and shell theories. On the other hand, laminated composite and sandwich plates/shells incorporate a significant complexity regarding their microscopic and macroscopic behavior. For this reason, extensive works have been performed on the development of the plate and shell theories to simplify the three-dimensional (3-D) complex problem into simpler one. In general, laminated plates and sandwich plates/shells are formulated using broadly following two theories: Equivalent single layer (ESL) and Layer-wise (LW) theories. The ESL theories are derived from 3-D elasticity theory by assuming appropriate displacement field or stress field through the thickness of the plates/shells. Based on these assumptions, a variety of the ESL theories are developed. The most simplified type of ESL theory is classical plate theory (CPT), also called the Kirchhoff theory (1850), which discards both transverse shear and through-the-thickness deformation. Therefore, this theory is accurate merely for very thin layered or sandwich plates/shells. Later on, the transverse shear deformation effects were taken into account

to propose first-order shear deformation theory (FSDT) employing Reissner–Mindlin model (Reissner, 1945; Mindlin, 1951). The FSDT provides much better accuracy than CPT for thick plates. However, this theory also experiences the shortcoming like the use of problem-dependent shear correction factor. To overcome the drawbacks of CLPT and FSDT, the higher-order shear deformation theories (HSDTs) have been introduced. Among all ESL theories, the HSDTs are most accurate and widely used structural theory to model laminated composite and sandwich plates/shells. Apart from ESL theories, some other refined theories such as layer-wise theories (LWT) and Zig-zag theories (ZZT) have been developed. This section is further divided into following subsections to understand clearly the systematic development of these different ESL and other theories.

1.3.3.1 Classical Plate Theory

The basis of the classical plate theory (CPT) lies on the Kirchhoff hypothesis (1850), which assumes that the transverse normals remain straight and perpendicular to the mid-surface after deformation and do not experience elongation. Thus, both transverse normal strain and transverse shear strains are discarded, which implies that the deformation is completely due to bending and in-plane stretching. The direct application of Kirchhoff hypothesis to laminated composites gives rise to classical laminated plate theory (CLPT) which has been developed by Reissner and Stavsky (1961), Stavsky (1961), Dong *et al*. (1962), and is summarized by Ashton and Whitney (1970). Pagano (1970) examined the validity of CLPT to predict the response of multi-layered bi-directional composites and sandwich plates and found that the results converge to the exact solution with increasing the length-to-thickness ratio. This theory which under-predicts deflections and over-predicts natural frequencies and buckling loads, is adequate only for very thin laminated plates/shells.

1.3.3.2 First-order Shear Deformation Theory

First-order shear deformation theory (FSDT) is an extension of the Reissner-Mindlin (Reissner, 1945; Mindlin, 1951) model to multi-layered composite plates. In general, the longitudinal modulus of composite laminates is much greater than their transverse shear modulus. This considerable material anisotropy may result in warping and transverse shear deformation for thick laminated composite plates. Hence, the effect of transverse shear deformation must be taken into consideration to predict its structural behavior accurately. Considering the effect of

shear deformation, a consistent stress-based plate theory was first provided by Reissner (1944, 1945). The assumptions made by Reissner (1944, 1945) provide a consistent stress distribution transversely, which would lead to consider through-thickness linearly varying in-plane displacements and invariant out-of-plane displacement. Mindlin (1951) used the same type of displacement field as given by Reissner (1944, 1945) without introducing corresponding stress distribution assumptions to develop a plate theory, known as "Mindlin plate theory". Medwadowski (1958) extended Reissner's theory to orthotropic laminates, while Yang *et al*. (1966) extended Mindlin's theory to symmetrically laminated anisotropic, orthotropic, and isotropic plates. Since, in FSDT, the transverse shear stresses are considered to be invariant with the thickness, shear correction factor must be introduced to adjust shear stress resultants. The shear correction factor is difficult to estimate especially for laminated composite and sandwich plates/shells because the factor depends not only on the lamination, geometric parameters, and face sheets-core material combinations but also loading, boundary, and other conditions (Vlachoutsis, 1992; Meunier and Shenoi, 1999).

1.3.3.3 Higher-order Shear Deformation Theory

In order to avoid the use of shear correction factor, to take account of proper cross-sectional warping, and to obtain the realistic through-thickness variation of the transverse shear strains and stresses, the higher-order shear deformation theories (HSDTs) have been developed. The HSDTs involve the higher-order terms in Taylor's expansion of the displacements in the coordinate normal to the mid-surface. Lo *et al.* (1977a, b) developed a higher-order theory for plate deformation considering nonlinear distributions of the in-plane displacement (four terms of Taylor's series expansion) and transverse displacement (three terms of Taylor's series expansion) in the thickness direction. Reddy (1984) modified the displacement model of Lo *et al*. (1977a, b), by ignoring the transverse normal stress effect and enforcing the transverse shear stress free conditions on the top and bottom surfaces. With this displacement model, the shear deformation theory, commonly known as Reddy's third-order shear deformation theory (TSDT), accounts for more realistic parabolic variation of the transverse shear stress across the thickness direction. However, the finite element (FE) formulation based on Reddy's TSDT kinematic conditions requires C^1 continuity which is computationally inefficient. In order to overcome this difficulty, a C^0 continuous displacement based FE formulation of a new HSDT has been developed by Pandya and Kant (1988a, 1988b), which is different from Reddy's TSDT in the

sense that the non-zero transverse shear force condition on the bounding surfaces. Later, Kant and Pandya (1988) developed a simple HSDT which enforces the zero transverse shear stress conditions on the outer surfaces. Generally, the order of the HSDTs more than three are not preferred since the accuracy achieved is so small that the effort needed to handle the large number of unknowns in the solution is not justified.

1.3.3.4 Layer-wise Theory

The layer-wise theories (LWTs) consider separate displacement field expansions within each material layer. In LWTs, the number of unknowns involved depends on the number of layers which is rather expensive for many cases of laminated composites and sandwich plates/shells. Srinivas (1973) developed a layer-wise theory wherein the displacements were assumed piecewise linear along the thickness direction for the static and dynamic analysis of laminated composite plates. Reddy (1987) presented a layer-wise laminate theory in which all the variables associated with the 3-D analysis were taken into the account. The author assumed linear variation of displacement components within each layer and the displacement field to be continuous across the laminate thickness.

1.3.4 REVIEW OF SHELL GEOMETRY

Shells may have a variety of geometries, which are determined by their curvature characteristics. The basic equations governing the shell geometries depend upon the selection of reference frame (Cartesian, polar, spherical or curvilinear), nature of Lame's parameters (constant or variable) and curvature (constant or variable). The shells of revolution are generated by revolving a generator (straight or curved line) about an axis. In engineering practice, the commonly found shells of revolution are cylindrical, conical, spherical, elliptical, hyperbolic paraboloid shells etc. These shells may be closed or open (segment of the closed shell). The literature of laminated composite and sandwich shells behavior is reviewed based on the shell geometry.

1.3.4.1 Cylindrical Shells

Cylindrical shells formed by revolving a straight line about an axis that is parallel to the line are the simplest type of shells of revolution. Following the pioneer work of Arnold and Warburton (1949), many researchers conducted the works on static and dynamic behavior of laminated and sandwich closed cylindrical shells and panels. Some of the noteworthy contributions are

discussed here for the sake of brevity. Lam and Loy (1998) used Love-type shell theory and Galerkin's method to study the free vibration of rotating thin laminated cylindrical shells and showed the influence of the boundary conditions on the natural frequencies of the rotating shells. Kardomateas (2001) presented the elasticity solution for orthotropic sandwich cylindrical shells subjected to external and/or internal pressure as well as axial load. The free vibration behavior of composite cylindrical shells with general boundary conditions was investigated by Shao and Ma (2007) using Love's shell theory in association with Fourier expansion method.

Song *et al*. (2016b) presented vibration analysis of laminated cylindrical shells reinforced with CNTs in thermal environments using Reddy's TSDT. Thanh *et al*. (2019) presented the non-linear dynamic and vibration analysis of temperature-dependent FG-CNTRC cylindrical shell surrounded by elastic foundation with the aid of Reddy's TSDT. Ansari *et al*. (2019b) investigated the free vibration behavior of sandwich cylindrical shells with FG-CNTRC face sheets and homogenous core resting on elastic foundation under internal pressure using HSDT. Shokri-Oojghaz *et al.* (2019) examined the stress and deflection distributions in sandwich cylindrical shells reinforced with aggregated CNTs subjected to internal and external pressures using axis symmetric FEM model. Kiani *et al.* (2020) studied the free and forced vibational response of FG-CNTRC sandwich cylindrical shell resting on the visco-Pasternak foundation with different boundary conditions. Yadav *et al*. (2021) carried out non-linear static analysis of sandwich cylindrical shells consisting of FG-CNTRC face sheets and FG porous core subjected to internal pressure with simply supported boundary conditions using HSDT. Rostami and Mohammadimehr (2022) presented an analytical approach based on the FSDT to study the vibration control of rotating sandwich cylindrical shell with CNTRC face sheets and porous core embedded with FG magneto-electro-elastic layers.

Based on Reddy's TSDT and Kármán-type kinematic nonlinearity, Shen *et al*. (2017) conducted nonlinear vibration analysis of graphene reinforced nanocomposite cylindrical shells. Liu *et al.* (2018) used 3-D elasticity theory to examine the buckling and free vibration behavior of GPL-reinforced multi-layered composite cylindrical shells under an axial stress. Shen and Xian (2018) investigated buckling and postbuckling behavior of laminated composite cylindrical shells reinforced with graphene sheets. Eyvazian (2021) analyzed the free vibration of sandwich cylindrical shells with FG-GPLRC face sheets and flexible core employing a novel unconstrained higher-order theory.

1.3.4.2 Conical Shells

Conical shells are special type of shells of revolution that are formed by revolving an inclined straight line about an axis keeping angle of inclination constant. The cross-section of conical shells may be circular or elliptic (where they are not shells of revolution). Due to the involvement of greater mathematical complexity to characterize their geometry, the dynamic behavior of conical shells has been studied to lesser extent than that of cylindrical shells. Among prior investigations of vibrating conical shells, Garnet and Kemper (1964) were the first to include the effect of transverse shear deformation and rotary inertia in the formulation. However, this study was restricted to the truncated conical shells made up of homogeneous isotropic materials. Bert and Ray (1969) carried out vibration behavior of orthotropic sandwich conical shells made up of glass fiber/epoxy composite face sheets and honeycomb core considering free-free boundary conditions using Rayleigh-Ritz inextensional method. Wilkins *et al*. (1970) investigated the symmetrical and unsymmetrical vibration modes of sandwich truncated conical shells with various boundary conditions using Love's first approximation shell theory, wherein the transverse shear effect is incorporated. Yang (1974) determined the natural frequencies and corresponding mode shapes of orthotropic conical shells using an integration method. Tong (1993) obtained exact solution for Donnell-type governing equations of vibrating composite laminated conical shells. Subsequently, Khatri (1995), Tripathi *et al*. (2007), Shadmehri *et al*. (2012), Viswanathan *et al*. (2015), and Sofiev (2018) investigated the buckling and free vibration analysis of conventional laminated truncated conical shells.

Heydarpour *et al*. (2014) employed FSDT and differential quadrature method (DQM) to examine the effects of centrifugal and Coriolis force on the free vibration behavior of composite truncated conical shells reinforced with CNTs. Mehri *et al.* (2016) investigated buckling and free vibration behavior of CNTRC conical shells with various CNTs grading patterns subjected to both external pressure and axial compression. Based on the FSDT and generalized differential quadrature (GDQ) method, Kamarian *et al.* (2016) studied the free vibration of composite conical shells reinforced with agglomerated CNTs. Ansari *et al*. (2019a) presented a non-linear vibration analysis of FG-CNTRC truncated conical shells based on the HSDT. Sofiyev *et al*. (2020) examined the stability of sandwich truncated conical shells with CNTRC coatings under external pressure using the modified Donnell-type shell theory and generalized FSDT.

Kiani (2019) performed an investigation on the bucking behavior of FG-GRC conical shells subjected to external pressure using FSDT. Afshari (2020) studied the influence of graphene nanoplatelets (GNPs) reinforcement on dynamic behavior of rotating truncated conical shells using FSDT. A non-linear dynamic model based on Hamilton's principle, the FSDT, and the von-Karman non-linearity was established for vibration analysis of FG-GPLRC truncated conical shells by Yang et al. (2021). Recently, Adab and Arefi (2022) presented a dynamic analysis of micro-conical sandwich shells with FG-GPLRC face sheets and porous polymeric core based on the modified couple stress theory and differential quadrature method (DQM).

1.3.4.3 Spherical Shells

Spherical shells are another special type of shells of revolution. To generate a spherical surface, a circular curve line instead of a straight line is revolved around an axis. These shells may be closed or open depending on the length of the circular arc. The pioneering work on axisymmetric vibration response of thin elastic spherical shells was done by Naghdi and Kalnins (1962). Based on FSDT kinematic conditions, Ansari *et al*. (2016) presented free vibration analysis of FG-CNTRC spherical shells resting on Pasternak elastic foundation. Sankar *et al.* (2017) analyzed the nonlinear axisymmetric dynamic behavior of sandwich spherical shells with CNTRC face sheets and titanium alloy core subjected to thermal loads using FSDT. Manh *et al*. (2020) used classical shell theory (CST) to study the nonlinear post-buckling behavior of sandwich annular spherical shell with CNTRC face sheets and homogeneous isotropic core in thermal environment. Heydarpour *et al.* (2019) investigated transient thermoelastic behavior of FG-GPLRC spherical shells subjected to thermo-mechanical loadings using Lord-Shulman thermoelasticity theory. Based on 3D elasticity theory, Liu *et al.* (2021) presented free vibration and static bending analysis of FG-GPLRC spherical shells.

1.3.4.4 Shallow Shells

Shallow shells are open shells which have rectangular, triangular, trapezoidal, circular, elliptic, rhombic, or other planforms and very large characteristic shell radii. These shells are sometimes called curved plates. The literature on shallow shells vibration research was reviewed by Qatu (1992) and Liew *et al*. (1997). Using Donnell shallow shell theory and FSDT, Mirzaei and Kiani (2016) investigated free vibration characteristics of CNTs-reinforced composite shallow cylindrical shells. Wang *et al*. (2017) analyzed free vibration characteristics of FG-CNTRC

shallow shells (spherical, cylindrical, and hyperbolic paraboloid) and plates employing the FSDT and the artificial spring boundary technique. By means of the HSDT and FEM, the free vibration and buckling behavior of CNTs-reinforced sandwich shells (spherical, elliptical, cylindrical, and hyperbolic) was investigated by Mehar and Panda (2018), and Mehar *et al*. (2018, 2019). Based on generalized HSDT, Setoodeh *et al*. (2019) presented free vibration analysis of doubly curved complete and incomplete sandwich shells (elliptical, cycloid, and parabolic) with porous core, FG-CNTRC face sheets and embedded with piezoelectric layers. Rout *et al*. (2019) developed finite element formulation based on the HSDT to analyze the free vibration of FG-GRC shallow shells (cylindrical, elliptic paraboloid, hyperbolic paraboloid, conoidal, and hypar) with arbitrary boundary conditions. Punera and Kant (2021) worked on the stress and free vibration analysis of CNTRC sandwich cylindrical panels using two dimensional kinematic models.

Wang *et al*. (2019) examined non-linear transient response of laminated doubly-curved shallow shells reinforced with GPLs under blast loads using HSDT. Sobhy and Zenkour (2019) analyzed free vibration of FG-GPLRC doubly curved shallow shells resting on elastic foundation using four-variable shear deformation shell theory. Qin *et al*. (2020) developed unified formulation to study the free vibration of FG-GPLRC shallow shells (cylindrical, spherical, and hyperbolic paraboloid) with different boundary conditions using FSDT.

1.3.4.5 Other Shells

Coupled conical-cylindrical shells are complicated types of shells which need great computational effort. Irie *et al*. (1984) employed transfer matrix method to determine the free vibration of coupled elastic cylindrical–conical shells. The vibration behavior of FG-CNTRC coupled conical-cylindrical shells was investigated by Ninh *et al.* (2021) using based on Donnell's shell theory. Using the same theory, Chai and Wang (2022) investigated traveling wave vibration characteristics of rotating GPLs-reinforced metal foam coupled cylindrical–conical shells. Owing to doubly-curved shallow configuration with a closed shape in the circumferential direction, modeling of toroidal shell segments is complex. Bidzard *et al.* (2019) presented finite element analysis based on FSDT to study the vibration behavior of FG-GPLRC toroidal shell panels restrained against rotation. Phuong *et al.* (2021) analyzed postbuckling behavior of FG-GRC toroidal shells surrounded by elastic foundation and subjected to uniform external pressure considering thermal effects.

1.3.5 FINITE ELEMENT MODELLING OF LAMINATED COMPOSITES AND SANDWICH STRUCTURES

A considerable amount of research has been devoted to the development of the finite element method for static and dynamic analysis of laminated composites and sandwich structures. Some of them which are important and relevant to the present research are discussed in this section. Pryor and Barker (1971) developed a finite element procedure which incorporates the effects of transverse shear deformation to study the static behavior of the laminated composite plates. The authors employed four-noded rectangular elements with twenty eight degrees of freedom (DOFs). Kolář and Němec (1973) analyzed various solutions of laminated plates which are obtained by using finite element method (FEM). Khatua and Cheung (1973) presented a finite element displacement analysis of multilayer sandwich plates composed of n stiff layers and $(n-1)$ weak cores. The author employed a rectangular plate element in which the transverse displacement was given by twelve term polynomial, whereas in-plane displacement components were specified by bilinear functions. Reddy (1980) developed a C^0 finite element based on the penalty/ Yang, Norris and Stavsky (YNS) theory to study the bending and free vibration behavior of laminated composite plates. Chao and Reddy (1984) developed a degenerated 3-D finite element t based on the total Lagrangian description of the motion of laminated composite shells. Pandya and Kant (1988c) formulated a C^0 finite element method based on higher-order shear deformation theory (HSDT) wherein nine-noded quadrilateral element with nine degrees-of-freedom per node was used for the analysis of laminated composite plates.

Chakrabarti and Sheikh (2004) developed an efficient six-noded triangular element in conjunction with refined plate theory to investigate the vibration behavior of sandwich plates with stiff laminated face sheets. Ray and Batra (2007) employed the finite element technique to study the active constrained layer damping (ACLD) treatment of a SWCNTs reinforced 1–3 piezoelectric composite structure. Pandit *et al.* (2008) proposed a computationally efficient C^0 finite element formulation based on an improved higher-order zigzag theory (HOZT) to investigate the static behavior of the laminated sandwich plates. Panda and Singh (2011) analyzed the large deflection free vibration response of thermally post-buckled composite doubly curved panels using non-linear finite element method (FEM) in which the geometric non-linearity is included. Moita *et al.* (2011) developed a non-conforming triangular finite element model having three nodes and eight degrees of freedom per node to study the static and vibration

analysis of active–passive damped multilayer sandwich plates. Zhu *et al.* (2012) performed the bending and free vibration analyses of thin to moderately thick FG-CNTRC plates using the finite element method (FEM) in conjunction with the first-order shear deformation theory (FSDT). Serdoun and Cherif (2016) employed a new C^1-HSDT p-element with eight degrees of freedom per node to analyze the free vibration of thick composite and sandwich plates. Belarbi *et al.* (2017) developed a simply four-noded C^0 continuous isoparametric element based on the layer-wise theory for vibration analysis of laminated composite and sandwich plates. Hajlaoui *et al.* (2019) employed a modified first-order enhanced solid-shell element formulation to investigate the buckling behavior of FG-CNTRC cylindrical shells under external pressure and axial compression. Using finite element procedure, Tran *et al.* (2020) carried out the forced vibration analysis of GPLRC shells in thermal environments.

1.3.6 THERMAL EFFECTS ON NANOCOMPOSITE SANDWICH PLATES AND SHELLS

By means of Reddy's TSDT, Shen and Zhang (2010) analyzed the buckling and postbuckling behavior of FG-CNTRC plates subjected to thermal loads with through thickness parabolic rise in temperature. The authors found that the buckling temperature and thermal postbuckling strength of the plate can be improved with special type of FG distribution (FG-X) of CNTs. Kiani (2017, 2018) presented the postbuckling analysis of FG-CNTRC plates and FG-CNTRC sandwich plates under uniform rise temperature conditions using a FSDT based analytical formulation which includes Kármán type of geometrical non-linearity. Hasrati *et al.* (2017) applied a numerical approach based on variational differential quadrature (VDQ) method to study the non-linear forced vibration of temperature-dependent FG-CNTRC cylindrical shells. Using VDQ in combination with kinematic conditions of FSDT and the von Karman geometric nonlinearity, Torabi and Ansari (2017) investigated nonlinear free vibration of FG-CNTRC annular plates under thermal loading. Safaei *et al.* (2018) analyzed the effects of thermal gradient load on the natural frequencies of the sandwich plates with agglomerated FG-CNTRC face sheets and isotropic core using FSDT and Eshelby-Mori-Tanaka method. Foroutan *et al*. (2019) reported the non-linear free and forced vibration of imperfect FG-CNTRC cylindrical panels subjected to external pressure in thermal environments assuming through thickness nonlinear temperature variation. Based on the classical shell theory, Hieu and Tung (2020a) investigated analytically the buckling and postbuckling behavior of FG-CNTRC cylindrical shells subjected

to external pressure under different thermal conditions. The authors assumed three different thermal conditions such as uniform temperature distribution, through-the-thickness temperature gradient, and in-plane linear temperature distribution. In another study, Hieu and Tung (2020b) presented buckling analysis of CNTRC cylindrical shells and toroidal shell segments enclosed by elastic foundation and subjected to lateral pressure and thermomechanical force at elevated temperatures.

Yang *et al*. (2017) used 3-D elasticity theory to investigate axisymmetric bending characteristics of FG-GPLRC circular and annular plates subjected to thermal and mechanical loads simultaneously. In their study, the plate was under a steady state temperature field along with through thickness temperature variation and three linear classical thermal boundary conditions were assumed to estimate the applied thermal loading. Based on the Reddy's TSDT and von Karman geometric nonlinearity, Shen *et al*. (2018) presented the linear and non-linear vibration analysis of FG-GRC cylindrical panels resting on elastic foundation in uniform thermal environments. The temperature-dependent thermoelastic properties of the GRC layers were determined using the extended Halpin-Tsai micromechanical model. Using the similar approach, Fan *et al*. (2019) examined the thermal effects on nonlinear dynamic behavior of FG-GRC laminated plates resting on visco-Pasternak foundations under various loading conditions. Dong *et al.* (2020) analyzed the non-linear harmonic resonance behavior of rotating FG-GPLRC cylindrical shells under different thermal conditions and external excitation. Mahani *et al*. (2020) applied a semi analytical approach based on the trigonometric expansion and GDQM to analyze the thermal buckling of FG-GPLRC conical shells subjected to uniform temperature rise.

1.3.7 DYNAMIC ANALYSES OF NANOCOMPOSITE SANDWICH PLATES AND SHELLS

As stated previously, the structural elements made up of laminated composites and sandwich constructions are subjected to various forms of dynamic loadings in their service life. Moreover, due to complicated effects involving the transverse shear and normal deformations, coupled material behaviors, thermal environments and centrifugal forces, the analytical and numerical prediction of dynamic behavior of the structures is really a challenging work. Some notable studies on free vibration and low-velocity impact analysis of composites/nanocomposites sandwich plates/shells are presented in this section.

1.3.7.1 Free Vibration Analysis

The recent review work of Sayyad and Ghugal (2015) revealed that a considerable amount of research works have been conducted on the free vibration analysis of conventional laminated composite and sandwich plates. A great variety of structural theories for modeling plate's kinematics and solutions methods for solving the governing equations are used to estimate the natural frequencies and mode shapes of the laminated composite and sandwich plates. However, the free vibration analysis of carbon nanofillers (CNTs and graphene) reinforced composite and sandwich structures have not been reported as conducted for conventional composites. Fan *et al.* (2017) introduced an analytical approach based on FSDT to study the free vibration of FG-CNTRC conical panels embedded with two piezoelectric layers subjected to elastically restrained boundary conditions. Zghal *et al.* (2018) examined the free vibration characteristics of functionally graded composite cylindrical shell panels reinforced with CNTs using a discrete double directors shell finite element technique which assumes the kinematic conditions of HSDT. Ansari *et al.* (2018) analyzed the free vibration behavior of embedded FG-CNTRC conical, cylindrical, and annular plates resting on Pasternak elastic foundation. Wang *et al*. (2018) adopted a layer-wise sandwich model for free vibration analysis of sandwich plates with CNTRC face sheets resting on elastic foundation at room temperature. Based on mesh-free method and FSDT, Moradi-Dastjerdi and Momeni-Khabisi (2018) studied the vibrational behavior of wavy CNTs-reinforced composite sandwich plates resting on elastic foundation. Beni (2019) developed the Carrera's Unified Formulation (CUF) to analyze the natural frequencies and vibration modes of annular sector sandwich plates with FG-CNTRC face-sheets and homogeneous core without considering the thermal effects. Zhao *et al.* (2019) used the modified Fourier series method, Ritz method and the assumptions of FSDT to investigate the free vibration characteristics of FG-CNTRC truncated conical shell panels with arbitrary edge conditions. Mehar *et al.* (2020) predicted the free vibration characteristics of CNT-reinforced sandwich plates using finite element technique in association with HSDT and verified the natural frequencies with those experimental results. Xiang *et al*. (2021) studied the natural frequencies and mode shapes of CNTRC conical shell panels with general boundary conditions employing element free kp-Ritz method based on the FSDT.

Reddy *et al.* (2018) used finite element approach in conjunction with FSDT for vibration analysis of GPLs reinforced composite thin, moderately thick, and thick plates with general

boundary conditions. Dong *et al.* (2018) analytically investigated the free vibration characteristics of rotating porous cylindrical shells reinforced by GPLs assuming the random distribution of GPLs and pores in the shell. In another work by Arefi *et al.* (2018), a two-variable sinusoidal shear deformation theory (SSDT) was applied to carry out the free vibration analysis of graphene nanoplatelets (GNPs)-reinforced nanocomposite plates with different grading patterns of nanoplatelets resting on elastic foundation. Free vibration behavior of porous FG-GPLRC truncated conical shell was studied by Bahaadini *et al.* (2019) based on Love's first approximation theory and general differential quadrature method (GDQM). Fazelzadeh *et al.* (2019) presented the analytical free vibration analysis of FG-GPLRC doubly curved shell panels (enneper and helicoid) in thermal environments with the aid of FSDT and Galerkin technique. An analytical method based on HSDT was developed by Qaderi et al. (2019) and Qaderi and Ebrahimi (2022) to study the free vibration response of temperature-dependent FG-GPLRC plates without and with viscoelastic support. Mohseni and Shakouri (2020) studied the vibration and damping characteristics of simply supported sandwich plates with GPLs-reinforced face sheets and viscoelastic core. Anvari *et al.* (2020) examined analytically the free vibration behavior of thick-walled sandwich cylindrical panels with FG-GPLRC face sheets and foam core supported by the elastic foundation utilizing modified couple stress theory. Afshari (2020) investigated free vibration behavior of composite truncated conical shells reinforced with GNPs using GDQM in combination with FSDT. Amirabadi *et al.* (2020) analyzed the forward and backward wave frequencies of rotating FG-GPLRC conical shells using Reddy's TSDT and GDQM. The effect of graphene grading pattern, stiffener, and temperature on the natural frequencies and mode shapes of the stiffened FG-GRC plates with arbitrary edge conditions in thermal environments was examined by Maji *et al.* (2021). Based on Donnell shell theory and refined Halpin-Tsai micromechanical approach, Zamani (2021) analyzed numerically the natural frequencies and mode shapes of rotating FG-GRC conical shells with different boundary conditions.

1.3.7.2 Low-velocity Impact Analysis

The most important issue that restricts the widespread usage of laminated composites and sandwich structures is their susceptibility to damage caused by localized impact loading. The failure mechanisms of these structures under low-velocity impact are quietly different those of the conventional metallic or alloy structures in which the damage begins from the surface and is

easily detectable. Many research works have been carried out to match experimental results with the vibration theories by assuming the presence of a quasi-elastic layer below the contact point. The pioneering work to include a theory of local indentation for static loading was based on a scheme proposed by Hertz (1881). The expression of local indentation of an elastic half-space under an elastic indenter is provided by the Hertzian contact law. The contact force between the impactor and target is expressed in terms of local indentation and a constant parameter which depends upon the radii of curvature at contact and the elastic properties of the impactor and the target.

The first attempt at a comprehensive coverage of the subject of the behavior of colliding solids was made by Goldsmith (1960). The author scrutinized the vibrational aspects of impact, contact phenomena due to the impact of elastic objects and the outcomes of impact experiments. Moon **(**1972, 1973) investigated the stress waves and dynamic stresses caused by the transverse impact on fiber-reinforced composite plates employing Mindlin's plate theory. The elastic wave analysis was used to determine the prefracture stresses induced by the impact forces. It was shown that the points of maximum stress travel along the fiber directions. Sun (1973) developed a simple analytical procedure to investigate nature of the wave fronts in laminated composite plates subjected to impact loading. Sun and Chattopadhyay (1975) investigated the dynamic response of laminated composite plates under initial stress to impact of a mass by solving a non-linear integral equation. Their results reveal that a higher initial tensile stress raises the peak contact force but decreases the contact period, the displacement, and the stresses. Yang and Sun (1982) carried out static indentation tests on glass/epoxy and graphite/epoxy multi-layered composites with a steel spherical impactor to determine power law indices for the loading, unloading, and reloading curves. Shivakumar *et al.* (1985) predicted the impact force and duration associated with low-velocity impact on circular composite plates employing the energy-balance and spring-mass models which incorporate the influence of bending, shear, and membrane deformations of the plate. Cairns and Legace (1989) investigated impact behavior of composite laminates using an analytical approach that includes the effects of shearing deformation, bending-twisting coupling, and nonlinear contact behavior. Abrate (2001) presented an overview of various types of mathematical models such as spring-mass models, energy-balance models, complete models, and an impact on infinite plate model which are employed to study the impact dynamics of composite structures.

Malekzadeh *et al.* (2006) predicted the impact behavior of composite sandwich panel with transversely-flexible core using an analytical method based on a novel equivalent three DOFs spring-mass-damper (SMD) model. Khalili *et al*. (2014) proposed an analytical method based on the high-order sandwich shell theory to investigate the impact response of circular cylindrical composite sandwich shells wherein the spring-mass model is employed to approximate the contact force between the impactor and the target. Zhu and Chai (2016) presented a comprehensive analytical approach based on the principle of minimum total potential energy to study the dynamic behavior of composite sandwich panel under low-velocity impact. A series of impact tests were conducted to validate the results obtained from the theoretical approach. Wang *et al*. (2021) investigated the load/displacement history, failure characteristics, and energy partition of sandwich panels with composite face sheets and foam core under low-velocity impact. It was shown that the impact response of the panels is greatly influenced by the core density, while the stacking sequence has small effect on it.

Apart from the conventional composites and sandwich structures, impact analysis of carbon nanofillers-based composites and sandwiches have been reported in many literatures. Wang *et al*. (2014) investigated the non-linear low-velocity impact response of CNTRC single-layer and sandwich plates in uniform thermal environments using an analytical method based on Reddy's HSDT, wherein the contact force is estimated via modified Hertzian contact law. Their results indicate that impact-induced dynamic behavior is affected significantly by CNTs volume fraction, CNTs grading pattern, initial stress, temperature change, facing-to-core thickness ratio, and impactor initial velocity. Using the same structural theory and method, Song *et al*. (2016a) and Zhang *et al.* (2017) analyzed dynamic behavior of FG-CNTRC plates and cylindrical shells subjected to impact loading. Selim *et al.* (2017) employed a novel element-free IMLS-Ritz model in association with Reddy's HSDT to analyze the dynamic behavior of CNTRC plates impacted by a spherical impactor without considering the thermal effects. Zarei *et al*. (2017) examined the impact response of temperature-dependent FG-CNTRC plates subjected to the simultaneous multiple masses. They obtained the solution of the governing equations using the fourth-order Runge-Kutta technique. Fallah *et al.* (2018) investigated the dynamic response of temperature-dependent FG-CNTRC plates with arbitrary geometry (circular and triangular) and general boundary conditions under low-velocity impact using HSDT, Hamilton's principle, and fourth-order Runge-Kutta method. Bayat *et al.* (2018) studied non-linear low-velocity impact

behavior of FG-CNTRC cylindrical shells using HSDT with a von Karman-type of kinematic non-linearity in thermal environments. The authors also employed a two-step perturbation technique to solve the equations of motion. Yang *et al*. (2018) presented the temporal variations of contact force and indentation of CNTRC shallow spherical shell under low-velocity impact in thermal environments using the Timoshenko-Mindlin theory. Azizi *et al*. (2019) employed the three DOFs spring-mass-damper (SMD) model to determine the contact force for low-velocity impact analysis of truncated conical sandwich shells with CNTRC facings considering various boundary conditions. Khalkhali *et al*. (2020) proposed an analytical model based on Reddy's HSDT to study the impact behavior of CNTs-reinforced nanocomposite sandwich plates considering various geometrical shapes of the impactor in thermal environments and the cylindrical impactor was found to cause more central displacement and indentation. Feli and Rashidi (2021) investigated the impact response of sandwich panels with CNTRC facings and homogeneous core using an analytical method wherein a three-DOF spring-mass model was employed to evaluate contact force

Fan *et al.* (2018) predicted the non-linear low-velocity impact behavior of FG-GRC plates resting on visco-Pasternak foundations in thermal environments. The governing equation of the target plate was formulated through HSDT in the framework of von Kármán type of kinematic non-linearity and solved employing a two-step perturbation technique. Song *et al.* (2019) presented an analytical approach based on the FSDT to study the effects of weight fraction and grading profile of GPLs on the dynamic response of FG-GPLRC plates subjected to impact loading, wherein the impact-induced contact force is computed using the modified Hertzian contact law. Dong *et al*. (2019) investigated the impact response of rotating FG-GPLRC cylindrical shells using Donnell's non-linear shell theory, Hamilton's principle, and Duhamel integration technique analytically. The authors adopted a single spring-mass model to estimate the contact force due to low-velocity impact with the spherical impactor on the target cylindrical shell. Lei and Tong (2019) developed an analytical procedure to carry out the transient analysis of temperature-dependent FG-GRC cylindrical shells subjected to impact loading using Reddy's HSDT and linearized contact law. Al-Furjan *et al.* (2021) focused on the dynamic analysis of sandwich conical frusta consisting of magnetostrictive layered facings and GPLs-reinforced nanocomposite core subjected to impact load wherein the interaction between the impactor and target was based on the three DOFs spring-mass-damper (SMD) model.

A number of researchers have employed finite element method to obtain the solution of the impact problem of the composite laminates and sandwich plates/shells. Lee *et al.* (1984) developed a three-dimensional finite element program in predicting transient response of rectangular layered composite plates subjected to impact loading. In their work, the dynamic equilibrium equation of the finite element system was solved using the central difference method. Tan and Sun (1985) developed the finite element procedure for impact analysis of the graphite/epoxy composite plates using 9-node isoparametric element and verified the theoretical results with those of statical indentation test. An experimentally established contact law was employed to model the interaction between the impactor and target plate. Later on, Sun and Chen (1985) extended this finite element impact analysis to the initially stressed ten-layered graphite/epoxy composite plates with simply supported boundary conditions. Newmark's time integration scheme was employed to solve the time-dependent equilibrium equations of the plate and the impactor. Using the in-house finite element computer codes with 8-point brick element, Wu and Fu-Kuo (1989) studied the transient laminated graphite/epoxy composite plates impacted by spherical elastic impactor. The contact force distributions during loading and unloading phases were determined employing the modified Hertzian contact law in association with Newton-Raphson method. Vaziri *et al.* (1996) investigated transient response of carbon fiber-reinforced laminated composite plates and cylindrical shells subjected to low-velocity impact loading using a super FEM that exhibits coarse-mesh accuracy. The analysis employs the classical theories incorporating von Karman kinematics assumptions to derive equilibrium equations of the impactor-target system.

Maity and Sinha (1996) developed a finite element formulation with nine noded Lagrangian elements in the framework of FSDT and HSDTs to analyze the low-velocity impact response of composite sandwich doubly-curved shells. Palazotto *et al.* (2000) studied impact response sandwich plates with composite face sheets and Nomex honeycomb core using a displacement-based, plate bending, finite element technique in which contact loading was simulated by Hertzian pressure distribution. Choi (2006) employed the general-purpose commercial FEM software with application of the spring element to analyze the contact force history of composite sandwich plates under low-velocity impact response and conducted the experiments for validity of the numerical results. Using 3-D finite element model, Foo *et al.* (2008) predicted the low-velocity impact response of sandwich plates with carbon/epoxy face

sheets and aluminum honeycomb core after the onset damage. Subsequently, an experimental examination on the sandwich plates under quasi-static indentation and low-velocity impact loading was performed to validate the model. Icardi and Ferrero (2009) presented a non-linear finite element simulation based on the zig-zag model with piece-wise high-order displacements to investigate the impact response of composite sandwich laminates. Shariyat and Hosseini (2014) carried out the eccentric low-velocity impact analysis of rectangular composite sandwich plates with viscoelastic core subjected to biaxial preloads using a second-order finite element technique. It was found that the biaxial tension increases the impact force and, thereby, leads to premature failures.

Malekzadeh and Dehbozorgi (2016) developed finite element formulation considering the kinematics of the FSDT to demonstrate the effect of CNTs grading pattern on impact behavior of CNTs-reinforced nanocomposite skew plates considering various aspect ratios and boundary conditions. The contact force between the projectile and plate was determined employing the Hertzian non-linear contact law while the solutions of the governing equations were obtained using Newmark's time integration scheme and Newton–Raphson algorithm. Ebrahimi and Habibi (2017) developed a finite element procedure with 15 DOFs per node in the framework of HSDT incorporating von Kármán geometrical non-linearity to study non-linear response of temperature-dependent FG-CNTRC plate under low-velocity impact. The effects of stacking sequence and lamination angle along with the other material and dynamic parameters on the impact response of the plates were examined. In another investigation, Ebrahimi and Habibi (2018) presented the non-linear finite element dynamic analysis of polymer-CNT-fiber multiscale nanocomposite plates resting on elastic foundation subjected to low-velocity eccentric impact in hygrothermal environments. By means of a nested micromechanical FEM, Rasoolpoor *et al*. (2020, 2021) examined the low-velocity impact responses of MWCNT/Aluminum nanocomposites and polymer-based hybrid nanocomposite plates reinforced with carbon fibers and CNTs. It was demonstrated that addition of CNTs in to the nanocomposite media would lead to increase the peak contact force and decrease both plate's displacement and contact duration. Li *et al*. (2021) investigated low-velocity impact response of sandwich plates with temperature dependent GRC face sheets and FG 3D lattice core using a full scale finite element simulation. In this work, 3D lattice cores were assumed to have two different FG configurations with negative effective Poisson's ratios.

1.4 RESEARCH GAPS IDENTIFIED

In the previous section, the available literature for the dynamic analysis of nanocomposite sandwich conical shell in thermal environment has been critically reviewed. The attempt has been made to take in all the significant contributions in the present area of interest. The following major research gaps as identified from the exhaustive literature review are broadly classified as:

a) Idealization of turbo-machinery blades with shallow conical shell

In majority of the research works, turbo-machinery blades were idealized as pretwisted plates or cylindrical shells. However, the width of actual turbo-machinery blades near hub region is normally greater than its width at free end. Accordingly, a cantilevered shallow open shell with trapezoidal palnform, definite pretwist, and variable chordwise surface curvature can be deemed as more practical model for turbo-machinery blades. The study on dynamic analysis of pretwisted shallow conical shell is very few although it has practical importance.

b) Sandwich conical shell with nanocomposite face sheets

The sandwich construction with nanocomposite (FG-CNTRC and FG-GRC) face sheets and stiff homogeneous core have broad application prospects in various weight-sensitive structures, especially for rotating blades of turbines, compressors, wind mills, helicopters, etc. The literature survey reveals that the behaviors of composite sandwich structures have been studied extensively, while a little attention has been focused on the behavior of sandwich plates and shells with nanocomposite face sheets. Moreover, there is no research work found on the use of nanocomposite sandwich construction in pretwisted shallow conical shell.

c) Thermal effects on nanocomposite sandwich conical shell

Generally, turbo-machinery blades work at different environmental temperatures depending on their applications. The behavior of the nanocomposite sandwich structures greatly influenced by the rise in environmental temperature because the properties of nanocomposite face sheets and homogenous core are temperature-dependent. The research works dealing with thermal effect on the behavior of sandwich turbo-machinery blades are found scanty. In the present research work, the thermal environment has been included in whole analysis to observe the structural responses of sandwich conical shell with nanocomposite face sheets.

d) Impact on nanocomposite sandwich conical shell in thermal environments

The composite sandwich components have to endure in low-velocity impacts from foreign masses during manufacturing, operation, and maintenance. It is fairly common in practice that space crafts, aircraft wings, automobile bodies, and blades of turbines, compressors, helicopters, ship hulls,and wind mills are subjected to impact with foreign bodies. A lot of research efforts have been made to investigate the impact response of laminated composite and composite sandwich plates and shells. To the best of the author' knowledge, the dynamic behavior of nanocomposite sandwich conical shell under low-velocity impact in thermal environment has not been investigated so far.

1.5 OBJECTIVES AND SCOPE OF THE PRESENT WORK

The critical review of published open literature reveals that although a good number of research works have been reported on the pretwisted composite plates and shells, nanocomposite structures, and composite sandwich structures but there is still a broad scope to carry out further research work, particularly in the field of dynamic analyses of pretwisted sandwich conical shells with nanocomposite face sheets. In this regard, a theoretical research effort is required to be performed for predicting the dynamic response of the nanocomposite sandwich conical shells impact in thermal environments. The present work is aimed at formulating finite element model based on the higher-order shear deformation theory (HSDT) for investigating some relevant problem areas in order to provide more thoughtful knowledge about the free vibration and impact behaviors of pretwisted sandwich shell with FG-CNTRC and FG-GRC face sheets in thermal environments. Based on this objective, the scope of the present research work comprises the following features:

a) A sandwich shallow conical shell with trapezoidal planform considered as the model for turbo-machinery blades is assumed to consist of carbon nanofillers (CNTs and graphene) reinforced composite face sheets and homogenous core. In each face sheet, the carbon nanofillers are either uniformly distributed or functionally graded along its thickness direction. The temperature-dependent material properties of both face sheets and core layers are estimated using micromechanical models.

b) The finite element formulation is developed using eight-noded isoparametric shell element wherein each node has seven degrees of freedom within the framework of the higher-order

shear deformation theory (HSDT) to model the sandwich shallow conical shell. The Gauss quadrature integration method is employed to determine the mass and stiffness matrices of the shell element. The effects of non-linearity arising out of the initial stresses due to thermal and centrifugal loads are incorporated via geometric stiffness based on Green-Lagrange's strains. The general dynamic equilibrium equation of cantilevered sandwich conical shell is formulated using Lagrange's equation of motion for moderate rotational speeds wherein Coriolis effect is neglected. In-house computer codes are developed based on the based on the present mathematical formulation. After ensuring the stability and the accuracy, the computer codes are used to obtain numerical results considering various set of parameters.

c) Numerical investigations to predict the free vibration characteristics of rotating pretwisted FG-CNTRC and FG-GRC sandwich conical shells in thermal environments are carried out separately. Natural frequencies are computed from solution of the eigen value problem employing QR iteration technique incorporated in the computer codes for different types of grading pattern of CNTs and graphene, CNTs volume fraction, core-to face sheets thickness ratio, pretwist angle, cone length to thickness ratio, rotational speed.

d) The dynamic behavior of the FG-CNTRC and FG-GRC sandwich conical shell under low-velocity impact considering thermal effects are also numerically predicted. Accordingly, the formulation includes the estimation of contact force between the impactor and the target sandwich shell using modified Hertzian contact law. The time-dependent dynamic equilibrium equations are solved employing Newmark's constant acceleration time integration scheme. Numerical results are depicted to scrutinize the influence of various important parameters such as grading pattern of CNTs and graphene, CNTs volume fraction, core-to face sheets thickness ratio, pretwist angle, temperature, impactor's size and initial velocity on the impact response of the FG-CNTRC and FG-GRC sandwich conical shell.

1.6 ORGANIZATION OF THE THESIS

Present chapter discusses the overview and motivation of the present research work. An extensive review of the available literature is then furnished highlighting the relevant aspects in connection to the research area, such as, nanocomposite sandwich plate/shell, modeling of turbo-machinery blades, plate/ shell theories, shell geometries, dynamic analyses nanocomposite sandwich shells and thermal effects on the nanocomposite plates/shells. The scope of the present

research is also furnished in this chapter to address the research gap as identified from the extensive literature review.

Chapter 2 covers the mathematical formulations developed for the proposed analysis of the FG-CNTRC sandwich conical shells and FG-GRC sandwich conical shells in thermal environments. The formulations are based on the basic equations, finite element formulation, general dynamic equilibrium equation, and solution procedure. The basic equations are derived in consideration of sandwich shallow conical shells with CNTRC and GRC face sheet layers, displacement field and strains based on HSDT and their thermoelastic stress-strain relationship. Using an eight noded isoparametric element with seven DOFs per node, the finite element formulation is developed. Gaussian quadrature method is employed to perform the numerical integration involved with the elemental stiffness and mass matrices as well as elemental load vector. Subsequently, the general dynamic equilibrium equations for rotating sandwich conical shells considering thermal effects are derived using Lagrange's equation of motion. The standard eigenvalue problem is solved using QR iteration technique to compute the natural frequencies. The modified Hertzian contact law is used to model the distribution of contact force between the impactor and the target shell. Finally, the time dependent dynamic equilibrium equations of both impactor and the target shell are numerically solved employing the Newmark's time integration scheme. Based on the present mathematical formulation, the inhouse computer codes are developed.

Chapter 3 presents the numerical investigation on the thermoelastic free vibration behavior of rotating pretwisted sandwich conical shells with FG-CNTRC face sheets. The convergence and comparison studies are performed to examine the stability and accuracy of the present formulation and the corresponding finite element codes. Afterward, the parametric study is conducted to analyze the effects of various parameters such as core-to-face sheets thickness ratio, pretwist angle, CNTs volume fraction, CNTs grading pattern, cone length to thickness ratio, temperature, rotational speed, and hub radius to length ratio on the natural frequencies of the rotating pretwisted sandwich conical shells. Some representative mode shapes of the conical shell are also presented.

Chapter 4 illustrates the numerical and graphical results of free vibration analysis of rotating pretwisted FG-GRC sandwich conical shells in thermal environments. A number of

examples of FG-GRC plates and FG-GRC sandwich construction are solved and the present results are compared with those of existing results. Some new results are presented to analyze the effects of various striking parameters including type of graphene grading pattern on the natural frequencies and mode shapes.

Chapter 5 deals with the numerical investigation on the behavior of temperature dependent FG-CNTRC sandwich conical shells under low-velocity impact. Mesh convergence and time step convergence of the present formulation are performed considering a specific problem. The ability of the present formulation to predict the low-velocity impact response is tested by comparing the present results with those of benchmarks results.

Chapter 6 analyzes the transient response of FG-GRC sandwich conical shells under low-velocity impact for different size and initial velocity of the impactor in thermal environments. Detailed parametric studies are conducted to examine the effects of geometrical and material properties on the transient response.

Chapter 7 summarizes the entire work, conclusions drawn from the present study, major contributions and the future scope of the present study.

CHAPTER 2

THEORETICAL FORMULATION

2.1 INTRODUCTION

This chapter contains the theoretical formulation and solution procedures for dynamic analysis of the rotating pretwisted composite sandwich conical shells. At first, the shallow conical shell model along with the geometrical features is introduced. A higher-order shear deformation theory is employed to define the displacement field within the sandwich conical shell. Afterward, stress resultants acting on the composite sandwich shell are derived from the stress-strain relationship considering the thermal effect. The entire trapezoidal planform of the conical shell is then discretized into eight-noded isoparametric shell element and the relevant finite element formulation for the present analysis is developed. The general dynamic equilibrium equation of the rotating shell is formulated using the Lagrange's equation of motion. The solution of the standard eigen value problem is obtained by using QR iteration scheme to compute the natural frequencies. For low-velocity impact problems, the dynamic equilibrium equation is used in the determination of the contact force which is estimated according to modified Hertzian contact law. The time-dependent equations of motion of the target shell and the impactor are solved by Newmark's constant acceleration time integration method. Finally, the micromechanical models are presented to evaluate the effective material properties of the nanocomposite face sheets of the sandwich conical shell.

2.2 BASIC EQUATIONS

In this section, the basic equations are derived for sandwich shallow conical shells with nanocomposite face sheets assuming a higher-order displacement field. After evaluating the strain components, the stress-strain relationship is presented considering the thermal effect.

2.2.1 SANDWICH SHALLOW CONICAL SHELL MODEL

Consider an untwisted sandwich conical shell panel that is formed by truncating a shallow cone with length s and vertex angle ϕ_v as depicted in **Fig. 2.1(a)**. The reference minor and major radii of the elliptical cross-section of the cone are denoted by p_0 and q_0, respectively. The sandwich panel is considered to consist of two composite face sheets and a homogenous core. The span length, base subtended angle, thicknesses of core and facings of the sandwich panel are indicated

by L, ϕ_0, and h_c and h_f, respectively. Accordingly, the overall thickness of the sandwich panel is $h = h_c + h_f$. The pretwisted sandwich conical shell having reference width b_0 is fixed at the periphery of a stiff hub of radius r rotating with a rotational speed Ω about $z-$axis as depicted in **Fig. 2.1 (b)**.

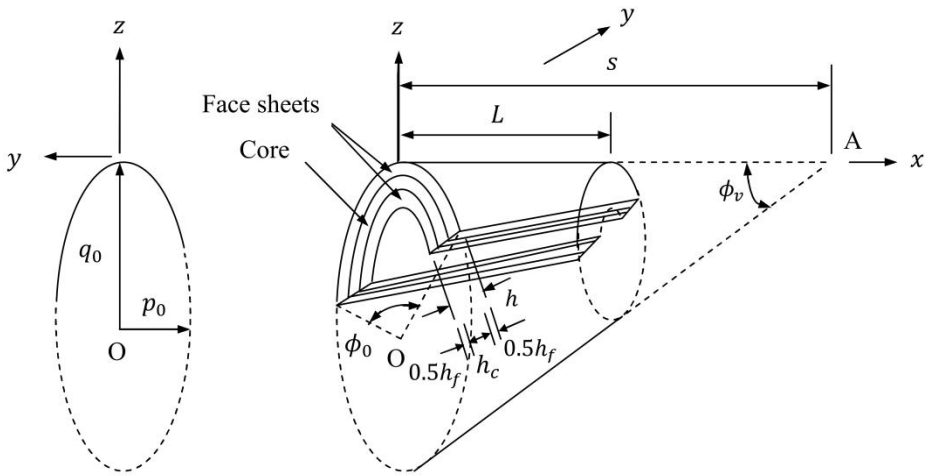

(a)

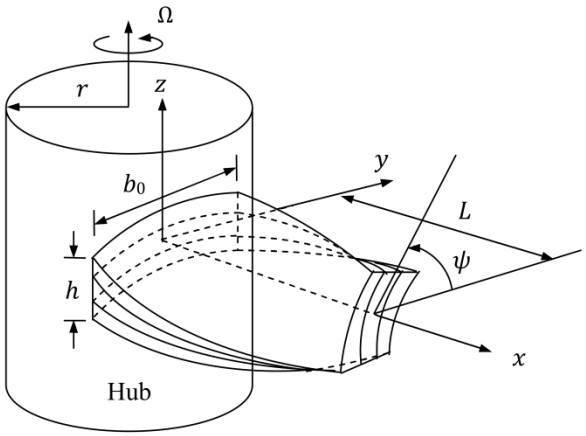

(b)

Fig. 2.1 Schematic diagram of sandwich shallow conical shell model: (a) untwisted shell and (b) pretwisted shell mounted on a rotating hub

According to Leissa *et al*. (1984), the mid-surface of any pretwisted shallow shell is characterized by

$$z = -\frac{1}{2}\left\{\frac{x^2}{r_x} + \frac{2xy}{r_{xy}} + \frac{y^2}{r_y}\right\} \tag{2.1}$$

where r_x and r_y are the curvature radii in *x* and *y*-directions, respectively, and r_{xy} is the pretwist radius. For a shallow conical shell, r_x is infinity ($r_x = \infty$), while r_y varies in the chordwise direction.

The curvature radius r_y given by Liew *et al*. (1994) can be expressed as

$$\left|r_y(x,y)\right| = \frac{1}{p^4 q}\left[p^4 + (q^2 - p^2)y^2\right]^{3/2} \tag{2.2}$$

where

$$q(x) = (s - x)\tan\frac{\phi_v}{2} \tag{2.3}$$

$$p(x) = \frac{b\,q\tan\frac{\phi_0}{2}}{\sqrt{4q^2\tan^2\frac{\phi_0}{2} - b^2}} \tag{2.4}$$

$$b = b_0(1 - x/s) \tag{2.5}$$

in which

$$b_0 = \frac{2s\sin\frac{\phi_v}{2}\tan\frac{\phi_0}{2}}{\sqrt{\cos^2\frac{\phi_v}{2} + \tan^2\frac{\phi_0}{2}}} \tag{2.6}$$

The pretwist radius (r_{xy}) can be expressed as

$$r_{xy} = -\frac{L}{\tan\psi} \tag{2.7}$$

2.2.2 NANOCOMPOSITE FACE SHEET LAYERS

Two types of nanocomposite face sheets are considered to be bonded with a homogeneous core to obtain the sandwich conical shell. These are CNTs-reinforced composite (CNTRC) face sheets and graphene-reinforced composite (GRC) face sheets.

2.2.2.1 CNTRC Face Sheets

The CNTRC face sheets are obtained by reinforcing the (10, 10) single-walled carbon nanotubes (SWCNTs) into a polymeric matrix. The SWCNTs are considered to align with span length and distributed either uniformly (UD) or functionally graded (FG) along its thickness direction. Five different types of CNTs distribution patterns, namely FG-UU, FG-VΛ, FG-ΛV, FG-OO, and FG-XX, are considered in the sandwich conical shell, as shown schematically in **Fig. 2.2**. The CNTs distribution functions across the thickness of both top and bottom face sheets for these five

different patterns are given in **Table 2.1,** wherein the total volume fraction of CNTs is expressed as

$$V_{CNT}^{*} = \frac{w_{CNT}}{w_{CNT} + \frac{\rho^{CNT}}{\rho^{m}} - \frac{\rho^{CNT}}{\rho^{m}} w_{CNT}} \tag{2.8}$$

in which w_{CNT} and ρ^{CNT} are mass fraction and mass density of the CNTs, respectively, whereas ρ^{m} is the mass density of matrix.

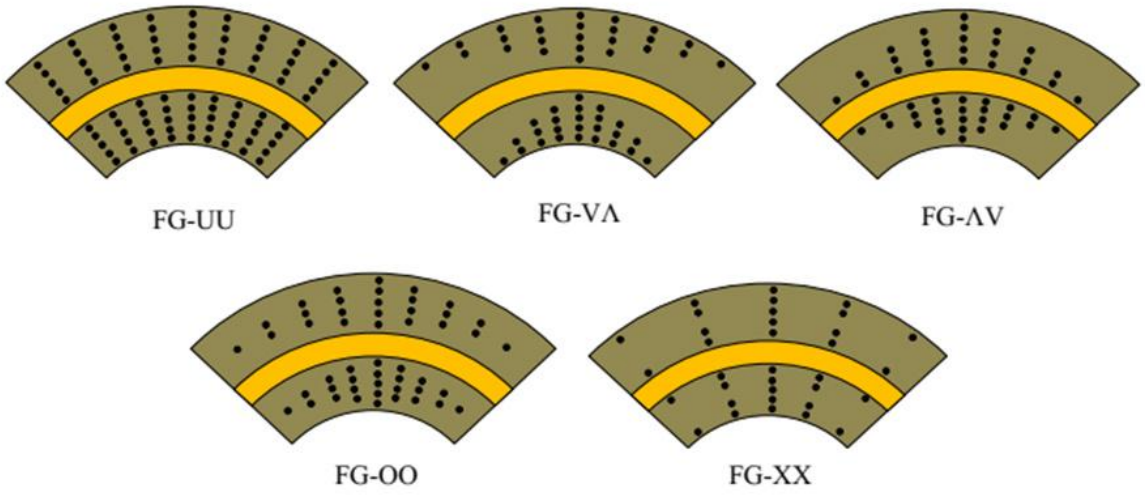

Fig. 2.2 Types of CNTs distribution patterns in sandwich shallow conical shell

In FG-UU type of grading profile, the CNTs volume fraction is uniform along its thickness direction for both CNTRC face sheets. In FG-VΛ type, the outermost surfaces of both face sheets contain maximum proportions of CNTs, while innermost surfaces neighboring to the core are free of CNTs. Besides, FG-ΛV type possesses a completely reverse distribution pattern of CNTs, i.e., outermost and innermost layers of the face sheets are free of CNTs and enriched with maximum proportions of CNTs, respectively. In FG-OO type, outermost and innermost layers of both face sheets are free of CNTs, whereas middle layers of the face sheets contain maximum proportions of CNTs. In FG-XX type, the outermost and innermost layers of the face sheets possess maximum proportions of CNTs, and the mid-surface layers of the face sheets are free of CNTs.

The effective elastic moduli of the CNTRC face sheets can be estimated using the extended rule of mixture (EROM) given as (Shen, 2009)

$$E_{11} = \eta_1 V_{CNT} E_{11}^{CNT} + V_m E^m \tag{2.9}$$

$$\frac{\eta_2}{E_{22}} = \frac{V_{CNT}}{E_{22}^{CNT}} + \frac{V_m}{E^m} \tag{2.10}$$

$$\frac{\eta_3}{G_{12}} = \frac{V_{CNT}}{G_{12}^{CNT}} + \frac{V_m}{G^m} \tag{2.11}$$

In the above expressions, E_{11}^{CNT}, E_{22}^{CNT}, and G_{12}^{CNT} are Young's and shear moduli of SWCNTs, respectively, while E^m and G^m signify the corresponding elastic moduli of the polymeric matrix.

Table 2.1 Volume fractions of CNTs for different distribution patterns

CNTs grading profiles	V_{CNT}	
	Top face sheet	Bottom face sheet
FG-UU	V_{CNT}^*	V_{CNT}^*
FG-VΛ	$2V_{CNT}^*\left(\frac{2z-h_c}{h_f}\right)$	$-2V_{CNT}^*\left(\frac{2z+h_c}{h_f}\right)$
FG-ΛV	$2V_{CNT}^*\left(\frac{h_c+h_f-2z}{h_f}\right)$	$2V_{CNT}^*\left(\frac{h_c+h_f+2z}{h_f}\right)$
FG-OO	$2V_{CNT}^*\left(1-\left\|\frac{4z-2h_c-h_f}{h_f}\right\|\right)$	$2V_{CNT}^*\left(1-\left\|\frac{4z+2h_c+h_f}{h_f}\right\|\right)$
FG-XX	$2V_{CNT}^*\left\|\frac{4z-2h_c-h_f}{h_f}\right\|$	$2V_{CNT}^*\left\|\frac{4z+2h_c+h_f}{h_f}\right\|$

Since the load transfer between the CNTs and polymeric matrix is not perfect (Qian *et al*., 2000; Seidel and Lagoudas, 2006), the terms $\eta_i (i = 1, 2, 3)$ known as efficiency parameters are introduced into **Eqs. (2.9)-(2.11)** to capture the size-dependent material properties. The efficiency parameters are estimated by matching the values of the elastic moduli of CNTRCs computed using EROM with corresponding values obtained from the molecular dynamics (MD) simulation (Shen, 2009). Furthermore, V_{CNT} and V_m denote the volume fractions of CNTs and matrix, respectively, and are interrelated as

$$V_{CNT} + V_m = 1 \tag{2.12}$$

It is assumed that the material properties of CNTs and polymeric matrix are dependent on temperature change. Therefore, effective material properties of CNTRCs like Young's and shear moduli and thermal expansion coefficients are dependent on the temperature change and

thickness coordinate. Besides, the Poisson's ratio depends weakly on temperature change and thickness coordinate and can be given as

$$\nu_{12} = V_{CNT}\nu_{12}^{CNT} + V_m\nu^m \tag{2.13}$$

where ν_{12}^{CNT} and ν_{12}^{m} signify Poisson's ratios of the SWCNTs and matrix, respectively.

The effective mass density ρ of the CNTRC layers is determined using a conventional rule of mixture (ROM) given as

$$\rho = V_{CNT}\rho^{CNT} + V_m\rho^m \tag{2.14}$$

The longitudinal and transverse thermal expansion coefficients of the CNTRCs can be expressed as

$$\alpha_{11} = V_{CNT}\alpha_{11}^{CNT} + V_m\alpha^m \tag{2.15}$$

$$\alpha_{22} = (1+\nu_{12}^{CNT})V_{CNT}\alpha_{22}^{CNT} + (1+\nu^m)V_m\alpha^m - \nu_{12}\alpha_{11} \tag{2.16}$$

in which α_{11}^{CNT}, α_{22}^{CNT}, and α^m denote the thermal expansion coefficients of the CNTs and matrix, respectively.

2.2.2.2 GRC Face Sheets

In GRC face sheets, either zigzag (specified as 0-ply) or armchair (specified as 90-ply) graphene sheets are reinforced into polymeric matrix. Each GRC face sheet is presumed to be a five-layered laminate (0/90/0/90/0) having either uniform distribution (UD) or functionally graded (FG) distribution of the graphene sheets across its thickness. For instance, the volume fraction of the graphene in the FG-V GRC face sheet is assumed to be distributed in decreasing order (0.11/0.09/0.07/0.05/0.03) from the top layer to bottom layer, while for FG-Λ GRC face sheet, the order of the volume fraction distribution is reversed, i.e., (0.03/0.05/0.07/0.09/0.11). Similarly, the UD GRC face sheet assumes a uniform distribution of graphene volume fraction (0.07/0.07/0.07/0.07/0.07). Accordingly, the material distributions in three different types of FG-GRC sandwich conical shells [(0°/90°/0°/90°/0°)/core/(0°/90°/0°/90°/0°)] along the thickness direction are considered as

- FG-UU: (UD GRC/Titanium alloy core /UD GRC)
- FG-VΛ: (FG-V GRC/Titanium alloy core/FG-Λ GRC)
- FG- ΛV: (FG-Λ GRC/Titanium alloy core/FG-V GRC)

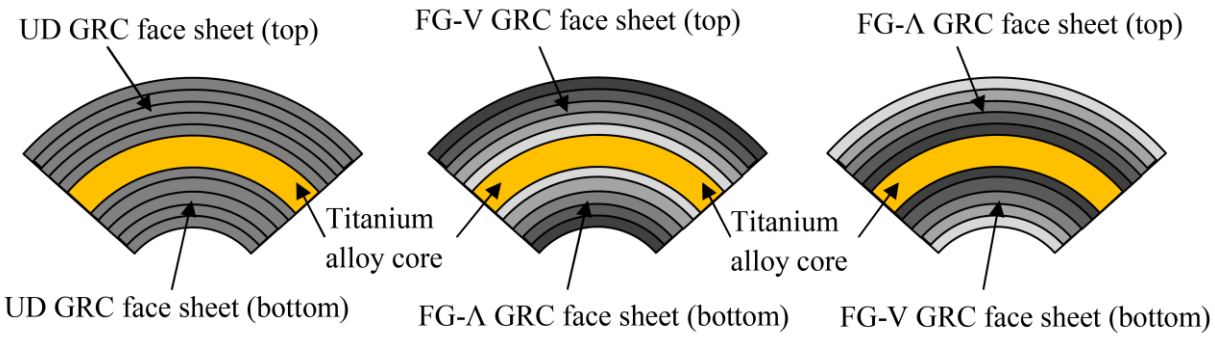

(a) FG-UU (b) FG-VΛ (c) FG- ΛV

Fig. 2.3 Types of graphene distribution patterns in sandwich shallow conical shell

According to the extended Halpin-Tsai model, the temperature-dependent effective elastic properties of the GRC layers are evaluated as follows (Shen *et al*., 2017)

$$E_{11} = \eta_1 \frac{1 + 2(L_G/h_G)\,\lambda_{11}V_G}{1 - \lambda_{11}V_G} E^m \tag{2.17}$$

$$E_{22} = \eta_2 \frac{1 + 2(b_G/h_G)\,\lambda_{22}V_G}{1 - \lambda_{22}V_G} E^m \tag{2.18}$$

$$G_{12} = \eta_3 \frac{1}{1 - \lambda_{12}V_G} G^m \tag{2.19}$$

where the geometrical dimensions L_G, b_G, and h_G correspond to the length, breadth, and effective thickness of the graphene sheet, respectively; E^m and G^m represent Young's modulus and shear modulus of the matrix, respectively. The required supplementary parameters λ_{ij} are computed using following expressions

$$\lambda_{11} = \frac{E_{11}^G/E^m - 1}{E_{11}^G/E^m + 2L_G/h_G} \tag{2.20}$$

$$\lambda_{22} = \frac{E_{22}^G/E^m - 1}{E_{22}^G/E^m + 2b_G/h_G} \tag{2.21}$$

$$\lambda_{12} = \frac{G_{12}^G/G^m - 1}{G_{12}^G/G^m} \tag{2.22}$$

where E_{11}^G, E_{22}^G, and G_{12}^G are Young's moduli in longitudinal and transverse directions, and shear modulus of the graphene sheet, respectively.

Similar to the cases of CNTRCs, the imperfect load transfer between graphene and polymer matrix leads to introduce efficiency parameters $\eta_j\,(j = 1, 2, 3)$in **Eqs. (2.17)-(2.19)** in order to take account of size-dependent effect and other effects in the material properties of GRCs. The

efficiency parameters are computed by comparing the elastic moduli obtained from MD simulation with those from extended Halpin-Tsai model. In **Eqs. (2.17)-(2.19),** V_G indicates graphene volume fraction and can be obtained from the following expression $V_G = 1 - V_m$, where V_m is the volume fraction of matrix. Using conventional ROM, the mass density (ρ) of the GRC can be as

$$\rho = V_G \rho^G + V_m \rho^m \tag{2.23}$$

where ρ^G and ρ^m are the mass densities of the graphene sheets and matrix, respectively.

The Poisson's ratio is weakly dependent on temperature change and can be expressed as

$$\nu_{12} = V_G \nu_{12}^G + V_m \nu^m \tag{2.24}$$

where ν_{12}^G and ν^m are the Poisson's ratio of the graphene sheet and matrix, respectively.

The determination of thermal expansion coefficients of the GRC layer is essential since both phases have temperature-dependent material properties. According to the Schapery model (Schapery, 1968), the thermal expansion coefficients of the GRC layer in the longitudinal and transverse directions can be expressed as

$$\alpha_{11} = \frac{V_G E_{11}^G \alpha_{11}^G + V_m E^m \alpha^m}{V_G E_{11}^G + V_m E^m} \tag{2.25}$$

$$\alpha_{22} = (1 + \nu_{12}^G) V_G \alpha_{22}^G + (1 + \nu^m) V_m \alpha^m - \nu_{12} \alpha_{11} \tag{2.26}$$

where α_{11}^G, α_{22}^G, and α^m are the thermal expansion coefficients of the graphene sheet and matrix, respectively.

2.2.3 DISPLACEMENT FIELD AND STRAINS

The displacement field within the sandwich conical shell panel is defined according to the HSDT as

$$u(x, y, z) = u_0(x, y) + z\beta_x(x, y) + z^2 u_0^*(x, y) + z^3 \beta_x^*(x, y) \tag{2.27}$$

$$v(x, y, z) = v_0(x, y) + z\beta_y(x, y) + z^2 v_0^*(x, y) + z^3 \beta_y^*(x, y) \tag{2.28}$$

$$w(x, y, z) = w_0(x, y) \tag{2.29}$$

where u, v, and w represent the displacement variables along x, y, and z directions, while u_0, v_0, and w_0 signify the corresponding mid-surface displacement variables; β_x and β_y symbolize the rotations of the normal to the mid-surface about y- and x-axes, respectively; u_0^*, v_0^*, β_x^*, and β_y^* signify the respective higher-order displacement variables. The modified

expressions of the displacement variables can be obtained from **Eqs. (2.27)-(2.29)** by enforcing zero transverse shear stresses ($\tau_{xz} = \tau_{yz} = 0$) on both top and bottom surfaces of the sandwich panel as

$$u = u_0 + z\beta_x + z^3\beta_x^* \tag{2.30}$$

$$v = v_0 + z\beta_y + z^3\beta_y^* \tag{2.31}$$

$$w = w_0 \tag{2.32}$$

where $\beta_x^* = -\frac{4}{3h^2}\left(\beta_x + \frac{\partial w_0}{\partial x}\right)$ and $\beta_y^* = -\frac{4}{3h^2}\left(\beta_y + \frac{\partial w_0}{\partial y}\right)$

Finally, the displacement variables can be rewritten as

$$\{\bar{u}\} = [\bar{Z}]\{\Delta\} \tag{2.33}$$

where $\{\bar{u}\}$, $\{\Delta\}$, and $[\bar{Z}]$ denote the displacement component vector, generalized displacement parameter vector, and transformation matrix, respectively, and are expressed as

$$\{\bar{u}\} = [u \quad v \quad w]^T \tag{2.34}$$

$$\{\Delta\} = [u_0 \quad v_0 \quad w_0 \quad \beta_x \quad \beta_y \quad \beta_x^* \quad \beta_y^*]^T \tag{2.35}$$

$$[\bar{Z}] = \begin{bmatrix} 1 & 0 & 0 & z & 0 & z^2 & 0 \\ 0 & 1 & 0 & 0 & z & 0 & z^2 \\ 0 & 0 & 1 & 0 & 0 & 0 & 0 \end{bmatrix} \tag{2.36}$$

Using **Eq.(2.33),** the velocity component vector $\{V\}$ can be obtained as

$$\{V\} = \frac{d\{\bar{u}\}}{dt} = [\bar{Z}]\{\dot{\Delta}\} \tag{2.37}$$

The expressions of the linear strain components are given as

$$\begin{Bmatrix} \varepsilon_{xx} \\ \varepsilon_{yy} \\ \gamma_{xy} \\ \gamma_{xz} \\ \gamma_{yz} \end{Bmatrix} = \begin{Bmatrix} u_{,x} \\ v_{,y} + w/r_y \\ u_{,y} + v_{,x} + w/r_{xy} \\ u_{,z} + w_{,x} \\ v_{,z} + w_{,y} - v/r_y \end{Bmatrix} = \begin{Bmatrix} \varepsilon_{xx}^0 \\ \varepsilon_{yy}^0 \\ \gamma_{xy}^0 \\ \varphi_{xz} \\ \varphi_{yz} \end{Bmatrix} + z\begin{Bmatrix} \kappa_{xx} \\ \kappa_{yy} \\ \kappa_{xy} \\ \kappa_{xz} \\ \kappa_{yz} \end{Bmatrix} + z^2\begin{Bmatrix} 0 \\ 0 \\ 0 \\ \varphi_{xz}^* \\ \varphi_{yz}^* \end{Bmatrix} + z^3\begin{Bmatrix} \kappa_{xx}^* \\ \kappa_{yy}^* \\ \kappa_{xy}^* \\ \kappa_{xz}^* \\ \kappa_{yz}^* \end{Bmatrix} \tag{2.38}$$

where

$$\begin{aligned} &\left[\varepsilon_{xx}^0 \quad \varepsilon_{yy}^0 \quad \gamma_{xy}^0 \quad \varphi_{xz} \quad \varphi_{yz}\right]^T \\ &= [u_{0,x} \quad v_{0,y} + w_0/r_y \quad u_{0,y} + v_{0,x} + 2w_0/r_{xy} \quad \beta_x + w_{0,x} \quad \beta_y + w_{0,y} - v_0/r_y]^T \end{aligned} \tag{2.39}$$

$$[\kappa_{xx} \quad \kappa_{yy} \quad \kappa_{xy} \quad \kappa_{xz} \quad \kappa_{yz}] = [\beta_{x,x} \quad \beta_{y,y} \quad \beta_{x,y} + \beta_{y,x} \quad 0 \quad \beta_y/r_y] \tag{2.40}$$

$$[0 \quad 0 \quad 0 \quad \varphi_{xz}^* \quad \varphi_{yz}^*] = [0 \quad 0 \quad 0 \quad 3\beta_x^* \quad 3\beta_y^*] \tag{2.41}$$

$$[\kappa_{xx}^* \quad \kappa_{yy}^* \quad \kappa_{xy}^* \quad \kappa_{xz}^* \quad \kappa_{yz}^*] = [\beta_{x,x}^* \quad \beta_{y,y}^* \quad \beta_{x,y}^* + \beta_{y,x}^* \quad 0 \quad \beta_y^*/r_y] \tag{2.42}$$

The linear strain component vector $\{\varepsilon_l\}$, as given in **Eq. (2.38)**, can be expressed in terms of mid-plane strain vector in the following compact form

$$\{\varepsilon_l\} = [\bar{T}]\{\varepsilon^0\} \tag{2.43}$$

where the mid-plane strain vector $\{\varepsilon^0\}$ and thickness coordinate matrix $[\bar{T}]$ are defined as

$$\{\varepsilon^0\} = \begin{bmatrix} \varepsilon_{xx}^0 & \varepsilon_{yy}^0 & \gamma_{xy}^0 & \kappa_{xx} & \kappa_{yy} & \kappa_{xy} & \kappa_{xx}^* & \kappa_{yy}^* & \kappa_{xy}^* & \varphi_{xz} & \varphi_{yz} & \kappa_{xz} & \kappa_{yz} & \varphi_{xz}^* & \varphi_{yz}^* & \kappa_{xz}^* & \kappa_{yz}^* \end{bmatrix}^T \tag{2.44}$$

$$[\bar{T}] = \begin{bmatrix} 1 & 0 & 0 & z & 0 & 0 & z^3 & 0 & 0 & 0 & 0 & 0 & 0 & 0 & 0 & 0 & 0 \\ 0 & 1 & 0 & 0 & z & 0 & 0 & z^3 & 0 & 0 & 0 & 0 & 0 & 0 & 0 & 0 & 0 \\ 0 & 0 & 1 & 0 & 0 & z & 0 & 0 & z^3 & 0 & 0 & 0 & 0 & 0 & 0 & 0 & 0 \\ 0 & 0 & 0 & 0 & 0 & 0 & 0 & 0 & 0 & 1 & 0 & z & 0 & z^2 & 0 & z^3 & 0 \\ 0 & 0 & 0 & 0 & 0 & 0 & 0 & 0 & 0 & 0 & 1 & 0 & z & 0 & z^2 & 0 & z^3 \end{bmatrix} \tag{2.45}$$

2.2.4 STRESS-STRAIN RELATIONSHIP

The composite sandwich shell is assumed to consist of a number of thin laminae, each with their different orientation of principal material coordinates with respect to the shell coordinates. For a typical lamina, the principal material axes 1 and 2 are considered to lie along and transverse to the fiber direction, respectively, as shown in **Fig. 2.4.** In reference to the material coordinates, Young's moduli are indicated as E_{11} and E_{22}, the shear moduli are indicated as G_{12}, G_{13}, and G_{23}, Poisson's ratio are indicated as ν_{12} and ν_{21}, and the thermal expansion coefficients are indicated by α_{11} and α_{22}.

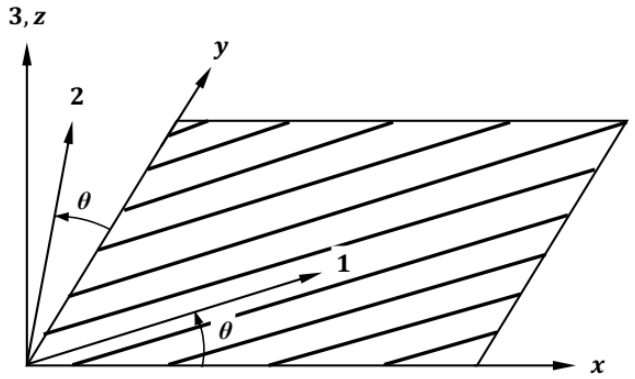

Fig. 2.4 A typical lamina with two reference systems

The stress-strain relations for a typical k^{th} lamina of linear thermoelastic materials with reference to material coordinates (1, 2, 3) can be expressed as

$$\begin{Bmatrix}\sigma_{11}\\ \sigma_{22}\\ \tau_{12}\\ \tau_{13}\\ \tau_{23}\end{Bmatrix}_k = \begin{bmatrix}Q_{11} & Q_{12} & 0 & 0 & 0\\ Q_{12} & Q_{22} & 0 & 0 & 0\\ 0 & 0 & Q_{66} & 0 & 0\\ 0 & 0 & 0 & Q_{44} & 0\\ 0 & 0 & 0 & 0 & Q_{55}\end{bmatrix}_k \left(\begin{Bmatrix}\varepsilon_{11}\\ \varepsilon_{22}\\ \gamma_{12}\\ \gamma_{13}\\ \gamma_{23}\end{Bmatrix} - \begin{Bmatrix}\alpha_{11}\\ \alpha_{22}\\ 0\\ 0\\ 0\end{Bmatrix} \Delta T \right)_k \tag{2.46}$$

where Q_{ij} 's are the on-axis reduced elastic constants of the k^{th} layer and can be expressed as

$$Q_{11} = \frac{E_{11}}{1-\nu_{12}\nu_{21}},\ Q_{22} = \frac{E_{22}}{1-\nu_{12}\nu_{21}},\ Q_{12} = \frac{\nu_{21}E_{11}}{1-\nu_{12}\nu_{21}},$$
$$Q_{66} = G_{12}, Q_{44} = G_{23},\ Q_{55} = G_{13} \tag{2.47}$$

and $\Delta T = T - T_0$ is the rise in temperature from reference temperature T_0 to any elevated temperature T.

Employing the usual transformation rule of stresses/strains as given by Jones (1975), the following stress-strain relations for the k^{th} lamina in the shell coordinates $(x-y-z)$ are obtained

$$\begin{Bmatrix}\sigma_{xx}\\ \sigma_{yy}\\ \tau_{xy}\\ \tau_{xz}\\ \tau_{yz}\end{Bmatrix}_k = \begin{bmatrix}\bar{Q}_{11} & \bar{Q}_{12} & \bar{Q}_{16} & 0 & 0\\ \bar{Q}_{12} & \bar{Q}_{22} & \bar{Q}_{26} & 0 & 0\\ \bar{Q}_{16} & \bar{Q}_{26} & \bar{Q}_{26} & 0 & 0\\ 0 & 0 & 0 & \bar{Q}_{44} & \bar{Q}_{45}\\ 0 & 0 & 0 & \bar{Q}_{45} & \bar{Q}_{55}\end{bmatrix}_k \left(\begin{Bmatrix}\varepsilon_{xx}\\ \varepsilon_{yy}\\ \gamma_{xy}\\ \gamma_{xz}\\ \gamma_{yz}\end{Bmatrix} - \begin{Bmatrix}\varepsilon_{xx}^{TH}\\ \varepsilon_{yy}^{TH}\\ \gamma_{xy}^{TH}\\ 0\\ 0\end{Bmatrix} \right)_k \tag{2.48}$$

where $\bar{Q}_{ij}$'s denote the off-axis reduced elastic coefficients and can be defined as

$$\begin{Bmatrix}\bar{Q}_{11}\\ \bar{Q}_{12}\\ \bar{Q}_{22}\\ \bar{Q}_{16}\\ \bar{Q}_{26}\\ \bar{Q}_{66}\\ \bar{Q}_{44}\\ \bar{Q}_{45}\\ \bar{Q}_{55}\end{Bmatrix} = \begin{bmatrix} m^4 & 2m^2n^2 & n^4 & 4m^2n^2 & 0 & 0\\ m^2n^2 & m^4+n^4 & m^2n^2 & -4m^2n^2 & 0 & 0\\ n^4 & 2m^2n^2 & m^4 & 4m^2n^2 & 0 & 0\\ m^3n & mn^3-m^3n & -mn^3 & -2m^3n+2mn^3 & 0 & 0\\ mn^3 & m^3n-mn^3 & -m^3n & 2m^3n-2mn^3 & 0 & 0\\ m^2n^2 & -2m^2n^2 & m^2n^2 & (m^2-n^2)^2 & 0 & 0\\ 0 & 0 & 0 & 0 & m^2 & n^2\\ 0 & 0 & 0 & 0 & -mn & mn\\ 0 & 0 & 0 & 0 & n^2 & m^2\end{bmatrix} \begin{Bmatrix}Q_{11}\\ Q_{12}\\ Q_{22}\\ Q_{66}\\ Q_{44}\\ Q_{45}\end{Bmatrix} \tag{2.49}$$

in which $m = \cos\theta$ and $n = \sin\theta$; θ is the lamination angle with the positive x −axis.

In the stress-strain relationship as expressed **Eq. (2.48),** the expressions of the thermal strains $(\varepsilon_{xx}^{TH}, \varepsilon_{yy}^{TH}, \gamma_{xy}^{TH})$ in reference to the shell coordinates can be obtained as

$$\begin{Bmatrix} \varepsilon_{xx}^{TH} \\ \varepsilon_{yy}^{TH} \\ \gamma_{xy}^{TH} \end{Bmatrix} = \begin{bmatrix} m^2 & n^2 \\ n^2 & m^2 \\ 2mn & -2mn \end{bmatrix} \begin{Bmatrix} \alpha_{11} \\ \alpha_{22} \end{Bmatrix} (T - T_0) \tag{2.50}$$

The resultant forces and moments acting on the composite sandwich shell obtained upon integration of the stresses through its thickness are given as

$$[\{N\} \quad \{M\} \quad \{M^*\}] = \left[\begin{Bmatrix} N_{xx} \\ N_{yy} \\ N_{xy} \end{Bmatrix} \quad \begin{Bmatrix} M_{xx} \\ M_{yy} \\ M_{xy} \end{Bmatrix} \quad \begin{Bmatrix} M_{xx}^* \\ M_{yy}^* \\ M_{xy}^* \end{Bmatrix} \right] = \int_{-h/2}^{h/2} \begin{Bmatrix} \sigma_{xx} \\ \sigma_{yy} \\ \tau_{xy} \end{Bmatrix}_k [1 \quad z \quad z^3] dz \tag{2.51}$$

$$[\{Q\} \quad \{Q^*\}] = \left[\begin{Bmatrix} Q_{xz} \\ Q_{yz} \end{Bmatrix} \quad \begin{Bmatrix} Q_{xz}^* \\ Q_{yz}^* \end{Bmatrix} \right] = \int_{-h/2}^{h/2} \begin{Bmatrix} \tau_{xz} \\ \tau_{yz} \end{Bmatrix}_k [1 \quad z^2] \, dz \tag{2.52}$$

$$[\{R\} \quad \{R^*\}] = \left[\begin{Bmatrix} R_{xz} \\ R_{yz} \end{Bmatrix} \quad \begin{Bmatrix} R_{xz}^* \\ R_{yz}^* \end{Bmatrix} \right] = \int_{-h/2}^{h/2} \begin{Bmatrix} \tau_{xz} \\ \tau_{yz} \end{Bmatrix}_k [z \quad z^3] \, dz \tag{2.53}$$

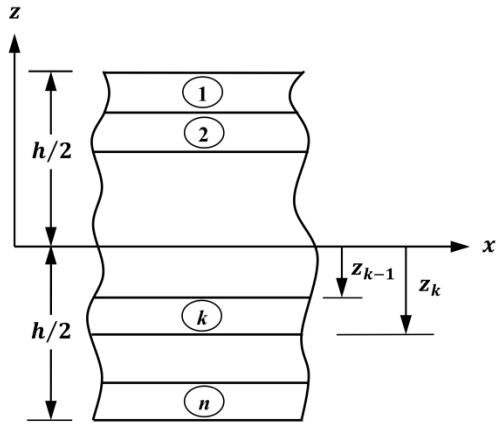

Fig. 2.5 Geometrical details of an n-layered laminate

Substituting the stress-strain relations in **Eq. (2.48)** into **Eqs. (2.51)-(2.53)**, the resultant forces and moments of laminate having n numbers of laminae **(Fig. 2.5)** becomes

$$\begin{Bmatrix} N_{xx} \\ N_{yy} \\ N_{xy} \end{Bmatrix} = \sum_{k=1}^{n} \begin{bmatrix} \bar{Q}_{11} & \bar{Q}_{12} & \bar{Q}_{16} \\ \bar{Q}_{12} & \bar{Q}_{22} & \bar{Q}_{26} \\ \bar{Q}_{16} & \bar{Q}_{26} & \bar{Q}_{66} \end{bmatrix}_k \left\{ \int_{z_{k-1}}^{z_k} \begin{Bmatrix} \varepsilon_{xx}^0 \\ \varepsilon_{yy}^0 \\ \gamma_{xy}^0 \end{Bmatrix} dz + \int_{z_{k-1}}^{z_k} \begin{Bmatrix} \kappa_{xx} \\ \kappa_{yy} \\ \kappa_{xy} \end{Bmatrix} z \, dz + \int_{z_{k-1}}^{z_k} \begin{Bmatrix} \kappa_{xx}^* \\ \kappa_{yy}^* \\ \kappa_{xy}^* \end{Bmatrix} z^3 \, dz \right\} \tag{2.54}$$

$$\begin{Bmatrix} M_{xx} \\ M_{yy} \\ M_{xy} \end{Bmatrix} = \sum_{k=1}^{n} \begin{bmatrix} \bar{Q}_{11} & \bar{Q}_{12} & \bar{Q}_{16} \\ \bar{Q}_{12} & \bar{Q}_{22} & \bar{Q}_{26} \\ \bar{Q}_{16} & \bar{Q}_{26} & \bar{Q}_{66} \end{bmatrix}_k \left\{ \int_{z_{k-1}}^{z_k} \begin{Bmatrix} \varepsilon_{xx}^0 \\ \varepsilon_{yy}^0 \\ \gamma_{xy}^0 \end{Bmatrix} z dz + \int_{z_{k-1}}^{z_k} \begin{Bmatrix} \kappa_{xx} \\ \kappa_{yy} \\ \kappa_{xy} \end{Bmatrix} z^2 dz + \int_{z_{k-1}}^{z_k} \begin{Bmatrix} \kappa_{xx}^* \\ \kappa_{yy}^* \\ \kappa_{xy}^* \end{Bmatrix} z^4 \, dz \right\} \quad (2.55)$$

$$\begin{Bmatrix} M_{xx}^* \\ M_{yy}^* \\ M_{xy}^* \end{Bmatrix} = \sum_{k=1}^{n} \begin{bmatrix} \bar{Q}_{11} & \bar{Q}_{12} & \bar{Q}_{16} \\ \bar{Q}_{12} & \bar{Q}_{22} & \bar{Q}_{26} \\ \bar{Q}_{16} & \bar{Q}_{26} & \bar{Q}_{66} \end{bmatrix}_k \left\{ \int_{z_{k-1}}^{z_k} \begin{Bmatrix} \varepsilon_{xx}^0 \\ \varepsilon_{yy}^0 \\ \gamma_{xy}^0 \end{Bmatrix} z^3 dz + \int_{z_{k-1}}^{z_k} \begin{Bmatrix} \kappa_{xx} \\ \kappa_{yy} \\ \kappa_{xy} \end{Bmatrix} z^4 dz + \int_{z_{k-1}}^{z_k} \begin{Bmatrix} \kappa_{xx}^* \\ \kappa_{yy}^* \\ \kappa_{xy}^* \end{Bmatrix} z^6 \, dz \right\} \quad (2.56)$$

$$\begin{Bmatrix} Q_{xz} \\ Q_{yz} \end{Bmatrix} = \sum_{k=1}^{n} \begin{bmatrix} \bar{Q}_{44} & \bar{Q}_{45} \\ \bar{Q}_{45} & \bar{Q}_{55} \end{bmatrix}_k \left\{ \int_{z_{k-1}}^{z_k} \begin{Bmatrix} \varphi_{xz} \\ \varphi_{yz} \end{Bmatrix} dz + \int_{z_{k-1}}^{z_k} \begin{Bmatrix} \kappa_{xz} \\ \kappa_{yz} \end{Bmatrix} z dz + \int_{z_{k-1}}^{z_k} \begin{Bmatrix} \varphi_{xz}^* \\ \varphi_{yz}^* \end{Bmatrix} z^2 dz + \int_{z_{k-1}}^{z_k} \begin{Bmatrix} \kappa_{xz}^* \\ \kappa_{yz}^* \end{Bmatrix} z^3 dz \right\} \quad (2.57)$$

$$\begin{Bmatrix} Q_{xz}^* \\ Q_{yz}^* \end{Bmatrix} = \sum_{k=1}^{n} \begin{bmatrix} \bar{Q}_{44} & \bar{Q}_{45} \\ \bar{Q}_{45} & \bar{Q}_{55} \end{bmatrix}_k \left\{ \int_{z_{k-1}}^{z_k} \begin{Bmatrix} \varphi_{xz} \\ \varphi_{yz} \end{Bmatrix} z dz + \int_{z_{k-1}}^{z_k} \begin{Bmatrix} \kappa_{xz} \\ \kappa_{yz} \end{Bmatrix} z^2 dz + \int_{z_{k-1}}^{z_k} \begin{Bmatrix} \varphi_{xz}^* \\ \varphi_{yz}^* \end{Bmatrix} z^3 dz + \int_{z_{k-1}}^{z_k} \begin{Bmatrix} \kappa_{xz}^* \\ \kappa_{yz}^* \end{Bmatrix} z^4 dz \right\} \quad (2.58)$$

$$\begin{Bmatrix} R_{xz} \\ R_{yz} \end{Bmatrix} = \sum_{k=1}^{n} \begin{bmatrix} \bar{Q}_{44} & \bar{Q}_{45} \\ \bar{Q}_{45} & \bar{Q}_{55} \end{bmatrix}_k \left\{ \int_{z_{k-1}}^{z_k} \begin{Bmatrix} \varphi_{xz} \\ \varphi_{yz} \end{Bmatrix} z^2 dz + \int_{z_{k-1}}^{z_k} \begin{Bmatrix} \kappa_{xz} \\ \kappa_{yz} \end{Bmatrix} z^3 dz + \int_{z_{k-1}}^{z_k} \begin{Bmatrix} \varphi_{xz}^* \\ \varphi_{yz}^* \end{Bmatrix} z^4 dz + \int_{z_{k-1}}^{z_k} \begin{Bmatrix} \kappa_{xz}^* \\ \kappa_{yz}^* \end{Bmatrix} z^5 dz \right\} \quad (2.59)$$

$$\begin{Bmatrix} R_{xz}^* \\ R_{yz}^* \end{Bmatrix} = \sum_{k=1}^{n} \begin{bmatrix} \bar{Q}_{44} & \bar{Q}_{45} \\ \bar{Q}_{45} & \bar{Q}_{55} \end{bmatrix}_k \left\{ \int_{z_{k-1}}^{z_k} \begin{Bmatrix} \varphi_{xz} \\ \varphi_{yz} \end{Bmatrix} z^3 dz + \int_{z_{k-1}}^{z_k} \begin{Bmatrix} \kappa_{xz} \\ \kappa_{yz} \end{Bmatrix} z^4 dz + \int_{z_{k-1}}^{z_k} \begin{Bmatrix} \varphi_{xz}^* \\ \varphi_{yz}^* \end{Bmatrix} z^5 dz + \int_{z_{k-1}}^{z_k} \begin{Bmatrix} \kappa_{xz}^* \\ \kappa_{yz}^* \end{Bmatrix} z^6 dz \right\} \quad (2.60)$$

where z_k and z_{k-1} are the distances of the bottom of the kth and $(k-1)$th layer from the mid-surface.

The thermal inplane stress resultant forces and moments

$$\begin{Bmatrix} N_{xx}^{TH} \\ N_{yy}^{TH} \\ N_{xy}^{TH} \end{Bmatrix} = \sum_{k=1}^{n} \begin{bmatrix} \bar{Q}_{11} & \bar{Q}_{12} & \bar{Q}_{16} \\ \bar{Q}_{12} & \bar{Q}_{22} & \bar{Q}_{26} \\ \bar{Q}_{16} & \bar{Q}_{26} & \bar{Q}_{66} \end{bmatrix}_k \int_{z_{k-1}}^{z_k} \begin{Bmatrix} \varepsilon_{xx}^{TH} \\ \varepsilon_{yy}^{TH} \\ \gamma_{xy}^{TH} \end{Bmatrix} dz \tag{2.61}$$

$$\begin{Bmatrix} M_{xx}^{TH} \\ M_{yy}^{TH} \\ M_{xy}^{TH} \end{Bmatrix} = \sum_{k=1}^{n} \begin{bmatrix} \bar{Q}_{11} & \bar{Q}_{12} & \bar{Q}_{16} \\ \bar{Q}_{12} & \bar{Q}_{22} & \bar{Q}_{26} \\ \bar{Q}_{16} & \bar{Q}_{26} & \bar{Q}_{66} \end{bmatrix}_k \int_{z_{k-1}}^{z_k} \begin{Bmatrix} \varepsilon_{xx}^{TH} \\ \varepsilon_{yy}^{TH} \\ \gamma_{xy}^{TH} \end{Bmatrix} z dz \tag{2.62}$$

$$\begin{Bmatrix} M_{xx}^{*TH} \\ M_{yy}^{*TH} \\ M_{xy}^{*TH} \end{Bmatrix} = \sum_{k=1}^{n} \begin{bmatrix} \bar{Q}_{11} & \bar{Q}_{12} & \bar{Q}_{16} \\ \bar{Q}_{12} & \bar{Q}_{22} & \bar{Q}_{26} \\ \bar{Q}_{16} & \bar{Q}_{26} & \bar{Q}_{66} \end{bmatrix}_k \int_{z_{k-1}}^{z_k} \begin{Bmatrix} \varepsilon_{xx}^{TH} \\ \varepsilon_{yy}^{TH} \\ \gamma_{xy}^{TH} \end{Bmatrix} z^3 dz \tag{2.63}$$

Combining **Eqs. (2.54)-(2.63),** the relations of the stress resultants, mid-plane strain, and curvature components can be expressed as

$$\{F\} = [D]\{\varepsilon^0\} - \{F^{TH}\} \tag{2.64}$$

where $\{F\}$, $\{F^{TH}\}$, $\{\varepsilon^0\}$, and $[D]$ are the stress resultant vector, thermal stress resultant vector, mid-plane strain vector, and elasticity matrix, respectively, and are given by

$$\{F_e\} = \left(N_{xx}, N_{yy}, N_{xy}, M_{xx}, M_{yy}, M_{xy}, M_{xx}^*, M_{yy}^*, M_{xy}^*, Q_{xz}, Q_{yz}, Q_{xz}^*, Q_{yz}^*, R_{xz}, R_{yz}, R_{xz}^*, R_{yz}^*\right)^T \tag{2.65}$$

$$\{F^{TH}\} = \left(N_{xx}^{TH}, N_{yy}^{TH}, N_{xy}^{TH}, M_{xx}^{TH}, M_{yy}^{TH}, M_{xy}^{TH}, M_{xx}^{*TH}, M_{yy}^{*TH}, M_{xy}^{*TH}, 0, 0, 0, 0, 0, 0, 0, 0\right)^T \tag{2.66}$$

$$\{\varepsilon^0\} = \left[\varepsilon_{xx}^0 \;\; \varepsilon_{yy}^0 \;\; \gamma_{xy}^0 \;\; \kappa_{xx} \;\; \kappa_{yy} \;\; \kappa_{xy} \;\; \kappa_{xx}^* \;\; \kappa_{yy}^* \;\; \kappa_{xy}^* \;\; \varphi_{xz} \;\; \varphi_{yz} \;\; \kappa_{xz} \;\; \kappa_{yz} \;\; \varphi_{xz}^* \;\; \varphi_{yz}^* \;\; \kappa_{xz}^* \;\; \kappa_{yz}^*\right]^T \tag{2.67}$$

$$[D] = \begin{bmatrix} [A_{ij}] & [B_{ij}] & [C_{ij}] & 0 & 0 & 0 & 0 \\ [B_{ij}] & [D_{ij}] & [E_{ij}] & 0 & 0 & 0 & 0 \\ [C_{ij}] & [E_{ij}] & [F_{ij}] & 0 & 0 & 0 & 0 \\ 0 & 0 & 0 & [A_{ij}^*] & [B_{ij}^*] & [D_{ij}^*] & [C_{ij}^*] \\ 0 & 0 & 0 & [B_{ij}^*] & [D_{ij}^*] & [C_{ij}^*] & [E_{ij}^*] \\ 0 & 0 & 0 & [D_{ij}^*] & [C_{ij}^*] & [E_{ij}^*] & [G_{ij}^*] \\ 0 & 0 & 0 & [C_{ij}^*] & [E_{ij}^*] & [G_{ij}^*] & [F_{ij}^*] \end{bmatrix}_{17\times 17} \tag{2.68}$$

where the stress resultants are defined as

$$\left(A_{ij}, B_{ij}, D_{ij}, C_{ij}, E_{ij}, F_{ij}\right) = \sum_{k=1}^{n} \int_{z_{k-1}}^{z_k} \bar{Q}_{ij} \left(1, z, z^2, z^3, z^4, z^6\right) dz \quad i, j = 1,2,6 \tag{2.69}$$

$$\left(A_{ij}^*, B_{ij}^*, D_{ij}^*, C_{ij}^*, E_{ij}^*, G_{ij}^*, F_{ij}^*\right) = \sum_{k=1}^{n} \int_{z_{k-1}}^{z_k} \bar{Q}_{ij} \left(1, z, z^2, z^3, z^4, z^5, z^6\right) dz \qquad i, j = 4,5 \tag{2.70}$$

2.3 FINITE ELEMENT FORMULATION

The trapezoidal planform of the sandwich shallow conical shell surface is discretized into eight-node isoparametric shell elements as shown in **Fig. 2.6.** Each node of the element has seven degrees of freedom (u_0, v_0, w_0, β_x, β_y, β_x^*, and β_y^*). In order to formulate the finite element analysis, an 8-node square master element, as shown in **Fig. 2.7(a)**, is mapped into a real quadrilateral element with curved side as shown in **Fig. 2.7(b).** The displacement field in the master element and geometrical relationship between the master element and real element are governed by the same interpolation function called shape function.

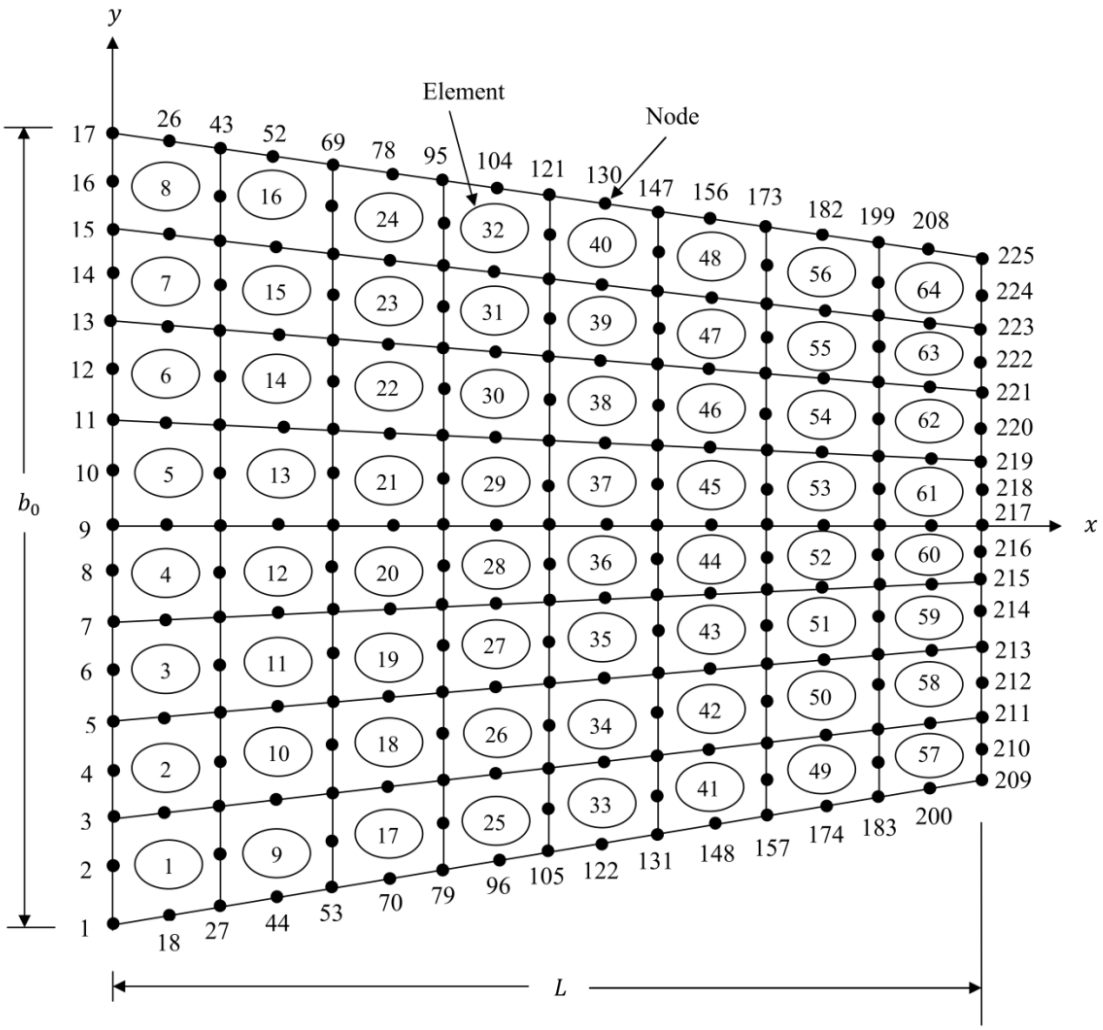

Fig. 2.6 Discretized trapezoidal planform of the sandwich shallow conical shell

For satisfactory representation of the displacement field over the element, the shape functions are derived from an interpolation polynomial in terms of the natural or intrinsic co-ordinates ξ and η.

The quadratic interpolation function or shape function that defines the variation of the displacement component u is assumed as

$$u(\xi,\eta) = c_1 + c_2\xi + c_3\eta + c_4\xi\eta + c_5\xi^2 + c_6\eta^2 + c_7\xi^2\eta + c_8\xi\eta^2 \quad (2.71)$$

where $c_i (i = 1,2,3, \ldots,8)$ are the generalized degrees of freedom.

The shape functions N_i at i^{th} node are derived from the interpolation function as (Cook *et al.*, 1989)

$$N_i = (1+\xi\xi_i)(1+\eta\eta_i)(\xi\xi_i+\eta\eta_i-1)/4 \quad \text{(for } i = 1, 2, 3, 4) \quad (2.72)$$

$$N_i = (1-\xi^2)(1+\eta\eta_i)/2 \quad \text{(for } i = 5, 7) \quad (2.73)$$

$$N_i = (1-\eta^2)(1+\xi\xi_i)/2 \quad \text{(for } i = 6, 8) \quad (2.74)$$

where ξ_i and η_i are the natural coordinates at i^{th} node.

The accurateness of the shape functions is examined from the following relations

$$\sum_{i=1}^{8} N_i = 1, \quad \sum_{i=1}^{8} \frac{\partial N_i}{\partial \xi} = 1, \quad \sum_{i=1}^{8} \frac{\partial N_i}{\partial \eta} = 1, \quad (2.75)$$

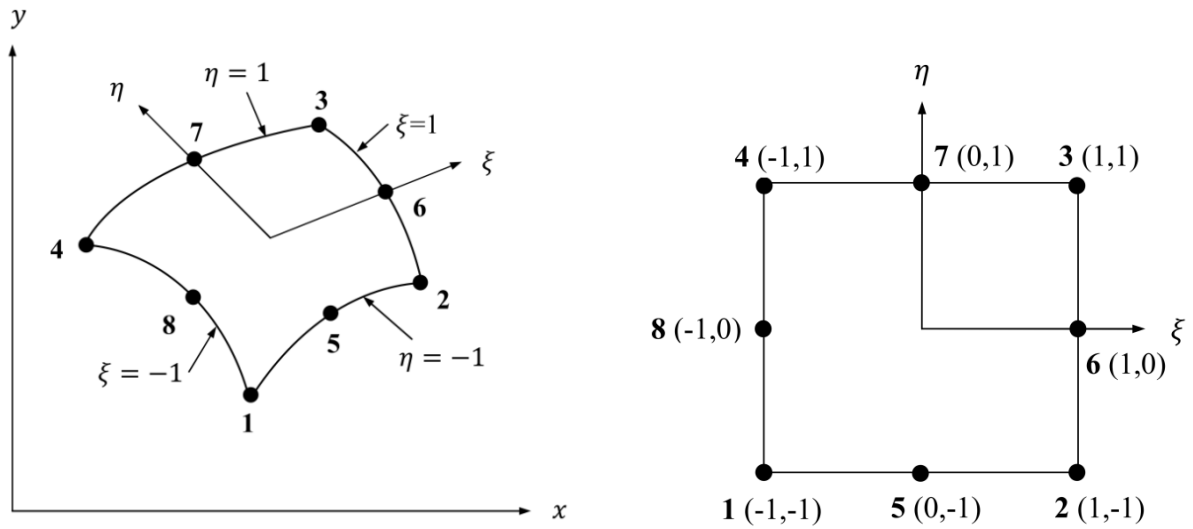

(a) (b)

Fig. 2.7 (a) Eight-node element in $x - y$ plane (b) The same element mapped into $\xi - \eta$ plane

The coordinates x and y of a point within the element can be expressed in terms of shape functions N_i and the nodal coordinates (x_i, y_i) as

$$x = \sum_{i=1}^{8} N_i\, x_i \qquad y = \sum_{i=1}^{8} N_i\, y_i \quad (2.76)$$

Using the isoparametric relation, the mid-plane displacement variables within the element can be expressed in terms of the corresponding nodal displacement parameters as

$$u_0 = \sum_{i=1}^{8} N_i\, u_{0i}\ ; \qquad v_0 = \sum_{i=1}^{8} N_i\, v_{0i}\ ; \qquad w_0 = \sum_{i=1}^{8} N_i\, w_{0i}\ ; \qquad \beta_x = \sum_{i=1}^{8} N_i\, \beta_{xi}\ ;$$
$$\beta_y = \sum_{i=1}^{8} N_i\, \beta_{yi}\ ; \qquad \beta_x^* = \sum_{i=1}^{8} N_i\, \beta_{xi}^*\ ; \qquad \beta_y^* = \sum_{i=1}^{8} N_i\, \beta_{yi}^* \tag{2.77}$$

and

$$\begin{Bmatrix} N_{i,x} \\ N_{i,y} \end{Bmatrix} = [J]^{-1} \begin{Bmatrix} N_{i,\xi} \\ N_{i,\eta} \end{Bmatrix} \tag{2.78}$$

where $[J]$ symbolizes Jacobian matrix and is given by

$$[J] = \begin{bmatrix} x_{,\xi} & y_{,\xi} \\ x_{,\eta} & y_{,\eta} \end{bmatrix} \tag{2.79}$$

The expressions of the displacement parameters in **Eq. (2.77)** can be expressed in the following compact form

$$\{\Delta\} = [N]\{\delta_e\} \tag{2.80}$$

where $\{\Delta\} = [u_0 \quad v_0 \quad w_0 \quad \beta_x \quad \beta_y \quad \beta_x^* \quad \beta_y^*]^T$ is the vector representing generalized displacement parameter and $\{\delta_e\} = [u_{0i} \quad v_{0i} \quad w_{0i} \quad \beta_{xi} \quad \beta_{yi} \quad \beta_{xi}^* \quad \beta_{yi}^*]^T$ represents nodal displacement parameter vector. The shape function matrix $[N]$ can be expressed as

$$[N] = \begin{bmatrix} N_i & 0 & 0 & 0 & 0 & 0 & 0 \\ 0 & N_i & 0 & 0 & 0 & 0 & 0 \\ 0 & 0 & N_i & 0 & 0 & 0 & 0 \\ 0 & 0 & 0 & N_i & 0 & 0 & 0 \\ 0 & 0 & 0 & 0 & N_i & 0 & 0 \\ 0 & 0 & 0 & 0 & 0 & N_i & 0 \\ 0 & 0 & 0 & 0 & 0 & 0 & N_i \end{bmatrix}_{i=1,2,3,\ldots,8} \tag{2.81}$$

Subsequently, the mid-plane strain vector $\{\varepsilon^0\}$ can be expressed in terms of nodal displacement parameter vector as

$$\{\varepsilon^0\} = [B]\{\delta_e\} \tag{2.82}$$

where $[B]$ is the strain-displacement matrix given as

$$[B] = \sum_{i=1}^{8} \begin{bmatrix} N_{i,x} & 0 & 0 & 0 & 0 & 0 & 0 \\ 0 & N_{i,y} & N_i/r_y & 0 & 0 & 0 & 0 \\ N_{i,y} & N_{i,x} & 2N_i/r_{xy} & 0 & 0 & 0 & 0 \\ 0 & 0 & 0 & N_{i,x} & 0 & 0 & 0 \\ 0 & 0 & 0 & 0 & N_{i,y} & 0 & 0 \\ 0 & 0 & 0 & N_{i,y} & N_{i,x} & 0 & 0 \\ 0 & 0 & 0 & 0 & 0 & N_{i,x} & 0 \\ 0 & 0 & 0 & 0 & 0 & 0 & N_{i,y} \\ 0 & 0 & 0 & 0 & 0 & N_{i,y} & N_{i,x} \\ 0 & 0 & N_{i,x} & N_i & 0 & 0 & 0 \\ 0 & -N_i/r_y & N_{i,y} & 0 & N_i & 0 & 0 \\ 0 & 0 & 0 & 0 & 0 & 0 & 0 \\ 0 & 0 & 0 & 0 & -N_i/r_y & 0 & 0 \\ 0 & 0 & 0 & 0 & 0 & 3N_i & 0 \\ 0 & 0 & 0 & 0 & 0 & 0 & 3N_i \\ 0 & 0 & 0 & 0 & 0 & 0 & 0 \\ 0 & 0 & 0 & 0 & 0 & 0 & -N_i/r_y \end{bmatrix}_{i=1,8} \tag{2.83}$$

2.4 GENERAL DYNAMIC EQUILIBRIUM EQUATION

Hamilton's principle applied to the dynamic analysis of elastic bodies states that "among all admissible displacements which satisfy the specific boundary conditions, the actual solution makes the functional $\int (T_k + U)\, dt$ stationary, where T_k and U are the kinetic energy and work done by conservative and non-conservative forces, respectively. The stationary value is actually a minimum".

2.4.1 KINETIC ENERGY OF ROTATING SANDWICH CONICAL SHELL

Consider two reference systems $\mathcal{R}_0(X, Y, Z)$ and $\mathcal{R}_1(x, y, z)$ to formulate the general dynamic equilibrium of a rotating sandwich conical shell as shown in the **Fig. 2.8**. The first one refers to the inertial Cartesian coordinate system with the unit vectors $(\mathbf{i_X}, \mathbf{i_Y}, \mathbf{i_Z})$ which is generally fixed to any arbitrary point with the axis of blade hub. The second one with the unit vectors $(\mathbf{i_x}, \mathbf{i_y}, \mathbf{i_z})$ is the shell coordinate system which is also known as local coordinate system. The vector $\mathbf{r_0} = \{X_0,\ Y_0,\ Z_0\}$ indicates the translational offsets of shell coordinate system from the inertial reference system.

The kinetic energy of the rotating sandwich conical shell can be described

$$T_K = \frac{1}{2}\int_{vol} \rho \mathbf{V}.\mathbf{V}\, d(vol) \tag{2.84}$$

where ρ symbolizes the mass density of the shell and $\mathbf{V}$ indicates the absolute velocity of an arbitrary point on the conical shell in $\mathcal{R}_0(X,Y,Z)$ reference system. The conical shell is assumed to rotate about the $\mathcal{R}_0(X,Y,Z)$ reference system with an angular velocity $\boldsymbol{\Omega} = \Omega \mathbf{i}_{\boldsymbol{Z}}$

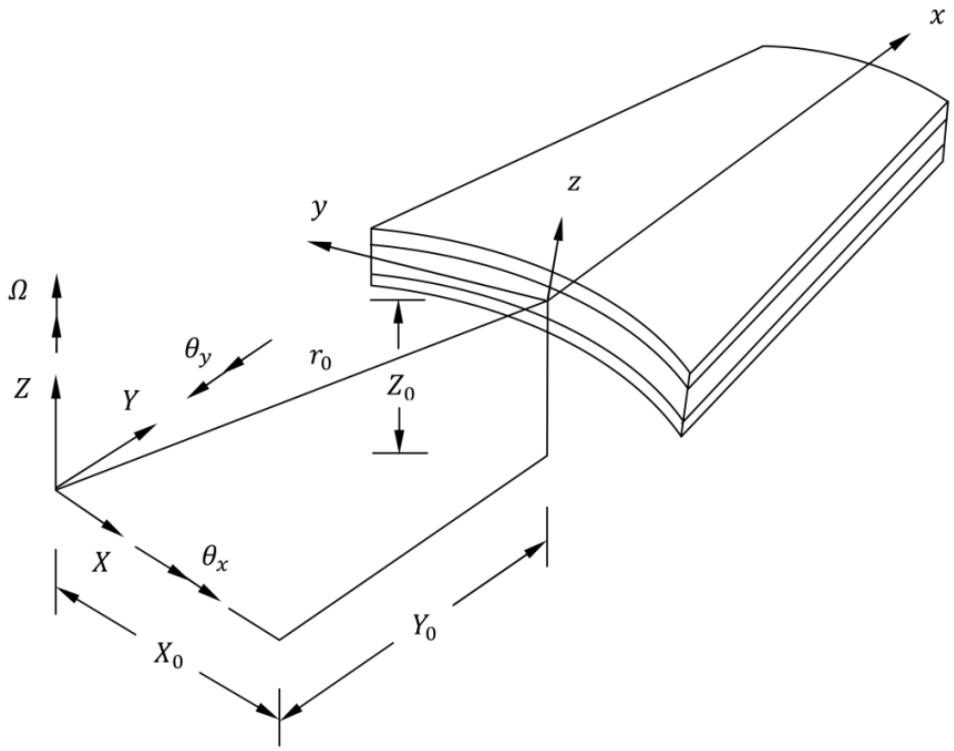

Fig. 2.8 Rotating sandwich shallow conical shell with two reference systems and their offsets

The components of angular velocity in the $\mathcal{R}_1(x,y,z)$ system can be given by

$$\{\Omega_x,\ \Omega_x,\ \Omega_x\} = \{0,\quad 0,\quad \Omega\}\left[T_{\theta y}\right]^T [T_{\theta x}]^T \tag{2.85}$$

where

$$[T_{\theta x}]^T = \begin{bmatrix} 1 & 0 & 0 \\ 0 & \cos(\theta_x) & -\sin(\theta_x) \\ 0 & \sin(\theta_x) & \cos(\theta_x) \end{bmatrix} \tag{2.86}$$

$$\left[T_{\theta y}\right]^T = \begin{bmatrix} \cos(\theta_y) & 0 & -\sin(\theta_y) \\ 0 & 1 & 0 \\ \sin(\theta_y) & 0 & \cos(\theta_y) \end{bmatrix} \tag{2.87}$$

where Ω symbolizes the rotational speed of the conical shell about Z axis of the $\mathcal{R}_0(X,Y,Z)$ system, θ_x indicates skew angle and θ_y signifies the precone angle. The order of rotations is θ_x and θ_y.

The fixed translational offsets expressed with reference to shell coordinate system are given as

$$\{l_x,\ l_y,\ l_z\} = \{X_0,\quad Y_0,\quad Z_0\}\left[T_{\theta y}\right]^T [T_{\theta x}]^T \tag{2.88}$$

According to Chasle's theorem,

$$\mathbf{V} = \frac{d\mathbf{r}}{dt} + \boldsymbol{\Omega} \times \mathbf{r} \tag{2.89}$$

where $\boldsymbol{r}$ indicates the position vector of the arbitrary point on the conical shell after deformation from the origin of the inertial reference frame and is given by

$$\mathbf{r} = (l_x + x + u)\mathbf{i_x} + \left(l_y + y + v\right)\mathbf{i_y} + (l_z + z + w)\mathbf{i_z} \tag{2.90}$$

where (x, y, z) are the coordinates of the point in the shell coordinate system (local coordinate axes), $\left(l_x, l_y, l_z\right)$ are the fixed translational offsets of the shell coordinate axes from the inertial axes expressed with reference to the shell coordinate system, and (*u*, *v*, *w*) are the elastic deflections.

The angular velocity vector **Ω** in **Eq. (2.89)** is given by

$$\boldsymbol{\Omega} = \Omega\mathbf{k_Z} = \Omega_x\mathbf{i_x} + \Omega_y\mathbf{i_y} + \Omega_z\mathbf{i_z} \tag{2.91}$$

where $\left(\Omega_x, \Omega_y, \Omega_z\right)$ are the components of angular velocity in the shell coordinate system.

Substituting the expressions of **r** and **Ω** into **Eq. (2.89)**, the absolute velocity **V** can be derived as

$$\begin{aligned} \boldsymbol{V} = &\left[\dot{u} + \Omega_y(l_z + z + w) - \Omega_z\left(l_y + y + v\right)\right]\mathbf{i_x} \\ &+ \left[\dot{v} + \Omega_z(l_x + x + u) - \Omega_x(l_z + z + w)\right]\mathbf{i_y} \\ &+ \left[\dot{w} + \Omega_x\left(l_y + y + v\right) - \Omega_y(l_x + x + u)\right]\mathbf{i_z} \end{aligned} \tag{2.92}$$

Computing $|\mathbf{V}|^2$ and canceling the terms which give no contribution when Lagrange's equation of motion is applied and substituting the result in kinetic energy expression, we have,

$$\begin{aligned} T_K = &\frac{1}{2}\int_{vol} \rho \begin{Bmatrix} \dot{u} \\ \dot{v} \\ \dot{w} \end{Bmatrix}^T \begin{Bmatrix} \dot{u} \\ \dot{v} \\ \dot{w} \end{Bmatrix} d(vol) + \frac{1}{2}\int_{vol} \rho \begin{Bmatrix} \dot{u} \\ \dot{v} \\ \dot{w} \end{Bmatrix}^T [A_1] \begin{Bmatrix} u \\ v \\ w \end{Bmatrix} d(vol) \\ &+ \frac{1}{2}\int_{vol} \rho \begin{Bmatrix} u \\ v \\ w \end{Bmatrix}^T [A_2] \begin{Bmatrix} u \\ v \\ w \end{Bmatrix} d(vol) + \frac{1}{2}\int_{vol} \rho \begin{Bmatrix} l_x + x \\ l_y + y \\ l_z + z \end{Bmatrix}^T [A_2] \begin{Bmatrix} u \\ v \\ w \end{Bmatrix} d(vol) \end{aligned} \tag{2.93}$$

where the matrices $[A_1]$ and $[A_2]$ are given by

$$[A_1] = \begin{bmatrix} 0 & -2\Omega_z & 2\Omega_y \\ 2\Omega_z & 0 & -2\Omega_x \\ -2\Omega_y & 2\Omega_x & 0 \end{bmatrix} \tag{2.94}$$

$$[A_2] = \begin{bmatrix} \Omega_y^2 + \Omega_z^2 & -\Omega_x\Omega_y & -\Omega_x\Omega_z \\ -\Omega_x\Omega_y & \Omega_x^2 + \Omega_z^2 & -\Omega_y\Omega_z \\ -\Omega_x\Omega_z & -\Omega_y\Omega_z & \Omega_x^2 + \Omega_y^2 \end{bmatrix} \tag{2.95}$$

Substituting $[u, \quad v, \quad w]^T = [\bar{Z}]\{\Delta\}$ as expressed in **Eq. (2.33)** into **Eq.(2.93),** the elemental kinetic energy becomes

$$T_{Ke} = \frac{1}{2}\int_{vol}\{\dot{\Delta}\}^T[\bar{Z}]^T\rho\,[\bar{Z}]\{\dot{\Delta}\}\,d(vol) + \frac{1}{2}\int_{vol}\{\dot{\Delta}\}^T[\bar{Z}]^T\rho[A_1]\,[\bar{Z}]\{\Delta\}\,d(vol)$$

$$+\frac{1}{2}\int_{vol}[\Delta]^T[\bar{Z}]^T\rho[A_2]\,[\bar{Z}]\{\Delta\}\,d(vol) + \int_{vol}\rho\begin{Bmatrix} l_x + x \\ l_y + y \\ l_z + z \end{Bmatrix}^T [A_2][\bar{Z}]\{\Delta\}d(vol) \tag{2.96}$$

Where $[m_I]$ refers to the matrix of inertia per unit area and can be expressed as

$$[m_I] = \int_{-h/2}^{h/2}[\bar{Z}]^T\rho\,[\bar{Z}]\,dz \tag{2.97}$$

Further, putting $\Delta = [N]\{\delta_e\}$ into **Eq. (2.96),** the elemental kinetic energy is finally expressed in the following form

$$T_{Ke} = \frac{1}{2}\{\dot{\delta}_e\}^T[M_e]\{\dot{\delta}_e\} + \frac{1}{2}\{\dot{\delta}_e\}^T[C_e]\{\delta_e\} + \frac{1}{2}\{\delta_e\}^T[K_{Re}]\{\delta_e\} + \{\delta_e\}^T\{F_{ce}\} \tag{2.98}$$

where $[M_e]$, $[C_e]$, $[K_{Re}]$, and $\{F_{\Omega e}\}$ denote the mass matrix, Coriolis matrix (skew-symmetric), rotational stiffness matrix (symmetric and positive definite), and centrifugal force vector for the shell element, respectively, and are defined as

$$[M_e] = \int_{-1}^{1}\int_{-1}^{1}[N]^T[m_I]\,[N]|J|d\xi d\eta \tag{2.99}$$

$$[C_e] = \rho\int_{vol}[N]^T[\bar{Z}]^T[A_1][\bar{Z}][N]\,d(vol) \tag{2.100}$$

$$[K_{Re}] = \rho\int_{vol}[N]^T[\bar{Z}]^T[A_2][\bar{Z}][N]\,d(vol) \tag{2.101}$$

$$\{F_{\Omega e}\} = \rho\int_{vol}[N]^T[\bar{Z}][A_2]\begin{Bmatrix} l_x + x \\ l_y + y \\ l_z + z \end{Bmatrix}^T d(vol) \tag{2.102}$$

On substitution of the expression of the transformation matrix $[\bar{Z}]$ into **Eq. (2.97),** the inertia matrix becomes

$$[m_I] = \begin{bmatrix} I_1 & 0 & 0 & I_2 & 0 & I_4 & 0 \\ 0 & I_1 & 0 & 0 & I_2 & 0 & I_4 \\ 0 & 0 & I_1 & 0 & 0 & 0 & 0 \\ I_2 & 0 & 0 & I_3 & 0 & I_5 & 0 \\ 0 & I_2 & 0 & 0 & I_3 & 0 & I_5 \\ I_4 & 0 & 0 & I_5 & 0 & I_3 & 0 \\ 0 & I_4 & 0 & 0 & I_5 & 0 & I_3 \end{bmatrix} \tag{2.103}$$

where $I_1$is the normal inertia, $I_2$is the rotary inertia and (I_3, I_4, I_5, I_7) are the higher-order inertias and are defined by

$$(I_1, I_2, I_3, I_4, I_5, I_7) = \sum_{k=1}^{n} \int_{z_{k-1}}^{z_k} \rho_k (1, z, z^2, z^3, z^4, z^6)\, dz \tag{2.104}$$

where ρ_k is the mass density of the k^{th} layer.

2.4.2 STRAIN ENERGY OF ROTATING SANDWICH CONICAL SHELL

The elastic strain energy of the sandwich conical shell element is expressed as

$$U_e^E = \frac{1}{2} \int_{vol} \{\varepsilon_l\}^T \{\sigma\}\, d(vol) \tag{2.105}$$

Using $\{\varepsilon_l\} = [\bar{T}]\{\varepsilon^0\}$ and $\{F\} = [D]\{\varepsilon^0\}$, the above expression can be rewritten

$$U_e^E = \frac{1}{2} \int_A \{\varepsilon^0\}^T\, [D]\{\varepsilon^0\} dA \tag{2.106}$$

in which $[D] = \int_{-h/2}^{h/2} [\bar{T}]^T \left[\bar{Q}_{ij}\right][\bar{T}] dz$ is the elasticity matrix.

Substituting $\{\varepsilon^0\} = [B]\{\delta_e\}$ in **Eq. (2.106),** the elemental elastic strain energy becomes

$$U_e^E = \frac{1}{2} \int_A \{\delta_e\}^T\, [B]^T [D][B]\{\delta_e\} dA = \frac{1}{2} \{\delta_e\}^T [K_e]\{\delta_e\} \tag{2.107}$$

where $[K_e]$ is the elastic stiffness matrix for the shell element that can be written as

$$[K_e] = \int_{-1}^{1} \int_{-1}^{1} [B]^T\, [D][B]|J| d\xi d\eta \tag{2.108}$$

The non-linear strain components according to the Green-Lagrange relations are given as (Cook *et al.*, 1989)

$$\{\varepsilon_{nl}\} = \begin{Bmatrix} \varepsilon_{xx} \\ \varepsilon_{yy} \\ \gamma_{xy} \\ \gamma_{xz} \\ \gamma_{yz} \end{Bmatrix}_{nl} =$$

$$\frac{1}{2}\begin{Bmatrix} (u_{,x})^2 + (v_{,x} + w/r_{xy})^2 + (w_{,x})^2 \\ (u_{,y} + w/r_{xy})^2 + (v_{,y} + w/r_y)^2 + (w_{,y} - v/r_y)^2 \\ 2[u_{,x}(u_{,y} + w/r_{xy}) + (v_{,x} + w/r_{xy})(v_{,y} + w/r_y) + w_{,x}(w_{,y} - v/r_y)] \\ 2[u_{,z}u_{,x} + v_{,z}(v_{,x} + w/r_{xy}) + w_{,z}w_{,x}] \\ 2[u_{,z}(u_{,y} + w/r_{xy}) + v_{,z}(v_{,y} + w/r_y) + w_{,z}(w_{,y} - v/r_y)] \end{Bmatrix} \tag{2.109}$$

The expressions of the nonlinear strain components in the **Eq. (2.109)** can be written in compact form as

$$\{\varepsilon_{nl}\} = \frac{1}{2}[\Gamma][G]\{\delta_e\} \tag{2.110}$$

where $[\Gamma]$ is obvious from **Eq. (2.109)** and **Eq. (2.110),** and $[G]$ is the matrix that contains the derivatives of shape functions as given below

$$[G] = \sum_{i=1}^{8} \begin{bmatrix} N_{i,x} & 0 & 0 & 0 & 0 & 0 & 0 \\ N_{i,y} & 0 & N_i/r_{xy} & 0 & 0 & 0 & 0 \\ 0 & N_{i,x} & N_i/r_{xy} & 0 & 0 & 0 & 0 \\ 0 & N_{i,y} & N_i/r_y & 0 & 0 & 0 & 0 \\ 0 & 0 & N_{i,x} & 0 & 0 & 0 & 0 \\ 0 & -N_i/r_y & N_{i,y} & 0 & 0 & 0 & 0 \\ 0 & 0 & 0 & N_{i,x} & 0 & 0 & 0 \\ 0 & 0 & 0 & N_{i,y} & 0 & 0 & 0 \\ 0 & 0 & 0 & 0 & N_{i,x} & 0 & 0 \\ 0 & 0 & 0 & 0 & N_{i,y} & 0 & 0 \\ 0 & 0 & 0 & 0 & 0 & N_{i,x} & 0 \\ 0 & 0 & 0 & 0 & 0 & N_{i,y} & 0 \\ 0 & 0 & 0 & 0 & 0 & 0 & N_{i,x} \\ 0 & 0 & 0 & 0 & 0 & 0 & N_{i,y} \\ 0 & 0 & 0 & 0 & 0 & 0 & 0 \\ 0 & 0 & 0 & 0 & -N_i/r_y & 0 & 0 \\ 0 & 0 & 0 & 0 & 0 & 0 & 0 \\ 0 & 0 & 0 & 0 & 0 & 0 & -N_i/r_y \end{bmatrix} \tag{2.111}$$

The elemental strain energy resulting from the initial stresses due to thermal and rotational loads is given as

$$U_e^{IS} = \int_{vol} \{\varepsilon_{nl}\}^T \{\sigma_{0TH}\}\, d(vol) + \int_{vol} \{\varepsilon_{nl}\}^T \{\sigma_{0R}\}\, d(vol) \tag{2.112}$$

where $\{\sigma_{0TH}\}$ and $\{\sigma_{0R}\}$ are the initial stress vectors induced due to the thermal and rotational loads, respectively.

The strain energy due to initial stresses, as given in **Eq. (2.112)**, can be rewritten using **Eq. (2.110)** as

$$U_e^{IS} = \frac{1}{2} \int_{vol} \{\delta_e\}^T [G]^T [\Gamma]^T \{\sigma_{0TH}\}\, d(vol) + \frac{1}{2} \int_{vol} \{\delta_e\}^T [G]^T [\Gamma]^T \{\sigma_{0R}\}\, d(vol) \tag{2.113}$$

Now the following integrations are obtained as

$$\int_{-h/2}^{h/2} [\Gamma]^T \{\sigma_{0TH}\} dz = [S_{TH}][G]\,\{\delta_e\} \tag{2.114}$$

$$\int_{-h/2}^{h/2} [\Gamma]^T \{\sigma_{0R}\} dz = [S_R][G]\,\{\delta_e\} \tag{2.115}$$

where $[S_{TH}]$ and $[S_R]$ are the matrices consisting of in-plane stress resultants induced due to thermal and rotational effects, respectively, as given in **Appendix.**

Finally, the elemental strain energy due to initial stresses can be reduced as

$$U_e^{IS} = \frac{1}{2}\{\delta_e\}^T [K_{\sigma THe}]\{\delta_e\} + \frac{1}{2}\{\delta_e\}^T [K_{\sigma Re}]\{\delta_e\} \tag{2.116}$$

in which $[K_{\sigma THe}]$ and $[K_{\sigma Re}]$ refer to the element geometric stiffness matrices due to thermal and rotational effects, respectively, and are given by

$$[K_{\sigma THe}] = \int_{-1}^{1}\int_{-1}^{1} [G]^T\, [S_{TH}][G]|J| d\xi d\eta \tag{2.117}$$

$$[K_{\sigma Re}] = \int_{-1}^{1}\int_{-1}^{1} [G]^T\, [S_R][G]|J| d\xi d\eta \tag{2.118}$$

The total strain energy for the element of sandwich conical shell considering thermal and rotational effects is given by

$$U_e = U_e^E + U_e^{IS} = \frac{1}{2}\{\delta_e\}^T [K_e]\{\delta_e\} + \frac{1}{2}\{\delta_e\}^T [K_{\sigma THe}]\{\delta_e\} + \frac{1}{2}\{\delta_e\}^T [K_{\sigma Re}]\{\delta_e\} \tag{2.119}$$

2.4.3 GOVERNING EQUATION OF MOTION

The governing equation for the dynamic equilibrium of the rotating composite sandwich conical panel is derived using Lagrange's equation of motion as given by

$$\frac{d}{dt}\left[\frac{\partial}{\partial\dot{\delta}}(T_K - U)\right] - \frac{\partial}{\partial\delta}(T_K - U) = \{F^{EX}\} \tag{2.120}$$

where $\{F^{EX}\}$ is the externally applied load vector.

Substituting the expressions of T_{Ke} and U_e into **Eq. (2.120),** the dynamic equilibrium equation of the sandwich conical shell element is derived as

$$[M_e]\{\ddot{\delta}_e\} + [C_e]\{\dot{\delta}_e\} + ([K_e] + [K_{\sigma THe}] + [K_{\sigma Re}] - [K_{Re}])\{\delta_e\} = \{F_{\Omega e}\} + \{P_e^{TH}\} + \{F_e\} \tag{2.121}$$

In the case of moderate rotating speed for which the matrices $[C_e]$ and $[K_{Re}]$ are ignored, the dynamic equilibrium equation of the sandwich conical shell element is reduced to

$$[M_e]\{\ddot{\delta}_e\} + ([K_e] + [K_{\sigma THe}] + [K_{\sigma Re}])\{\delta_e\} = \{F_{\Omega e}\} + \{P_e^{TH}\} + \{F_e\} \tag{2.122}$$

where $[M_e]$, $[K_e]$, $[K_{\sigma THe}]$, $[K_{\sigma Re}]$, and $\{P_e^{TH}\}$ represent the elemental mass matrix, elemental elastic stiffness matrix, elemental geometric stiffness matrix due to thermal load, elemental geometric stiffness matrix due to rotational load, and elemental thermal load vector, respectively, and are defined as

$$[M_e] = \int_{-1}^{1}\int_{-1}^{1}[N]^T[m_I][N]|J|d\xi d\eta \tag{2.123}$$

$$[K_e] = \int_{-1}^{1}\int_{-1}^{1}[B]^T[D][B]|J|d\xi d\eta \tag{2.124}$$

$$[K_{\sigma THe}] = \int_{-1}^{1}\int_{-1}^{1}[G]^T[S_{TH}][G]|J|d\xi d\eta \tag{2.125}$$

$$[K_{\sigma Re}] = \int_{-1}^{1}\int_{-1}^{1}[G]^T[S_R][G]|J|d\xi d\eta \tag{2.126}$$

$$\{P_e^{TH}\} = \int_{-1}^{1}\int_{-1}^{1}[B]^T[F^{TH}]|J|d\xi d\eta \tag{2.127}$$

The integrals in the above expressions are numerically evaluated by using Gaussian quadrature of orders 2 (4 points) (Cook *et al.,* 1989).

The following global form of the dynamic equilibrium equation is obtained by assembling all the elemental matrices and force vectors in reference to the common global coordinates

$$[M]\{\ddot{\delta}\} + ([K] + [K_{\sigma TH}] + [K_{\sigma R}])\{\delta\} = \{F(\Omega^2)\} + \{P^{TH}\} + \{F\} \tag{2.128}$$

where $[M], [K], [K_{\sigma TH}],$ and $[K_{\sigma R}]$ indicate the global mass matrix, global elastic stiffness matrix, global geometric stiffness matrices due to thermal and rotational loads, respectively, $\{\delta\}$

represents the global displacement vector, $F(\Omega^2)$ is the nodal equivalent centrifugal load vector, $\{F\}$ signifies the global externally applied load vector, and $\{P^{TH}\}$ signifies the global thermal load vector.

The matrix $[K_{\sigma R}]$ depends on initial stress distribution due to rotational load and is estimated by iterative procedure (Sreenivasamurthy and Ramamurti, 1981) upon solving:

$$([K] + [K_{\sigma TH}] + [K_{\sigma R}])\{\delta\} = \{F(\Omega^2)\} \tag{2.129}$$

First, stresses due to rotational load are converged to zero, and the above equation becomes

$$([K] + [K_{\sigma TH}])\{\delta\} = \{F(\Omega^2)\} \tag{2.130}$$

Solving **Eq. (2.130)** gives the first set of stress distribution, then **Eq. (2.129)** becomes

$$(([K] + [K_{\sigma TH}]) + [K_{\sigma R}]_1)\{\delta\} = \{F(\Omega^2)\} \tag{2.131}$$

The solution of the above equation gives a new set stress distribution and the stresses are found to converge within two iterations.

2.5 SOLUTION PROCEDURE

2.5.1 BOUNDARY CONDITIONS

In the finite element analysis, boundary conditions are imposed by considering or vanishing the generalized displacements $u, v, w, \beta_x, \beta_y, \beta_x^*,$ and β_x^* at the different nodes of the discretized structure.

The essential boundary conditions of the cantilevered sandwich conical shell are:

$$u = v = w = \beta_x = \beta_y = \beta_x^* = \beta_y^* = 0 \ ; \ x = 0 \tag{2.132}$$

2.5.2 FORMULATING FREE VIBRATION PROBLEM

The natural frequencies and eigenvectors are obtained about the deformed configuration. For static analysis, the time-dependent terms in **Eq. (2.128)** are neglected and the following form is obtained

$$([K] + [K_{\sigma TH}] + [K_{\sigma R}])\{\delta_{static}\} = \{F(\Omega^2)\} \tag{2.133}$$

where δ_{static} is the static equilibrium solution as a result of the combined effects of thermal and centrifugal loads.

In case of the dynamic analyses, both the static as well as the time-dependent components are considered where the displacement vector $\{\delta\}$ is expressed as the sum of a static and a dynamic term. Thus,

$$\{\delta\} = \{\delta_{static}\} + \{\delta_p\} \tag{2.134}$$

where $\{\delta_p\}$ is a small linear time-dependent perturbation about the static deflected position $\{\delta_{static}\}$.

The equation of motion for free vibration is given by

$$[M]\{\ddot{\delta}\} + ([K] + [K_{\sigma TH}] + [K_{\sigma R}])\{\delta\} = 0 \tag{2.135}$$

Assuming harmonic vibrations, $\{\delta\} = \{\delta\}\exp(i\omega_n t)$ we have

$$\left[([K] + [K_{\sigma TH}] + [K_{\sigma R}]) - \omega_n^2[M]\right]\{\delta\} = 0 \tag{2.136}$$

This is a standard eigenvalue problem and is solved for the eigenvalues and eigenvectors by the QR iteration algorithm (Bathe, 1990)

$$[\mathcal{A}]\{\delta\} = \lambda\{\delta\} \tag{2.137}$$

where $[\mathcal{A}] = ([K] + [K_\sigma]_{TH} + [K_\sigma]_R)^{-1}[M]$, and $\lambda = 1/\omega_n^2$

2.5.3 FORMULATING LOW-VELOCITY IMPACT PROBLEM

In the impact problem, the pretwisted nanocomposite sandwich conical shell is subjected to impact with a solid spherical object of mass m_{imp}, radius r_{imp}, and initial velocity V_0 (**Fig. 2.9**). To simplify the problem, the radius of the hub is neglected.

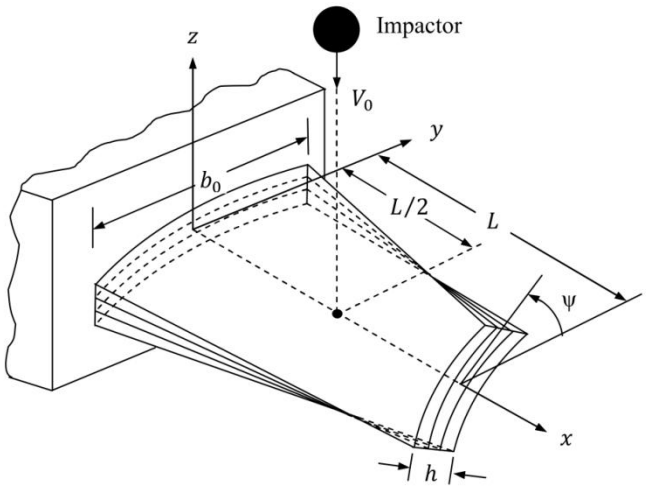

Fig. 2.9 Pretwisted nanocomposite sandwich shallow conical shell impacted with an impactor

Incorporating the contact force resulted in due to the impact, the dynamic equilibrium equation can be expressed as

$$[M]\{\ddot{\delta}\} + ([K] + [K_{\sigma TH}] + [K_{\sigma R}])\{\delta\} = \{F(\Omega^2)\} + \{P^{TH}\} + \{F_C\} \tag{2.138}$$

where $\{F_C\}$ signifies the contact force vector resulted in due to impact and is expressed as

$$\{F_C\} = \{0 \quad 0 \quad 0 \ldots F_{ci} \ldots 0 \quad 0 \quad 0\} \tag{2.139}$$

where F_{ci} is the contact force at the i^{th} node where impact occurs.

The dynamic equilibrium equation of the impactor can be expressed as (Sun and Chen, 1985)

$$m_{imp}\,\ddot{w}_{imp} + F_c = 0 \tag{2.140}$$

where m_{imp} and $\ddot{w}_{imp}$ are the mass and acceleration of the impactor, respectively.

The estimation of the contact force is dependent on a contact law that relates the contact force with the indentation. The local indentation $a(t)$ at the impacted point on the target is defined as

$$a(t) = w_{imp} - w_s \cos\psi \tag{2.141}$$

where w_{imp} denotes the impactor displacement and w_s indicates the mid-surface shell displacement.

According to modified Hertzian contact law (Sun and Chen, 1985), the contact force during loading cycle of impact is determined as

$$F_C = k_c a^{1.5} \quad 0 < a \leq a_m \tag{2.142}$$

where a_m symbolize the maximum indentation during loading cycle and k_c is the modified contact stiffness.

According to Yang and Sun (1982), the modified contact stiffness (k_c) is given by

$$k_c(T) = \frac{4}{3}\frac{\left[\frac{1}{r_{imp}} + \frac{1}{2r_y(L/2,0)}\right]^{-1/2}}{\left[\frac{1-\nu_{imp}^2}{E_{imp}} + \frac{1}{E_{22}(T)}\right]} \tag{2.143}$$

where the terms E_{imp} and ν_{imp} indicate Young's modulus and Poisson's ratio of the spherical impactor, while $E_{22}(T)$ and r_y denote Young's modulus in transverse direction and radius of curvature in $y-$ direction of the target composite sandwich conical shell, respectively.

Permanent indentation takes place even at comparatively less value of impact load, and the unloading phase of the impact process differs notably from the loading phase. Conversely, the reloading curve is different from the unloading curve during subsequent reloading. The contact force upon unloading and reloading can be given as

$$F_C = F_m \left(\frac{a - a_p}{a_m - a_p} \right)^{2.5} \quad \text{for loading cycle} \tag{2.144}$$

$$F_C = F_m \left(\frac{a - a_p}{a_m - a_p} \right)^{1.5} \quad \text{for reloading cycle} \tag{2.145}$$

where F_m is the maximum contact force at the commencement of the unloading cycle and a_p indicates the permanent indentation during contact period and is estimated from the following expression

$$a_p = \begin{cases} 0 & \text{if } a_m < a_{cr} \\ \beta_c (a_m - a_{cr}) & \text{if } a_m \geq a_{cr} \end{cases} \tag{2.146}$$

where $\beta_c = 0.094$ and $a_{cr} = 1.667 \times 10^{-1}$ mm

The dynamic equilibrium equations **Eq (2.138)** and **Eq. (2.140)** of the rotating composite sandwich conical shell and the impactor include the time-dependent contact force F_c. These equations can be treated as a system of ordinary differential equations with constant coefficients and are made to be satisfied at discrete time intervals Δt apart. Newmark's direct integration scheme (Bathe, 1990) is used to obtain the approximate time derivatives and solution of the forced vibration equations. Accordingly, the dynamic equilibrium equations can be written at the time $(t + \Delta t)$ as

$$[M]\{\ddot{\delta}\}^{t+\Delta t} + ([K] + [K_\sigma]_{TH})\{\delta\}^{t+\Delta t} = \{F_c\}^{t+\Delta t} \tag{2.147}$$

$$m_{imp}\{\ddot{w}_{imp}\}^{t+\Delta t} + \{F_c\}^{t+\Delta t} = 0 \tag{2.148}$$

Now, **Eq. (2.147)** can be rewritten in the following form

$$[\hat{K}]\{\delta\}^{t+\Delta t} = \{F_c\}^{t+\Delta t} + \{\hat{R}\}^{t+\Delta t} \tag{2.149}$$

where the effective stiffness matrix $[\hat{K}]$ and effective load vector $\{\hat{R}\}$ for the target sandwich panel are determined as

$$\left[\hat{K}\right] = a_0[M] + [K] + [K_\sigma]_{TH} \tag{2.150}$$

$$\left\{\hat{R}\right\}^{t+\Delta t} = [M](a_0\{\delta\}^t + a_2\left\{\dot{\delta}\right\}^t + a_3\left\{\ddot{\delta}\right\}^t) \tag{2.151}$$

Similarly, **Eq. (2.148)** is rearranged as

$$\hat{k}_{imp}\, w_{imp}{}^{t+\Delta t} = \hat{f}_{imp}{}^{t+\Delta t} \tag{2.152}$$

where the effective stiffness $\hat{k}_{imp}$ and effective load vector $\hat{f}_{imp}$ for the impactor are expressed as

$$\hat{k}_{imp} = a_0 m_{imp} \tag{2.153}$$

$$\hat{f}_{imp}{}^{t+\Delta t} = m_{imp}\left(a_0 w_{imp}{}^t + a_2 \dot{w}_{imp}{}^t + a_3 \ddot{w}_{imp}{}^t\right) - F_C^t \tag{2.154}$$

For each time step, the acceleration and the velocity of the target sandwich panel are obtained from the following expressions

$$\left\{\ddot{\delta}\right\}^{t+\Delta t} = a_0(\{\delta\}^{t+\Delta t} - \{\delta\}^t) - a_2\left\{\dot{\delta}\right\}^t - a_3\left\{\ddot{\delta}\right\}^t \tag{2.155}$$

$$\left\{\dot{\delta}\right\}^{t+\Delta t} = \{\delta\}^t + a_6\left\{\ddot{\delta}\right\}^t + a_7\left\{\ddot{\delta}\right\}^{t+\Delta t} \tag{2.156}$$

Similarly, the acceleration and the velocities of the impactor are obtained as

$$\left\{\ddot{w}_{imp}\right\}^{t+\Delta t} = a_0\left(\left\{w_{imp}\right\}^{t+\Delta t} - \left\{w_{imp}\right\}^t\right) - a_2\left\{\dot{w}_{imp}\right\}^t - a_3\left\{\ddot{w}_{imp}\right\}^t \tag{2.157}$$

$$\left\{\dot{w}_{imp}\right\}^{t+\Delta t} = \left\{w_{imp}\right\}^t + a_6\left\{\ddot{w}_{imp}\right\}^t + a_7\left\{\ddot{w}_{imp}\right\}^{t+\Delta t} \tag{2.158}$$

The following initial conditions are considered in the present analysis

$$\{\delta\}_{t=0} = \left\{\dot{\delta}\right\}_{t=0} = \left\{\ddot{\delta}\right\}_{t=0} = 0 \tag{2.159}$$

$$\left(w_{imp}\right)_{t=0} = \left(\ddot{w}_{imp}\right)_{t=0} = 0; \qquad \left(\dot{w}_{imp}\right)_{t=0} = V_0 \tag{2.160}$$

The integration constants a_i $(i = 1,2,3,4,5,6,7)$ used in **Eqs. (2.150)-(2.158)** are expressed as

$$\begin{gathered} a_0 = \frac{1}{\alpha_n \Delta t^2}; \quad a_1 = \frac{\beta_n}{\alpha_n \Delta t}; \quad a_2 = \frac{1}{\alpha_n \Delta t}; \quad a_3 = \frac{1}{2\alpha_n} - 1; \\ a_4 = \frac{\beta_n}{\alpha_n} - 1; \quad a_5 = \frac{\Delta t}{2}\left(\frac{\beta_n}{\alpha_n} - 2\right); \quad a_6 = \Delta t(1 - \beta_n); \quad a_7 = \beta_n \Delta t \end{gathered} \tag{2.161}$$

where the values $\alpha_n = 0.25$ and $\beta_n = 0.5$ are adopted for constant average acceleration method. **Eq. (2.152)** is solved by the Gauss elimination technique, and the dynamic stresses are obtained at each time step. The time step for each impact case is chosen to satisfy the convergence of the time-based responses.

CHAPTER 3

THERMOELASTIC FREE VIBRATION ANALYSIS OF ROTATING PRETWISTED FG-CNTRC SANDWICH CONICAL SHELLS

3.1 INTRODUCTION

Rotating blades are the key components of turbo-machines which generally work in hot thermal environments under high centrifugal and excitation forces. Consequently, the blades experience fatigue failure caused by the resonance vibration which results in catastrophic failure of the turbo-machines. Hence, the free vibration characteristics of the rotating turbo-machinery blades in thermal environments must be investigated assuming an appropriate model. A pretwisted shallow conical shell is one of the appropriate models for turbo-machinery blades with low aspect ratios. It is seen that the blades are always mounted on a rigid hub (disk) forming the rotating system. In other words, the pretwisted shallow conical shell attached to rotating hub is more practical idealization of the turbo-machinery blades. The sandwich structures with CNTs reinforced composites face sheets and homogeneous core may be the future materials for turbo-machinery blades due to their extraordinarily high stiffness-to-weight ratio and other preferred properties. In this chapter, free vibration characteristics of rotating pretwisted sandwich conical shells with FG-CNTRC face sheets considering the effect of hub radius in thermal environments are investigated. The numerical results and discussions followed by convergence, comparison, and parametric studies are presented systematically.

3.2 NUMERICAL RESULTS AND DISCUSSIONS

In-house computer codes based on the proposed mathematical formulation have been developed to investigate the free vibration characteristics of the cantilevered sandwich conical shells with FG-CNTRC face sheets and homogenous core considering the effect of hub radius. In this work, poly methyl methacrylate (PMMA) and (10, 10) armchair SWCNTs are considered as matrix and reinforcing constituents for the CNTRC face sheets, respectively. The temperature-dependent material properties of PMMA are taken as (Wang and Shen, 2012): $E^m = (3.52 - 0.0034T)$

GPa, $\nu^m = 0.34$, $\rho^m = 1150$ kg/m^3, and $\alpha^m = 45.0(1 + 0.0005\Delta T) \times 10^{-6}$/K, where $T = T_0 + \Delta T$ and $T_0 = 300$ K. The effective material properties and effectiveness parameters of SWCNTs are listed in **Table 3.1** and **Table 3.2,** respectively (Mehar and Panda, 2018). Titanium alloy (Ti-6Al-4V) is considered as homogeneous core with the following material properties (Wang and Shen, 2012): $E_c = 122.56(1 - 4.586 \times 10^{-4}T)$ GPa, $\nu_c = 0.29$, $\rho_c = 4429$ kg/m^3, and $\alpha_c = 7.5788(1 + 6.638 \times 10^{-4}T - 3.147 \times 10^{-4}T^2) \times 10^{-6}$/K.

The following geometrical dimensions of the FG-CNTRC sandwich conical shells are considered: $s = 0.4$ m, $L/s = 0.7$, $\phi_0 = \phi_v = 20°$.

Table 3.1 Material properties of SWCNTs (10, 10) at different levels of temperature **[** L= 9.26 nm, R = 0.68 nm, h = 0.067 nm, ν_{12}^{CNT}= 0.175, ρ_{CNT} = 1400 kg/m^3] (Mehar and Panda, 2018)

Temp, T (K)	E_{11}^{CNT} (GPa)	E_{22}^{CNT} (GPa)	G_{12}^{CNT} (GPa)	α_{11}^{CNT} (10^{-6}/K)	α_{22}^{CNT} (10^{-6}/K)
300	5646.6	7080.0	1944.5	3.4584	5.1682
400	5567.9	6981.4	1970.3	4.1496	5.0905
500	5530.8	6934.8	1964.3	4.5361	5.0189
700	5474.4	6864.1	1964.4	4.8877	4.8943

Table 3.2 Effectiveness parameters of the SWCNTs (Mehar and Panda, 2018)

V_{CNT}^*	η_1	η_2	η_3
0.12	0.137	1.022	0.715
0.17	0.142	1.626	1.138
0.28	0.141	1.585	1.109

3.3 CONVERGENCE STUDY

In mesh convergence study, the fundamental frequencies (Hz) of non-rotating FG-CNTRC sandwich conical shell with three different types of CNTs distribution patterns (FG-UU, FG-VΛ, and FG-ΛV) obtained from the present FEM considering different mesh sizes of 4×4, 6×6, 8×8, and 10×10 for two values of pretwist angles ($\psi = 0°$ and 30°) at two different levels of temperatures $T = 300$ K and 500 K are plotted in **Fig. 3.1**. It is evident that the fundamental frequencies of the FG-CNTRC conical shell converge with the mesh size of 8×8 irrespective of CNTs grading pattern, pretwist angle, and temperature. On the basis of this convergence study, a

converged mesh size of 8×8 with 64 elements and 225 nodes has been adopted in the finite element vibration analysis of the pretwisted FG-CNTRC sandwich conical shells.

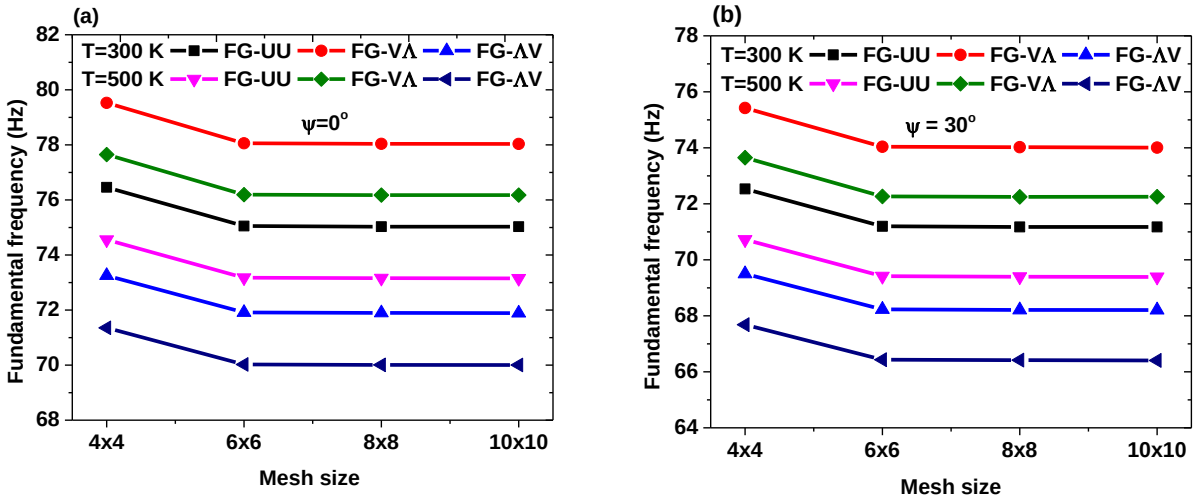

Fig. 3.1 Convergence study of FG-CNTRC sandwich conical shells with three different CNTs distribution patterns in thermal environments for two pretwist angles (a) ψ =0º and (b) ψ =30º [$s = 0.4$ m, $L/s = 0.7, \phi_0 = \phi_v = 20°, s/h = 100, h_c/h_f = 2,\ \Omega^{\mathrm{ND}} = 0.0$]

3.4 COMPARISON STUDY

The accuracy of the computer codes developed is examined by comparing the results with those benchmark results available in open literature. In the first comparative study, the non-dimensional fundamental frequencies $\left(\varpi = \omega_n {b_0}^2\sqrt{\rho h/D}\right)$ of non-rotating isotropic shallow conical shell corresponding to different pretwist angles ($\psi = 0°$, 15°, 30°, and 45°) and span length to cone length ratios ($L/s = 0.6$, 0.7, and 0.8) are determined from the present FEM and are compared with those obtained by Liew *et al.* (1994) as furnished in **Table 3.3.** A second comparative study considers a simply supported FG-CNTRC plate with four different grading patterns (UD, FG-V, FG-O, and FG-X). For this example, the first three non-dimensional natural frequencies $\left(\varpi = \omega L^2/h\sqrt{\rho_0/E_0}\right)$ of the FG-CNTRC plates at three levels of temperatures $T =$ 300 K, 500 K, and 700 K are compared with those of Lei *et al*. (2013) as presented in **Table 3.4**. In the third example, the first three non-dimensional natural frequencies $\left(\varpi = \omega_n L^2/h\sqrt{\rho_{c0}/E_{c0}}\right)$ of simply supported sandwich plates with FG-CNTRC face sheets and

titanium alloy core (Ti-6Al-4V) for different core-to-face sheets thickness ratios ($h_c/h_f = 8$, 6, and 4) and CNTs volume fractions (V_{CNT}^{*} =0.12, 0.17, and 0.28) at reference temperature $T_0 = 300$ K are presented for comparison with those reported by Wang and Shen (2012) in **Table 3.5**.

Table 3.3 Non-dimensional fundamental frequencies $\left(\varpi = \omega_n {b_0}^2\sqrt{\rho h/D}\right)$ of pretwisted shallow conical shells with different pretwist angles [$s/h = 1000$, ϕ_v =15°, ϕ_0=30°, $\nu = 0.3$, $D = Eh^3/12(1-\nu^2)$].

Pretwist	Present FEM			Liew *et al.* (1994)		
angle (ψ)	$L/s = 0.6$	$L/s = 0.7$	$L/s = 0.8$	$L/s = 0.6$	$L/s = 0.7$	$L/s = 0.8$
0º	0.35690	0.30446	0.27699	0.35997	0.30608	0.27832
15º	0.33858	0.29278	0.26853	0.34116	0.29410	0.26964
30º	0.28692	0.25699	0.24133	0.28828	0.25725	0.24179
45º	0.21010	0.19645	0.19114	0.21015	0.19603	0.19070

Table 3.4 Non-dimensional natural frequencies $\left(\varpi = \omega_n L^2/h\sqrt{\rho_0/E_0}\right)$ of FG-CNTRC plates with different CNTs grading patterns in thermal environments [$V_{CNT}^{*} = 0.12$, L/b =1, b/h =10, $\eta_1 = 0.137$, η_2 =1.002, $\eta_3 = 0.7$].

Temp.	Mode	Present FEM				Lei *et al*. (2013)			
(T), K	sequence	UD	FG-V	FG-O	FG-X	UD	FG-V	FG-O	FG-X
300	1	12.2763	11.6057	10.3734	13.2021	12.1261	11.3095	10.4535	13.1289
	2	17.0105	16.6848	15.7180	17.1311	16.5545	16.2611	15.353	17.1045
	3	17.0766	17.1778	17.1311	17.1311	16.9835	17.0406	17.0365	17.3901
500	1	10.8682	10.3243	9.2258	11.5985	10.9644	10.2442	9.5378	11.6675
	2	14.1692	14.1780	13.2971	14.2316	14.4941	14.2264	13.4627	14.5948
	3	14.4573	14.2755	14.2317	14.5212	14.5494	14.5404	14.5394	15.1371
700	1	9.0761	8.7134	7.8185	9.5626	9.2518	8.7751	8.2728	9.6982
	2	10.5513	10.7270	10.5567	10.6789	11.5159	11.5436	11.1033	11.5519
	3	11.3727	11.3039	10.6793	11.4105	11.8279	11.5514	11.509	12.2867

Table 3.5 Non-dimensional natural frequencies $\left(\varpi = \omega_n L^2/h\sqrt{\rho_{c0}/E_{c0}}\right)$ of FG-CNTRC sandwich plates at reference temperature $T_0 = 300$ K [L/b =1, $b/h = 20$, h_f = 1 mm]

h_c/h_f	Mode sequence	Present FEM			Wang and Shen (2012)		
		V^*_{CNT} =0.12	V^*_{CNT} =0.17	V^*_{CNT} =0.28	V^*_{CNT} =0.12	V^*_{CNT} =0.17	V^*_{CNT} =0.28
8	1	5.0808	5.2954	5.6610	5.0775	5.2927	5.6588
	2	11.7129	11.8772	12.0651	11.6798	11.8455	12.0346
	3	14.1040	15.1690	17.0176	14.0903	15.1634	17.0354
6	1	4.9139	5.1913	5.6559	4.9119	5.1905	5.6569
	2	11.0112	11.2306	11.4820	10.9850	11.2067	11.4603
	3	14.1188	15.4387	17.6698	14.1158	15.4544	17.7366
4	1	4.6828	5.0709	5.7004	4.6845	5.0763	5.7131
	2	9.8842	10.2120	10.5866	9.8689	10.1018	10.5823
	3	14.2543	15.9656	18.7339	14.3043	16.0716	18.9850

Table 3.6 Natural frequencies (Hz) of cantilevered MWCNT-reinforced composite sandwich plates with different aspect ratios [Weight fraction of MWCNT= 0.3%, $h = 0.0048$ m, $b = 0.15$ m].

L/b	Source	Mode sequence				
		1	2	3	4	5
1	Present FEM	64.61	156.85	394.16	502.28	568.84
	Mehar *et al*. (2020) FEM	65.82	159.11	404.85	510.84	584.11
	Mehar *et al.* (2020) Experiment	63.82	154.34	388.66	469.97	549.66
1.2	Present FEM	44.78	125.16	276.44	437.24	469.64
	Mehar *et al.* (2020) FEM	45.17	127.12	285.08	449.86	477.13
	Mehar *et al.* (2020) Experiment	44.26	123.31	273.67	413.87	448.50
1.4	Present FEM	32.84	103.82	203.53	353.45	450.31
	Mehar *et al.* (2020) FEM	33.14	105.56	210.40	364.15	457.76
	Mehar *et al.* (2020) Experiment	32.48	102.39	201.98	335.02	430.30

Table 3.7 Non-dimensional fundamental frequencies $\left(\varpi = \omega_n L^2\sqrt{\rho h^2/D}\right)$ of cantilevered isotropic plate rotating at different rotational speeds [L/b =1, h/L = 0.12, $D = Eh^3/12(1-\nu^2)$, $\nu = 0.3$].

Non-dimensional rotational speed (Ω^{ND})	Present FEM	Sreenivasamurthy and Ramamurthi (1981b)
0.0	3.41684	3.43685
0.2	3.49410	3.51858
0.4	3.71598	3.75280
0.6	4.05798	4.12875
0.8	4.49133	4.56786
1.0	4.99059	5.09167

A fourth example follows the theoretical and experimental studies by Mehar *et al.* (2020) on the free vibration of MWCNT-reinforced nanocomposite sandwich plates with cantilever boundary conditions. The first five natural frequencies (Hz) of the nanocomposite sandwich plates with three different aspect ratios (L/b = 1, 1.2, and 1.4) are also presented in **Table 3.6** for comparison with the theoretical and experimental results of Mehar *et al.* (2020). Finally, the non-dimensional fundamental frequencies of cantilevered isotropic plates rotating at different non-dimensional rotational speeds (Ω^{ND} = 0.0, 0.2, 0.4, 0.6, 0.8, and 1.0) are determined and compared with those of Sreenivasamurthy and Ramamurthi (1981b) as furnished in **Table 3.7**. All these comparative studies show that the results obtained from the computer codes agree well with those reported in the literature, thus verifying the accuracy of the present formulation.

3.5 PARAMETRIC STUDY

Once the proposed formulation and solution method have been validated, parametric studies are carried out in this section. The effects of some important parameters such as core-to-face sheets thickness ratio, temperature, cone length-to-thickness ratio, and non-dimensional rotational speed ($\Omega^{ND} = \Omega/\omega_0$; ω_0 being the natural frequency of non-rotating sandwich conical shell) on the natural frequencies of the pretwisted FG-CNTRC sandwich conical shells with different CNTs grading patterns, CNTs volume fractions and pretwist angles in uniform thermal environments are scrutinized.

3.5.1 EFFECT OF CORE-TO-FACE SHEETS THICKNESS RATIO

The variations of the first three natural frequencies (Hz) against core-to-face sheets thickness ratio h_c/h_f of the pretwisted FG-CNTRC sandwich conical shells corresponding to five different CNTs distribution patterns (FG-UU, FG-VΛ, FG-ΛV, FG-OO, and FG-XX), three values of CNTs volume fraction (V_{CNT}^* =0.12, 0.17, and 0.28), and four values of pretwist angle ($\psi = 0°$, 15°, 30°, and 45°) at temperature $T = 500$ K are shown in **Figs. 3.2-3.4**. It is seen that the frequency values decrease monotonically with increasing h_c/h_f ratio for all the cases considered until about $h_c/h_f = 10$, after which the frequency curves become almost flat. The type of CNTs distribution pattern is seen to affect the predicted values of the natural frequency for the whole range of h_c/h_f; in particular, the FG-VΛ type of distribution pattern results in the highest value of frequency followed by FG-XX, FG-UU, FG-OO, and then FG-ΛV types, respectively, as shown in **Fig. 3.2.** The special feature of FG-VΛ pattern, i.e., maximum and minimum distributions of CNTs near to outer and inner surfaces of the face sheets, respectively, lead to make stiffer sandwich shell and higher values of natural frequencies compared to other types of distribution patterns. In contrast, completely reverse distribution pattern of CNTs in the face sheets for FG-ΛV type pattern lead to make more flexible sandwich shell and lower values of frequency. Note that the frequency values of FG-XX, FG-UU, and FG-OO patterns are approximately the same. However, the effect of distribution pattern on the frequencies is more evident for lower values of the h_c/h_f since the strength contribution of the CNTRC face sheets decreases considerably with increasing h_c/h_f ratio. Clearly, the maximum rate of reduction in frequency with respect to h_c/h_f ratio is noticed in the case of FG-VΛ, while the minimum rate of reduction is found for FG-ΛV. **Fig. 3.3** portrays the effect of CNTs volume fraction V_{CNT}^* on the variation of the first three natural frequencies of pretwisted (ψ =15°) FG-VΛ CNTRC sandwich conical shells with the core-to-thickness ratio h_c/h_f at temperature $T = 500$K. It is found that the higher values of V_{CNT}^* always result in higher values of frequencies because the elastic properties of the CNTs are larger than the polymer matrix in the CNTRC face sheets. In addition, the relative decrease in frequencies due to increasing h_c/h_f ratio is found to be higher for $V_{CNT}^* = 0.28$ and lower for $V_{CNT}^* = 0.12$ compared to that of $V_{CNT}^* = 0.17$. The first three natural frequencies of FG-VΛ CNTRC sandwich conical shells having CNTs volume fraction $V_{CNT}^* = 0.12$ for four different values of pretwist angles $\psi =$ 0°, 15°, 30°, and 45° are plotted against the core-to-thickness ratio h_c/h_f in **Fig. 3.4**. It can be noted that frequency values for the

first and second modes decrease with increasing pretwist angle, while a completely reverse trend of frequency variation with pretwist angle is found for the third mode for the whole range of h_c/h_f ratio. This may be due to the reduction of the structural stiffness with an increase in pretwist angle in the case of the first two modes, while for the third mode it may be due to the coupling effect of bending and torsion. However, the effect of pretwist angle on the variation of the frequencies with h_c/h_f ratio is almost negligible.

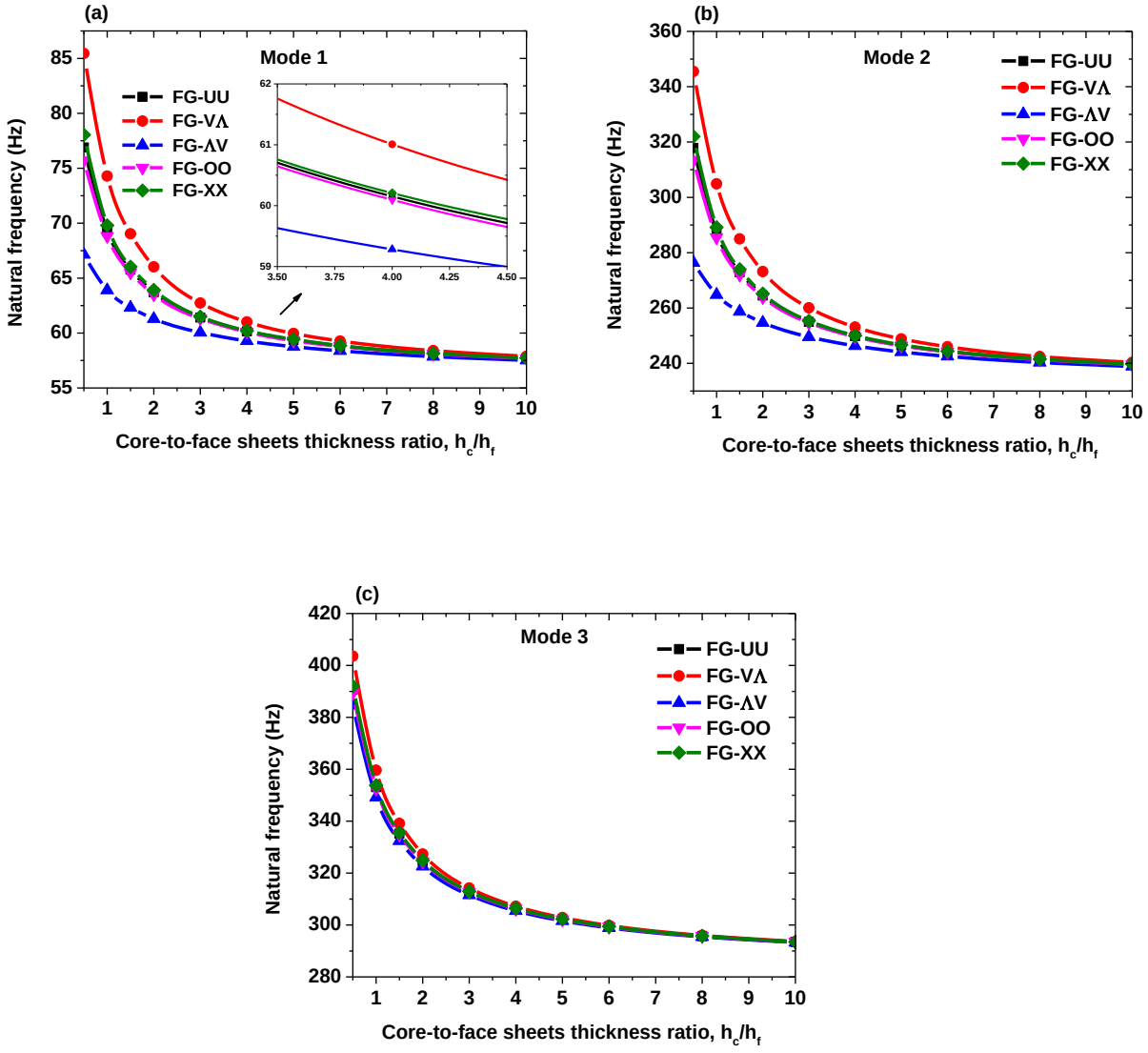

Fig. 3.2 Variation of natural frequencies (Hz) of the pretwisted FG-CNTRC sandwich conical shells against core-to-face sheets thickness ratio for different CNTs grading patterns at temperature $T = 500$ K: (a) Mode 1, (b) Mode 2, and (c) Mode 3 $[s = 0.4$ m, $L/s = 0.7$, $\phi_0 = \phi_v = 20°$, $s/h = 100$, $\psi = 15°$, $r/L = 1$, $V^*_{CNT} = 0.12$, $\Omega^{ND} = 0.0]$

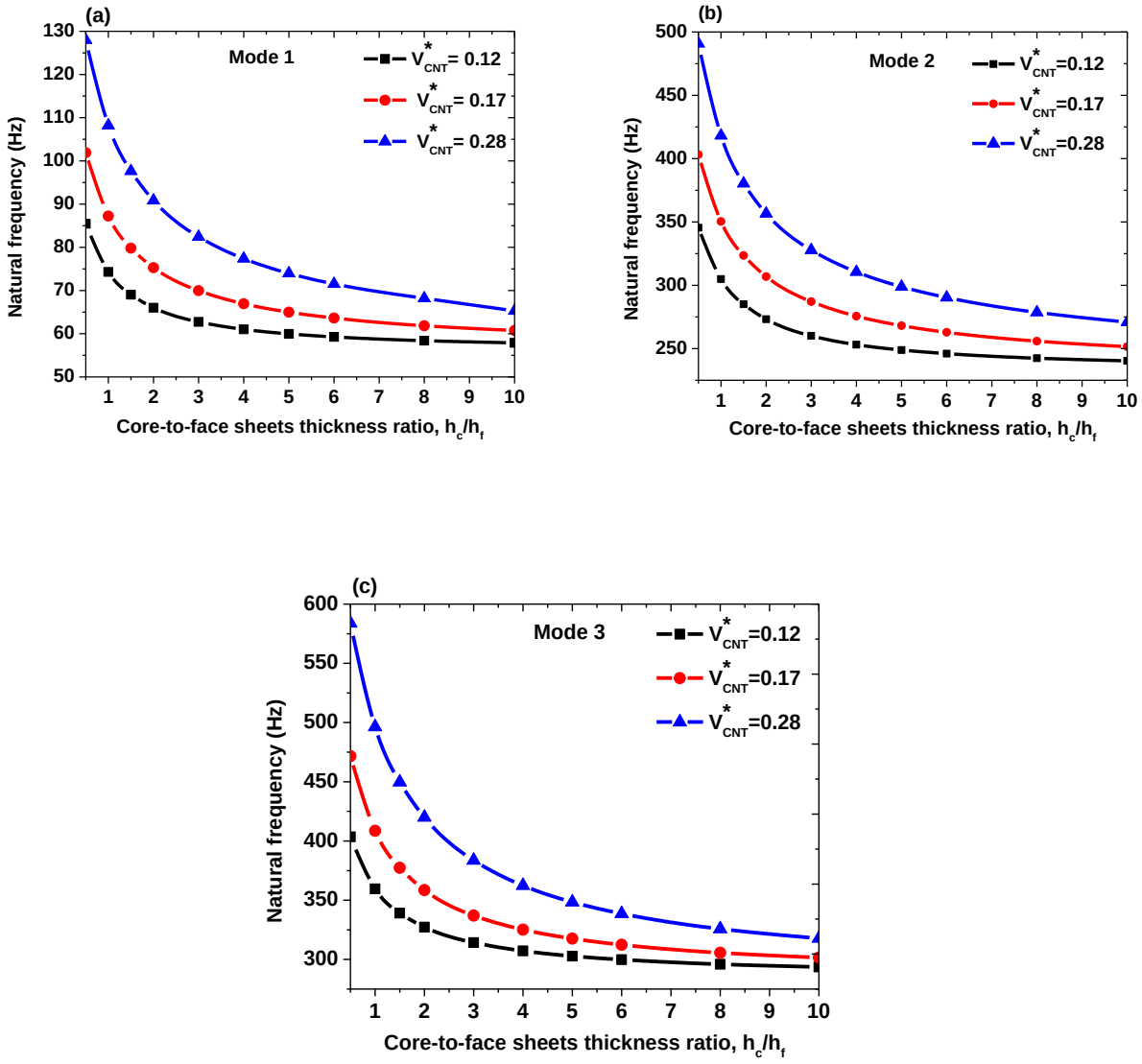

Fig. 3.3 Variation of natural frequencies (Hz) of the pretwisted FG-VΛ CNTRC sandwich conical shells against core-to-face sheets thickness ratio for different values of CNTs volume fraction at temperature $T = 500$ K: (a) Mode 1, (b) Mode 2, and (c) Mode 3 [$s =$ 0.4 m, $L/s =$ 0.7, $\phi_0 = \phi_v = 20°$, $s/h = 100$, $\psi = 15°$, $r/L = 1$, $\Omega^{ND} = 0.0$]

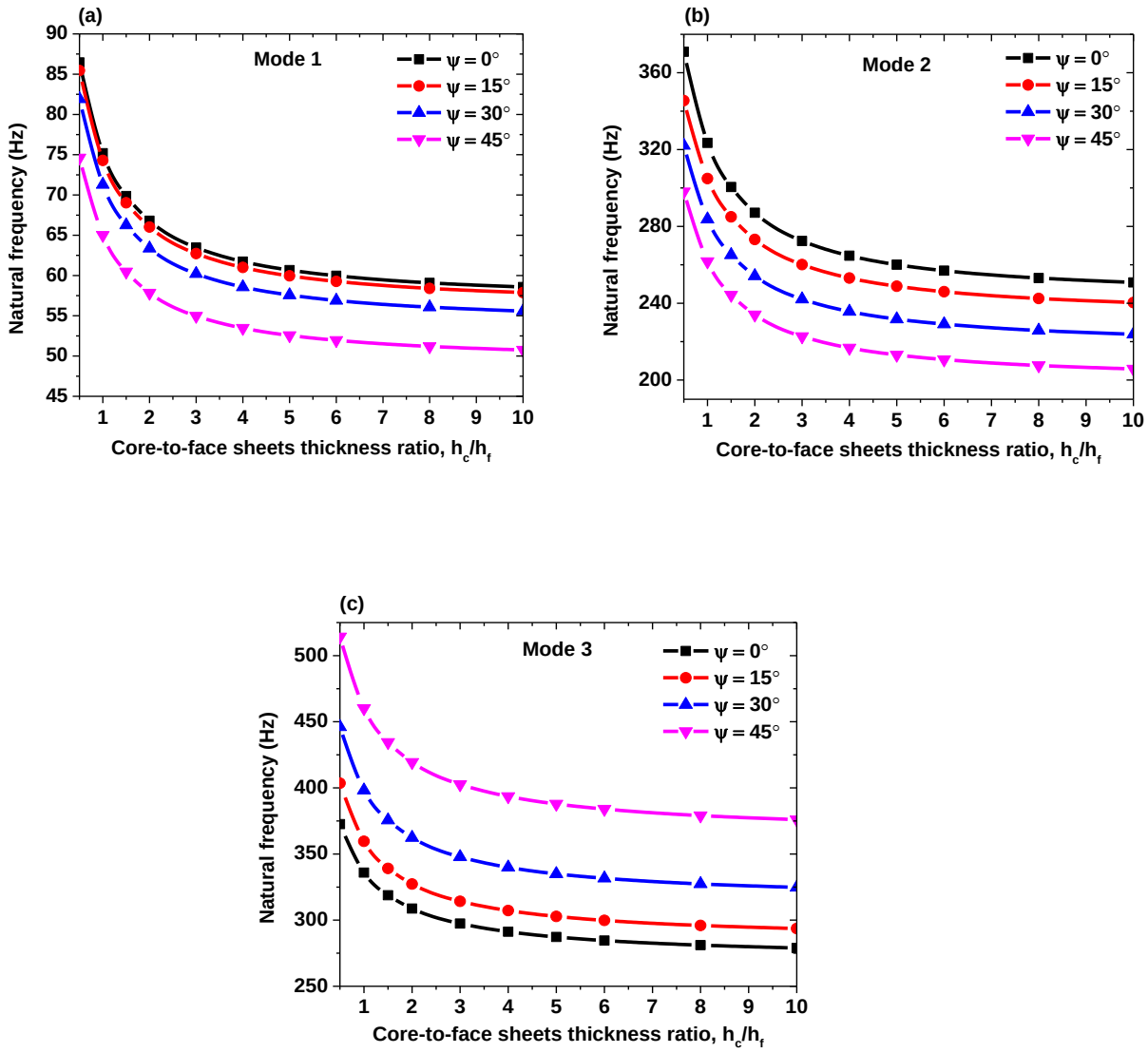

Fig. 3.4 Variation of natural frequencies (Hz) of the pretwisted FG-VΛ CNTRC sandwich conical shells against core-to-face sheets thickness ratio for different values of pretwist angle at temperature $T = 500$ K: (a) Mode 1, (b) Mode 2, and (c) Mode 3 [$s =$ 0.4 m, $L/s = 0.7$, $\phi_0 = \phi_v = 20°$, $s/h = 100$, $r/L = 1$, $V_{CNT}^{*} = 0.12$, $\Omega^{ND} = 0.0$]

3.5.2 EFFECT OF TEMPERATURE

The variations of the first three natural frequencies of pretwisted sandwich conical shells with temperature for different CNTs distribution patterns (FG-UU, FG-VΛ, FG-ΛV, FG-OO, and FG-XX), CNTs volume fraction values ($V_{CNT}^{*} = 0.12$, 0.17, and 0.28), pretwist angles ($\psi = 0°$, 15°, 30°, and 45°), and core-to-face sheets thickness ratios ($h_c/h_f = 0.5$, 1, 2, 5, and 10) are shown

in **Figs. 3.5-3.8,** respectively**.** As expected, the decrease in all frequencies with the rise in temperature is clearly seen for all the cases considered. It is due to the fact that the increase in temperature degrades the material properties of both the CNTRC face sheets and titanium alloy core constituents of the sandwich shell in addition to inducing internal thermal strains resulting in a decrease in the overall stiffness of the pretwisted sandwich conical shell panel.

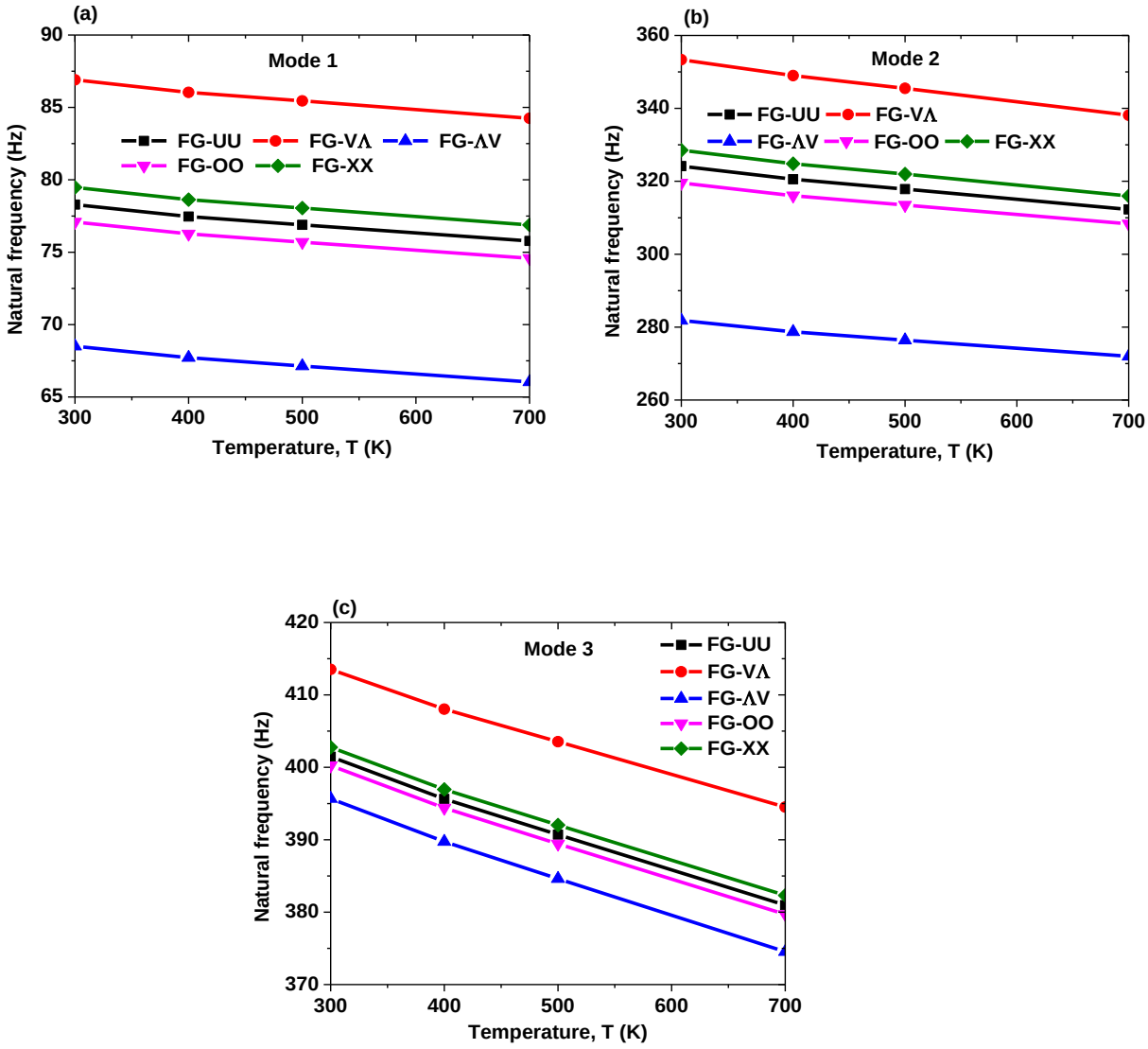

Fig. 3.5 Variation of natural frequencies (Hz) of the pretwisted FG-CNTRC sandwich conical shells against temperature for different CNTs distribution patterns: (a) Mode 1, (b) Mode 2, and (c) Mode 3 [$s =$ 0.4 m, $L/s = 0.7$, $\phi_0 = \phi_v = 20°$, $s/h = 100$, $\psi = 15°$, $r/L = 1$, $V_{CNT}^{*} = 0.12$, $\Omega^{ND} = 0.0$]

As seen from **Figs. 3.5-3.7,** the frequency variation curves are almost parallel to each other, indicating that the thermal strains induced are almost independent of the CNTs grading pattern, CNTs volume fraction, and pretwist angle. However, the effect of temperature on natural frequencies is more apparent for higher values of h_c/h_f ratio than its lower values, as displayed in **Fig. 3.8**. It is due to the higher stiffness degradation of the titanium alloy core layer than the CNTRC face sheets with an increase in temperature.

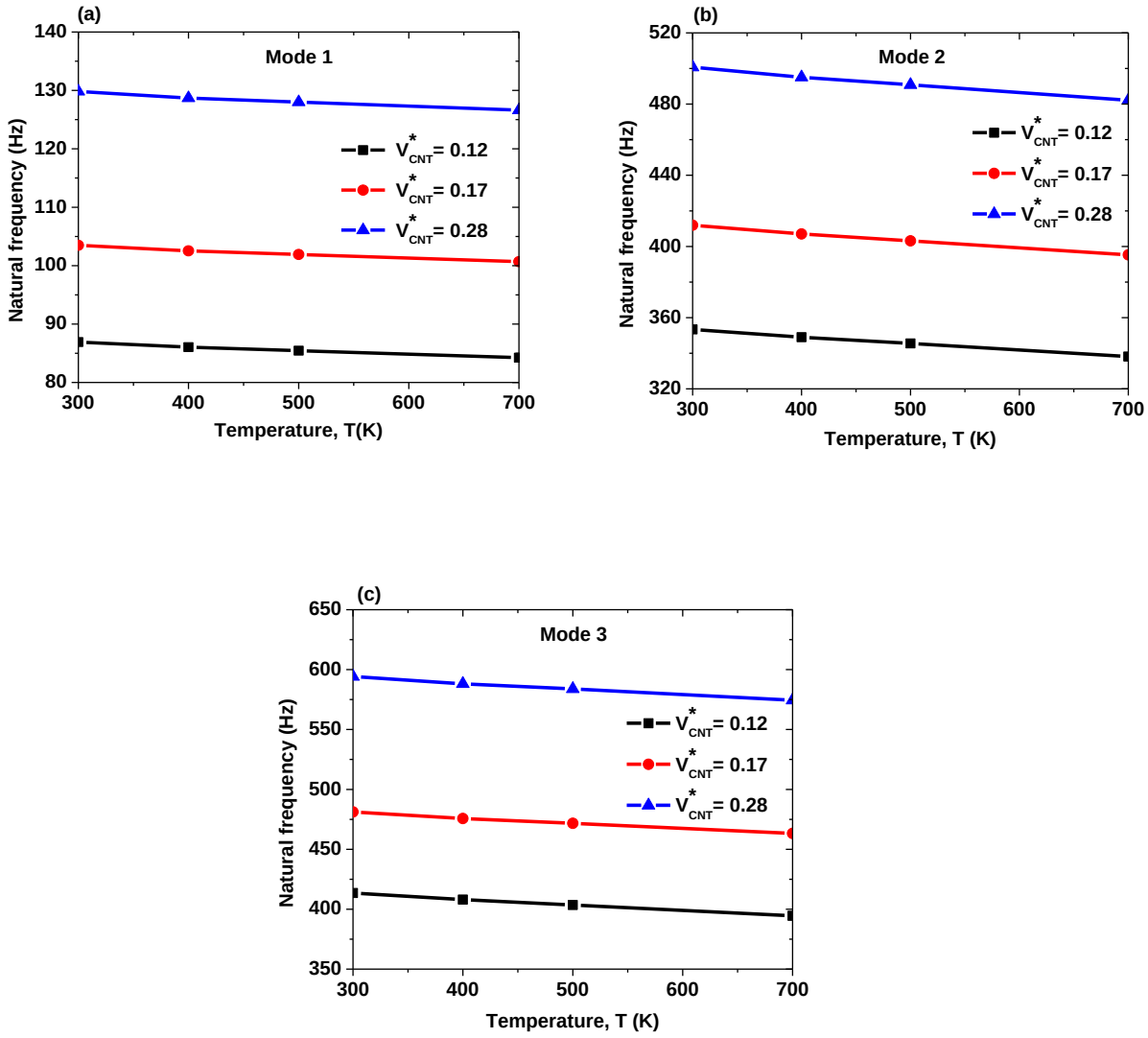

Fig. 3.6 Variation of natural frequencies (Hz) of the pretwisted FG-VΛ CNTRC sandwich conical shells against temperature for different CNTs volume fractions: (a) Mode 1, (b) Mode 2, and (c) Mode 3 [$s =$ 0.4 m, $L/s = 0.7$, $\phi_0 = \phi_v = 20°$, $s/h = 100$, $\psi = 15°$, $r/L = 1$, $V^*_{CNT} = 0.12$, $h_c/h_f = 0.5$, $\Omega^{ND} = 0.0$]

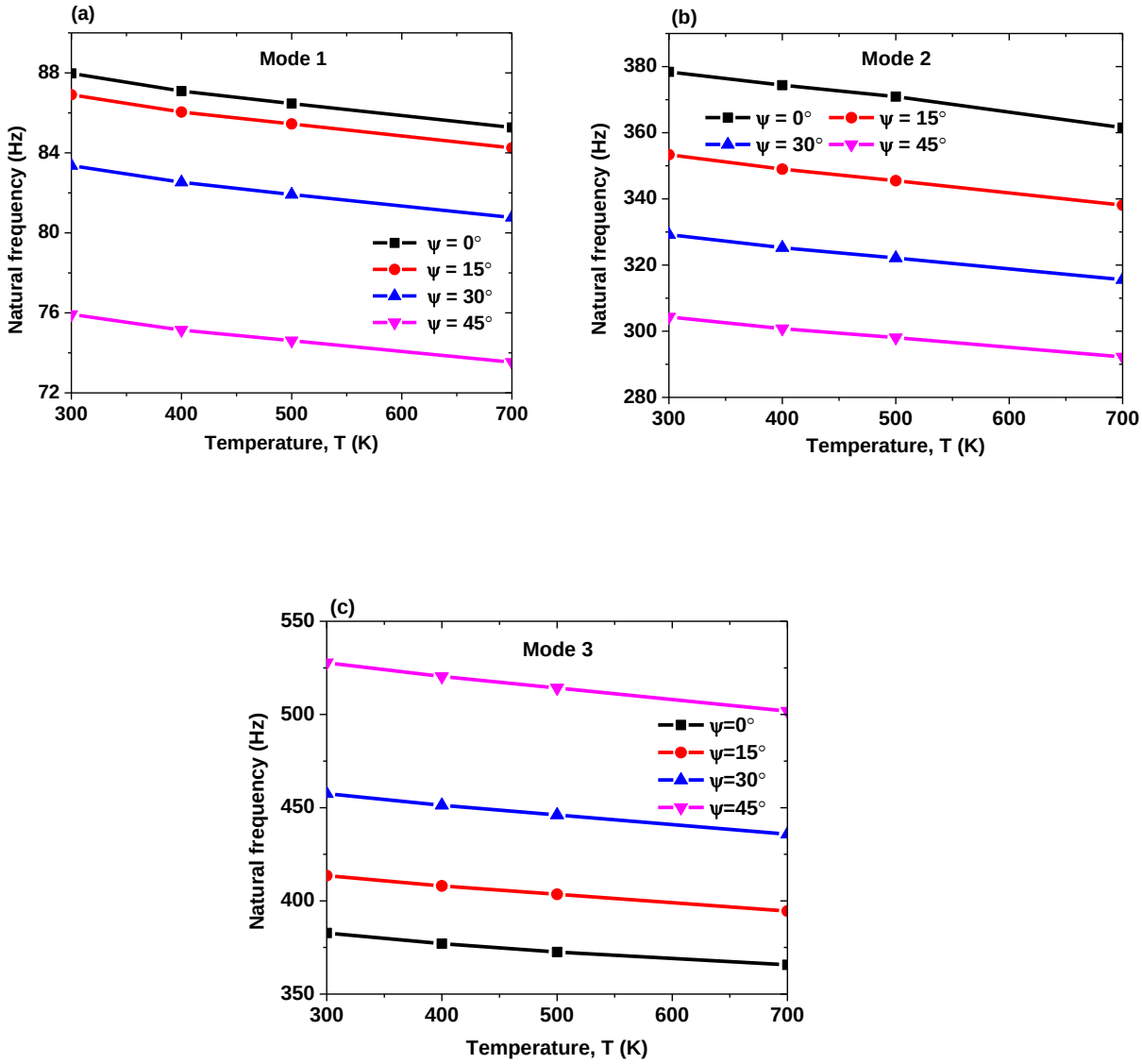

Fig. 3.7 Variation of natural frequencies (Hz) of the pretwisted FG-VΛ CNTRC sandwich conical shells against temperature for different pretwist angles: (a) Mode 1, (b) Mode 2, and (c) Mode 3 [$s =$ 0.4 m, $L/s = 0.7$, $\phi_0 = \phi_v = 20°$, $s/h = 100$, $r/L = 1$, $h_c/h_f = 0.5$, $V_{CNT}^{*} = 0.12$, $\Omega^{ND} = 0.0$]

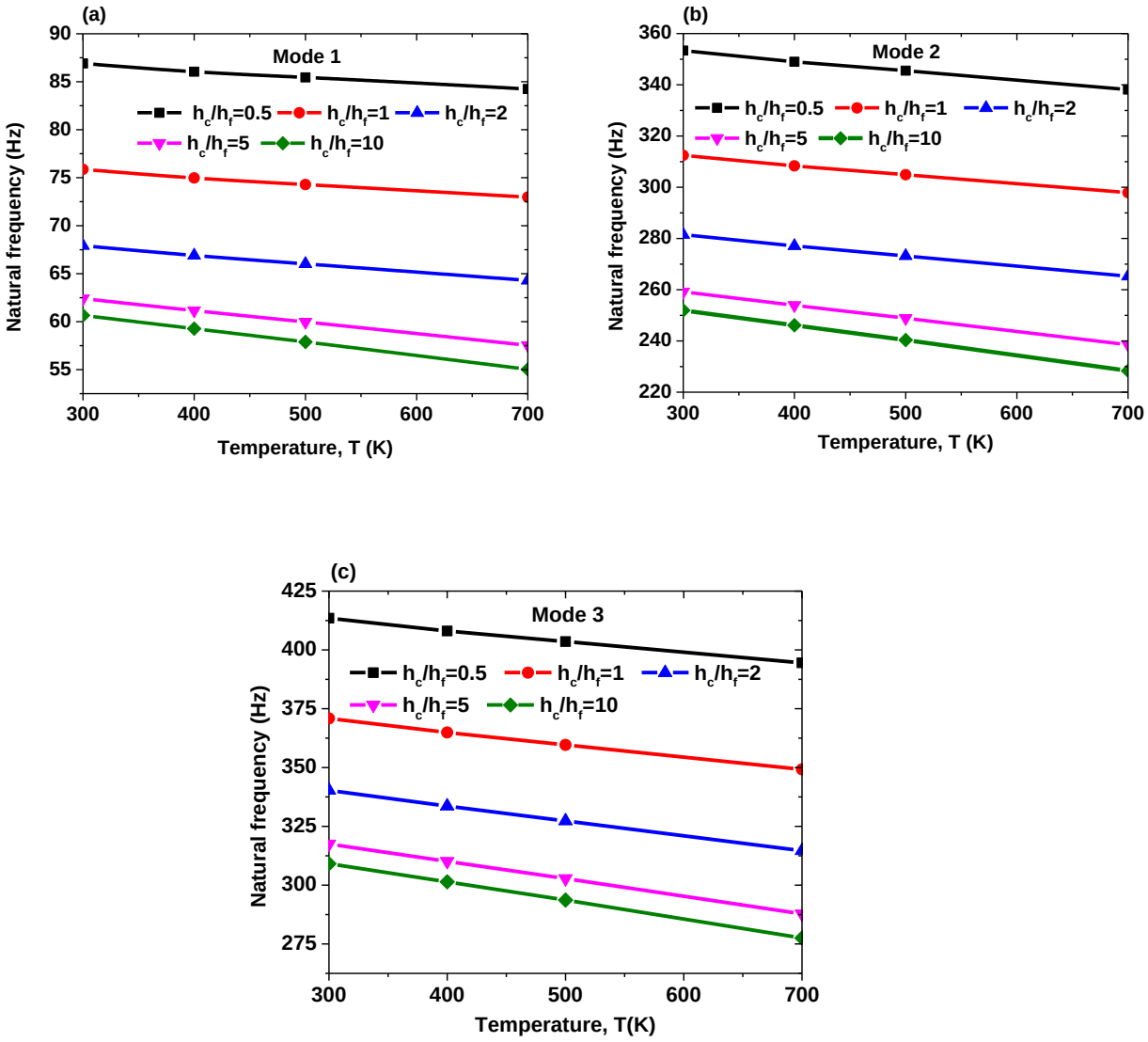

Fig.3.8 Variation of natural frequencies (Hz) of the pretwisted FG-VΛ CNTRC sandwich conical shell panels against temperature for different core-to-face sheets thickness ratio: (a) Mode 1, (b) Mode 2, and (c) Mode 3 [$s =$ 0.4 m, $L/s = 0.7$, $\phi_0 = \phi_v = 20°$, $s/h = 100$, $r/L = 1$, $\psi = 15°$, $V_{CNT}^{*} = 0.12$, $\Omega^{ND} = 0.0$]

3.5.3 EFFECT OF CONE LENGTH-TO-THICKNESS RATIO

The variation of the fundamental frequency against cone length-to-thickness ratio s/h of the pretwisted FG-CNTRC sandwich conical shells for different CNTs grading patterns (FG-UU, FG-VΛ, FG-ΛV, FG-OO, and FG-XX), CNTs volume fraction values (V_{CNT}^{*} =0.12, 0.17, and

0.28), pretwist angles (ψ =0°, 15°, 30°, and 45°), and core-to-face sheets thickness ratios (h_c/h_f = 0.5, 1, 2, 5, and 10) are illustrated in **Fig. 3.9.**

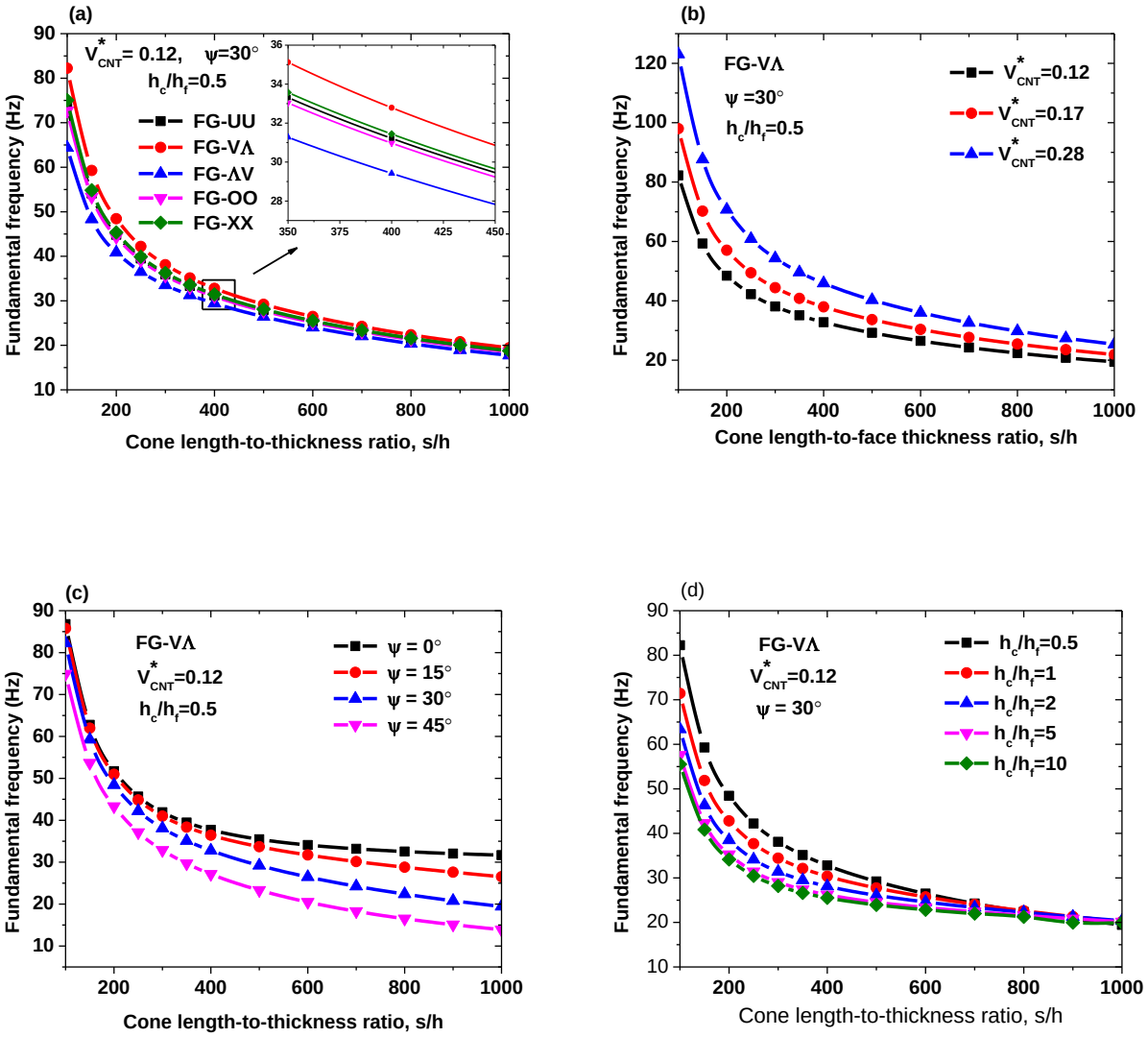

Fig.3.9 Variation of fundamental frequency (Hz) of the pretwisted FG-CNTRC sandwich conical shells with cone length-to-thickness ratio [$s =$ 0.4 m, $L/s =$ 0.7, $\phi_0 = \phi_v = 20°$, $r/L = 1$, $\Omega^{ND} = 0.0$, $T = 500$ K]

The obtained results imply that the fundamental frequency decreases monotonically with respect to the s/h ratio for all scenarios considered. This may be attributed due to the fact that the sandwich conical shell becomes more flexible when its thickness decreases. It is observed that the fundamental frequency value of the pretwisted CNTRC sandwich conical shell with

FG-VΛ type grading pattern is the maximum, while its minimum value is found for FG-ΛV type grading pattern in the whole range of the s/h ratio as displayed in **Fig. 3.9(a).** Further, the effect of the grading pattern on the fundamental frequency becomes comparatively weak as the s/h ratio increases. It is evident from **Fig. 3.9(b)** that the relative decrease of fundamental frequency for FG-VΛ pattern in the range of s/h ratio is larger for $V_{CNT}^{*} = 0.28$ and smaller for $V_{CNT}^{*} = 0.12$ in comparison with that of $V_{CNT}^{*} = 0.17$. **Fig. 3.9(c)** shows that the change in fundamental frequency values of FG-VΛ type grading pattern with respect to pretwist angle ψ is found to be more pronounced for higher values of s/h ratios than its lower values**.** In other words, the effect of pretwist angle on fundamental frequency is more significant for thinner sandwich conical shells than that for thicker ones. Besides, the effect of h_c/h_f ratio on fundamental frequency is considerable and indistinguishable for lower and higher values of the s/h ratios, respectively, as shown in **Fig. 3.9(d).**

3.5.4 EFFECT OF ROTATIONAL SPEED

Figs. 3.10-3.14 present the variations of the first four natural frequencies of pretwisted FG-CNTRC sandwich conical shells with non-dimensional rotational speed Ω^{ND} for different CNTs grading patterns (FG-UU, FG-VΛ, FG-ΛV, FG-OO, and FG-XX), pretwist angles ($\psi = 0°$, 15°, 30°, and 45°), core-to-face sheets thickness ratios ($h_c/h_f =$ 0.5, 1, 2, 5, and 10), thermal conditions ($T =$ 300 K, 400 K, 500 K, and 700 K), and hub radius-to-span length ratios ($r/L =$ 0.0, 0.5,1, 1.5, and 2). The results obtained for all cases indicate that the frequency values increase monotonically with increasing non-dimensional rotational speed Ω^{ND}. The increase in natural frequency may be attributed to the centrifugal stiffening, i.e., increase in structural stiffness of the sandwich conical shell with the increase in rotational speed. It can be seen from **Fig. 3.10** that sandwich shell having FG-VΛ type grading pattern exhibits the largest value of frequency, while the smallest value of frequency is found in case of FG-ΛV type grading pattern in the range of rotational speed $\Omega^{ND} \in (0, 1)$ for all four modes. However, the centrifugal stiffening in terms of increase of frequency with respect to Ω^{ND} is affected by the type of CNTs grading pattern. For example, the fundamental frequencies of pretwisted ($\psi = 30°$) sandwich conical shell with $s/h = 100$, $r/L = 1$, and $h_c/h_f = 2$ for the patterns FG-UU, FG-VΛ, FG-ΛV, FG-OO, and FG-XX increase by factors 1.8646, 1.8814, 1.8477, 1.8478, and

1.8813, respectively in the range of rotational speeds $\Omega^{ND} \in (0, 1)$ at elevated temperature $T = 500$ K.

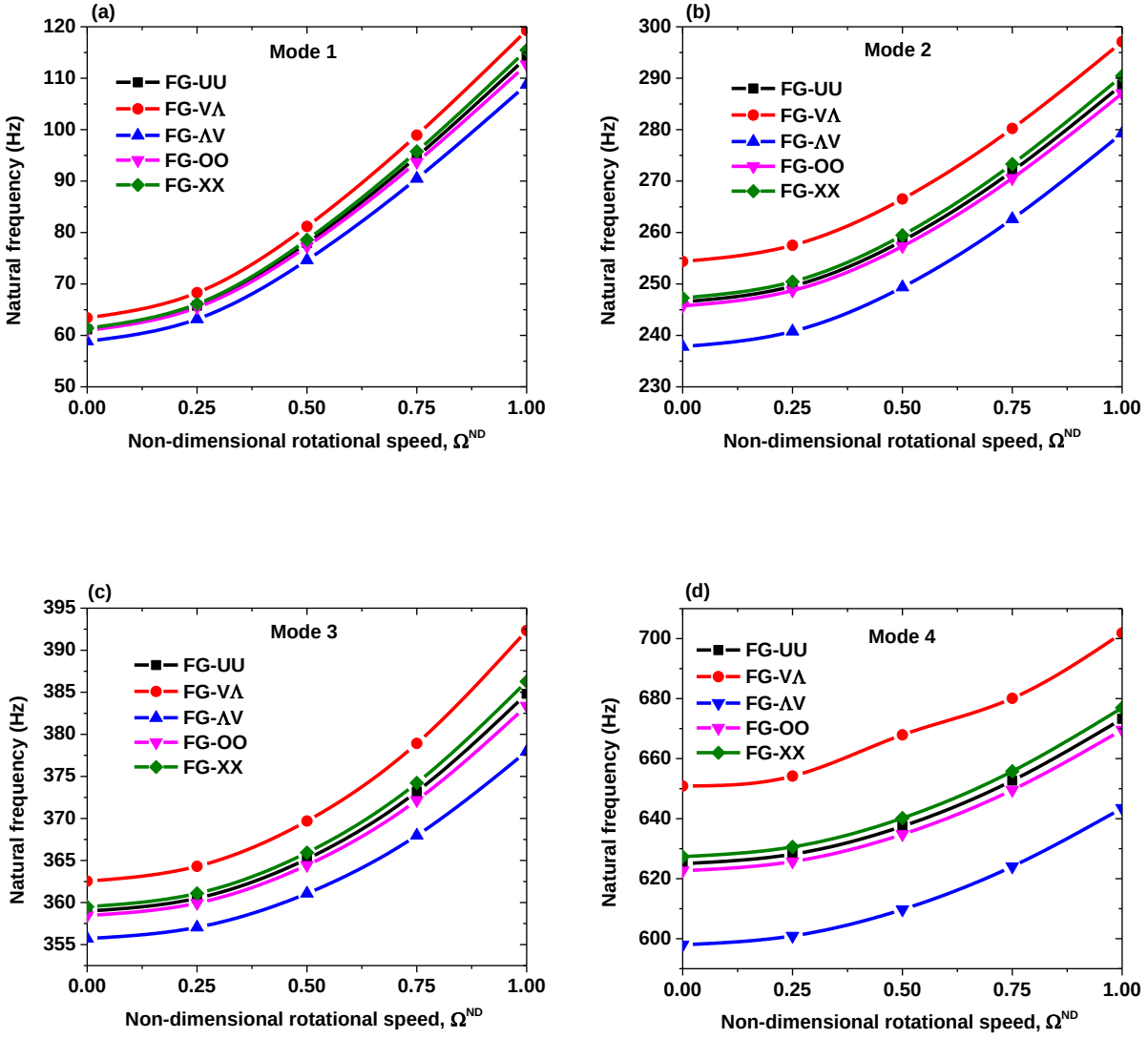

Fig.3.10 Variation of natural frequencies (Hz) of the pretwisted FG-CNTRC sandwich conical shells against non-dimensional rotational speed for different CNTs grading pattern at elevated temperature $T = 500$ K: (a) Mode 1, (b) Mode 2, (c) Mode 3, and (d) Mode 4 [$s = 0.4$ m, $L/s = 0.7$, $\phi_0 = \phi_v = 20°$, s/h =100, $r/L = 1$, $\psi = 30°$, $h_c/h_f = 2$, $V^*_{CNT} = 0.12$]

The effect of pretwist angle on the centrifugal stiffening of the FG-CNTRC sandwich conical shell is found to be considerable, as evident in **Fig. 3.11**. For a particular case of FG-VΛ sandwich conical shell with $s/h = 100$, $r/L = 1$, and $h_c/h_f = 2$, the fundamental frequency

values increase by the factors 1.8595, 1.8641, 1.8814, and 1.9148 for pretwist angles $\psi = 0°$, 15°, 30°, and 45°, respectively, in the range of rotational speed $\Omega^{ND} \in (0, 1)$ at $T = 500$ K. These results specify that the rise in fundamental frequency due to centrifugal force increases with the increase of pretwist angle.

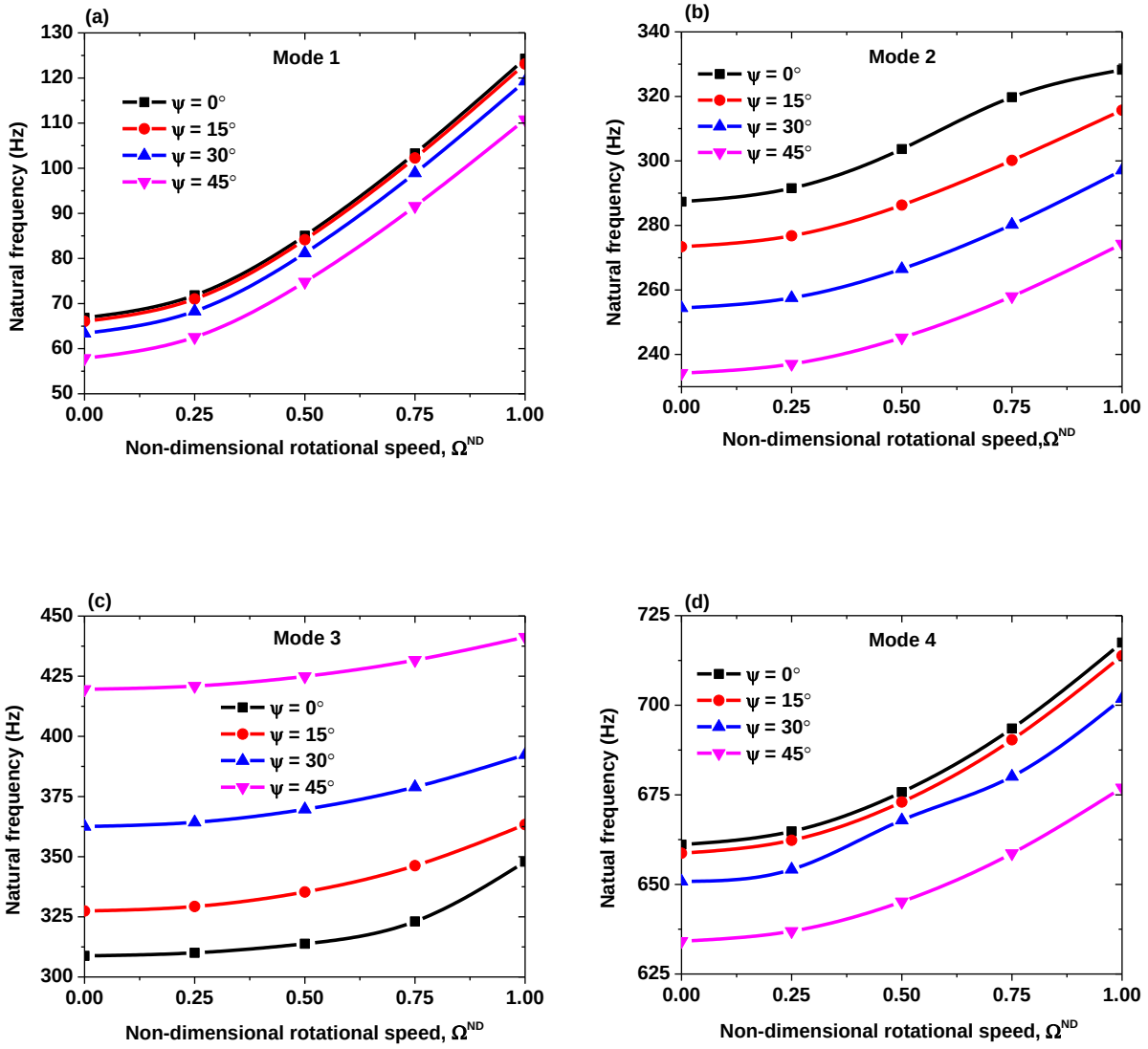

Fig.3.11 Variation of natural frequencies (Hz) of the pretwisted FG-VΛ CNTRC sandwich conical shells against non-dimensional rotational speed for different pretwist angles at elevated temperature $T = 500$ K: (a) Mode 1, (b) Mode 2, (c) Mode 3, and (d) Mode 4 [$s = 0.4$ m, $L/s = 0.7$, $\phi_0 = \phi_v = 20°$, $s/h = 100$, $r/L = 1$, $h_c/h_f = 2$, $V^*_{CNT} = 0.12$]

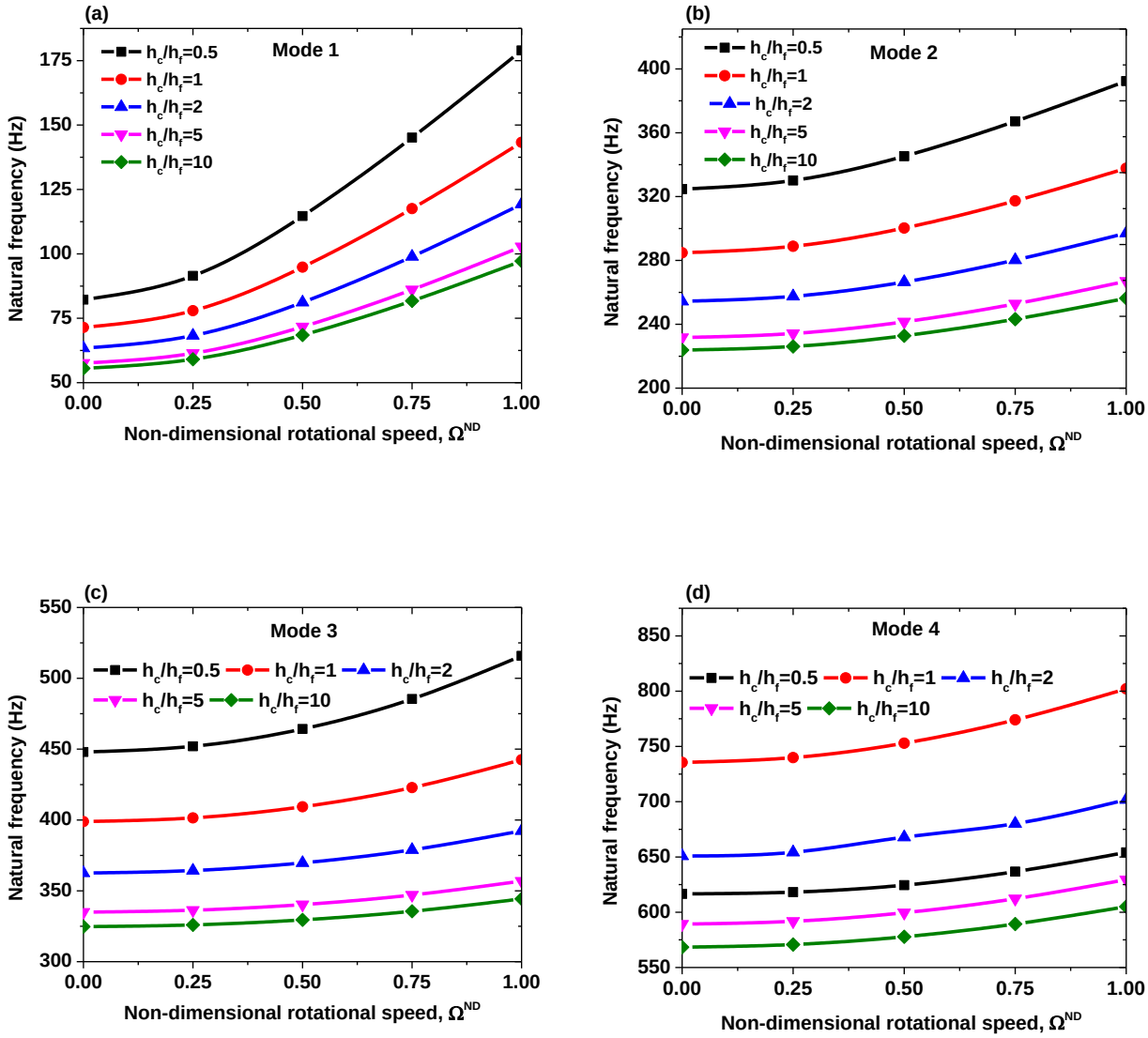

Fig. 3.12 Variation of natural frequencies (Hz) of the pretwisted FG-VΛ CNTRC sandwich conical shells against non-dimensional rotational speed for different values of core-to-face sheets thickness ratios at elevated temperature $T = 500$ K: (a) Mode 1, (b) Mode 2, (c) Mode 3, and (d) Mode 4 [$s =$ 0.4 m, $L/s = 0.7$, $\phi_0 = \phi_v = 20°$, s/h =100, $r/L = 1$, $\psi = 30°$, $V_{CNT}^{*} = 0.12$]

Fig. 3.12 shows the influence of the ratio h_c/h_f on the variation of the natural frequencies of pretwisted ($\psi = 30°$) FG-VΛ type CNTRC sandwich conical shell with the rotational speed at $T = 500$ K. The rate of increase in frequency with rotational speed (i.e., gradient of the frequency versus rotational speed curve) is found to decrease with the

increasing h_c/h_f ratio. It indicates that the contribution of CNTRC face sheets is more than the homogenous core for the centrifugal stiffening of the FG-CNTRC sandwich conical shell. On the other hand, the centrifugal stiffening of the pretwisted FG-VΛ type CNTRC sandwich conical shell is found to be almost invariant with temperature, as shown in **Fig. 3.13.** For the whole range of rotational speeds $\Omega^{ND} \in (0, 1)$, the highest and lowest natural frequencies are observed for T = 300 K and T = 700 K, respectively.

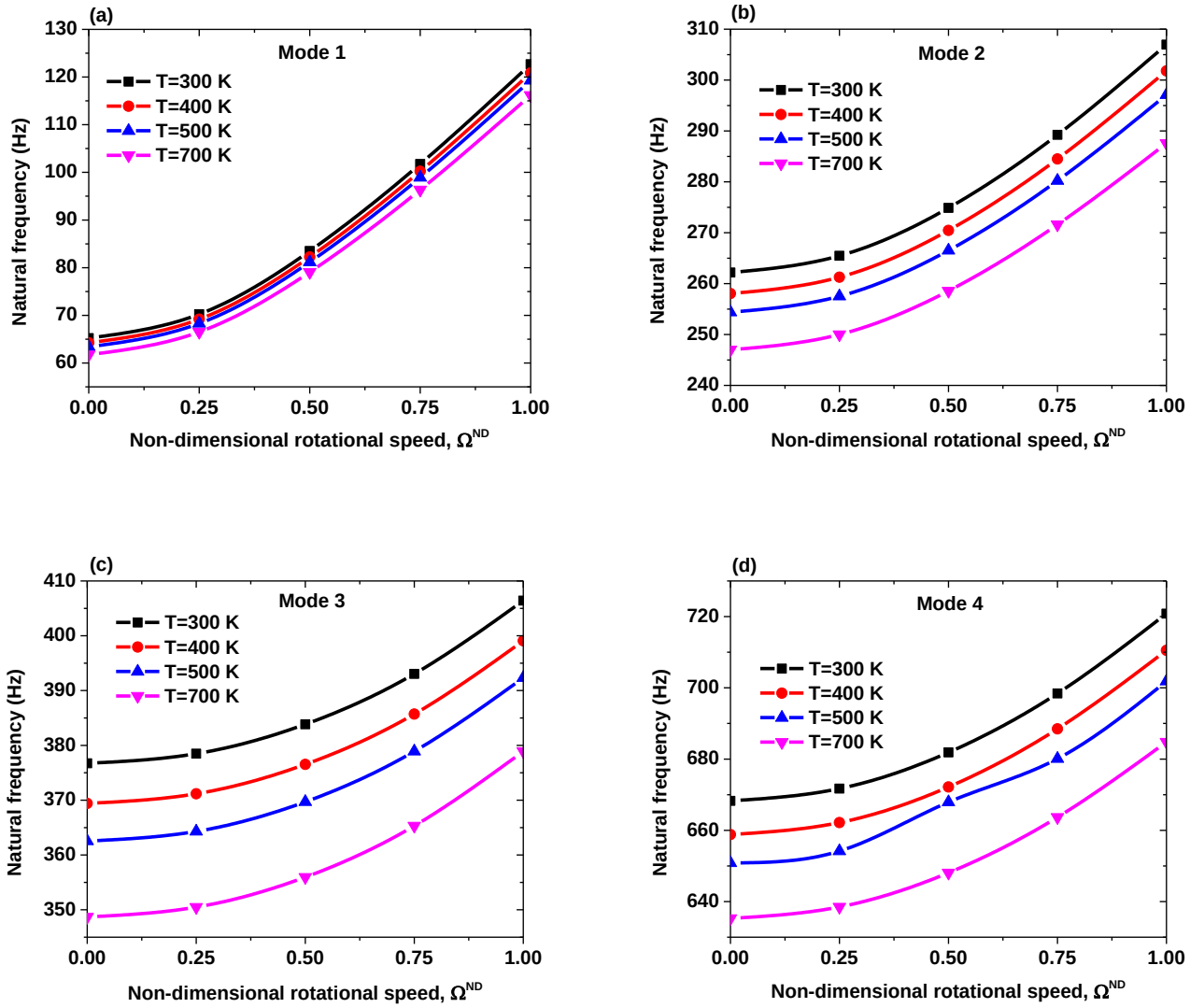

Fig.3.13 Variation of natural frequencies (Hz) of the pretwisted FG-VΛ CNTRC sandwich conical shells against non-dimensional rotational speed for different levels of temperature: (a) Mode 1, (b) Mode 2, (c) Mode 3, and (d) Mode 4 [$s =$ 0.4 m, $L/s = 0.7$, $\phi_0 = \phi_v = 20°$, s/h =100, $r/L = 1$, $\psi = 30°$, $h_c/h_f = 2$, $V_{CNT}^* = 0.12$]

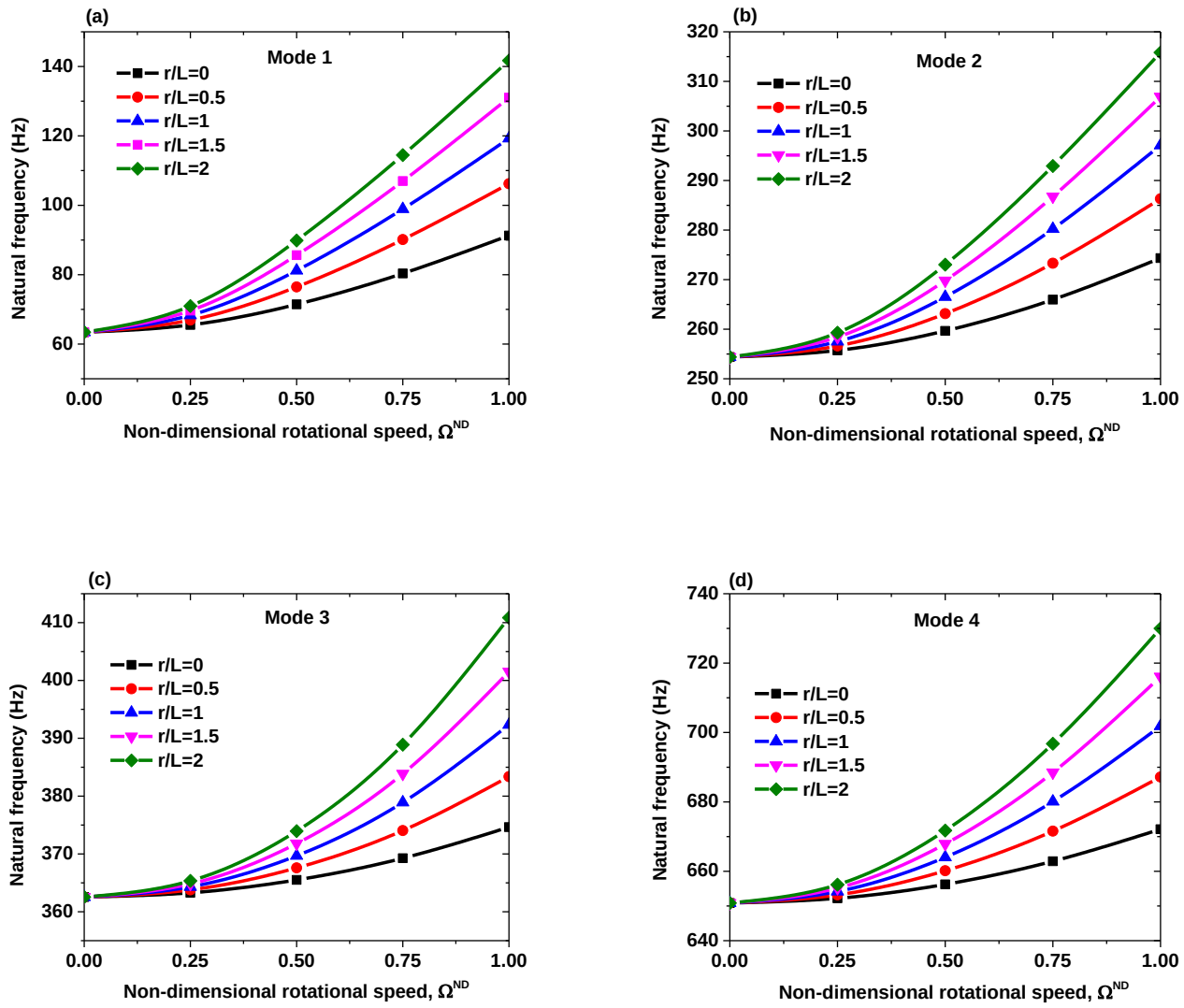

Fig.3.14 Variation of natural frequencies (Hz) of the pretwisted FG-VΛ CNTRC sandwich conical shells against non-dimensional rotational speed for different values of hub radius-to-length ratios at temperature $T = 500$ K: (a) Mode 1, (b) Mode 2, (c) Mode 3, and (d) Mode 4 [$s =$ 0.4 m, $L/s = 0.7$, $\phi_0 = \phi_v = 20°$, s/h =100, $\psi = 30°$, $h_c/h_f = 2$, $V^*_{CNT} = 0.12$]

Fig. 3.14 presents the variation of natural frequency (Hz) of pretwisted FG-VΛ CNTRC sandwich conical shell with non-dimensional rotational speed for different values of the hub radius-to-span length ratios ($r/L = 0$, 0.5, 1, 1.5, and 2) at $T = 500$K. From **Fig. 3.14,** it is clear that all first four frequencies of rotating FG-VΛ CNTRC sandwich conical shells increase with the increase of hub radius-to-span length ratio, while the frequencies of non-rotating ($\Omega^{ND} = 0.0$)

sandwich conical shells are independent of the choice of the r/L ratios. As such, the ratio r/L has a marked influence on the variation of the natural frequencies, especially at higher rotational speeds for a particular temperature and CNTs grading pattern.

3.6 MODE SHAPES

The first four mode shapes of FG-CNTRC sandwich conical shell panels with three different CNTs distribution patterns (FG-UU, FG-VΛ, and FG-ΛV) and two different values of pretwist angles ($\psi = 0°$ and 30°) at reference temperature $T = 300$ K are shown in **Table 3.8.** Here, 3D surface plots along with contour plots underneath the mode shapes are presented to understand the vibration patterns of the sandwich conical shells. It can be observed that the first and third modes of untwisted ($\psi = 0°$) sandwich conical shell are the first two spanwise bending modes, the third mode corresponds the first torsional mode, and the fourth mode is coupled bending and torsional modes irrespective of the type of CNTs grading pattern. Besides, the first, second, and fourth modes of pretwisted ($\psi = 30°$) sandwich conical shell are the first three bending modes, and the third mode corresponds the first torsional modes for all CNTs distribution patterns. **Table 3.9** presents the first four mode shapes of both untwisted and pretwisted FG-VΛ CNTRC conical shell panels for three different values non-dimensional rotational speeds $\Omega^{ND} = 0.0$, 0.5, and 1.0 at elevated temperature $T = 700$ K. It is worth mentioning that the first four mode shapes are weakly dependent on the rotational speed and temperature.

Table 3.8 Mode shapes of FG-CNTRC sandwich conical shells with three types of CNTs distribution patterns and two values of pretwist angles at reference temperature $T = 300$ K [$s = 0.4$ m, $L/s = 0.7$, $\phi_0 = \phi_v = 20°$, s/h =1000, $r/L = 1$, $h_c/h_f = 0.5$, $V^*_{CNT} = 0.12$, $\Omega^{ND} = 0.0$]

Type	ψ	1st mode	2nd mode	3rd mode	4th mode
FG-UU	0°	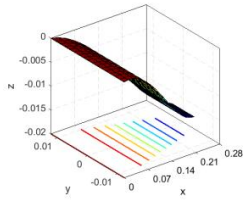	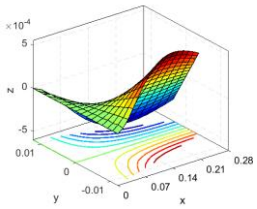	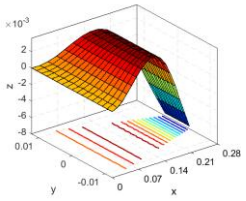	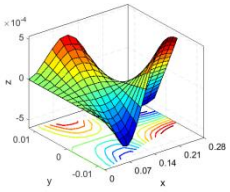
	30°	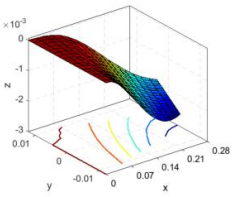	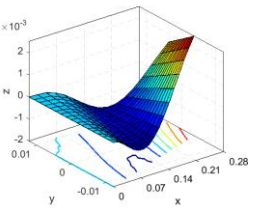	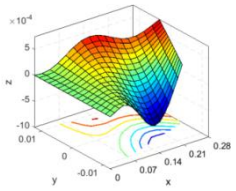	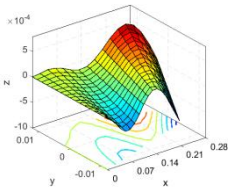
FG-VΛ	0°	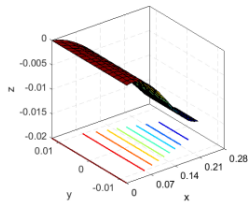	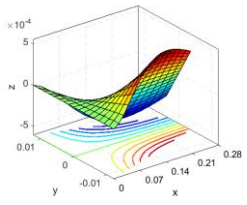	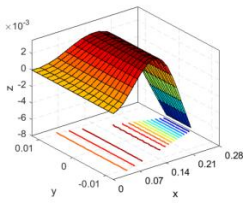	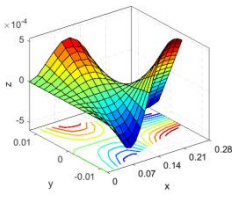
	30°	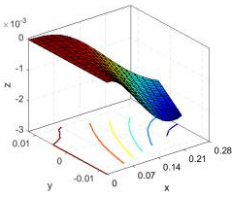	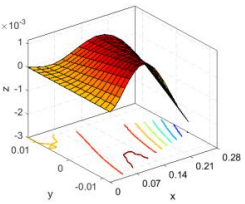	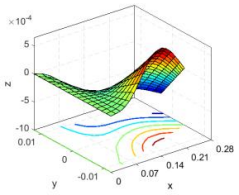	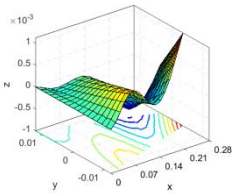
FG-ΛV	0°	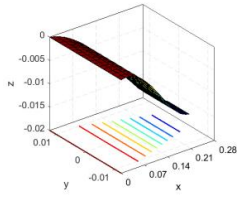	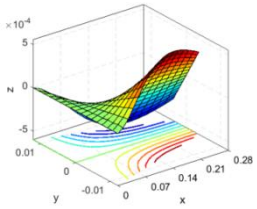	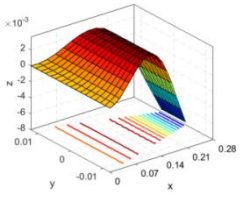	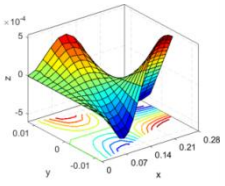
	30°	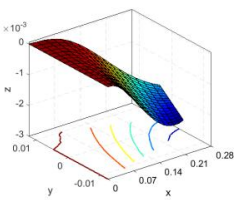	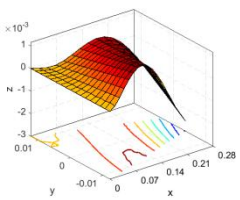	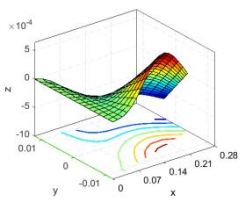	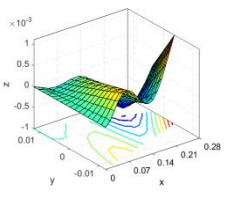

Table 3.9 Mode shapes of FG-VΛ CNTRC sandwich conical shells for three values of rotational speeds and two values of pretwist angles at elevated temperature $T = 700$ K [$s = 0.4$ m, $L/s = 0.7$, $\phi_0 = \phi_v = 20°$, $s/h = 1000$, $r/L = 1$, $h_c/h_f = 0.5$, $V^*_{CNT} = 0.12$]

Ω^{ND}	ψ	1st mode	2nd mode	3rd mode	4th mode
0.0	0°	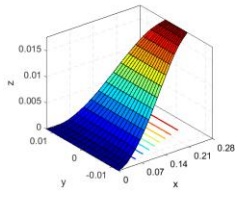	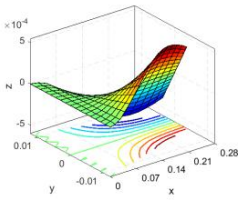	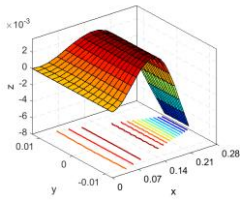	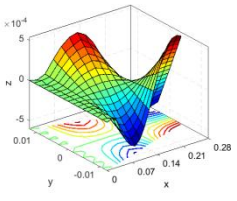
	30°	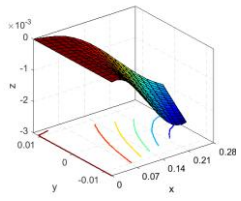	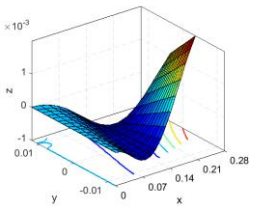	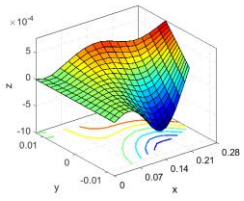	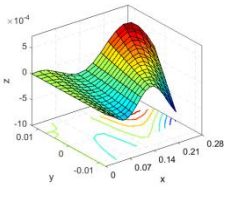
0.5	0°	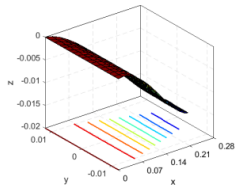	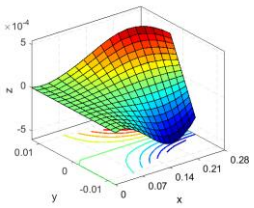	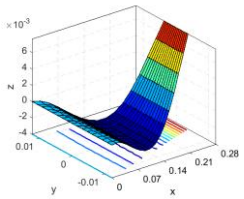	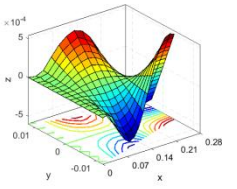
	30°	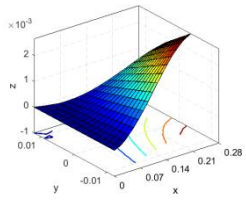	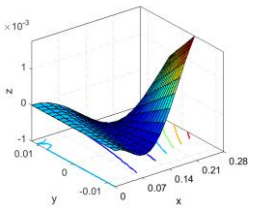	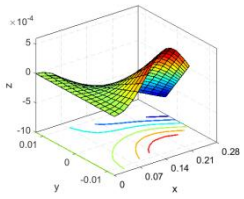	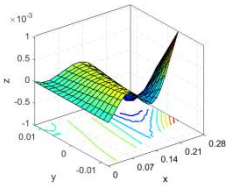
1.0	0°	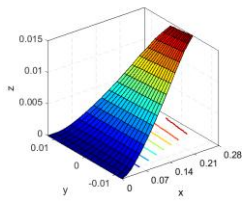	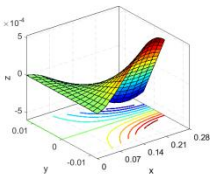	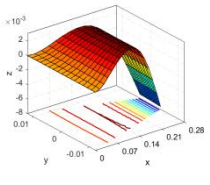	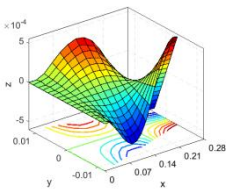
	30°	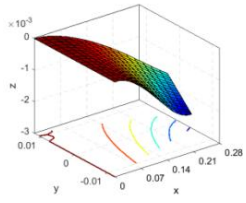	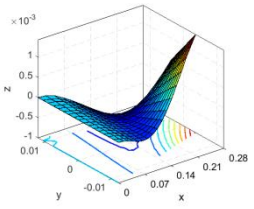	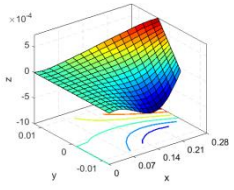	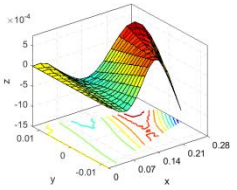

CHAPTER 4

FREE VIBRATION ANALYSIS OF ROTATING PRETWISTED FG-GRC SANDWICH CONICAL SHELLS IN THERMAL ENVIRONMENTS

4.1 INTRODUCTION

Recently, graphene and its derivatives have attracted many researchers because of its excellent mechanical, electrical, and thermal properties. Graphene sheets can strengthen the polymeric matrix significantly without increasing its weight. The graphene reinforced composites (GRC) have attracted immense attention, especially in designing turbo-machinery blades. In this chapter, free vibration analysis of rotating pretwisted sandwich conical shells with GRC face sheets and homogeneous core in thermal environments is conducted. In order to simplify the blade model, the radius of the hub on which the blade is attached is neglected ($r = 0$). At first, the general numerical results and discussions are presented to state the material properties of the constituents and geometrical dimensions of the FG-GRC sandwich conical shells. Thereafter, convergence and comparison studies are performed to examine the ability of the present method for predicting the vibration response of FG-GRC sandwich structures under different thermal conditions. Finally, parametric studies are performed considering some new numerical examples.

4.2 NUMERICAL RESULTS AND DISCUSSIONS

In the present free vibration analysis, the cantilevered pretwisted sandwich conical shells with two symmetric GRC face sheets and a homogeneous core is considered. The GRCs are obtained by reinforcing the zigzag type (referred to as 0-ply) of graphene sheets having effective thickness $h_G = 0.188$ nm and mass density $\rho_G = 4118$ kg/m^3 into poly methyl methacrylate (PMMA) matrix. The temperature-dependent material properties (Lin *et al.,* 2017) of the graphene sheets and efficiency parameters of graphene/PMMA nanocomposite (Shen *et al.,* 2017) are listed in **Table 4.1** and **Table 4.2**, respectively, while $G_{13} = G_{12}$ and $G_{23} = 0.5G_{12}$ are assumed. The material properties of PMMA are considered as ρ^m =1150 kg/m^3,$\nu^m = 0.34$, $\alpha^m = 45(1 + 0.0005\,\Delta T) \times 10^{-6}$/K, and $E^m = (3.52 - 0.0034T)$ GPa in which $T = T_0 + \Delta T$ and $T_0 = 300$ K (reference temperature). Titanium alloy (Ti-6Al-4V) is chosen for the homogenous

core layer, which has the following temperature-dependent Young's modulus and thermal expansion coefficient (Wang and Shen, 2018) of $E_c = 122.56(1 - 4.586 \times 10^{-4}T)$ GPa and $\alpha_c = 7.5788(1 + 6.638 \times 10^{-4}T - 3.147 \times 10^{-6}T^2) \times 10^{-6}$/K. Besides, the Poisson's ratio is assumed to be a constant, and ν_c = 0.29, and ρ_c = 4429 kg/m^3.

Table 4.1 Temperature-dependent material properties for monolayer graphene **[**L_G=14.76 nm, b_G=14.77 nm, h_G= 0.188 nm,ν_{12}^G= 0.177, ρ_G= 4118 kg/m^3] (Lin *et al.*, 2017)

T (K)	E_{11}^G(GPa)	E_{22}^G (GPa)	G_{12}^G (GPa)	α_{11}^G (10^{-6}/K)	α_{22}^G (10^{-6}/K)
300	1812	1807	683	-0.90	-0.95
400	1769	1763	691	-0.35	-0.40
500	1748	1735	700	-0.08	-0.08

Table 4.2 Temperature-dependent efficiency parameters for graphene/PMMA nanocomposites (Shen *et al.*, 2017)

Temp. (K)	V_G	η_1	η_2	η_3
300	0.03	2.929	2.855	11.842
	0.05	3.068	2.962	15.944
	0.07	3.013	2.966	23.575
	0.09	2.647	2.609	32.816
	0.11	2.311	2.260	33.125
400	0.03	2.977	2.896	13.928
	0.05	3.128	3.023	15.229
	0.07	3.060	3.027	22.588
	0.09	2.701	2.603	28.869
	0.11	2.405	2.337	29.527
500	0.03	3.388	3.382	16.712
	0.05	3.544	3.414	16.018
	0.07	3.462	3.339	23.428
	0.09	3.058	2.936	29.754
	0.11	2.736	2.665	30.773

4.3 CONVERGENCE STUDY

In mesh convergence study, the fundamental frequencies (Hz) of non-rotating FG-GRC sandwich conical shells with three different graphene distribution patterns (FG-UU, FG-VΛ, and FG-ΛV) obtained from the present FE formulation corresponding to the mesh sizes of 4×4, 6×6, 8×8, and 10×10 for pretwist angles $\psi = 0^{o}$ and 30^{o} under two different thermal conditions (T =300 K and 500 K) are illustrated in **Fig. 4.1.** It is found that the fundamental frequencies of both untwisted ($\psi = 0^{o}$) and pretwisted (ψ =30^{o}) FG-GRC sandwich conical shells are converged with the mesh size of 8×8 irrespective of the distribution pattern and thermal condition. On the basis of this convergence study, a converged mesh size of 8×8 has been adopted to determine the fundamental frequencies of the pretwisted FG-GRC sandwich conical shells throughout the study.

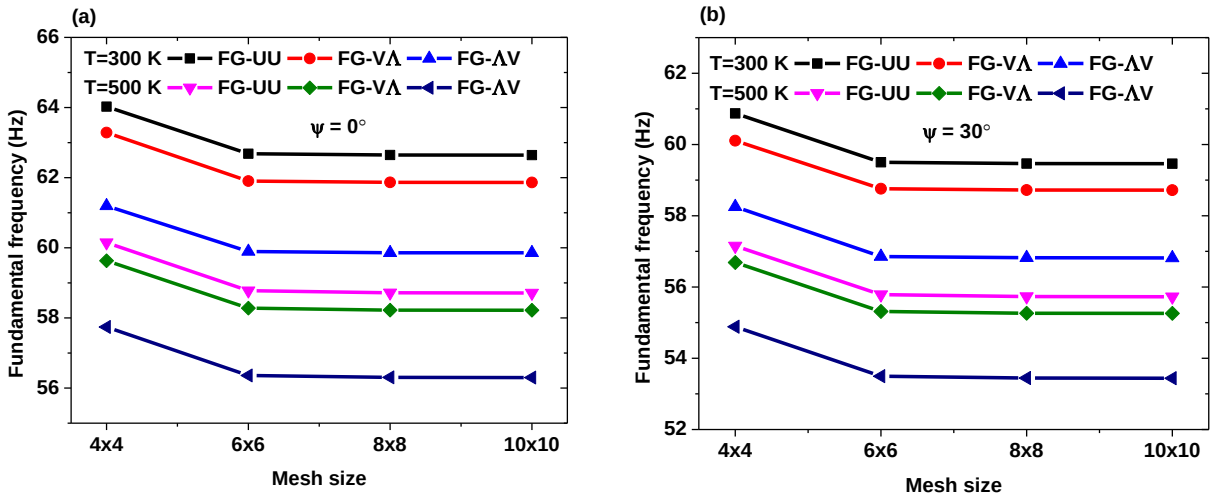

Fig. 4.1 Convergence study for fundamental frequencies (Hz) of the pretwisted FG-GRC sandwich conical shells with three graphene grading patterns for two different pretwist angles: (a) $\psi = 0^{o}$ and (b) $\psi = 30^{o}$ [$s = 0.4$m, L/s =0.7, $\phi_0 = \phi_v = 20°$, $s/h = 100$, $h_c/h_f = 2$, Ω^{ND}= 0.0]

4.4 COMPARISON STUDY

As a part of the validation of the present method, the non-dimensional fundamental frequencies (ϖ) of simply supported square FG-GRC plate with four different types of graphene grading patterns (UD, FG-X, FG-O, and FG-V) at temperatures T =300 K, 400 K, and 500 K are

determined and compared with those reported by Shen *et al.* (2017) and Kiani (2018) as listed in **Table 4.3**. In another example, the first four non-dimensional natural frequencies $\left(\varpi = \omega_n L^2/h\sqrt{\rho_{c0}/E_{c0}}\right)$ of simply supported square sandwich plate [(0º/90º/0º/90º/0º/core/0º/90º/0º/90º/0º] with FG-GRC face sheets and Ti-6Al-4V core for three different values of core-to-face sheets thickness ratios (h_c/h_f = 4, 3, and 2) at reference temperature T =300 K are determined and compared in **Table 4.4** with results of Wang and Shen (2018). These comparisons demonstrate that the results from the present method are in good agreement with the benchmark results.

Table 4.3 Non-dimensional fundamental frequencies ($\varpi = \omega_n L^2/h\sqrt{\rho_0/E_0}$) of simply supported square GRC plate [$(0º/90º/0º/90º/0º)_s$] with different types of grading pattern at T =300 K, 400 K and 500 K [$L/b = 1,\ b/h = 10$, h = 2 mm]

Type	Temp. (K)	Present FEM	Shen et al. (2017)	Kiani (2018)
UD	300	28.3245	28.0982	28.0794
	400	22.1702	21.9591	21.9430
	500	14.8961	15.0773	15.0636
FG-X	300	30.4058	29.5212	30.0881
	400	24.7077	23.8137	24.3027
	500	18.6427	18.2243	18.7757
FG-O	300	23.7205	23.5769	23.4260
	400	17.5861	17.5580	17.4008
	500	9.3903	9.8081	9.5522
FG-V	300	26.2855	25.3900	26.2182
	400	20.8845	19.7323	20.4385
	500	14.7250	14.8437	14.1465

Table 4.4 Non-dimensional natural frequencies ($\varpi = \omega_n L^2/h\sqrt{\rho_{c0}/E_{c0}}$) of simply supported square sandwich plate [(0º/90º/0º/90º/0º/core/0º/90º/0º/90º/0º] with FG-GRC face sheets and Ti-6Al-4V core at reference temperature T =300 K [$L/b = 1,\ b/h = 20$, h_f = 1 mm.]

h_c/h_f	Mode	FG-UU		FG-VΛ		FG-ΛV	
		Present FEM	Wang and Shen (2018)	Present FEM	Wang and Shen (2018)	Present FEM	Wang and Shen (2018)
4	1	6.0307	6.0295	6.0234	6.0229	5.7692	5.7670
	2	15.0534	15.0355	14.9697	14.93553	14.3617	14.3438
	3	15.0539	15.0449	14.9725	14.9663	14.3696	14.3476
	4	23.6456	23.6186	23.6175	23.5992	22.6542	22.6111
3	1	6.1299	6.1304	6.1555	6.1568	5.7867	5.7856
	2	15.3122	15.3060	15.2958	15.2933	14.4220	14.4084
	3	15.3190	15.3172	15.3054	15.3074	14.4255	14.4120
	4	24.0220	24.0177	24.1182	24.1246	22.7237	22.6959
2	1	6.3356	6.3385	6.4308	6.4344	5.8504	5.8510
	2	15.8348	15.8444	15.9686	15.9802	14.5998	14.5950
	3	15.8484	15.8580	15.9857	15.9993	14.6007	14.5978
	4	24.7955	24.8238	25.1544	25.1928	22.9652	22.9605

4.5 PARAMETRIC STUDY

In this section, the effects of some important parameters such as pretwist angle, cone length-thickness ratio, core-to-face sheets thickness ratio, temperature, and rotational speed on the natural frequencies (Hz) of the pretwisted FG-GRC sandwich conical shells are analyzed. The relevant geometrical parameters of the sandwiched conical shells are utilized as: $s = 0.4$m, $L/s = 0.7$, $\phi_0 = \phi_v = 20°$.

4.5.1 EFFECT OF PRETWIST ANGLE

The effect of pretwist angle on the first two natural frequencies (Hz) of the FG-GRC sandwich conical shells with three different distribution patterns (FG-UU, FG-VΛ, and FG-ΛV) corresponding to core-to-face sheets thickness ratio $h_c/h_f = 0.5$ and temperatures $T = 300$ K and 500 K are depicted in **Fig. 4.2.**

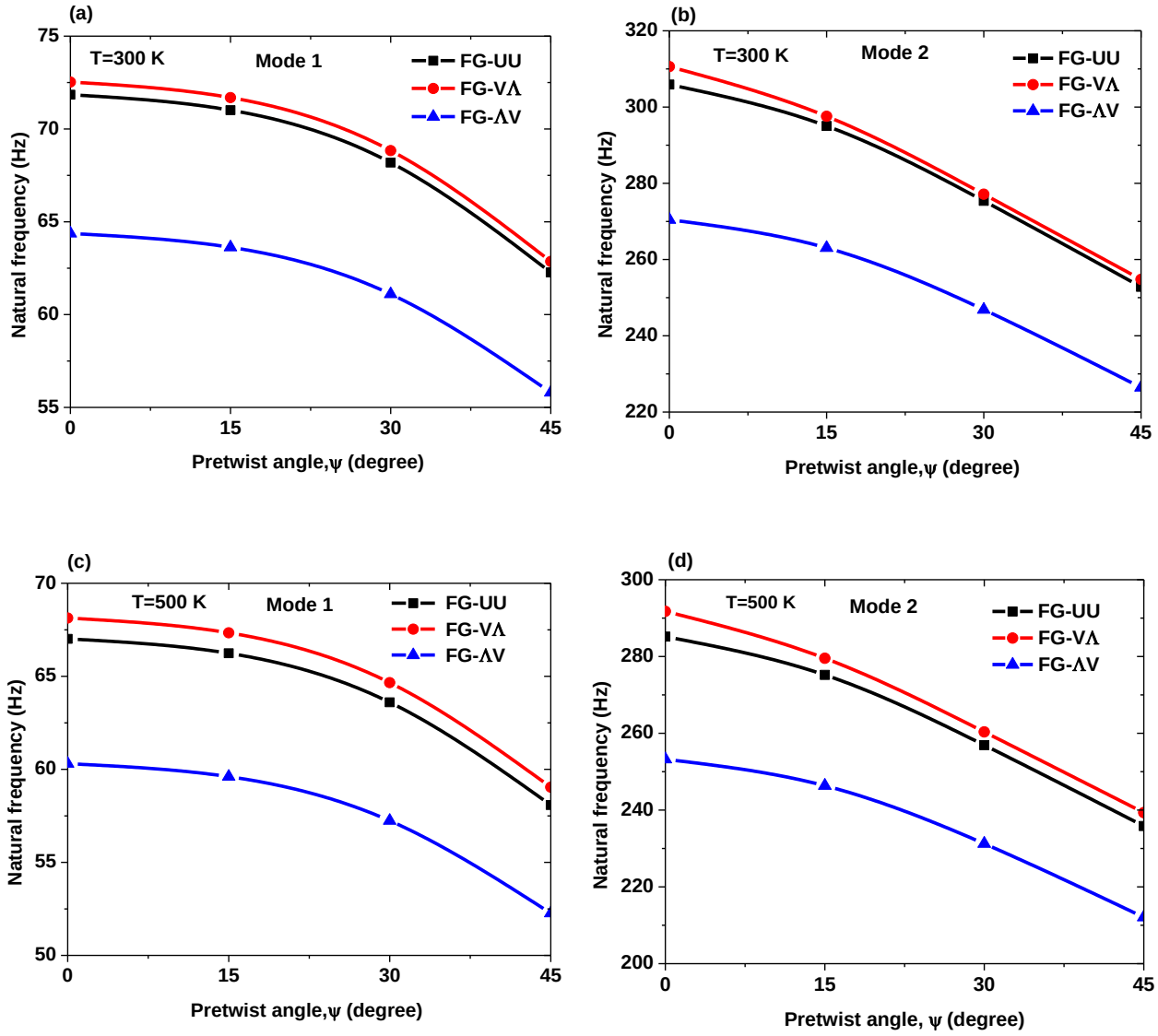

Fig. 4.2 Effect of pretwist angle (ψ) on the natural frequencies (Hz) of FG-GRC sandwich conical shells with three different distribution patterns at two temperature levels: (a) $T = 300$ K, Mode 1, (b) $T = 300$ K, Mode 2, (c) $T = 500$ K, Mode 1, and (d) $T = 500$ K, Mode 2 [$s = 0.4$ m, $L/s = 0.7$, $\phi_0 = \phi_v = 20°$, s/h =100, $\Omega^{ND} = 0.0$]

In general, the natural frequency values of the pretwisted FG-GRC sandwich conical shells are found to be lower at elevated temperatures at all pretwist angles and graphene grading patterns**.** Further**,** it is also noted that the first two natural frequencies exhibit a monotonic decrease with the increase in pretwist angle irrespective of the types of distribution pattern and thermal conditions. This reduction in natural frequencies of FG-GRC sandwich conical shells is similar to those observed for the pretwsited isotropic shells, as reported by Liew *et al.* (1994),

and can be attributed to a decrease in bending stiffness of the sandwich conical shell with an increase in pretwist angle. The fundament frequencies of the pretwisted GRC sandwich conical shells with FG-UU, FG-VΛ, and FG-ΛV grading patterns corresponding to $h_c/h_f = 0.5$ are reduced by 13.33%, 13.34%, and 13.32%, respectively, at room temperature T =300 K, while the percentage reduction in fundamental frequencies at elevated temperature T =500 K are found to be 13.34%, 13.35%, and 13.33%, respectively as the pretwist angle is increased from 0° to 45°. It implies that the percentage reduction in the fundamental frequencies with an increase in the pretwist angle is almost independent of the choice of the grading pattern and temperature increment. Furthermore, the effect of pretwist angle on the fundamental frequencies is slightly higher at elevated temperatures than at room temperature.

4.5.2 EFFECT OF CONE LENGTH-TO-THICKNESS RATIO

Fig. 4.3 illustrates the effect of cone length-to-thickness ratio s/h on the fundamental frequencies of the pretwisted FG-GRC sandwich conical shells with three different graphene grading patterns (FG-UU, FG-VΛ, and FG-ΛV) for three different values of the core-to-face sheets thickness ratios ($h_c/h_f = 0.5$, 2, and 10) at two level of temperatures T =300 K and 500 K**.** The fundamental frequencies are found to decrease rapidly with an increase in the s/h ratios up to $s/h = 400$, after which the drop in the frequency values becomes negligible. This rapid reduction in the fundamental frequency at lower values of the s/h ratio is observed for all graphene grading patterns and h_c/h_f ratios, and may be attributed to a rapid increase in the flexibility of the sandwich conical shell. The percentage decrease in fundamental frequencies of the pretwisted sandwich conical shells with FG-UU grading pattern due to the increase in the s/h ratio from 100 to 1000 for $h_c/h_f = 0.5$, 2, and 10 at T =300 K are 62.68%, 62.29%, and 62.92%, respectively, while the corresponding percentage decrease in case of the FG-VΛ grading pattern are 63.31%, 62.10%, and 62.51%, respectively. Similarly, for FG-ΛV grading pattern, the percentages of decrease in fundamental frequency are 60.50%, 61.29%, and 62.45%, respectively. It indicates that at a particular temperature, the effect of the s/h ratio on the predicted fundamental frequency is more pronounced in the case of the FG-VΛ and FG-UU grading patterns for lower and higher values of the core-to-face sheets thickness ratio, respectively. Therefore, it may be inferred that the effect of thickness on the fundamental frequency vaules are widely dependent on the graphene grading patterns and core-to-face sheets thickness ratio.

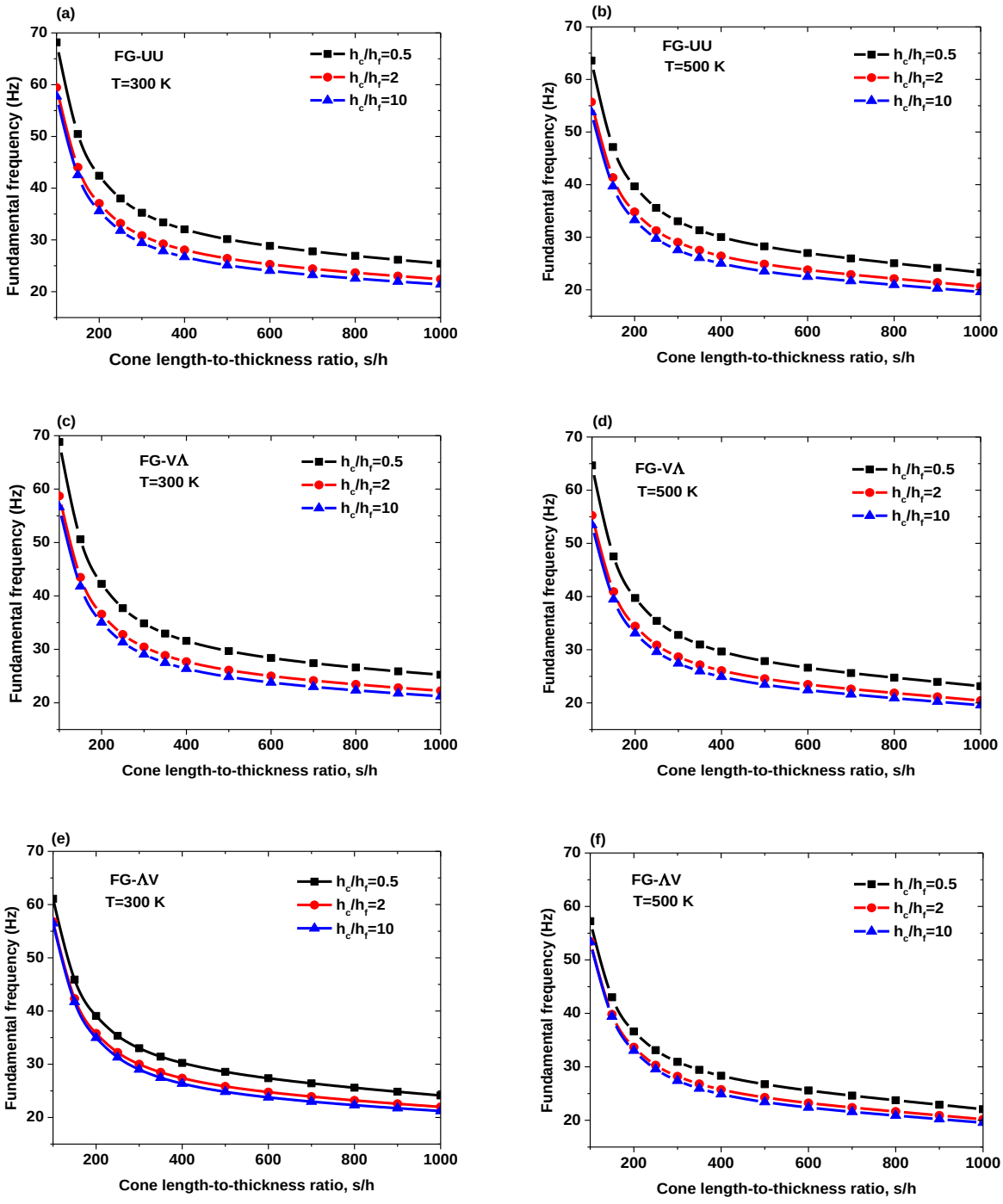

Fig. 4.3 Effect of cone length-to-thickness ratio (s/h) on the fundamental frequencies (Hz) of the pretwisted FG-GRC sandwich conical shells with different graphene grading patterns and temperature levels: (a) FG-UU, T =300 K, (b) FG-UU, T =500 K, (c) FG-VΛ, T =300 K, (d) FG-VΛ, T =500 K, (e) FG-ΛV, T =300 K, and (f) FG-ΛV, T =500 K. [s = 0.4 m, L/s = 0.7, $\phi_0 = \phi_v = 20°$, $\psi = 30°$, $\Omega^{ND} = 0.0$]

4.5.3 EFFECT OF CORE-TO-FACE SHEETS THICKNESS RATIO

The influence of core-to-face sheets thickness ratio h_c/h_f on the first two natural frequencies (Hz) of the pretwisted FG-GRC sandwich conical shells with three different graphene grading patterns (FG-UU, FG-VΛ, and FG-ΛV) for pretwist angle ψ =30° at two levels of temperatures T =300 K and 500 K are shown in **Fig. 4.4**. The obtained results signify that the first two natural frequencies of the pretwisted sandwich conical shells having FG-UU and FG-VΛ type grading patterns decrease monotonically as the ratio h_c/h_f increases for all thermal conditions. In contrast, for the case of FG-ΛV grading pattern, with an increase in the ratio h_c/h_f, the first two natural frequencies decrease first to attain their minimum values and then increase slightly. From the mechanical properties considered, it is evident that the titanium alloy core is siffer as well as heavier than GRC faces sheets. The increase in the ratio h_c/h_f leads to the lower proportion of GRC face sheets relative to titanium alloy core, thereby increasing the structural stiffness of the sandwich conical shells with higher values of the total structural mass. In this case, the decrease in natural frequencies of the sandwich conical shells due to increase in its overall structural mass is more than the increase in natural frequencies due to increase in its overall stiffness. Simultaneously, the layers of GRC face sheets adjacent to the core ($z = \pm h_c/2$) shift away from the mid-surface of the sandwich conical shell with increasing the ratio h_c/h_f. In case of the FG-ΛV pattern, shifting away of the layers in GRC face sheets possessing high volume fraction ($V_G = 0.11$) from mid-surface causes an increase in structural stiffness, which may compensate the general reduction in stiffness due to the lowering of GRC face sheets proportion. It is noticeable that the first two natural frequencies in case of the FG-VΛ pattern are found to be the largest and followed by FG-UU, then FG-ΛV patterns for the lower values of core-to-face sheets thickness ratio (h_c/h_f = 0.5) at any thermal condition. Besides, the sandwich conical shell with the FG-UU type pattern is found to exhibit the largest natural frequencies and followed by FG-VΛ and then FG-ΛV patterns for higher values of the core-to-face sheets thickness ratio ($h_c/h_f \geq 1$). **Fig. 4.5** portrays the percentage decrease in the first two natural frequencies of the pretwisted sandwich conical shells due to increase in the ratio h_c/h_f with reference to h_c/h_f = 0.5 at two different levels of temperatures T = 300 K and 500 K. It is observed from the results that the highest percentage decrease in the natural frequencies is found in case of the FG-VA type grading pattern and followed by FG-UU then FG-ΛV type grading patterns irrespective of

temperature. Further, the rates of decrease in the natural frequencies seem to be more apparent for lower values of the ratio h_c/h_f.

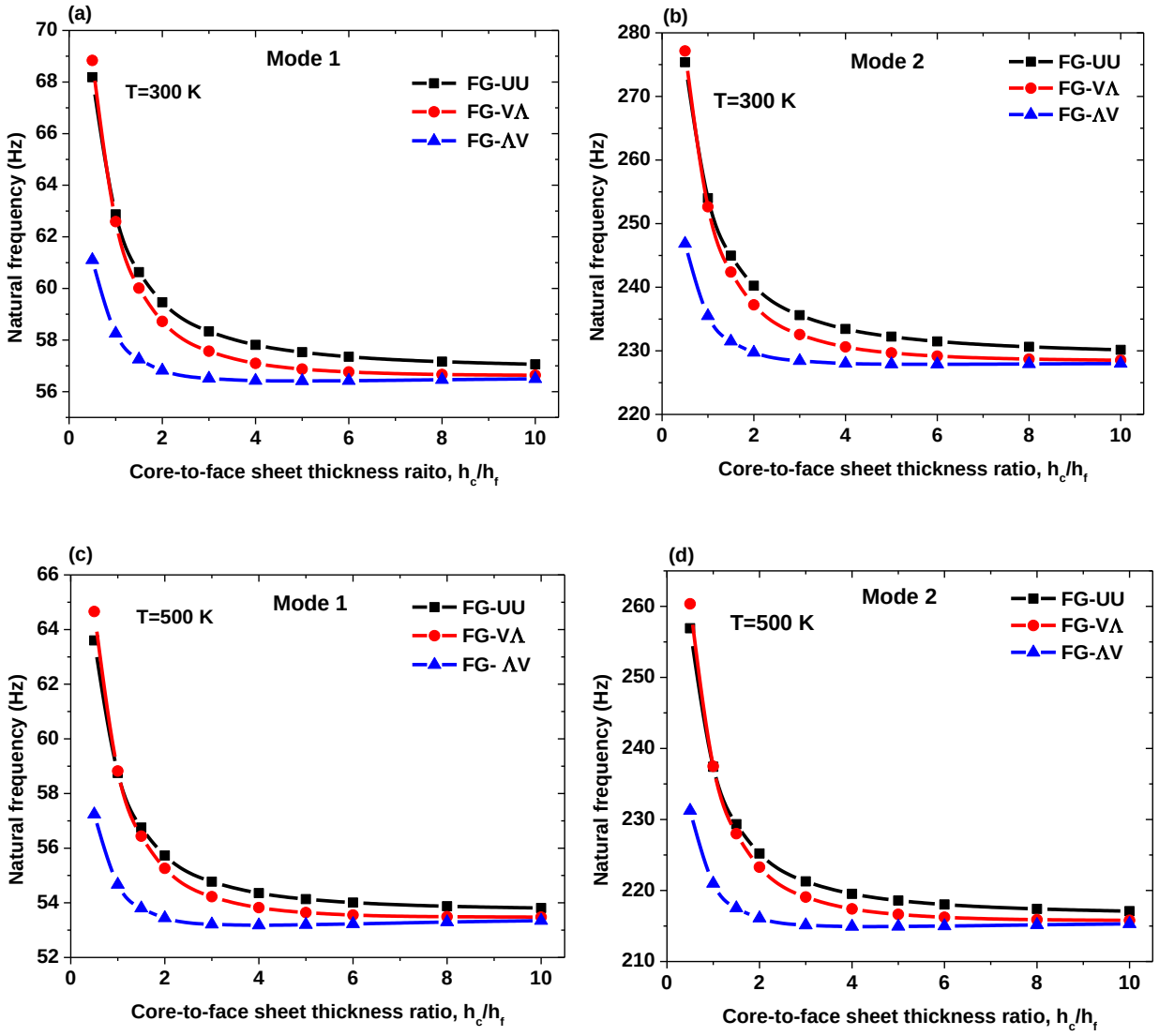

Fig. 4.4 Effect of core-to-face sheets thickness ratio (h_c/h_f) on the natural frequencies (Hz) of the pretwisted FG-GRC sandwich conical shells at two temperature levels: (a) $T = 300$ K, Mode 1, (b) $T = 300$ K, Mode 2, (c) $T = 500$ K, Mode 1, and (d) $T = 500$ K, Mode 2 [$s = 0.4$ m, $L/s = 0.7$, $\phi_0 = \phi_v = 20°$, $\psi = 30°$, $s/h = 100$, $\Omega^{ND} = 0.0$]

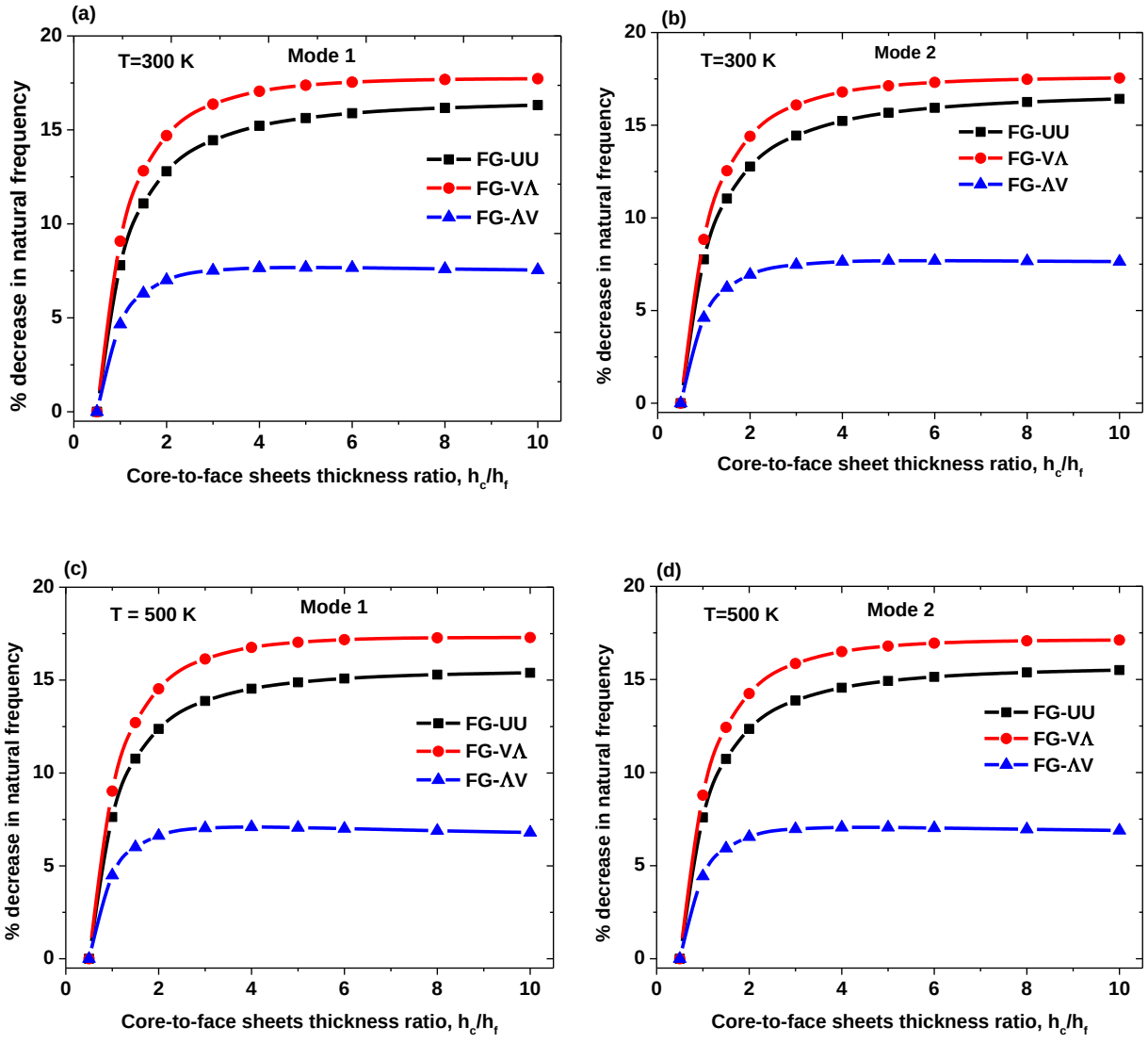

Fig. 4.5 Percentage decrease in natural frequencies of the pretwisted FG-GRC sandwich conical shells for two levels of temperatures: (a) $T = 300$ K, Mode 1, (b) $T = 300$ K, Mode 2, (c) $T = 500$ K, Mode 1, and (d) $T = 500$ K, Mode 2 [$s = 0.4$ m, $L/s = 0.7$, $\phi_0 = \phi_v = 20°$, $\psi = 30°$, $s/h = 100$, $\Omega^{ND} = 0.0$]

4.5.4 EFFECT OF TEMPERATURE

The effect of varying temperature on the first two natural frequencies (Hz) of the pretwisted FG-GRC sandwich conical shells with three different graphene grading patterns (FG-UU, FG-VΛ, and FG-ΛV) and three different values of core-to-face sheets thickness ratio ($h_c/h_f = 0.5$, 2, and 10) is depicted in **Fig. 4.6**.

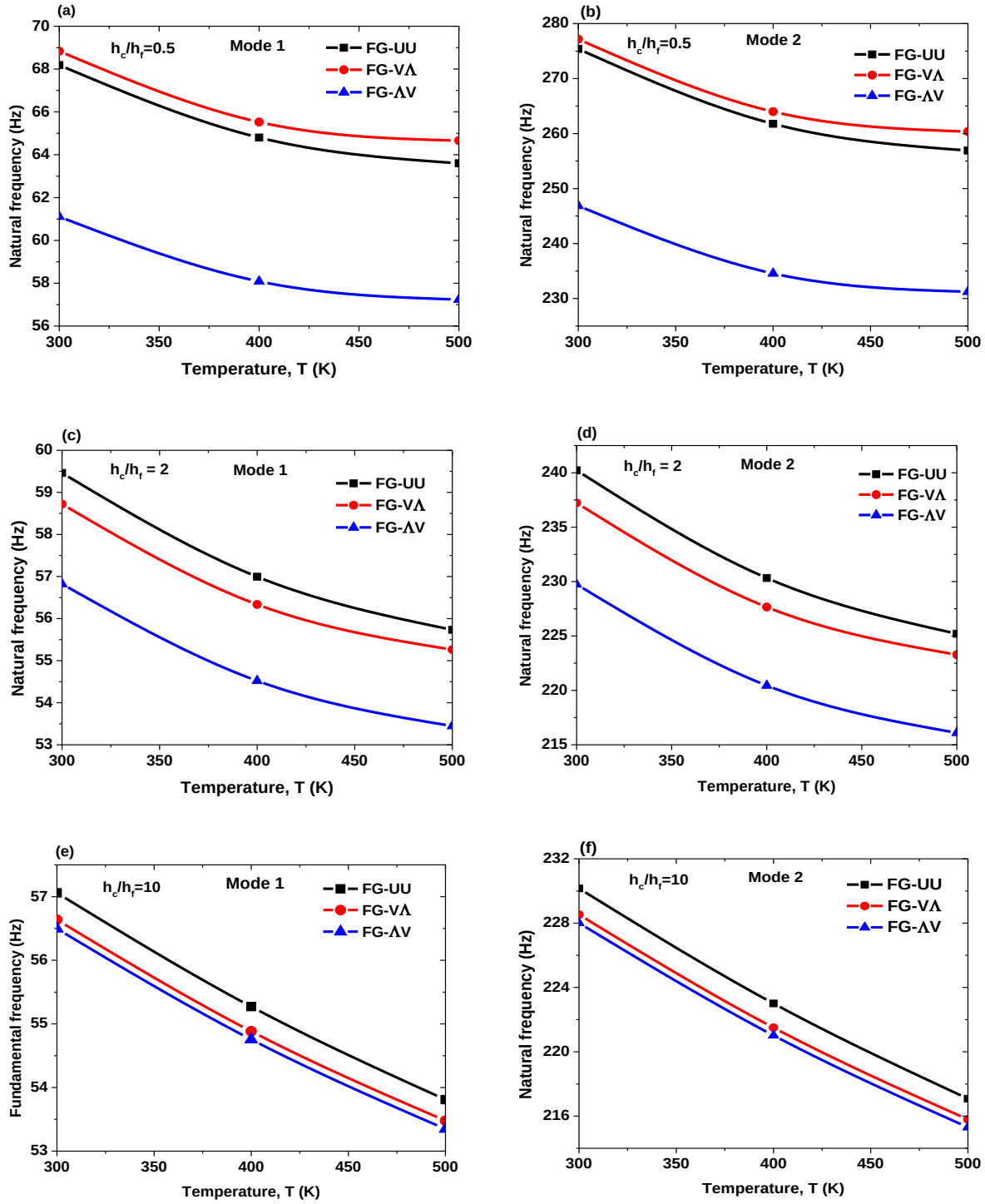

Fig. 4.6 Effect of temperature on the natural frequencies (Hz) of pretwisted FG-GRC sandwich conical shells for three values of h_c/h_f ratios: (a) h_c/h_f =0.5, Mode 1, (b) h_c/h_f =0.5, Mode 2, (c) h_c/h_f = 2, Mode 1, (d) h_c/h_f = 2, Mode 2, (e) h_c/h_f =10, Mode 1, and (f) h_c/h_f =10, Mode 2 [s = 0.4 m, L/s = 0.7, $\phi_0 = \phi_v$ = 20°, ψ = 30°, s/h = 100, Ω^{ND} = 0.0]

The first two natural frequencies of the pretwisted FG-GRC sandwich conical shells are found to decrease monotonically with a rise in temperature for all the cases considered, as shown in **Fig. 4.6**. This decreasing trend is expected because the rise in temperature causes thermal stress, which in turn degrades the overall structural stiffness of the sandwich conical shells considerably. Moreover, the rise in temperature reduces the mechanical strengths of both the GRC face sheets and titanium alloy core constituents, resulting in reduction of strength of the sandwich conical shells. **Fig. 4.7** shows the percentage decreases in the first two natural frequencies of the pretwisted FG-GRC sandwich conical shells due to the rise in temperature up to 400 K ($\Delta T = 100$ K) and 500 K ($\Delta T = 200$ K) from a baseline temperature of 300 K, for three different values of the core-to-face sheets thickness ratio $h_c/h_f = 0.5$, 2, and 10. The highest percentage decrease in the natural frequencies is noticed in case of the FG-UU type pattern for all values of the ratio h_c/h_f. It signifies that the thermal effects on natural frequencies are found more pronounced for the FG-UU type pattern in pretwisted FG-GRC sandwich conical shells. In addition, the thermal effects with respect to the types of graphene grading patterns are indistinguishable for lower proportions of GRC face sheets in the sandwich conical shells. The percentage decreases in the natural frequencies are also found to be more pronounced at lower values of the ratio h_c/h_f. It is due to the higher degradation in the mechanical properties occurring in GRC face sheets compared to the titanium alloy core with an increase in temperature from T=300K to 500K. As such, the drop in the natural frequencies is significant at lower h_c/h_f values in FG-VΛ and FG-ΛV patterns, while for higher h_c/h_f values, the titanium alloy core strength plays a significant role compared to the graphene-nanoparticle distributions as in FG-UU type pattern.

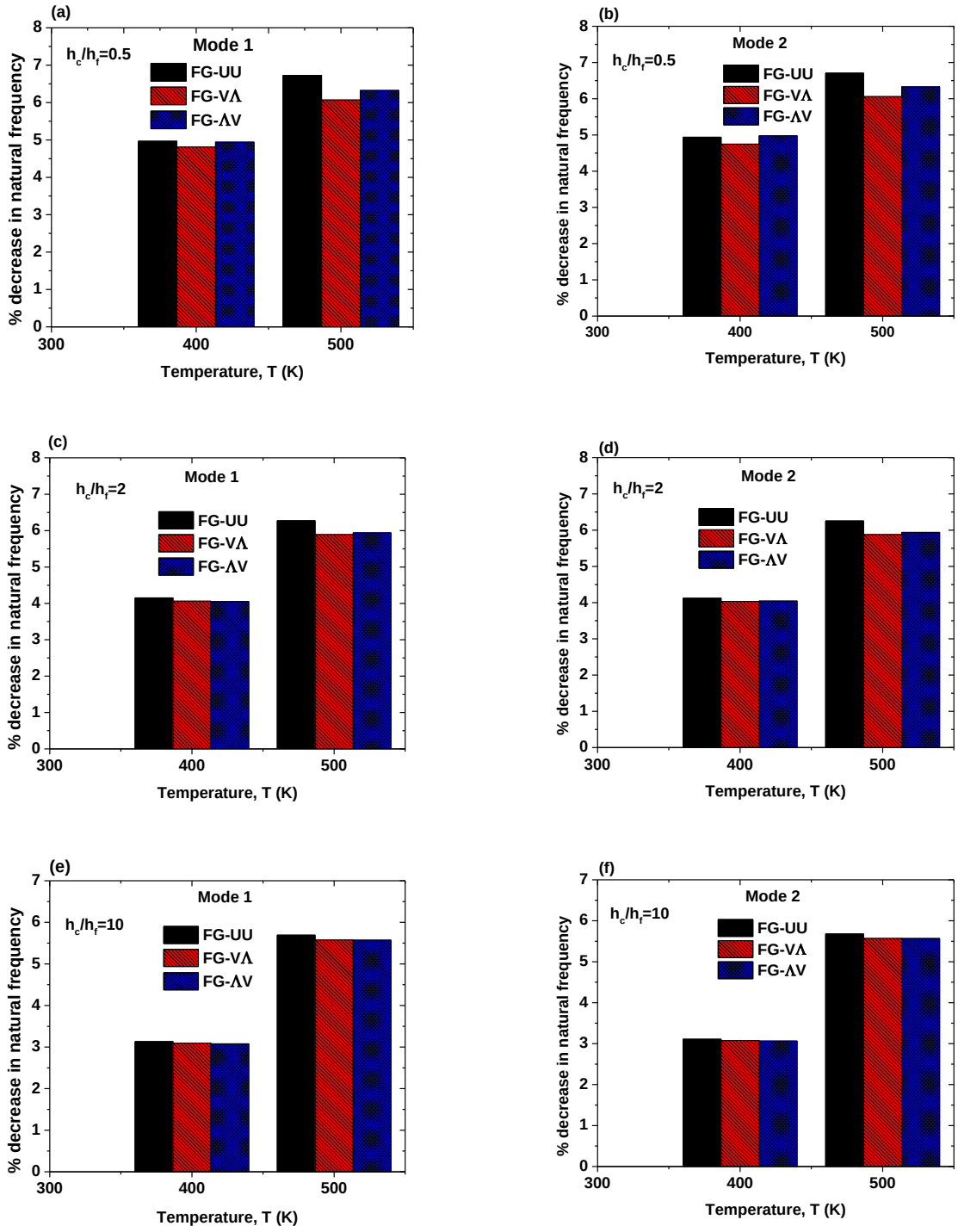

Fig. 4.7 Percentage decreases in natural frequencies of the pretwisted FG-GRC sandwich conical shells for three values of h_c/h_f ratios: (a) h_c/h_f =0.5, Mode 1, (b) h_c/h_f =0.5, Mode 2, (c) h_c/h_f = 2, Mode 1, (d) h_c/h_f = 2, Mode 2, (e) h_c/h_f =10, Mode 1, and (f) h_c/h_f =10, Mode 2 [s = 0.4 m, L/s = 0.7, $\phi_0 = \phi_v$ = 20°, ψ = 30°, s/h = 100, Ω^{ND} = 0.0]

4.5.5 EFFECT OF ROTATIONAL SPEED

The effects of non-dimensional rotational speed Ω^{ND} on the first two natural frequencies of FG-GRC sandwich conical shells with three different types of graphene grading pattern (FG-UU, FG-VΛ, and FG-ΛV) for pretwist angles $\psi = 0°$ and 30° at elevated temperature $T = 500$ K are displayed in **Figs. 4.8** and **4.9,** respectively. In this numerical example, the results are obtained for three different values of core-to-face sheets thickness ratios ($h_c/h_f = 0.5$, 2, and 10)**.** It can be found that the first two natural frequencies increase monotonically with an increase in non-dimensional rotational speed irrespective of the types of graphene grading pattern, values of the pretwist angle, and core-to-face sheets thickness ratio. This is due to the fact that the rotating sandwich shell becomes more centrifugally stiffened as the rotational speed is increased, thereby exhibiting higher values of natural frequencies. The rate of increase in the natural frequency with respect to the rotational speed is found to be more significant for higher values of the rotational speed Ω^{ND}. The fundamental frequency of the untwisted ($\psi = 0°$) GRC sandwich conical shell with FG-VΛ pattern corresponding to $h_c/h_f = 0.5$, 2, and 10 increase by factors 1.6597, 1.4939, and 1.4187, respectively, while for the case of pretwisted ($\psi = 30°$) sandwich conical shell, the values of these factors are 1.6824, 1.5115, and 1.4736, respectively, in the range of rotational speed of interest (Ω^{ND} = 0,1). Similar observations can be seen in case of the FG-UU and FG-ΛV grading patterns of the FG-GRC sandwich conical shells. It implies that the centrifugal stiffening is more apparent in case of the pretwisted FG-GRC sandwich conical shell than the untwisted FG-GRC sandwich conical shell for all types of graphene grading patterns and values of the ratio h_c/h_f. Furthermore, the centrifugal stiffening is found to decrease with an increase in the ratio h_c/h_f irrespective of graphene grading pattern and pretwist angle. In addition, the influence of the rotational speed in terms of increasing fundamental frequency is found to be maximum in case of FG-VΛ pattern and followed by FG-UU and FG-ΛV patterns, irrespective of the pretwist angle and ratio h_c/h_f. For instance, the fundamental frequencies for FG-VΛ, FG-UU, and FG-ΛV patterns with pretwist angle $\psi = 30°$ corresponding to $h_c/h_f = 2$ increase by factors 1.5115, 1.4773 and 1.4265, respectively, in the range of rotational speed $\Omega^{ND} \in (0, 1)$.

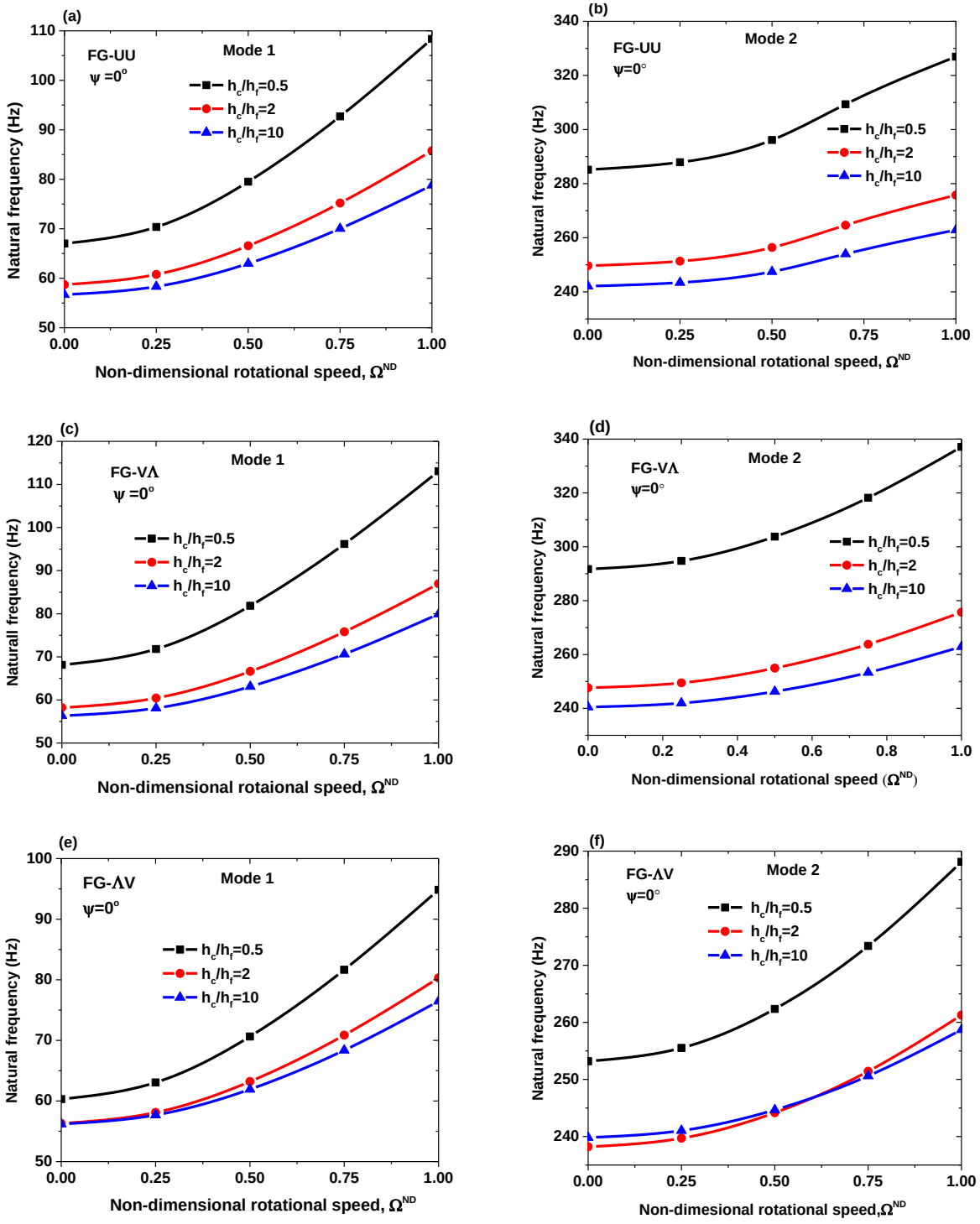

Fig. 4.8 Effect of non-dimensional rotational speed on the natural frequencies (Hz) of untwisted ($\psi = 0°$) FG-GRC sandwich conical shells with three different distribution patterns at T =500 K: (a) FG-UU, Mode 1, (b) FG-UU, Mode 2, (c) FG-VΛ, Mode 1, (d) FG-VΛ, Mode 2, (e) FG-ΛV, Mode 1, and (f) FG-ΛV, Mode 2 [$s = 0.4$ m, $L/s = 0.7$, $\phi_0 = \phi_v = 20°$, $\psi = 30°$, $s/h = 100$]

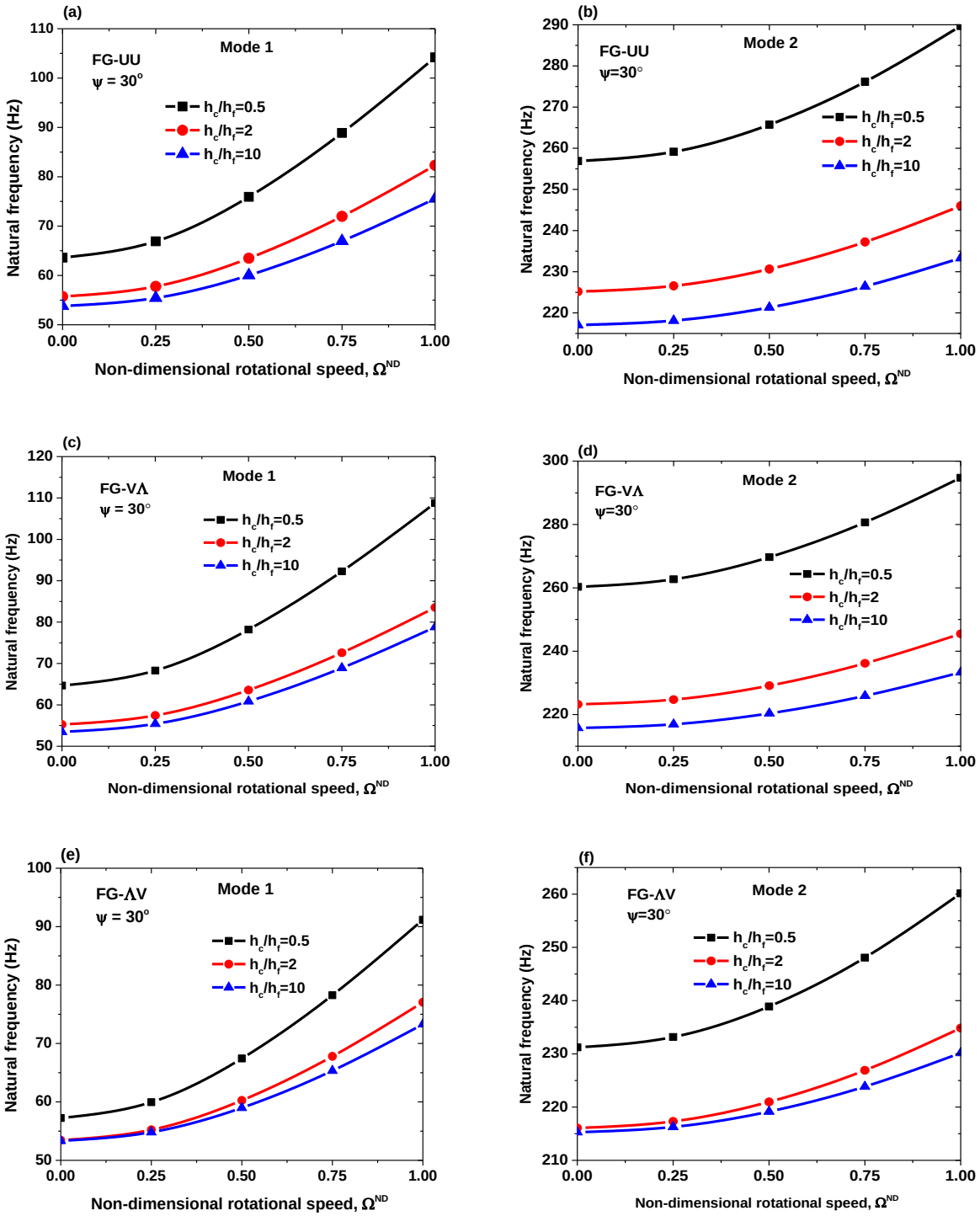

Fig. 4.9 Effect of non-dimensional rotational speed on the natural frequencies (Hz) of pretwisted ($\psi = 30°$) FG-GRC sandwich conical shells with three different distribution patterns at $T = 500$ K: (a) FG-UU, Mode 1, (b) FG-UU, Mode 2, (c) FG-VΛ, Mode 1, (d) FG-VΛ, Mode 2, (e) FG-ΛV, Mode 1, and (f) FG-ΛV, Mode 2 [$s = 0.4$ m, $L/s = 0.7$, $\phi_0 = \phi_v = 20°$, $\psi = 30°$, $s/h = 100$]

4.6 MODE SHAPES

Table 4.5 and **Table 4.6** display the first four mode shapes of the FG-VΛ GRC sandwich conical shells for pretwist angles ψ = 0° and 30°, respectively, under two different thermal conditions (T = 300 K and 500 K) and three rotational speeds (Ω^{ND}= 0.0, 0.5, and 1.0). Here, three-dimensional surface plots along with contour plots underneath the mode shapes are depicted to comprehend the vibration patterns executed by the FG-GRC sandwich conical shells. It is noticed that the first two modes of the untwisted ($\psi = 0°$) FG-GRC sandwich conical shells correspond to the first span-wise bending mode (1B) and second span-wise bending mode (2B), respectively, irrespective of rotational speeds and thermal conditions. The third and fourth modes of untwisted FG-GRC sandwich conical shells indicate third span-wise bending mode (3B) and first twisting mode (1T), respectively, for T =300 K, while the corresponding modes are found to be first twisting mode (1T) and third span-wise bending mode (3B), respectively for T =500 K. It is also observed that the first three modes of the pretwisted (ψ = 30°) FG-GRC sandwich conical shells, i.e., first span-wise bending (1B), second span-wise bending (2B) and third span-wise bending (3B) modes are similar for all temperatures and rotational speeds, while the next mode corresponds the fourth bending mode (4B) and first twisting mode (1T) for temperatures 300 K and 500 K, respectively.

Table 4.5 Effects of temperature and rotational speed on the mode shapes of the untwisted ($\psi = 0°$) GRC sandwich conical shells with FG-VΛ grading pattern [$s = 0.4$ m, $L/s = 0.7, \phi_0 = \phi_v = 20°, s/h = 1000, h_c/h_f = 0.5$]

Ω^{ND}	Temp. (K)	Mode 1	Mode 2	Mode 3	Mode 4
0.0	300	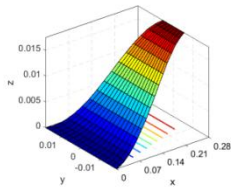	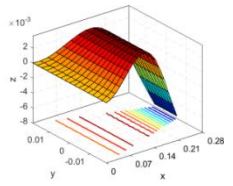	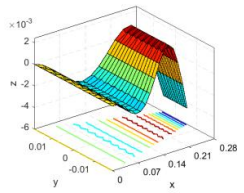	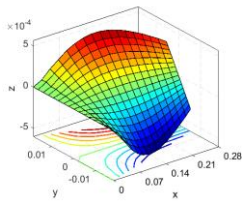
	500	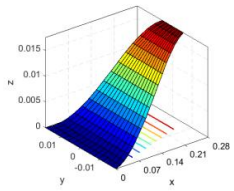	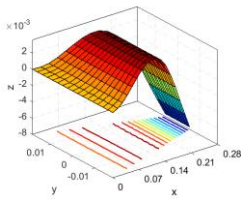	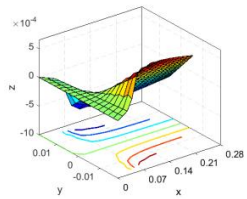	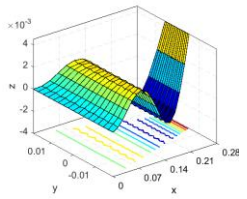
0.5	300	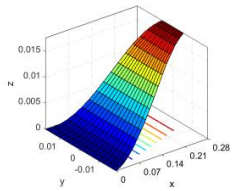	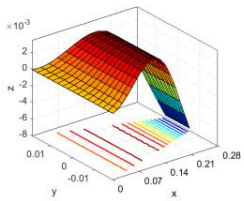	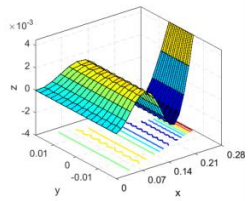	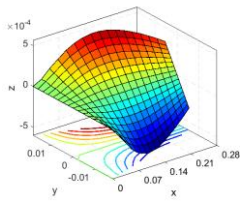
	500	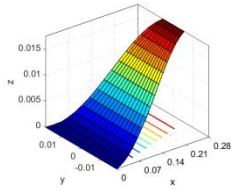	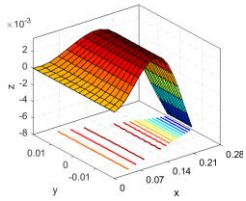	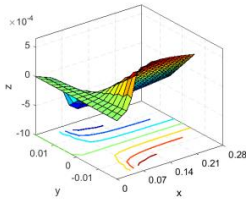	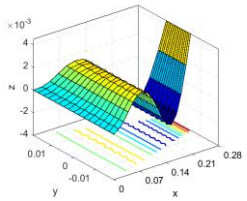
1.0	300	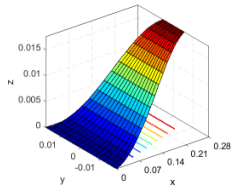	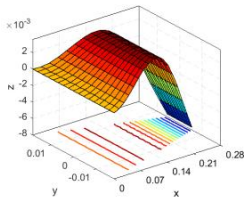	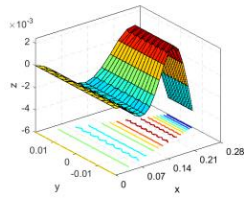	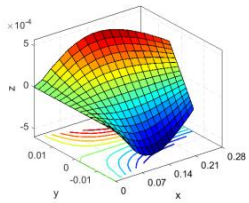
	500	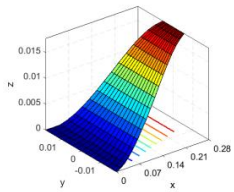	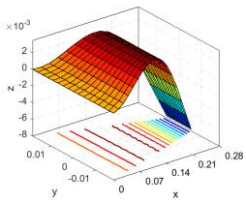	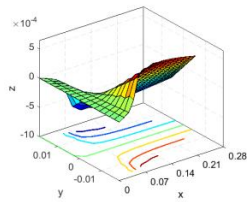	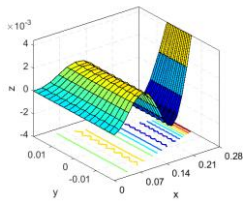

Table 4.6 Effects of temperature and rotational speed on the mode shapes of the pretwisted ($\psi = 30°$) GRC sandwich conical shells with FG-VΛ grading pattern [$s = 0.4$ m, $L/s = 0.7$, $\phi_0 = \phi_v = 20°$, $s/h = 1000$, $h_c/h_f = 0.5$]

Ω^{ND}	Temp .(K)	Mode 1	Mode 2	Mode 3	Mode 4
0.0	300	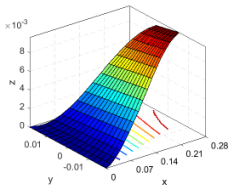	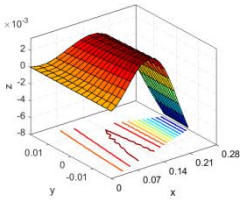	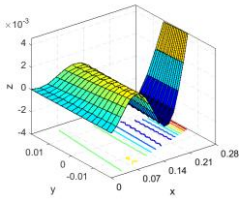	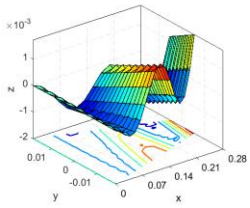
	500	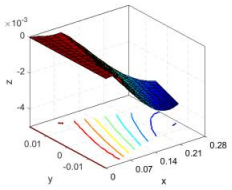	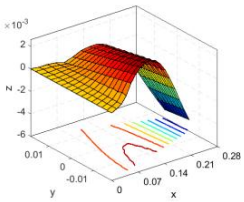	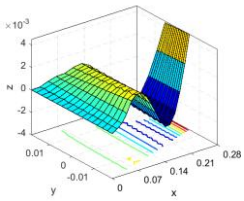	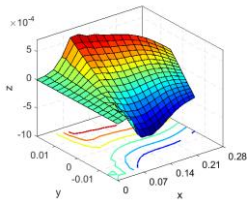
0.5	300	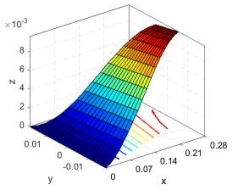	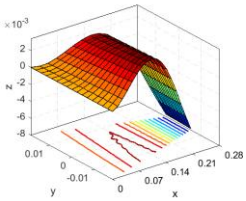	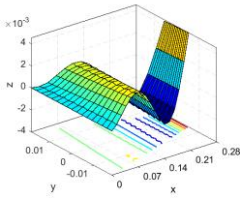	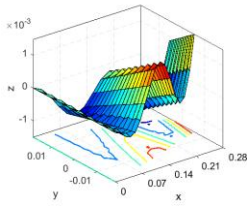
	500	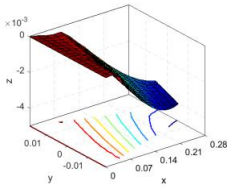	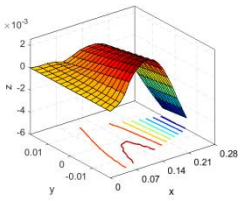	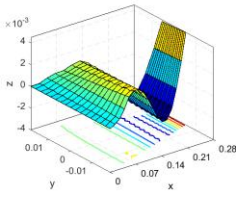	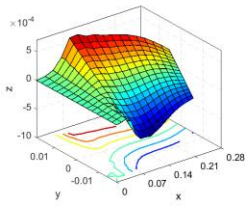
1.0	300	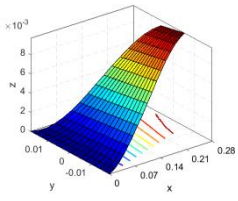	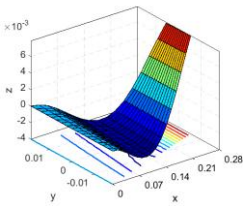	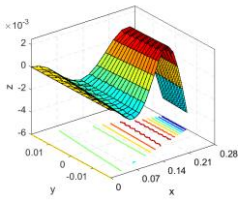	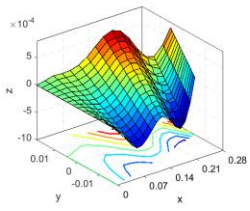
	500	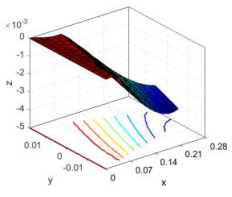	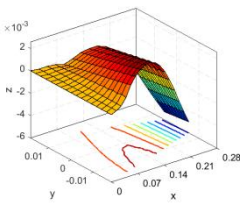	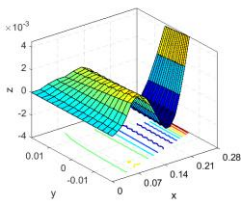	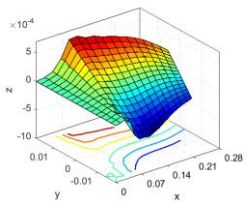

CHAPTER 5

DYNAMIC BEHAVIOR OF TEMPERATURE-DEPENDENT FG-CNTRC SANDWICH CONICAL SHELLS UNDER LOW-VELOCITY IMPACT

5.1 INTRODUCTION

The impact loadings are regarded as the most severe type of loading for composite materials. During manufacturing, operation, maintenance, and transportation, the laminated composites and sandwich structures are frequently subjected to impact with foreign bodies of different sizes and shapes. The impact with foreign objects at low-velocity (typically less than 10 m/s) results in invisible and undetectable damages such as facing/core debonding, delamination in the composite facings, fiber breakage, matrix cracking, and cracking in the core is generally found in aircraft wings, fan blades in jet engine and protruded section in automobiles. Turbo-machinery blades are under a preload resulting from centrifugal forces, and as a consequence, the initial stresses may worsen the damage due to impact, especially in thermal environments. However, the impact resistance can be improved by using carbon nanofillers reinforcement (CNTs and graphene) with functionally graded distribution. The transient responses of these structures are mostly dependent on the presence of initial stresses arising during manufacture or from environmental effects like thermal strain.

5.2 NUMERICAL RESULTS AND DISCUSSIONS

The numerical results obtained from the developed formulation are presented to analyze the impact behavior of the cantilever pretwisted sandwich conical shells having CNTs-reinforced nanocomposite (CNTRC) facings and homogenous core. Firstly, convergence and validation studies are performed for examining the stability and correctness of the present formulation for predicting the impact response. Secondly, parametric studies are carried out to analyze the effect of different parameters on the low-velocity impact behavior of the FG-CNTRC sandwich conical shells. This work also considers poly methyl methacrylate (PMMA) as matrix and (10, 10) armchair SWCNTs reinforcing constituents for the CNTRC face sheets, as considered in Chapter 3. The temperature-dependent required properties of PMMA are also assumed as (Wang and

Shen, 2012): $E^m = (3.52 - 0.0034T)$ GPa, $\nu^m = 0.34$, $\rho^m = 1150$ kg/m^3, and $\alpha^m = 45.0(1 + 0.0005\Delta T) \times 10^{-6}$/K. The temperature-dependent elastic properties and efficiency parameters of SWCNTs are already given in **Table 3.1** and **Table 3.2,** respectively, in Chapter 3. Further, Titanium alloy (Ti-6Al-4V) is selected as core layer with the following material properties (Wang and Shen, 2012): $E_c = 122.56(1 - 4.586 \times 10^{-4}T)$ GPa, $\nu_c = 0.29$, $\rho_c = 4429$ kg/m^3, and $\alpha_c = 7.5788(1 + 6.638 \times 10^{-4}T - 3.147 \times 10^{-4}T^2) \times 10^{-6}$/K.

The following geometrical dimensions of the FG-CNTRC sandwich conical shells are considered: $s = 0.4$ m, $L/s = 0.7$, $\phi_0 = \phi_v = 20°$.

5.3 CONVERGENCE STUDY

In order to ensure the convergence of the FE mesh and steadiness of the time integration technique, the time histories of contact force and central shell displacement for FG-UU CNTRC sandwich conical shells are determined at an elevated temperature $T = 500$ K with the following parameters: $s = 0.4$ m, $L/s = 0.7$, $\phi_0 = \phi_v = 20°$, $s/h = 100$, $\psi = 30°$, $h_c/h_f = 2$, $V^*_{CNT} = 0.12$, $d_{imp} = 12.7$ mm, $V_0 = 3$ m/s.

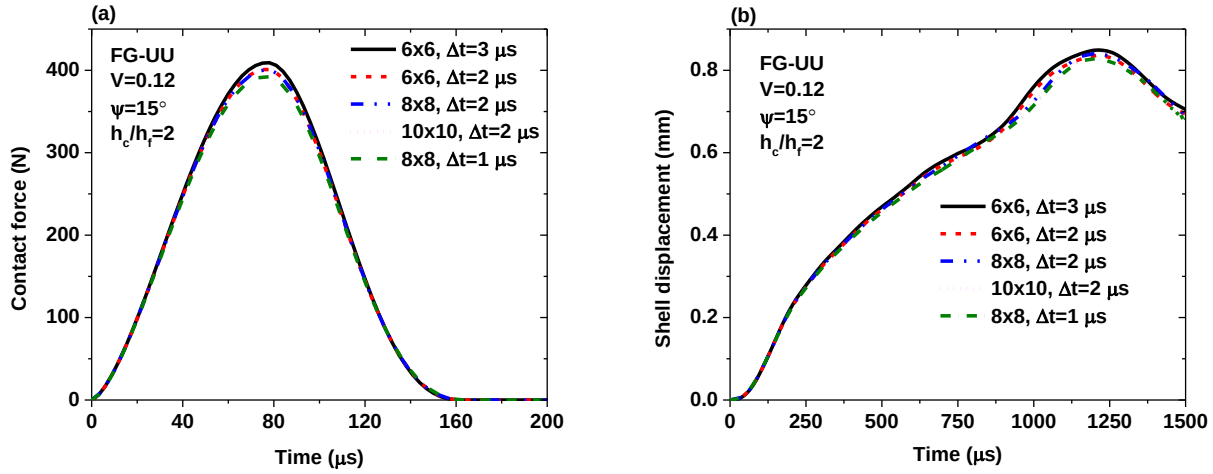

Fig. 5.1 Convergence of (a) contact force and (b) central shell displacement for pretwisted FG-CNTRC sandwich conical shell at an elevated temperature $T = 500$ K

The obtained results are illustrated in **Fig. 5.1**, considering a variety of mesh sizes and time steps. The error among the results is found to decrease when the mesh becomes finer and the time step becomes smaller. Hence, an 8×8 mesh size with a time step of 2 μs is reasonably considered for the subsequent analyses.

5.4 COMPARISON STUDY

After the convergence study, two different examples are selected from the literature for the validation of the present formulation and solution method. In the first example, the temporal variations of contact force and normalized plate displacement of a graphite/epoxy composite [(0/90/0/90/0)$_s$] plate due to low-velocity impact are obtained from the present method and compared with those reported by Sun and Chen (1985), as shown in **Fig. 5.2**. The following geometrical and material properties of the composite plates considered: $L = b = 0.2$ m, $h = 0.00269$ m, $E_1 = 120$ GPa, $E_2 = 7.9$ GPa, $G_{12} = G_{23} = G_{13} = 5.5$ GPa, $\nu_{12} = 0.30$, $\rho = 1.58\times10^{-5}$ N-s^2 /cm^4. Here, a spherical steel impactor with diameter $d_{imp} = 12.7$ mm is assumed to impact centrally on the simply-supported (SSSS) composite plate at the initial velocity of $V_0 = 3$ m/s. As evident in this figure, the results of the present approach are in good conformity with those reported results.

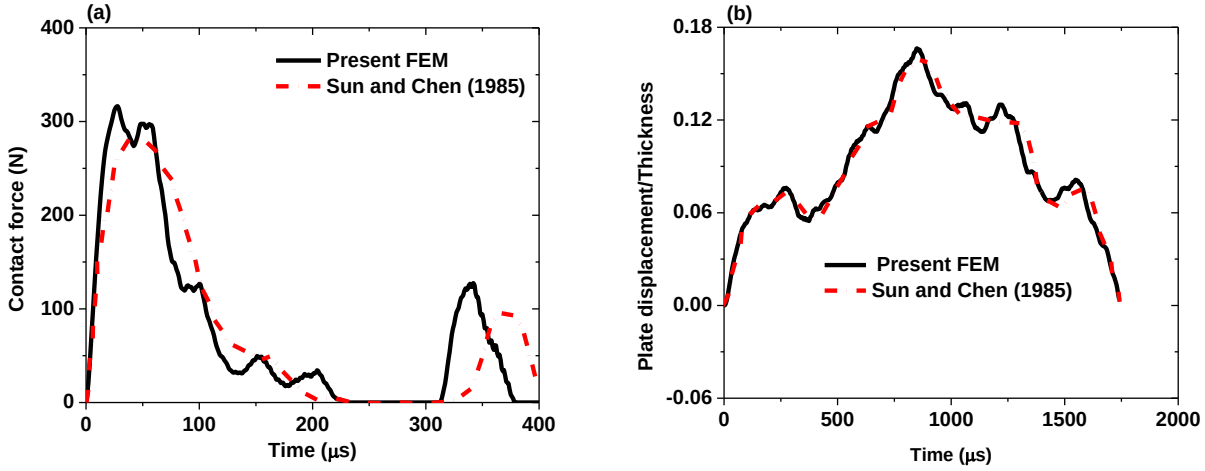

Fig. 5.2 Temporal variations of (a) contact force and (b) central plate displacement of an SSSS graphite/epoxy composite plate due to low-velocity

Another example is extracted from the work of Wang *et al.* (2014) to validate the present method with respect to the impact response of nanocomposite sandwich plate with FG-CNTRC face sheets and titanium alloy core. In this example, a simply supported FG-VΛ type CNTRC sandwich plate is considered to be impacted centrally with a spherical impactor ($d_{imp} = 12.7$ mm, $V_0 = 3$ m/s). The following geometrical properties are considered here:

$L/b = 1, b/h = 10,\ h_f = 1$ mm, $h_c = 8$ mm. The temporal variations of the contact force and plate deflection, along with those of Wang *et al.* (2014), are illustrated in **Fig. 5.3**. It is evident that the results of the present method agree with their reference values reasonably, and the difference found between the results is due to the exclusion of kinematic nonlinearity in the present model.

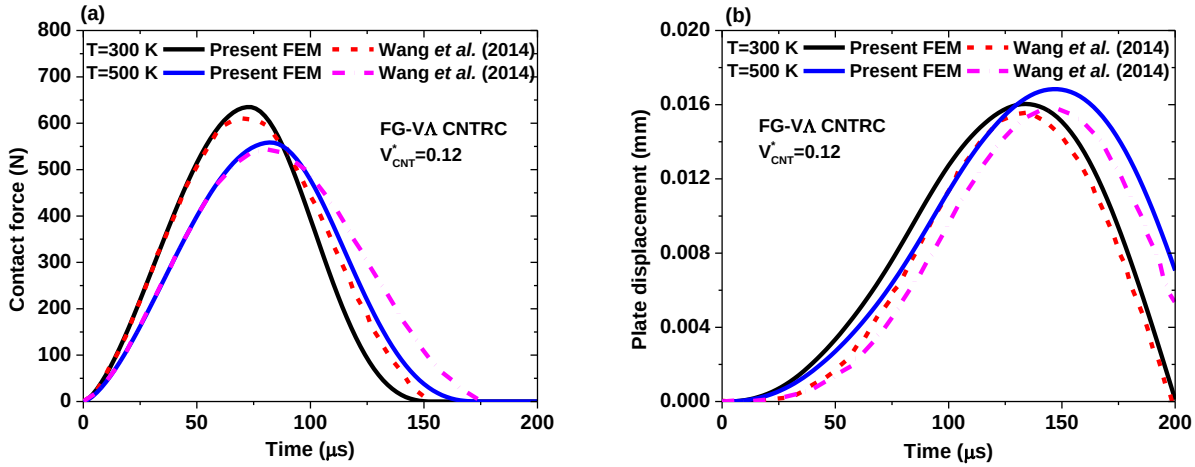

Fig. 5.3 Temporal variations of (a) contact force and (b) central plate displacement of an SSSS FG-VΛ CNTRC sandwich plate under low-velocity impact at two different temperatures $T =$ 300 K and 500 K

5.5 PARAMETRIC STUDY

After convergence and validation of the present model, the effects of various parameters on the impact response of pretwisted sandwich conical shells with FG-CNTRC face sheets and titanium alloy core are investigated considering the following geometrical dimensions: $s = 0.4$ m, $L/s = 0.7$, $\phi_0 = \phi_v = 20°$. A steel impactor having material properties $E_{imp} = 207$ GPa, $\nu_{imp} = 0.3$, and $\rho_{imp} = 7960$ kg/m^3 is assumed to impact at the central point $(x = L/2,\ y = 0)$ of the target sandwich panel. If otherwise not stated, the cone length-to-thickness ratio, impactor diameter, and initial velocity of the impactor are considered as $s/h = 100$, $d_{imp} = 12.7$ mm, and $V_0 = 3$ m/s, respectively.

5.5.1 INFLUENCE OF CNTs GRADING PATTERN

The influence of CNTs grading pattern on the impact response of pretwisted FG-CNTRC sandwich conical shell panel at the reference temperature ($T = 300$ K) is illustrated in **Fig. 5.4**. Here, five different CNTs grading patterns, namely, FG-UU, FG-VΛ, FG-ΛV, FG-OO, and FG-XX, are taken into consideration. The CNTs volume fraction, core-to-facing thickness ratio, and pretwist angle are assumed to be $V_{CNT}^{*} = 0.12$, $h_c/h_f = 0.5$, and $\psi = 15°$, respectively.

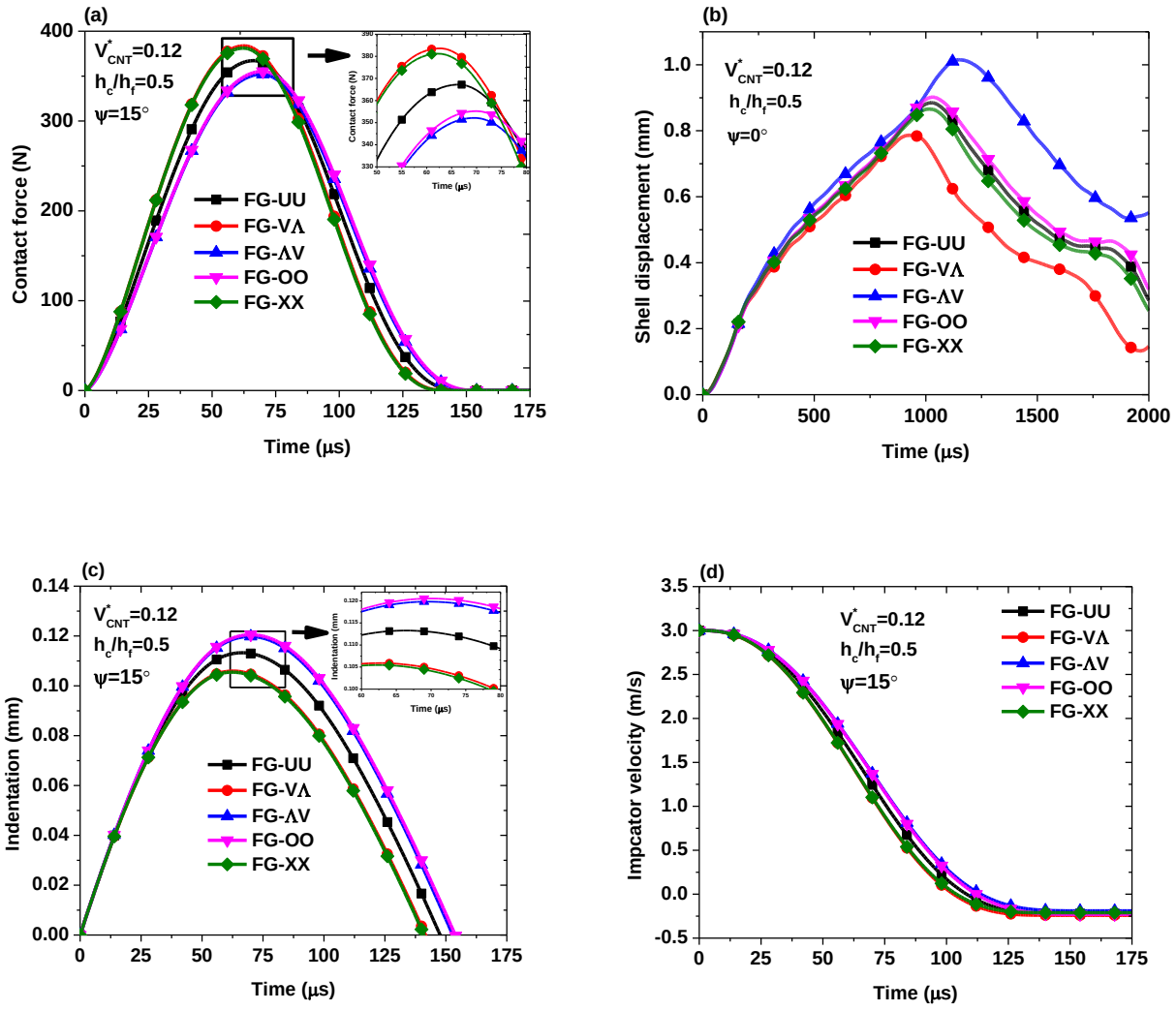

Fig. 5.4 Influence of CNTs grading pattern on impact response of FG-CNTRC sandwich conical shell panel at the reference temperature $T = 300$ K: (a) contact force, (b) central shell displacement, (c) indentation, and (d) impactor velocity

As depicted in **Fig. 5.4(a),** the case of FG-VΛ possesses the maximum peak value of contact force with the shortest contact duration, while the case of FG-ΛV possesses the minimum value of contact force with the longest contact duration among the five grading patterns considered. This is due to the highest transverse Young's moduli of the surface with densely populated CNTs in the case of the FG-VΛ pattern, as evident from the CNTs distribution pattern in **Fig. 2.2**. It is worth mentioning that the material properties of the impact surfaces can affect the contact force. However, the contact force for the sandwich conical panels having FG-VΛ grading profile is slightly larger than FG-XX, although their contact surfaces have the same material properties. It can be inferred that the contact force is affected by the material properties of the contact surface. For the same reason, FG-VΛ has the lowest central shell displacement and impactor velocity, while FG-ΛV has the highest central shell displacement and impactor velocity**.** However, the effect of CNTs grading pattern on the shell displacement becomes more apparent as time elapses. The highest and lowest indentations are found in the case of grading profiles FG-OO and FG-XX, respectively.

5.5.2 INFLUENCE OF CNTs VOLUME FRACTION

The influence of CNTs volume fraction V_{CNT}^{*} on the impact response of pretwisted CNTRC sandwich conical shells with FG-VΛ grading profile at the reference temperature $T = 300$ K is demonstrated in **Fig. 5.5**. The time histories of contact force, central shell displacement, indentation, and impactor velocity are determined considering three different values of $V_{CNT}^{*} =$ 0.12, 0.17, and 0.28 with $h_c/h_f = 0.5$ and $\psi = 15°$. It is seen from the time history of contact force in **Fig. 5.5(a)** that an increase in CNTs volume fraction V_{CNT}^{*} results in higher contact force and shorter contact duration. This is due to the fact that an increase in the CNTs volume fraction results in an increase in the contact stiffness of the sandwich conical shell with FG-VΛ grading pattern at the impact point. This increase in the contact stiffness is also responsible for the reduction in the central shell displacement, indentation, and impactor velocity with an increment of V_{CNT}^{*}, as shown in **Figs. 5.5(b)-(d).** It is further to note that the times for attaining the peak contact force, shell displacement, and indentation become shorter as V_{CNT}^{*} increases due to the increase in effective stiffness of the shell.

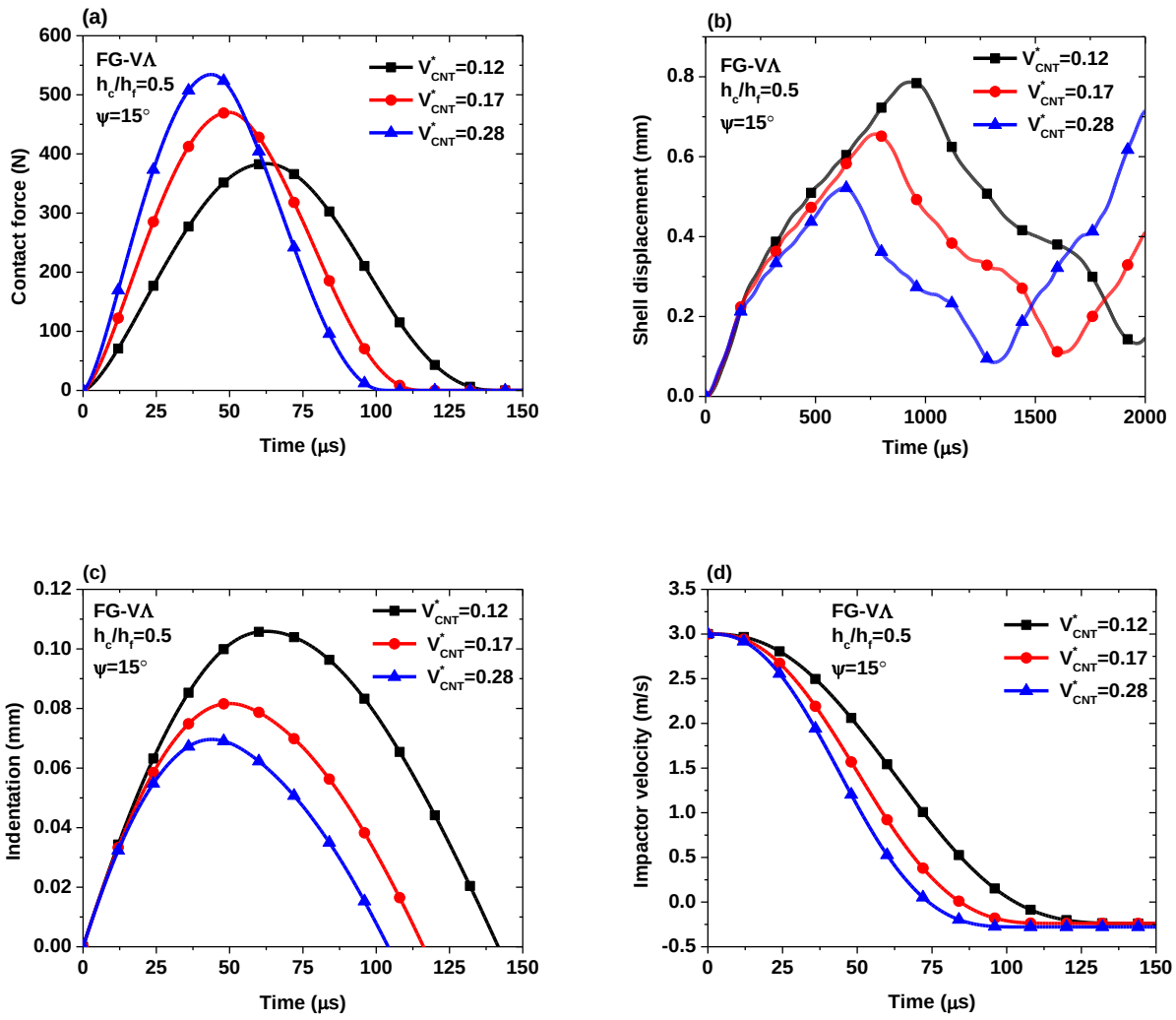

Fig. 5.5 Influence of CNTs volume fraction on impact response of FG-CNTRC sandwich conical shell at the reference temperature $T = 300$ K: (a) contact force, (b) central shell displacement, (c) indentation, and (d) impactor velocity

5.5.3 INFLUENCE OF THERMAL ENVIRONMENT

The influence of thermal environment on the impact response of pretwisted FG-CNTRC sandwich conical shell is depicted in **Fig. 5.6**. In this figure, the results are obtained for three different temperatures $T = 300$ K, 500 K, and 700 K considering two CNTs grading patterns, namely, FG-VΛ and FG-ΛV with CNTs volume fraction $V_{CNT}^{*} = 0.12$, core-to-facing thickness ratio $h_c/h_f = 0.5$, and pretwist angle $\psi = 15°$. A rise in temperature of the environment results in a lower peak value of the contact force with a longer contact duration irrespective of the CNTs

grading pattern, as evident in **Fig. 5.6(a)**. In contrast, the peak central shell deflection, peak indentation, and impactor velocity are found to increase with the rising of temperature, as depicted in **Figs. 5.6(b)-(d),** respectively. It is obvious because the elastic properties of both facing and core layers decrease with an increase in the service temperature. In addition, there is a decrease in the contact stiffness $k_c(T)$, which in turn is dependent on the transverse Young's modulus $E_{22}(T)$ of the facing on which the impact occurs. As such, with an increase in the temperature, the sandwich construction becomes more flexible, which results in lower contact force, longer contact duration, and higher values of shell displacement, indentation, and impactor velocity.

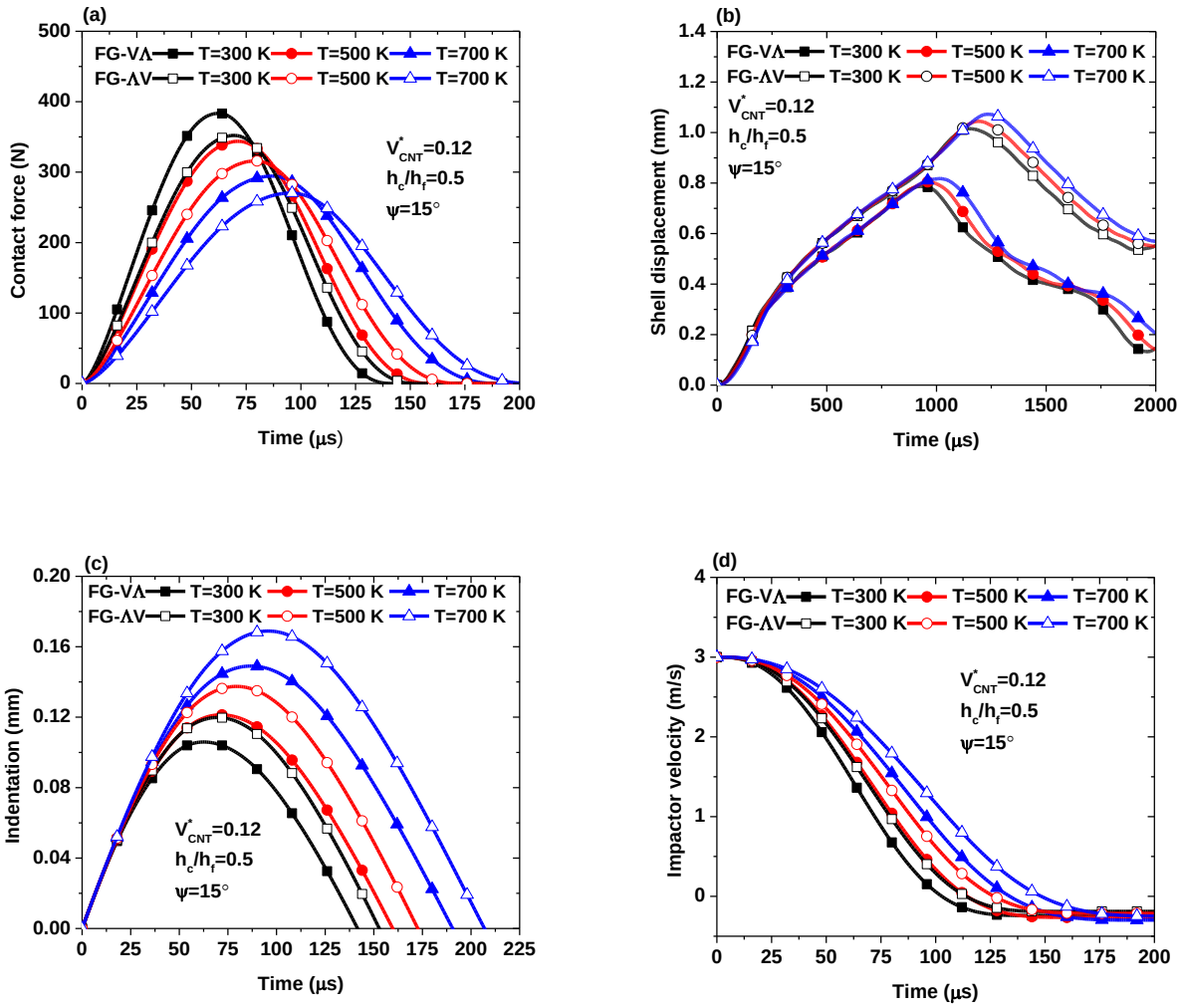

Fig. 5.6 Influence of temperature on impact response of FG-CNTRC sandwich conical shell: (a) contact force, (b) central shell displacement, (c) indentation, and (d) impactor velocity

5.5.4 INFLUENCE OF PRETWIST ANGLE

Fig. 5.7 illustrates the influence of pretwist angle ($\psi = 0°$, 15°, and 30°) on the impact behavior of FG-VΛ CNTRC sandwich conical shell with CNTs volume fraction $V_{CNT}^{*} = 0.12$ and core-to-facing thickness ratio $h_c/h_f = 0.5$ at an elevated temperature $T = 500$ K.

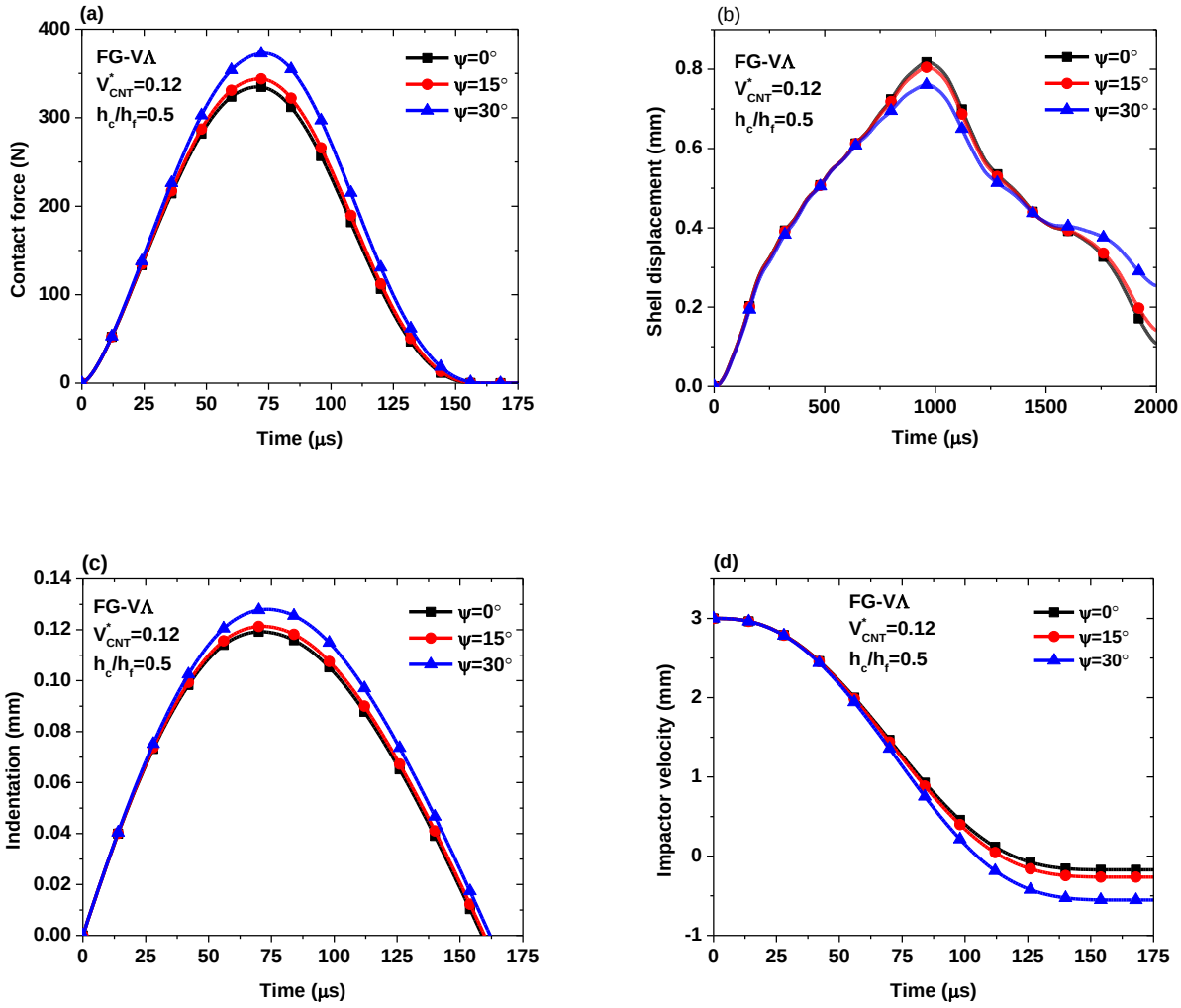

Fig. 5.7 Influence of pretwist angle on impact behavior of FG-CNTRC sandwich conical shell at an elevated temperature of $T = 500$ K: (a) contact force, (b) central shell displacement, (c) indentation, and (d) impactor velocity

From the time history of contact force, as displayed in **Fig. 5.7(a),** it is clear that the peak value of contact force increases with an increase in pretwist angle. Obviously, the pretwisted structures are less stiff than the untwisted structures since the structural stiffness decreases with

increasing pretwist angle. However, an increase in pretwist angle results in a higher local indentation at the impact point (estimated using **Eq.(2.141)**), which in turn increases the resulting contact force. Further, the maximum shell displacement and impactor velocity are found to decrease with an increase in pretwist angle, as shown in **Fig. 5.7(b)** and **(d),** respectively. Besides, the contact duration, peak time of contact force, and the peak time of shell displacement are found to be almost independent of the pretwist angle.

5.5.5 INFLUENCE OF CORE-TO-FACE SHEETS THICKNESS RATIO

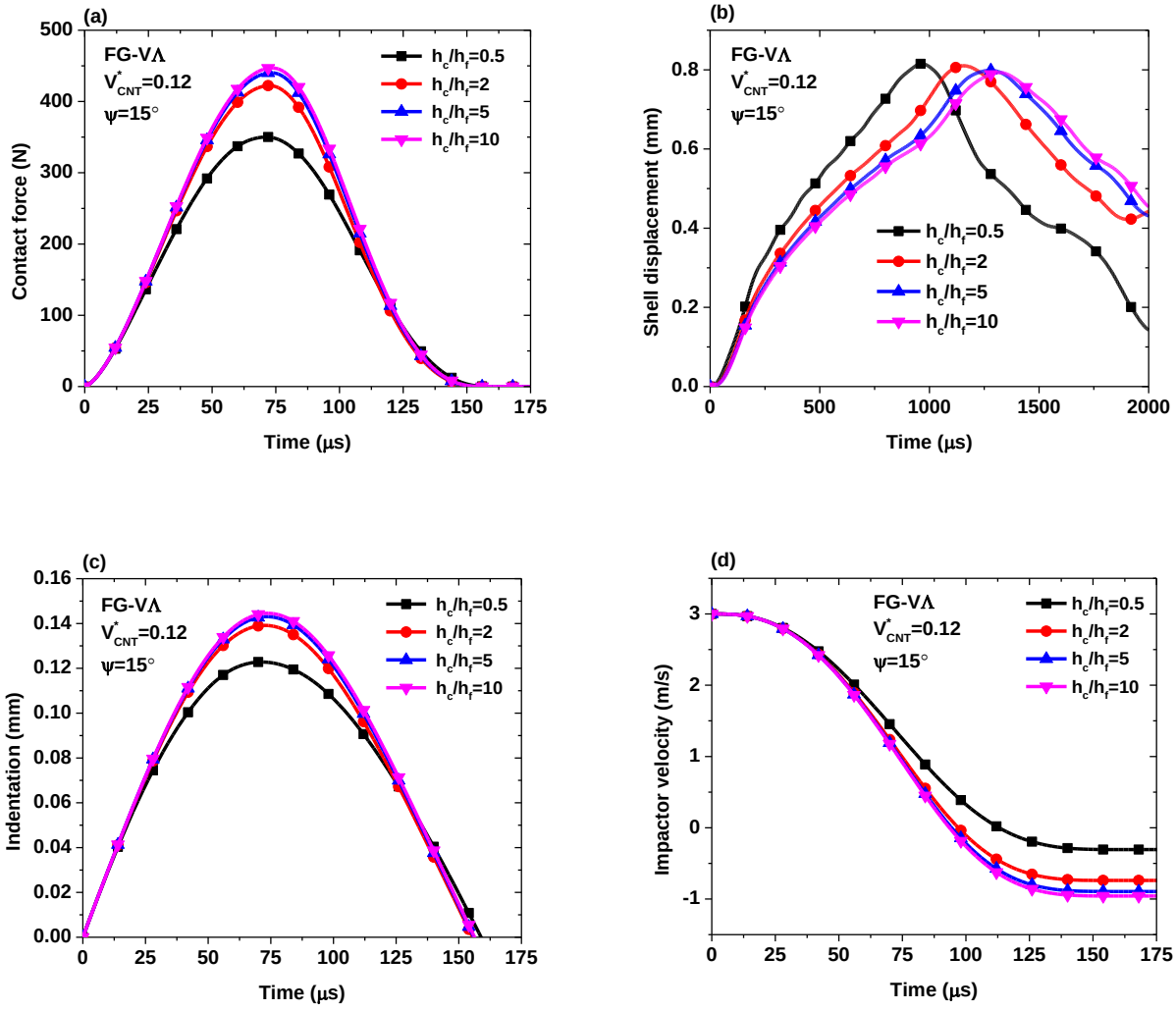

Fig. 5.8 Influence of core-to-face sheets thickness ratio on impact response of FG-CNTRC sandwich conical shell at the elevated temperature of $T = 500$ K: (a) contact force, (b) central shell displacement, (c) indentation, and (d) impactor velocity

The influence of core-to-face sheets thickness ratio h_c/h_f on the impact behavior of pretwisted FG-CNTRC sandwich conical shell with FG-VΛ grading profile, CNTs volume fraction $V_{CNT}^{*} = 0.12$, and pretwist angle $\psi = 15°$ is presented in **Fig. 5.8**. In this regard, temporal variations of the contact force, shell displacement, indentation, and impactor velocity for four different values of core-to-face sheets thickness ratios $h_c/h_f = 0.5$, 2, 5, and 10 at the elevated temperature $T = 500$ K are obtained and presented in **Figs. 5.8(a)-(d)**, respectively. As seen from these figures, an increase in the h_c/h_f ratio leads to higher values of contact force and indentation while the shell displacement and impactor velocity increase. In view of the fact that the overall thickness of the sandwich panel is constant, therefore, increasing h_c/h_f ratio involves a thicker core and thinner facings. Obviously, the higher thickness of the titanium alloy core causes higher stiffness as the core is stiffer than the CNTRC facings, which in turn leads to higher contact force and indentation. Accordingly, the central shell displacement and impactor velocity decrease when the ratio h_c/h_f is increased. It is further noted that the contact duration and peak time of contact force remain unaltered, whereas the peak time of shell displacement becomes longer with an increase in the h_c/h_f ratio.

5.5.6 INFLUENCE OF CONE LENGTH-TO-THICKNESS RATIO

The influence of cone length-to-thickness ratio s/h on the impact response of pretwisted FG-CNTRC sandwich conical shell having FG-VΛ type of CNTs grading pattern at elevated temperature $T = 500$ K is analyzed as depicted in **Fig. 5.9**. The time histories of contact force, shell displacement, indentation, and impactor velocity for three different values of the ratios $s/h = 50$, 100, and 200 are evaluated and furnished in **Figs. 5.9(a)-(d),** respectively. Here, the CNTs volume fraction, core-to-facing thickness ratio, and pretwist angle are considered as $V_{CNT}^{*} = 0.12$, $h_c/h_f = 2$, and $\psi = 15°$, respectively. It is seen that an increase in cone length-to-thickness ratio leads to a decrease in contact force and indentation while the central shell displacement and impactor velocity increase. The contact duration is found to be almost invariant with the increase in s/h ratio. Further, the peaks of contact force and indentation shift toward the left, while the peak of the shell displacement shifts toward the right as the s/h ratio is increased. Such a type of impact response of this structure is anticipated because the sandwich conical shell panel turns less stiff when the ratio s/h is increased.

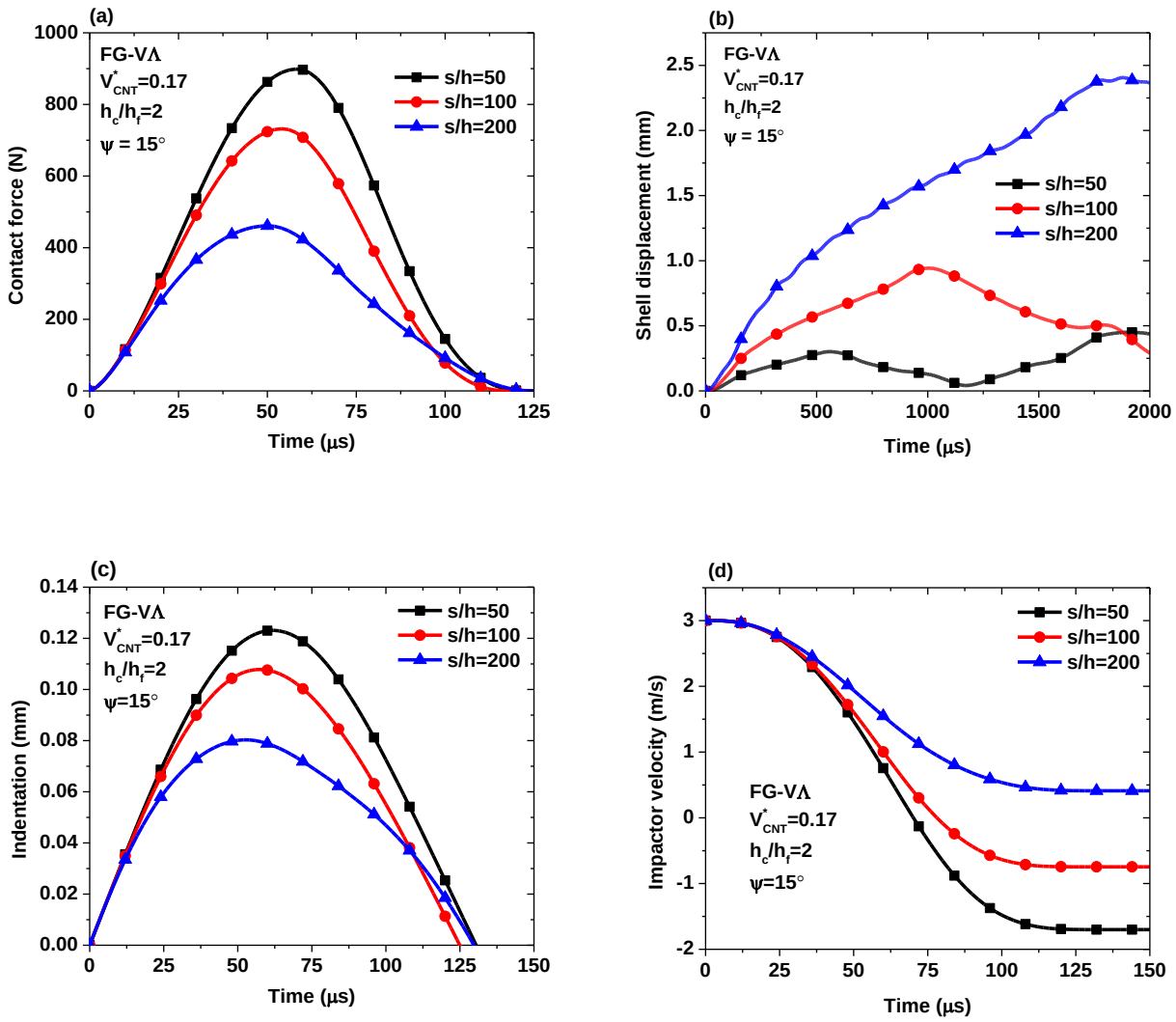

Fig. 5.9 Influence of cone length-to-thickness ratio on impact response of FG-CNTRC sandwich conical shell panel at an elevated temperature of $T = 500$ K: (a) contact force, (b) central shell displacement, (c) indentation, and (d) impactor velocity

5.5.7 INFLUENCE OF INITIAL VELOCITY OF THE IMPACTOR

In this part, the effect of initial impactor velocity on the impact behavior of FG-CNTRC sandwich conical shell having core-to-facing thickness ratio $h_c/h_f = 5$ and pretwist angle $\psi = 15°$ at an elevated temperature $T = 500$ K is analyzed. An FG-VΛ grading pattern with CNTs volume fraction $V_{CNT}^{*} = 0.17$ in the CNTRC sandwich conical shell is considered. Three different low-range initial velocities of the spherical steel impactor, i.e., $V_0 = 1$ m/s, 3 m/s, and 5 m/s are assumed to obtain the contact force, central shell displacement, indentation, and impactor

velocity within the considered time span. The temporal variations of contact force, central shell displacement, indentation, and impactor velocity are displayed in **Figs. 5.10(a)-(d),** respectively.

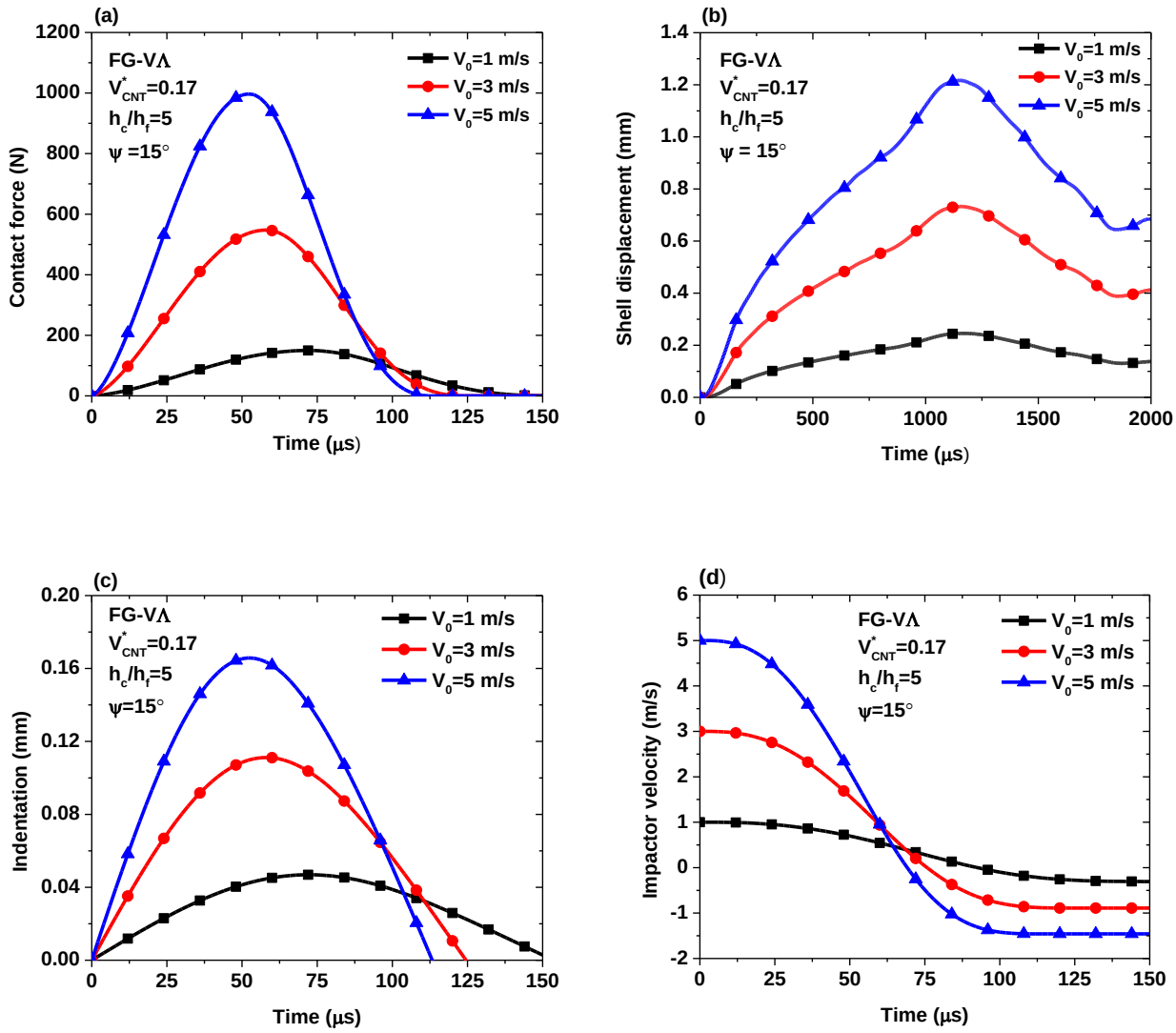

Fig. 5.10 Effect of initial velocity of impactor on impact response of FG-VΛ CNTRC sandwich conical shell at an elevated temperature of $T = 500$ K: (a) contact force, (b) central shell displacement, (c) indentation, and (d) impactor velocity

As observed in **Fig. 5.10**, the maximum contact force, maximum shell displacement, and maximum indentation are found to increase with an increase in initial velocity of the impactor, while the contact duration decreases due to an increase in initial kinetic energy of the impactor. The times reaching the peak of contact force and maximum indentation become shorter, while the peak time of the central shell displacement is unaltered with the increase of

initial velocity. It is also found that the impactor velocity increases with an increase in initial impactor velocity in the loading phase, whereas it decreases in the unloading phase.

5.5.8 INFLUENCE OF SIZE OF THE IMPACTOR

Fig. 5.11 illustrates the effect of impactor size on the impact response of the CNTRC sandwich conical shell with FG-VΛ type of CNTs grading pattern.

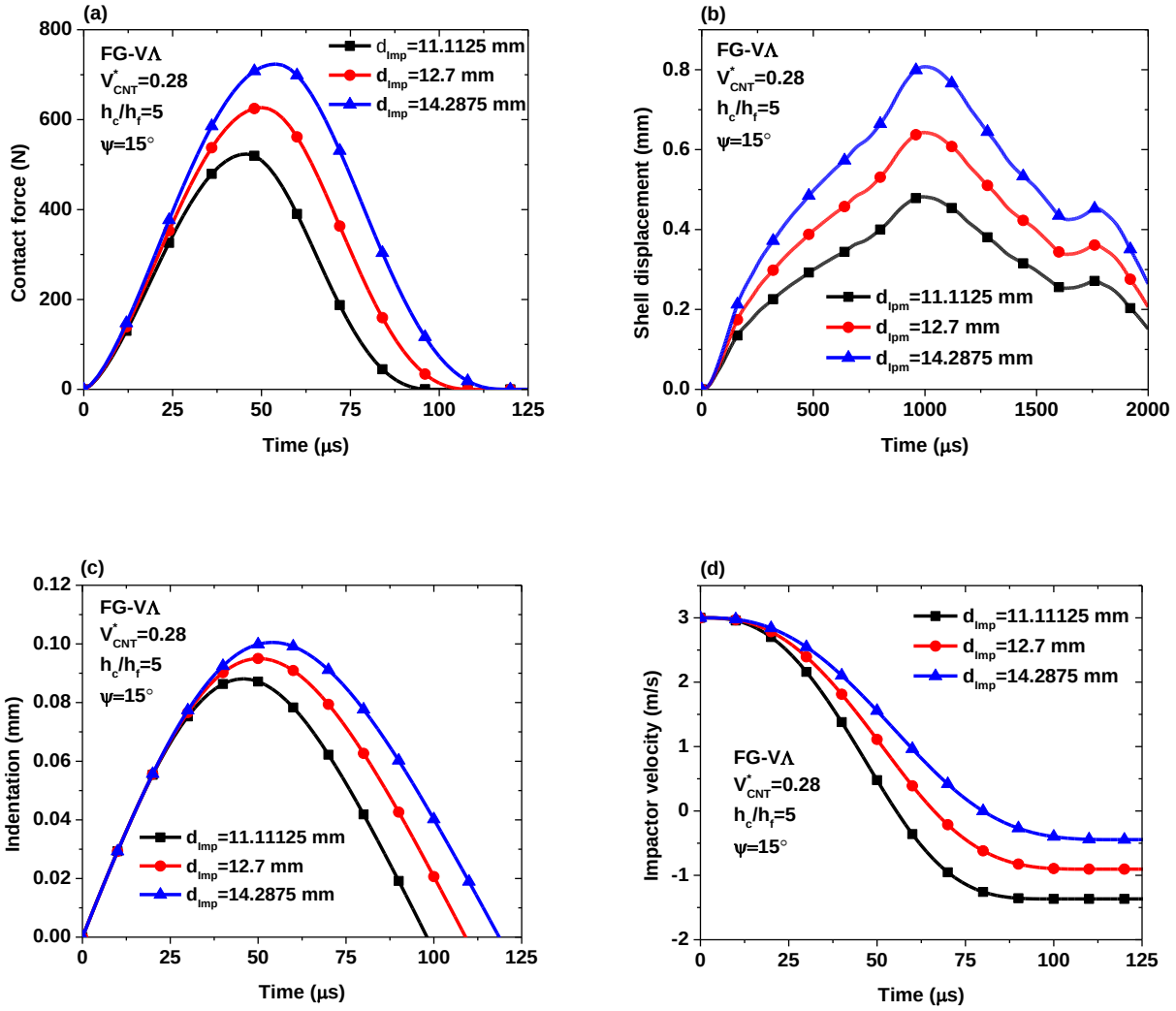

Fig. 5.11 Effect of impactor size on impact response of FG-VΛ CNTRC sandwich conical shell at an elevated temperature of $T = 500$ K: (a) contact force and (b) central shell displacement, (c) indentation, and (d) impactor velocity

In this case, the results are obtained for the CNTs volume fraction $V_{CNT}^{*} = 0.28$, core-to-facing thickness ratio $h_c/h_f = 5$, and pretwist angle $\psi = 15°$ at an elevated temperature $T = 500$ K. Also, three different diameters of spherical steel impactor, i.e., $d_{imp} = 11.1125$ mm $\left(\frac{7"}{16}\right)$, 12.7 mm $\left(\frac{1"}{2}\right)$, and 14.2875 mm $\left(\frac{9"}{16}\right)$ are selected. As observed in the figures, an increase in impactor diameter would lead to higher values of peak contact force, contact duration, central shell displacement, indentation, and impactor velocity within the considered time span. This may be attributed due to the higher value of contact stiffness of the system and the larger mass and kinetic energy of the impactor with its bigger diameter. Further, the peak times of contact force and indentation become longer for the impactor of bigger diameter, whereas the peak time of central shell displacement is nearly invariant with the impactor diameter.

CHAPTER 6

TRANSIENT RESPONSE OF FG-GRC SANDWICH CONICAL SHELL UNDER LOW-VELOCITY IMPACT IN THERMAL ENVIRONMENTS

6.1 INTRODUCTION

In this chapter, the dynamic response of the FG-GRC sandwich conical shells under low-velocity impact in thermal environments are investigated using the present mathematical formulation. A spherical impactor is assumed to impact centrally on the FG-GRC sandwich conical shells. The time histories of contact force, shell displacement, indentation, and impactor velocities are presented in the subsequent sections.

6.2 NUMERICAL RESULTS AND DISCUSSIONS

The numerical results are obtained from the developed computer codes to study the transient analysis of the cantilevered pretwisted sandwich conical shells with two symmetric GRC face sheets and a homogeneous core under low-velocity impact. The GRCs are assumed to reinforce with the zigzag graphene sheets having effective thickness $h_G = 0.188$ nm and mass density $\rho_G = 4118$ kg/m^3 into PMMA matrix as considered in Chapter 4. The temperature-dependent material properties of graphene sheets and efficiency parameters of graphene/PMMA nanocomposite are already given in **Table 4.1** and **Table 4.2**, respectively, while $G_{13} = G_{12}$ and $G_{23} = 0.5G_{12}$ are assumed. The material properties of PMMA are considered as ρ^m =1150 kg/m^3,ν^m =0.34, $\alpha^m = 45(1 + 0.0005\,\Delta T) \times 10^{-6}$/K, and $E^m = (3.52 - 0.0034T)$ GPa in which $T = T_0 + \Delta T$ and $T_0 = 300$ K (reference temperature). Titanium alloy (Ti-6Al-4V) is seleccted for the homogenous core part which has the following temperature-dependent Young's modulus and thermal expansion coefficient (Wang and Shen 2018) of $E_c = 122.56(1 - 4.586 \times 10^{-4}T)$ GPa and $\alpha_c = 7.5788(1 + 6.638 \times 10^{-4}T - 3.147 \times 10^{-6}T^2) \times 10^{-6}$/K. Besides, the Poisson's ratio is assumed to be a constant, and ν_c = 0.29, and ρ_c = 4429 kg/m^3.

6.3 CONVERGENCE STUDY

The convergence of contact force of the pretwisted FG-GRC sandwich conical shell with FG-UU type of graphene grading pattern at $T = 500$ K is performed considering two cases. The geometrical dimensions of the cantilever pretwisted sandwich conical shells are considered as: $s = 0.4,\ L/s = 0.7,\ \phi_0 = \phi_v = 20°, s/h = 100,\ h_c/h_f = 2,\ \psi = 15°$. A steel ball of diameter 12.7 mm is assumed o impact centrally with an initial velocity 3 m/s on the sandwich conical shell. **Fig. 6.1(a)** shows the convergence with different mesh sizes (4×4, 6×6, 8×8, and 10×10) and constant time step ($\Delta t = 2$ μs), while **Fig. 6.1(b)** presents the convergence with different time steps ($\Delta t = 1$, 2, 3, and 4 μs) and constant mesh size (8×8). From **Figs. 6.1(a)** and **(b),** it is observed that the contact force converges for a mesh size of 8×8 and a time step of 2 μs, which are adopted in the subsequent analysis.

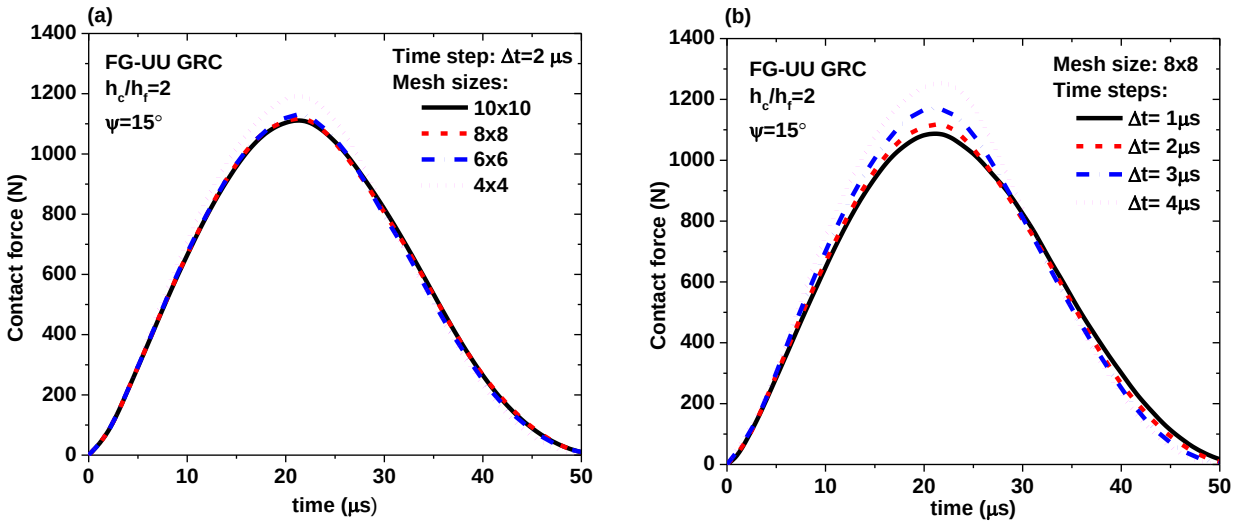

Fig. 6.1 Convergence study of contact force of GRC sandwich conical shell with FG-UU type graphene grading pattern at $T = 500$ K: (a) mesh convergence at constant time step, $\Delta t = 2$ μs and (b) time step convergence at constant mesh size, 8×8

6.4 PARAMETRIC STUDY

After examining the stability and accuracy of the present mathematical model, the influences of various critical parameters on the transient response of pretwisted FG-GRC sandwich conical shells impacted centrally with a spherical steel ball in thermal environments are analyzed considering the following geometrical dimensions: $s = 0.4$ m, $L/s = 0.7$, $\phi_0 = \phi_v = 20°$. The

material properties of steel impactor are considered as: $E_{imp} = 207$ GPa, $\nu_{imp} = 0.3$, and $\rho_{imp} = 7960$ kg/m^3. If otherwise not stated, the cone length-to-thickness ratio, impactor's diameter, and initial velocity of the impactor are considered as $s/h = 100$, $d_{imp} = 12.7$ mm, and $V_0 = 3$ m/s, respectively.

6.4.1 EFFECT OF GRAPHENE GRADING PATTERN

The effect of graphene grading pattern (FG-UU, FG-VΛ, and FG-ΛV) on the impact response of pretwisted FG-GRC sandwich conical shell with pretwist angle $\psi = 15°$ and core-to-facings thickness ratio $h_c/h_f = 0.5$ at temperature $T = 300$ K is presented in **Fig. 6.2**. In this case, diameter and initial velocity of the impactor are set as $d_{imp} = 12.7$ mm, and $V_0 = 3$ m/s, respectively. As is observed in **Fig. 6.2(a),** the sandwich conical shell with FG-VΛ grading profile exhibits the highest peak value of contact force with the shortest contact duration among the three graphene grading patterns considered due to the highest value of contact stiffness k_c (**Eq. (2.144)**). Besides, the case of FG-VΛ grading pattern possesses the lowest peak of contact force with the longest contact duration due to the least value of Young's moduli (E_{22}) of the impacted layer of the top facing. The shell displacement at the impact point $(x = L/2, y = 0)$ in case of FG-ΛV grading profile is the maximum and followed by the grading profiles FG-UU and FG-VΛ as displayed in **Fig. 6.2(b**). This may be attributed to the presence of minimum graphene volume fraction $(V_G = 0.03)$ in the outermost layer and maximum graphene volume fraction $(V_G = 0.11)$ in the innermost layer of both facings with FG-ΛV grading profile which results in its least flexural stiffness. It is worth to note that the sandwich panels with FG-VΛ type of graphene grading profile respond (time of attaining displacement peaks) faster than the other type of grading profiles considered. From the maximum to minimum local indentation on the target shell surface are found in the order of FG-ΛV, FG-UU, and FG-VΛ, respectively, as evident in **Fig. 6.2(c).** The higher surface stiffness of the target panel results in lower values of the indentation. For similar reasons, impactor velocity are found to be maximum for the FG-ΛV grading profile and minimum for the FG-VΛ grading profile, as depicted in **Fig. 6**.2**(d)**, respectively.

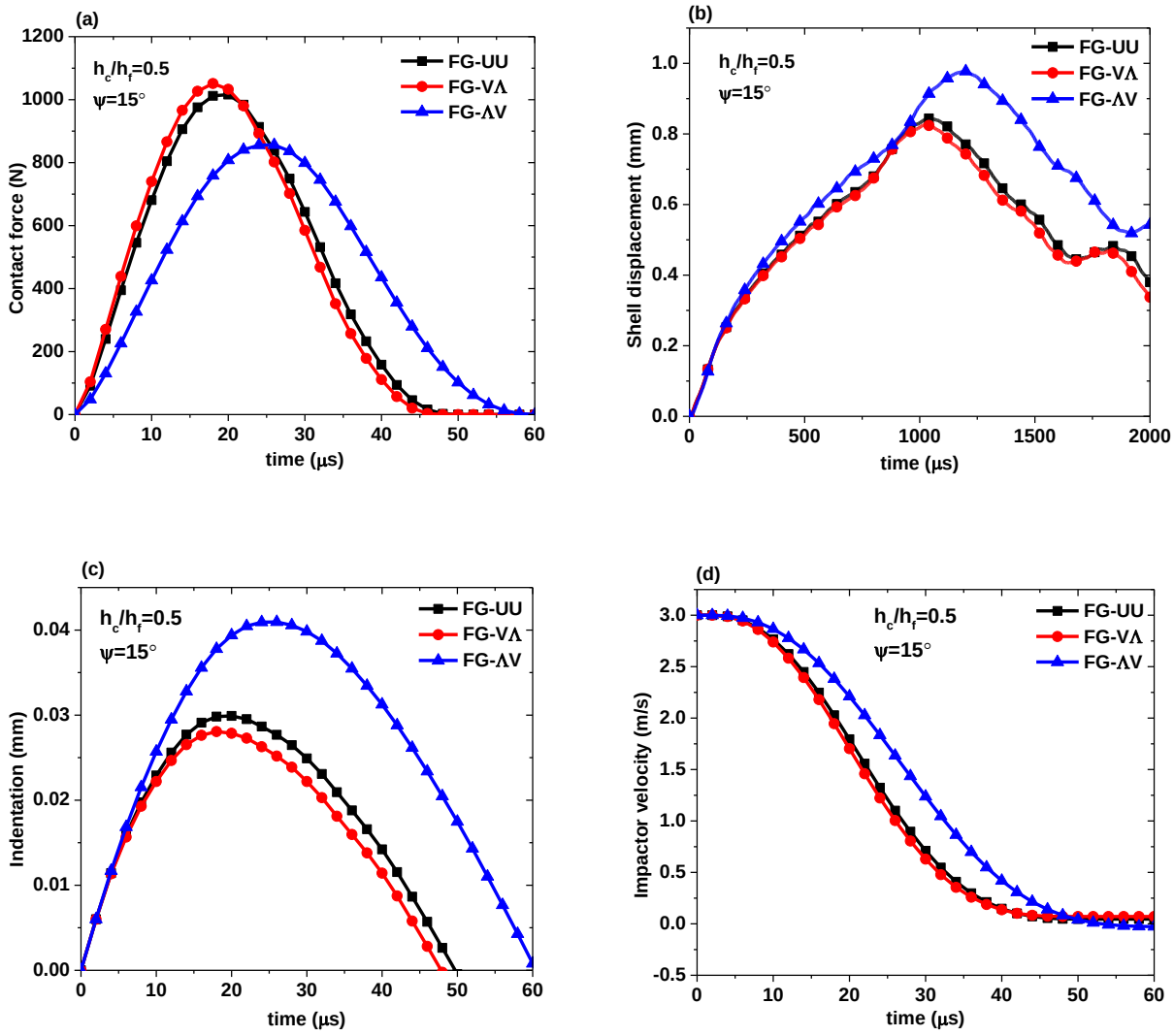

Fig. 6.2 Effect of graphene grading profile on impact behavior of FG-GRC sandwich conical shell at T =300 K: (a) contact force, (b) central shell displacement, (c) indentation, and (d) impactor velocity

6.4.2 EFFECT OF TEMPERATURE

The thermal effect on the impact behavior of the FG-GRC sandwich conical shell is indispensable as the material properties of both GRC facings and titanium alloy core are temperature-dependent. The temporal variations of contact force, central shell displacement, indentation, and impactor velocity of the FG-GRC sandwich conical shell with two graphene grading profiles (FG-VΛ and FG-ΛV), pretwist angle $\psi = 15°$ and core-to-facings thickness ratio $h_c/h_f = 0.5$ at three different levels of temperature $T = 300$ K, 400 K, and 500 K are

thereby illustrated in **Figs. 6.3(a)-(d)**, respectively. The size and initial velocity of the impactor are selected same as in the previous case.

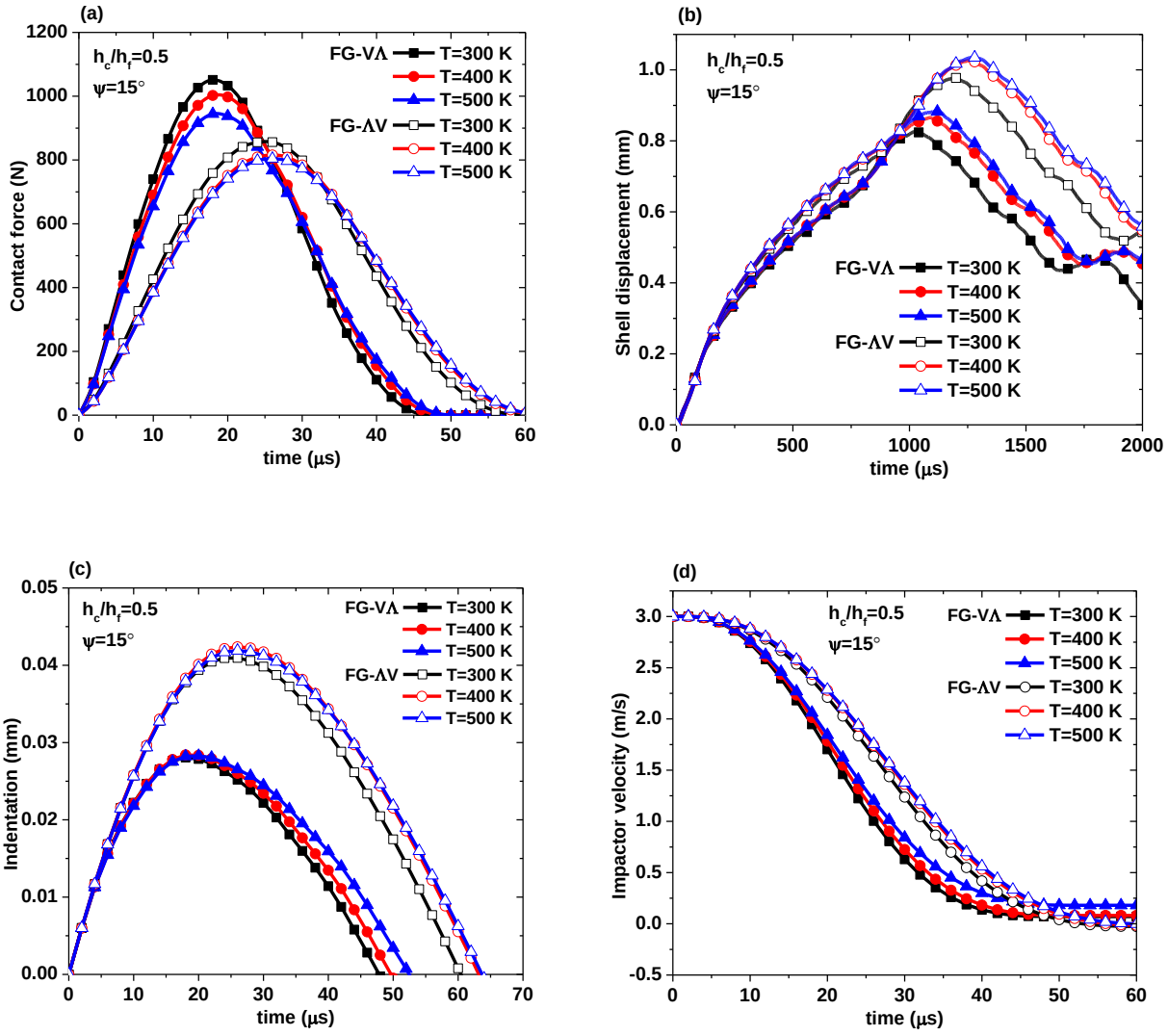

Fig. 6.3 Effect of temperature on impact behavior of pretwisted FG-GRC sandwich conical shells with FG-VΛ and FG-ΛV graphene grading profiles: (a) contact force, (b) central shell displacement, (c) indentation, and (d) impactor velocity

The obtained results in **Fig. 6.3** indicate that the value of the peak contact force decreases with an increase in temperature for both graphene grading profiles. On the other hand, the contact duration, as well as the values of shell displacement, indentation and impactor velocity, are found to increase when the temperature is raised. It is caused by the softening effect of the thermal stress as the elevation of temperature from its reference value (T =300 K) lessens the

elastic moduli of both GRC facings and Ti-6Al-4V core. Moreover, the decrease in transverse Young's modulus of the impacted surface $E_{22}(T)$ causes the degradation of the contact stiffness $k_c(T)$, which in turn leads to decrease the contact force.

6.4.3 EFFECT OF PRETWIST ANGLE

The effects of pretwist angle (ψ) on impact response of pretwisted FG-GRC sandwich conical shell with the ratio $h_c/h_f = 0.5$ at the temperature level of T =500 K are illustrated in **Fig. 6.4**.

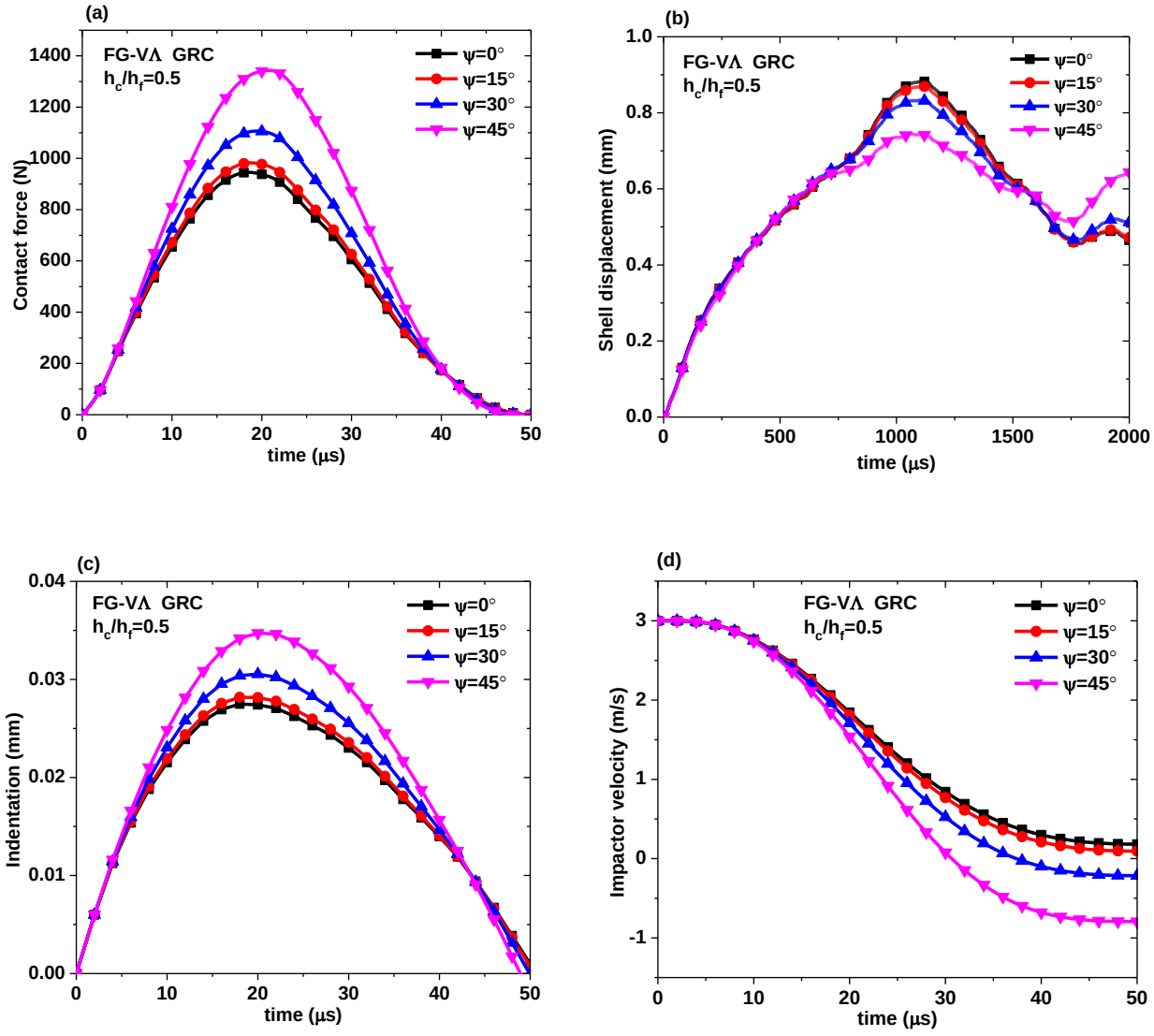

Fig. 6.4 Effect of pretwist angle on impact behavior of FG-GRC sandwich conical panel with FG-VΛ graphene grading profile at T = 500 K: (a) contact force, (b) central shell displacement, (c) indentation, and (d) impactor velocity

The results are obtained for FG-VΛ type of graphene grading profile in FG-GRC sandwich conical shell with four different values of pretwist angles ψ = 0°, 15°, 30°, and 45°. In **Fig. 6.4**, the impact responses of the pretwisted sandwich conical shell are compared with those of untwisted sandwich conical shell. The increase in pretwist angle from 0° to 45° results in larger peak contact force, smaller central shell displacement, larger peak indentation, and smaller impactor velocity. As reported earlier, the structural stiffness of the pretwisted conical shell is reduced for a larger pretwist angle. In addition, the local indentation at the impacted point is found to decrease with increasing pretwist angle which would lead to an increase the value of contact force. However, the pretwist angle has a negligible effect on the contact duration and time attaining the peak displacement of the sandwich conical shell.

6.4.4 EFFECT OF CORE-TO-FACE SHEETS THICKNESS RATIO

Fig. 6.5 displays the results of impact response of pretwisted FG-GRC sandwich conical shell for four different values of the core-to-face sheets thickness ratios (i.e., $h_c/h_f = 0.5$, 2, 5, and 10). The results are obtained for FG-VΛ graphene grading profile, pretwist angle $\psi = 15°$, and temperature T =500 K. Based on the obtained results, it is evident that an increase in the ratio h_c/h_f from 0.5 to 10 results in an increased value of the peak contact force and decreased value of peak shell displacement as evident in **Figs. 6.5(a)** and **(b)**. However, the contact duration is almost invariant to the value of h_c/h_f ratio. Since the total thickness of the sandwich conical shell is constant; therefore, the higher value of the ratio h_c/h_f refers to the shell with a thicker core which has higher flexural stiffness. Interestingly, the sandwich panel with a thicker core responds to the low-velocity impact slower than that of the thinner core. Further, the higher values of the ratio h_c/h_f result in higher values of peak indentation and lower values of impactor velocity as demonstrated in **Figs. 6.5(c)** and **(d)**, respectively. It can also be noted that the effect of the ratio h_c/h_f on the impactor velocity is more apparent in the unloading phase than in the loading phase.

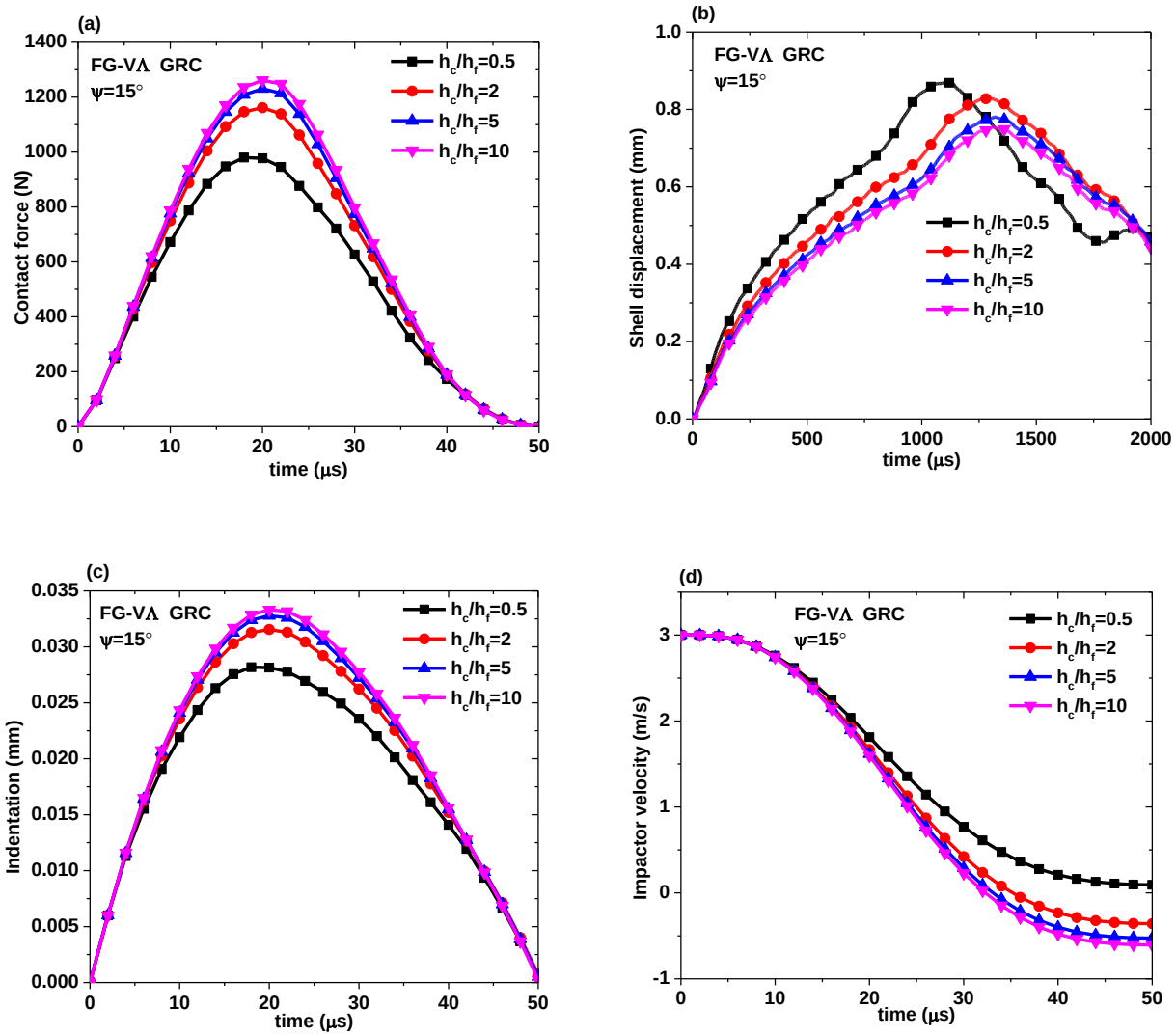

Fig. 6.5 Effect of core-to-face sheets thickness ratio on impact behavior of FG-GRC sandwich conical shell with FG-VΛ graphene grading profile at elevated temperature $T = 500$ K: (a) contact force, (b) central shell displacement, (c) indentation, and (d) impactor velocity

6.4.5 EFFECT OF SPAN-TO-CONE LENGTH RATIO

The effect of span-to-cone length ratio (L/s) on the impact response of the FG-GRC sandwich conical shell with FG-VΛ graphene grading profile at the elevated temperature $T = 500$ K is demonstrated in **Fig. 6.6**. The results are obtained for three different values of the span-to-cone length ratios L/s =0.6, 0.7, and 0.8 of the pretwisted sandwich shallow conical shell with $h_c/h_f = 2$ and $\psi = 15°$. Based on the obtained results, it is evident that the values of peak contact force and indentation decrease with increasing the ratio L/s, while the values of peak

shell displacement and impactor velocity are found to increase as the ratio L/s is increased. This can be attributed to the fact that the flexural stiffness of the cantilever sandwich conical shell decreases with an increase in the ratio L/s which in turn results in an increase in shell displacement and a decrease in the indentation and contact force although contact stiffness of the impacted surface is unaltered. The higher values of the ratio L/s result in faster attainment of peak contact force and slower attainment of peak shell displacement. However, the effect of L/s on the transient response is found to be more apparent in the loading phase than in the unloading phase.

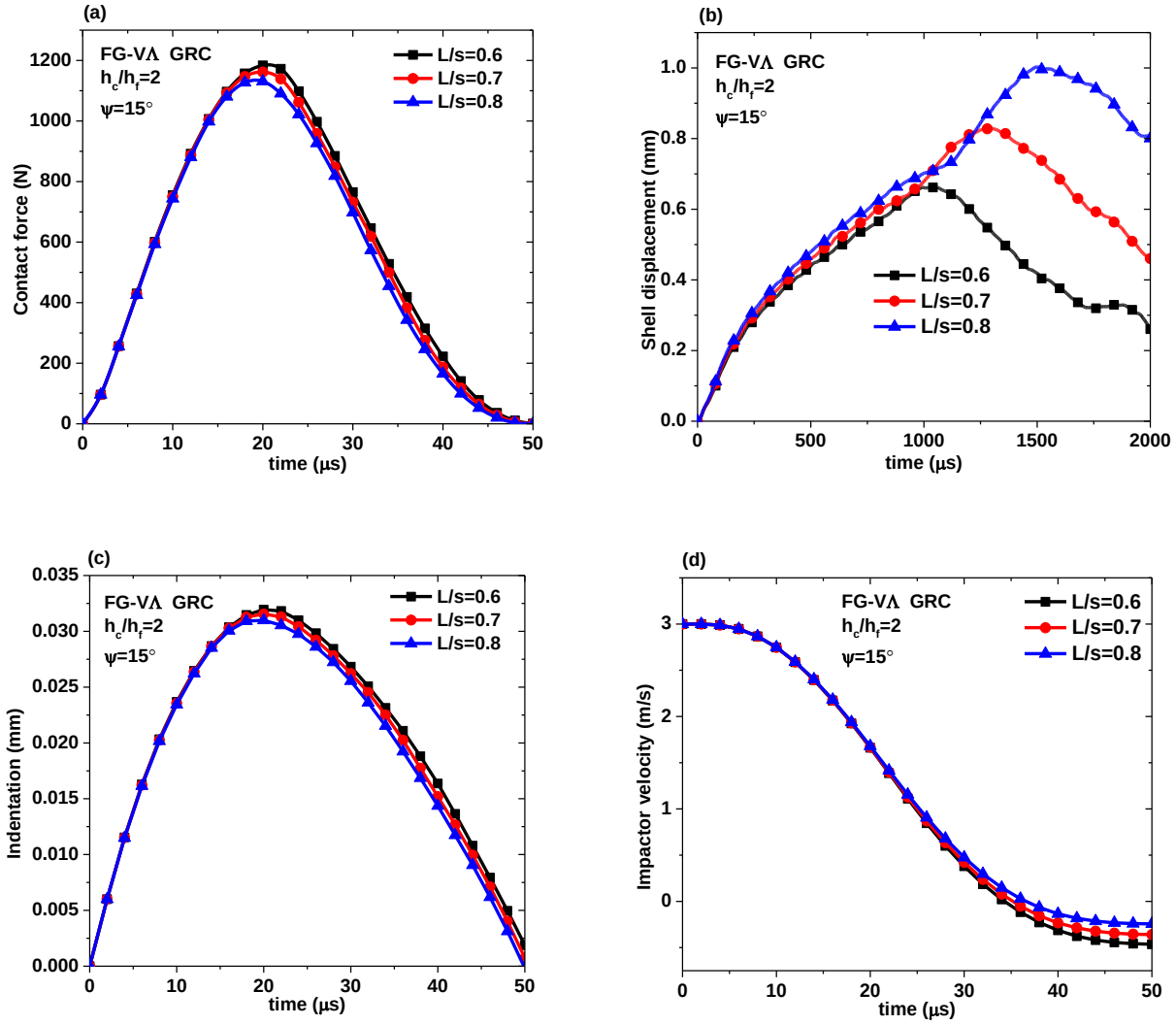

Fig. 6.6 Effect of span-to-cone length ratio (L/s) on impact behavior of FG-GRC sandwich conical shell with FG-VΛ graphene grading profile at the elevated temperature $T = 500$ K: (a) contact force, (b) central shell displacement, (c) indentation, and (d) impactor velocity

6.4.6 EFFECT OF INITIAL VELOCITY OF IMPACTOR

Fig. 6.7 illustrates the influence of initial impactor velocity on the impact response of the pretwisted FG-GRC sandwich conical shell with FG-VΛ graphene grading profile, pretwist angle ψ =15° and the ratio h_c/h_f = 5 at the elevated T = 500 K.

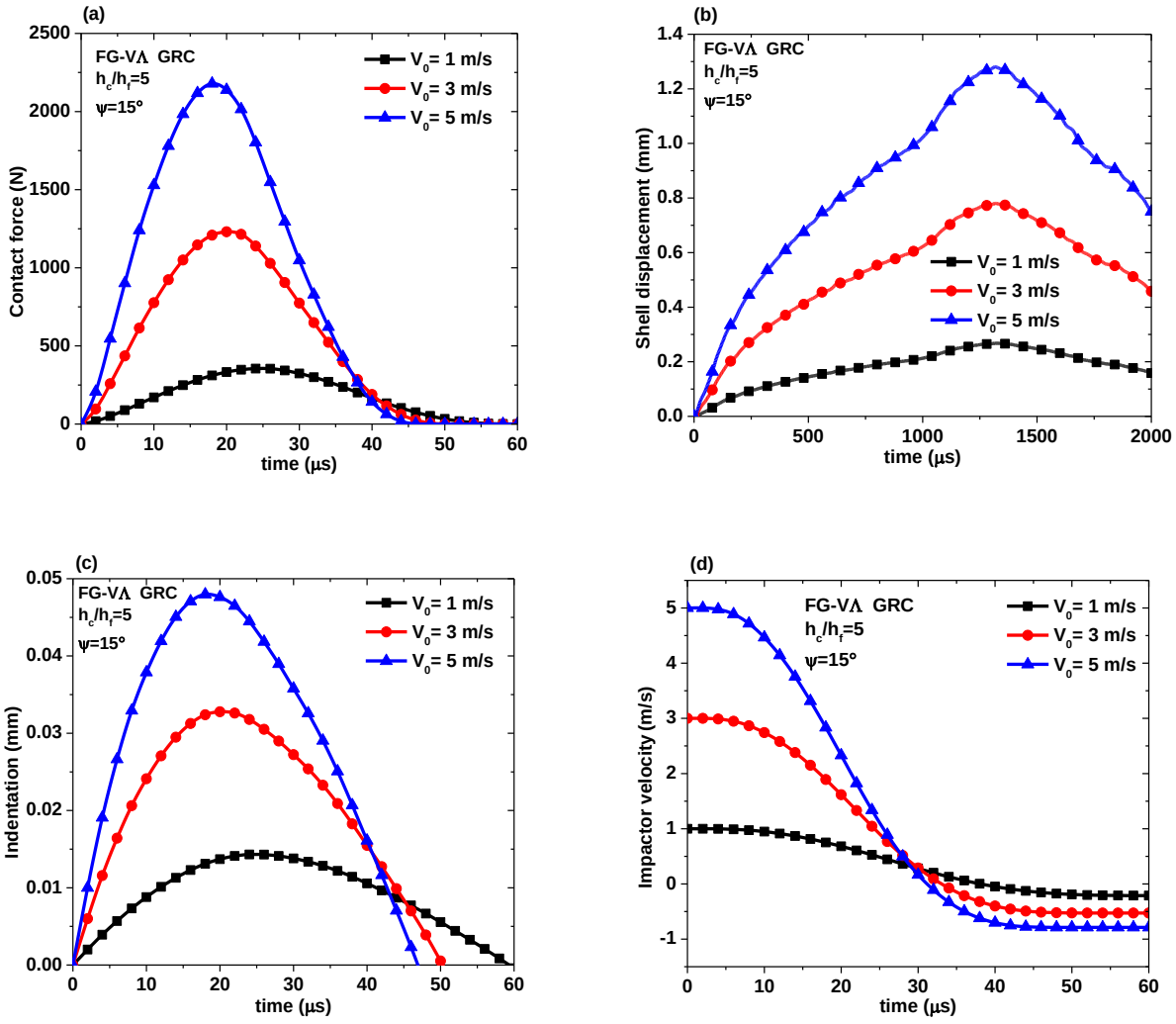

Fig. 6.7 Effect of initial velocity of impactor on impact behavior of FG-GRC sandwich conical shell with FG-VΛ graphene grading profile at the elevated temperature T = 500 K: (a) contact force, (b) central shell displacement, (c) indentation, and (d) impactor velocity

In this case, the ball impactor of diameter d_{imp} = 12.7 mm is assumed to strike centrally on the sandwich conical shell with three different initial velocities V_0 = 1 m/s, 3 m/s, and 5 m/s. As illustrated in **Figs. 6.7(a)-(d),** the values of peak contact force, peak shell displacement, peak indentation, and impactor velocity become higher when the initial velocity of the impactor is

increased. This behavior is expected as the higher value of initial velocity results in higher impact energy absorbed by the FG-GRC sandwich conical shell, which leads to higher values of peak contact force, peak shell displacement, peak indentation, and impactor velocity. Further, the contact duration becomes shorter along with faster attainment of the peak contact force as well as peak indentation when the value of impactor's intial velocity is increased. However, the response time of the sandwich conical shell to the low-velocity impact in terms of attainment of the peak shell displacement is almost invariant with initial velocity of the impactor.

6.4.7 EFFECT OF SIZE OF IMPACTOR

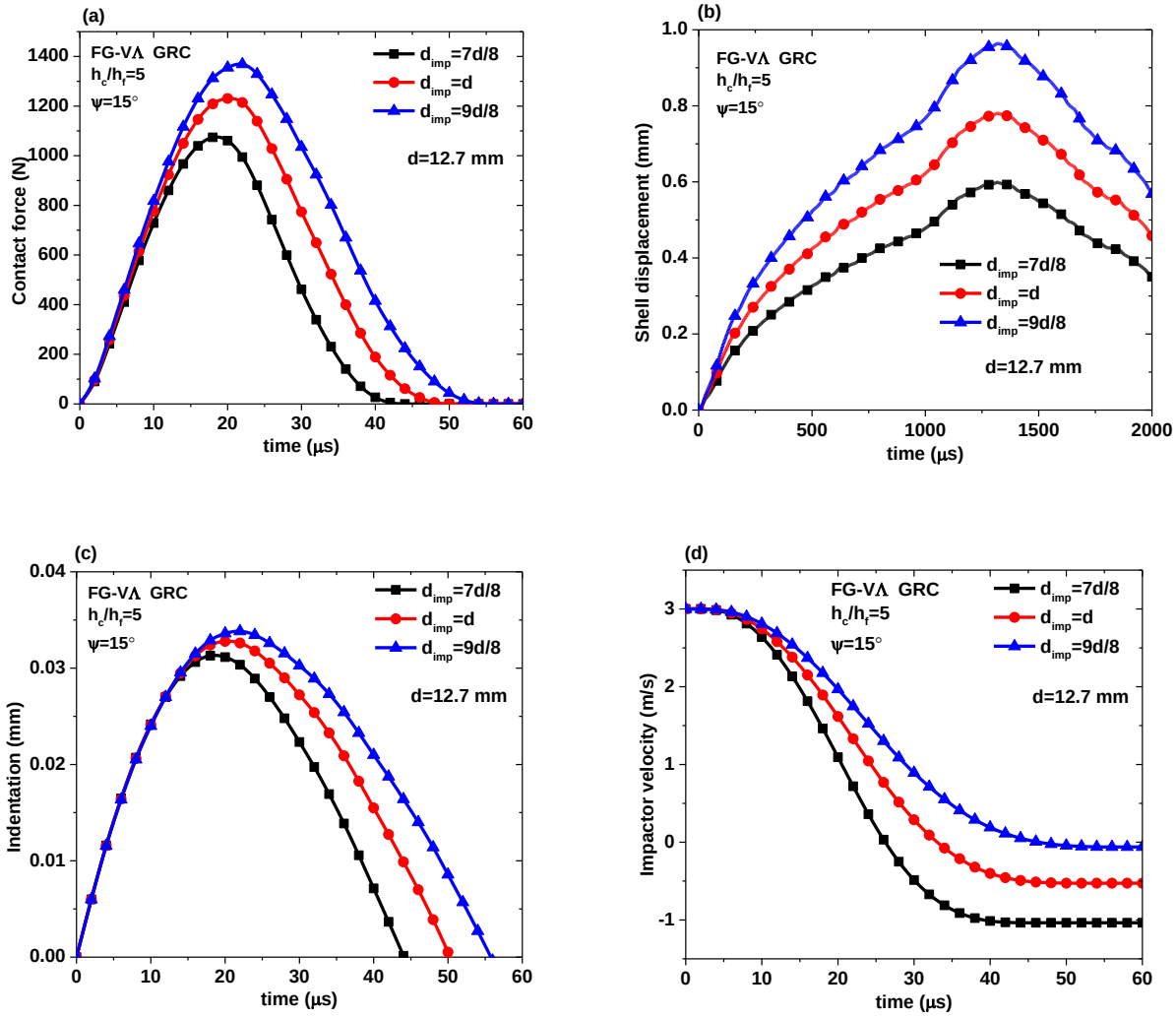

Fig. 6.8 Effect of impactor size on impact behavior of FG-GRC sandwich conical shell with FG-VΛ graphene grading profile at the elevated temperature $T = 500$ K: (a) contact force, (b) central shell displacement, (c) indentation, and (d) impactor velocity

The influence of size of the impactor on the impact behavior of the pretwisted FG-GRC sandwich conical shell with FG-VΛ graphene grading profile for ψ =15° and $h_c/h_f = 5$ at the elevated temperature $T = 500$ K are depicted in **Fig. 6.8**. The results are obtained considering three different diameters of the ball impactor $d_{imp} = \frac{7d}{8}, d,$ and $\frac{9d}{8}$, where, d =12.7 mm. The values of peak contact force, contact duration, peak shell displacement, peak indentation, and impactor velocity are found to increase as the impactor diameter increases. This is due to the involvement of higher kinetic energy and mass of the larger-sized impactor. In addition, an increase in impactor diameter increases the contact stiffness (k_c) of the panel, as estimated in **Eq. (2.143)**, which would lead to an increase in contact force. The attainments of peak contact force and peak indentation become slower when impactor diameter increases, while the central shell displacement is attained almost at the same instant of time, irrespective of the impactor diameter.

CHAPTER 7

CONCLUSIONS

7.1 INTRODUCTION

This dissertation is concerned with the dynamic analysis of cantilever pretwisted sandwich conical shells composed of CNTs-reinforced composite (CNTRC) face sheets and graphene reinforced composite (GRC) face sheets under different thermal conditions. The reinforcements of CNTs and graphene sheets are assumed to be either uniform or piece-wise functionally graded across the thickness direction of the shell. The temperature-dependent material properties of the CNTRC and GRC layers are estimated using the micromechanical models. A finite element formulation with eight noded isoparametric elements is derived in the framework of the higher-order shear deformation theory (HSDT). Based on this formulation, in-house computer codes are developed to obtain the numerical results for free vibration and transient behavior under low-velocity impact of the pretwisted sandwich conical shells with CNTRC face sheets and GRC face sheets. The convergence and comparison studies are performed to establish the stability and accuracy of the present method. Thereafter, the numerical results are presented graphically to scrutinize the effects of some important parameters on the free vibration and transient behavior under low-velocity impact of the shell. The important conclusions drawn from the present investigation and discussed thoroughly in Chapter 3, Chapter 4, Chapter 5, and Chapter 6 are listed in Section 7.2. Afterward, the major contribution of the research and the scope of future research in the context of the present work and its related problem areas are outlined in the subsequent sections.

7.2 CONCLUDING REMARKS

7.2.1 FREE VIBRATION ANALYSIS OF FG-CNTRC SANDWICH CONICAL SHELLS

a) The parametric study reveals that natural frequencies of the pretwisted sandwich conical shells decrease monotonically with an increase in the core-to-face sheets thickness ratio irrespective of CNTs grading pattern, CNTs volume fraction, and pretwist angle.

However, the rate of decrease in natural frequencies is more apparent for lower proportions of the homogenous core.

b) Among five considered CNTs grading patterns in the CNTRC sandwich conical shell, the FG-VΛ type of grading pattern exhibits the highest value of the natural frequencies and followed by FG-XX, FG-UU, FG-OO, and then FG-ΛV types, for all considered cases. The effect of CNTs grading pattern on the frequencies is more obvious for higher proportions of the CNTRC face sheets. Interestingly, the natural frequency values for FG-XX, FG-UU, and FG-OO type CNTs grading patterns are very close.

c) CNTs volume fraction has a significant effect on the natural frequencies of the FG-CNTRC sandwich conical shells. For whole ranges of core-to-face sheets thickness ratio, temperature, and non-dimensional rotational speed, the natural frequencies increase as the CNTs volume fraction increases. It indicates that the FG-CNTRC conical shells become more stiffened as more amounts of CNTs are reinforced.

d) The first two natural frequencies of the pretwisted FG-CNTRC conical shell decrease monotonically with increasing pretwist angle, whereas the reverse trend of frequency variation with pretwist angle is found in the case of the third mode.

e) It is found that the natural frequencies of FG-CNTRC sandwich conical shells are highly sensitive to the temperature of the environment. The natural frequencies are found to decrease with the increase in temperature. The thermal effect on the frequencies is almost independent of CNTs distribution pattern, CNTs volume fraction, and pretwist angle, while the stiffness degradation is highly dependent on the core-to-face sheets thickness ratio. For instance, higher proportions of homogeneous core result in higher stiffness degradation indicating the homogenous core part is more thermally affected than the CNTRC face sheet part.

f) With an increase in rotational speed, the natural frequencies of the rotating pretwisted FG-CNTRC sandwich conical shell increase monotonically due to centrifugal stiffening under a constant thermal load. However, centrifugal stiffening of the sandwich conical shell is weekly dependent on the CNTs grading pattern and thermal load, while it is highly sensitive to the change of pretwist angle, core-to-face sheets thickness ratio, and hub radius-to-span length ratio. It is also found that the natural frequencies of the rotating

shell increase with an increase in hub radius to length ratio for whole considered range of the speed.

g) The effects of CNTs grading pattern, rotational speed, and temperature on the first four mode shapes are found to be weak. Besides, the effect of pretwist angle on these mode shapes is considerable irrespective of the thermal conditions.

7.2.2 FREE VIBRATION ANALYSIS OF FG-GRC SANDWICH CONICAL SHELLS

a) The first two natural frequencies of the pretwisted FG-GRC sandwich conical shell decrease monotonically with an increase in pretwist angle irrespective of the types of graphene grading pattern and thermal condition.

b) With the increase in core-to-face sheets thickness ratio, the natural frequencies decrease monotonically in case of FG-VΛ and FG-UU patterns. Besides, the frequency of FG-ΛV type sandwich conical shells first decreases to reach its minimum value and then increases slightly with increasing core-to-face sheets thickness ratio. Among three types of distribution patterns in sandwich conical shells, the FG-VΛ pattern is found to have the natural frequencies for thicker GRC face sheets, while the FG-UU type pattern exhibits the highest natural frequencies for thinner GRC face sheets.

c) The rise in temperature reduces the frequency values wherein the rates of reduction in the natural frequencies are affected by the types of graphene grading pattern and proportion of the GRC face sheets in the sandwich conical shells.

d) The fundamental frequency of the rotating FG-GRC sandwich conical shell increases significantly with an increase in rotational speed. The effect of rotational speed on the fundamental frequency is dependent on the pretwist angle, core-to-face sheets thickness ratio, and types of distribution patterns.

e) The first two mode shapes of the FG-VΛ GRC sandwich conical shells are weakly influenced by the rotational speed and pretwist angle while the fourth mode shape is significantly altered by the pretwist angle.

7.2.3 DYNAMIC BEHAVIOR OF FG-CNTRC SANDWICH CONICAL SHELLS UNDER LOW-VELOCITY IMPACT

a) Among the considered five different CNTs grading profiles in the FG-CNTRC sandwich conical shell panel, the FG-VΛ type exhibits the largest contact force, shortest contact

duration, smallest shell displacement, and highest impactor velocity. In contrast, the smallest contact force, longest contact duration, largest shell displacement, and lowest highest impactor velocity are evident in the case of FG-ΛV type. However, the highest and lowest indentations are found in the case of grading profiles FG-OO and FG-XX, respectively.

b) The impact responses are highly affected by CNTs volume fraction. For instance, the higher value of CNTs volume fraction results in higher contact force with shorter contact duration, lower shell displacement, lower indentation, and lower impactor velocity.
c) With the rise in temperature of the environment, the contact force decreases, whereas contact duration, shell displacement, indentation, and impactor velocity increase.
d) The contact force and indentation increase with an increase in pretwist angle while the shell displacement and impactor velocity decrease.
e) With the increase of core-to-facing thickness ratio, the contact force, as well as indentation increases and shell displacement decreases.
f) The cone length-to-thickness ratio of a conical shell panel is an important parameter affecting its low-velocity impact response. The numerical results exhibit that an increase in cone length-to-thickness ratio results in a decrease in the values of contact force and indentation, whereas the central shell displacement and impactor velocity are evident to increase.
g) The contact force, shell displacement, and indentation are found to increase when the initial velocity and size of the impactor are increased.

7.2.4 DYNAMIC BEHAVIOR OF FG-GRC SANDWICH CONICAL SHELLS DUE TO LOW-VELOCITY IMPACT

a) The higher value of peak contact force while lower values of peak central shell displacement, peak indentation and impactor velocity are observed for FG-VΛ type graphene grading pattern which has graphene-rich layers at the impact side than the other considered patterns.
b) An increase in temperature results in a decrease in peak values of contact force and an increase in panel displacement, indentation, and impactor velocity due to the degradation of structural stiffness.

c) The higher values of pretwist angle and core-to-facing thickness ratio of the sandwich panel result in higher peak contact force, higher peak indentation, and lower peak central panel displacement.
d) Both peak contact force and peak indentation decrease while the peak central shell displacement increases with an increase in span length to cone length ratio due to an increase in flexibility of the shell.
e) The larger size and higher initial velocity of the impactor result in higher peak contact force, peak central shell displacement, and peak indentation due to higher kinetic energy absorbed.

7.3 SIGNIFICANT CONTRIBUTIONS OF THE THESIS

The significant contributions of the present research are stated below:

a) A finite element formulation-based mathematical model in the framework of the higher-order shear deformation theory (HSDT), which accounts for cubic distribution of in-plane displacement components and uniform distribution of transverse displacement component through the entire thickness, is developed considering one of the most sensitive parameters like thermal load. This formulation is well-versed in analyzing and predicting the dynamic response of rotating shallow shells with any geometrical shapes operating at any environmental temperature.
b) Using the developed mathematical model, the free vibration and impact response of the pretwisted sandwich conical shells with CNTRC face sheets and GRC face sheets in thermal environments have been studied.
c) The prevalent and fascinating feature of the present study is that it proposes a pretwisted sandwich shallow conical shell model for turbo-machinery blades. The proposed sandwich-type blades with nanocomposite (CNTRC and GRC) face sheets and homogenous core would be advantageous for different weight-sensitive applications. Thus, the results of the present analysis may have enormous technical importance for future reference.
d) The appropriate selection of grading pattern of CNTs and graphene in the nanocomposite face sheets of the sandwich blades provides its improved vibration and impact behavior.

7.4 SCOPE OF THE FUTURE WORK

This section discusses some of the possible areas of research to which the present investigation may be extended in the future. Some of the future works which may be undertaken in line with the present work are as follows:

a) The present investigation based on linear elastic analysis can be extended to the nonlinear analysis of the nanocomposite sandwich conical shells wherein the effect of geometric as well as material nonlinearity is included.
b) The present work can be extended to the sandwich conical shells with porous core and/or porous face sheets.
c) The present work can be extended to the dynamic analysis of the nanocomposite sandwich structures under multiple impacts.
d) Fluid-structure interaction may be an exciting research area as the nanocomposite sandwich structure is proposed as rotating blades of turbo-machines.
e) A quantitative comparison between the dynamic behavior of sandwich conical shells with FG-CNTRC face sheets and FG-GRC face sheets can be performed in the future.
f) The experimental verification of the theoretical models developed in this study is really a challenging work that can be taken up for further research.

REFERENCES

Abrate, S. (2001), Modeling of Impacts on Composite Structures, Composite structures, Vol. 51, No. 2, pp. 129-138.

Adab, N., and Arefi, M. (2022), Vibrational Behavior of truncated Conical Porous GPL-Reinforced Sandwich Micro/Nano-Shells, Engineering with Computers, DOI: 10.1007/s00366-021-01580-8.

Afshari, H. (2020), Efect of Graphene Nanoplatelet Reinforcements on the Dynamics of Rotating Truncated Conical Shells, Journal of the Brazilian Society of Mechanical Sciences and Engineering, Vol. 42, 519.

Afshari, H. (2020), Free Vibration Analysis of GNP-reinforced truncated Conical Shells with Different Boundary Conditions, Australian Journal of Mechanical Engineering, https://doi.org/10.1080/14484846.2020.1797340.

Al-Furjan, M.S.H., Farrokhian, A., Mahmoud, S.R., and Kolahchi, R. (2021), Dynamic Deflection and Contact Force Histories of Graphene Platelets Reinforced Conical Shell Integrated with Magnetostrictive Layers Subjected to Low-Velocity Impact, Thin-Walled Structures, Vol. 163, 107706.

Amirabadi, H., Farhatnia, F., Eftekhari, S.A., and Hosseini-Ara, R. (2020), Free Vibration Analysis of Rotating Functionally Graded GPL-reinforced Truncated Thick Conical Shells Under Different Boundary Conditions, Mechanics Based Design of Structures and Machines, https://doi.org/10.1080/15397734.2020.1822183.

Andrews, R., and Weisenberger, M.C. (2004), Carbon Nanotube Polymer Composites, Current Opinion in Solid State and Materials Science, Vol. 8, pp. 31–37.

Ansari, R., Torabi, J., and Shojaei, M.F. (2016), Vibrational Analysis of Functionally Graded Carbon Nanotube-Reinforced Composite Spherical Shells Resting on Elastic Foundation using the Variational Differential Quadrature Method, European Journal of Mechanics - A/Solids, Vol. 60, pp. 166-182.

Ansari, R., Hasrati, E., and Torabi, J. (2019a), Nonlinear Vibration Response of Higher-Order Shear Deformable FG-CNTRC Conical Shells, Composite Structures, Vol. 222, 110906.

Ansari, R., Hasrati, E., and Torabi, J. (2019b), Vibration Analysis of Pressurized Sandwich FG-CNTRC Cylindrical Shells based on the Higher-order Shear Deformation Theory, Materials Research Express, Vol. 6, 045049.

Ansari, R., Torabi, J., and Shojaei, M.F. (2018), Free Vibration Analysis of Embedded Functionally Graded Carbon Nanotube-Reinforced Composite Conical/ Cylindrical Shells and Annular Plates Using A Numerical Approach, Journal of Vibration and Control, Vol. 24, No. 6, 1123-1144.

Anvari, M., Mohammadimehr, M., and Amiri, A. (2020), Vibration Behavior of a Micro Cylindrical Sandwich Panel Reinforced by Graphene Platelet, Journal of Vibration and Control, Vol. 26, No. 13-14, pp. 1311-1343.

Arefi, M., Bidgoli, E.M.R., Dimitri, R., and Tornabene, F. (2018), Free Vibrations of Functionally Graded Polymer Composite Nanoplates Reinforced with Graphene Nanoplatelets, Aerospace Science and Technology, Vol. 81, pp. 108-117.

Arnold, R., and Warburton, G.B. (1949), Flexural Vibrations of the Walls of Thin Cylindrical Shells have Freely Supported Ends, Proceedings of the Royal Society London A, Vol. 197, pp. 238–256.

Ashton, J. E., and Whitney, J. M. (1970), Theory of Laminated Plates, Stanford, CT: Technomic.

Azizi, A., Khalili, S.M.R., and Fard, K.M. (2019), Low-velocity Impact Response of Sandwich Conical Shell with Agglomerated Single-Walled Carbon Nanotubes-Reinforced Face Sheets considering Structural Damping, Journal of Sandwich Structures and Materials, Vol. 21, No.4, pp. 1481-1519.

Bahaadini, R., Saidi, A.R., Arabjamaloei, Z., and Ghanbari-Nejad-Parizi, A. (2019), Vibration Analysis of Functionally Graded Graphene Reinforced Porous Nanocomposite Shells, International Journal of Applied Mechanics, Vol. 11, No. 07, 1950068.

Bakshi, S.R., Lahiri, D., and Agarwal, A. (2010), Carbon Nanotube Reinforced Metal Matrix Composites – A Review, International Materials Reviews, Vol. 55, No. 1, pp. 41-64.

Bandyopadhyay, T., and Karmakar, A. (2015), Bending Characteristics of Delaminated Cross-Ply Composite Shallow Conical Shells in Hygrothermal Environment, Journal of Reinforced Plastics and Composites, Vol. 34, No. 20, pp. 1724-1735.

Bandyopadhyay, T., Karmakar, A., and Kishimoto, K. (2014), Hygrothermal Effects on the Free Vibration Characteristics of Delaminated Composite Pretwisted Rotating Conical Shells, JSME Mechanical Engineering Journal, Vol. 1, No. 6, pp. SMM0059(1-18).

Bathe, K.J. (1990), Finite Element Procedures in Engineering Analysis, New Delhi: Prentice Hall of India.

Bayat, M.R., Rahmani, O., and Mashhadi, M.M. (2018), Nonlinear Low-Velocity Impact Analysis of Functionally Graded Nanotube-Reinforced Composite Cylindrical Shells in Thermal Environments, Polymer Composites, Vol. 39, No. 3, pp. 730-745.

Belarbi, M.O., Tati, A., Ounis, H., and Khechai, A. (2017), On the Free Vibration Analysis of Laminated Composite and Sandwich Plates: A Layerwise Finite Element Formulation, Latin American Journal of Solids and Structures, Vol.14, pp. 2265-2290.

Beni, N.N. (2019), Free Vibration Analysis of Annular Sector Sandwich Plates with FG-CNT Reinforced Composite Face-Sheets Based on the Carrera's Unified Formulation, Composite Structures, Vol. 214, pp. 269-292.

Bert, C.W., and Ray, J.D. (1969), Vibrations of Orthotropic Sandwich Conical Shells with Free Edges, International Journal of Mechanical Sciences, Vol. 11, pp. 767-779.

Bidzard, A., Malekzadeh, P., and Mohebpour, S.R. (2019), Vibration of Multilayer FG-GPLRC Toroidal Panels with Elastically Restrained Against Rotation Edges, Thin-Walled Structures, Vol. 143, 106209.

Birman, V., and Kardomateas, G.A. (2018), Review of Current Trends in Research and Applications of Sandwich Structures, Composites Part B: Engineering, Vol. 142, pp. 221-240.

Cairns, D.S., and Lagace, P.A. (1989), Transient Response of Graphite/Epoxy and Kevlar/Epoxy Laminates Subjected to Impact, AIAA Journal, Vol. 27, No.11, pp.1590-1596.

Cao, D.X., Liu, B.Y., Yao, M.H., and Zhang, W. (2017), Free Vibration Analysis of a Pretwisted Sandwich Blade with Thermal Barrier Coatings Layers, Science China Technological Sciences, Vol. 60, pp.1747–1761.

Carrera, E., and Brischetto, S. (2009), A Survey with Numerical Assessment of Classical and Refined Theories for the Analysis of Sandwich Plates, Applied Mechanics Reviews, Vol. 62, No. 1, pp. 010803(1-17).

Chai, Q., and Wang, Y.Q. (2022), Traveling Wave Vibration of Graphene Platelet Reinforced Porous Joined Conical-Cylindrical Shells in a Spinning Motion, Engineering Structures, Vol. 252, 113718.

Chakrabarti, A., and Sheikh, A.H. (2004), Vibration of Laminate-Faced Sandwich Plate by a New Refined Element, Journal of Aerospace Engineering, Vol. 17, No. 3, pp. 123-134.

Chao, W.C., and Reddy, J.W. (1984), Analysis of Laminated Composite Shells using a Degenerated 3-D Element, International Journal for Numerical Methods in Engineering, Vol. 20, pp. 1991-2007.

Chen, C., Li, Y., Gu, Y., Li, M., and Zhang, Z. (2017), Improvement in Skin–Core Adhesion of Multiwalled Carbon Nanotubes Modified Carbon Fiber Prepreg/Nomex Honeycomb Sandwich Composites, Journal of Reinforced Plastics and Composites, Vol. 36, No. 8, pp. 608-618.

Chen, J., and Li, Q-S. (2019), Vibration Characteristics of a Rotating Pre-twisted Composite Laminated Blade, Composite Structures, Vol. 208, pp.78-90.

Cheng, H., Li, C.F., and Jiang, Y. (2022), Free Vibration Analysis of Rotating Pre-twisted Ceramic Matrix Carbon Nanotubes Reinforced Blades, Mechanics of Advanced Materials and Structures, Vol. 29, No. 14, pp. 2040-2052.

Choi, I.H. (2006), Contact Force History Analysis of Composite Sandwich Plates Subjected to Low-Velocity Impact, Composite Structures, Vol. 75, pp. 582-58.

Choi, S.C., Park, J.S., and Kim, J.H. (2007), Vibration Control of Pre-twisted Rotating Composite Thin-Walled Beams with Piezoelectric Fiber Composites, Journal of Sound and Vibration, Vol. 300, No.1–2, pp.176-196.

Cook, R.D., Malkus, D.S., and Plesha, M.E. (1989), Concepts and Applications of Finite Element Analysis, John Wiley & Sons, New York.

Deep, N., and Mishra, P. (2018), Evaluation of Mechanical Properties of Functionalized Carbon Nanotube Reinforced PMMA Polymer Nanocomposite, Karbala International Journal of Modern Science, Vol. 4, No. 2, pp. 207-215.

Dokainish, M.A., and Rawtani, S. (1971), Vibration Analysis of Rotating Cantilevered Plates, International Journal for Numerical Methods in Engineering, Vol. 3, pp. 233–248.

Dong, S.B., Pister, K., and Taylor, R.L. (1962), On the Theory of Laminated Anisotropic Shells and Plates, Journal of Aerospace Science, Vol. 29, pp. 969-975.

Dong, Y., Li, X., Gao, K., Li, Y., and Yang, J. (2020), Harmonic Resonances of Graphene-Reinforced Nonlinear Cylindrical Shells: Effects of Spinning Motion and Thermal Environment, Nonlinear Dynamics, Vol. 99, 5696, https://doi.org/10.1007/s11071-019-05297-8.

Dong, Y.H., Li, Y.H., Chen, D., and Yang, J. (2018), Vibration Characteristics of Functionally Graded Graphene Reinforced Porous Nanocomposite Cylindrical Shells with Spinning Motion, Composites Part B: Engineering, Vol. 145, pp. 1-13.

Dong, Y.H., Zhu, B., Wang, Y., He, L.W., Li, Y.H., and Yang, J. (2019), Analytical Prediction of the Impact Response of Graphene Reinforced Spinning Cylindrical Shells under Axial and Thermal Loads, Applied Mathematical Modelling, Vol. 71, pp. 331-348.

Ebrahimi, F., and Habibi, S. (2017), Low-velocity Impact Response of Laminated FG-CNT Reinforced Composite Plates in Thermal Environment, Advances in Nano Research, Vol. 5, No. 2, pp. 69-97.

Ebrahimi, F., and Habibi, S. (2018), Nonlinear Eccentric Low-Velocity Impact Response of Polymer-CNT-fiber Multiscale Nanocomposite Plate Resting on Elastic Foundations in Hygrothermal Environments, Mechanics of Advanced Materials and Structures, Vol. 25, No. 5, No. 425-438.

Erkliğ, A., and Doğan, N.F. (2020), Nanographene Inclusion Effect on the Mechanical and Low Velocity Impact Response of Glass/Basalt Reinforced Epoxy Hybrid Nanocomposites, Journal of Brazilian Society of Mechanical Sciences and Engineering, Vol. 42, 83.

Eyvazian, A., Sebaey, T.A., Zur, K.K., Khan, A., Zhang, H., and Wong, S.H.F. (2021), On the Dynamics of FG-GPLRC Sandwich Cylinders Cased on an Unconstrained Higher-order Theory, Composite Structures, Vol. 267, 113879.

Fallah, M., Daneshmehr, A.R., Zarei, H., Bisadi, H., and Minak, G. (2018), Low Velocity Impact Modeling of Functionally Graded Carbon Nanotube Reinforced Composite (FG-CNTRC) Plates with Arbitrary Geometry and General Boundary Conditions, Composite Structures, Vol. 187, pp. 554-565.

Fan, J., Huang, J., Ding, J., and Zhang, J. (2017), Free Vibration of Functionally Graded Carbon Nanotube-Reinforced Conical Panels Integrated with Piezoelectric Layers subjected to Elastically Restrained Boundary Conditions, Advances in Mechanical Engineering, Vol. 9, No.7, pp. 1-17.

Fan, Y., Xiang, Y., and Shen, H.S. (2019), Nonlinear Forced Vibration of FG-GRC Laminated Plates Resting on Visco-Pasternak Foundations, Composite Structures, Vol. 209, 443-452.

Fan, Y., Xiang, Y., Shen, H.S., and Hui, D. (2018), Nonlinear low-Velocity Impact Response of FG-GRC Laminated Plates Resting on Visco-Elastic Foundations, Composites Part B: Engineering, Vol. 144, 184-194.

Fang, M., Wang, K., Lu, H., Yang, Y., and Nutt, S. (2009), Covalent Polymer Functionalization of Graphene Nanosheets And Mechanical Properties of Composites, Journal of Material Chemistry, Vol. 19, No. 38, pp. 7098-7105.

Fazelzadeh, S.A., Rahmani, S., Ghavanloo, E., and Marzocca, P. (2019), Thermoelastic vibration of Doubly-curved Nano-composite Shells Reinforced by Graphene Nanoplatelets, Journal of Thermal Stresses,Vol. 42, 2019, No. 1, pp. 1-17.

Feli, S., and Rashidi, E. (2021), Analytical Modeling of Carbon Nanotubes Effects and Their Distribution Patterns on the Low Velocity Impact Response of Sandwich Panels, Journal of Sandwich Structures and Materials, Vol. 23, No. 4, pp. 1403-1423.

Fidelus, J.D., Wiesel, E., Gojny, F.H., Schulte, K., and Wagner, H.D. (2005), Thermo-mechanical Properties of Randomly Oriented Carbon/Epoxy Nanocomposites, Composites Part A: Applied Science and Manufacturing, Vol. 36, No.11, pp. 1555–1561.

Foo, C.C., Chai, G.B., and Seah, L.K. (2008), A Model to Predict Low-Velocity Impact Response and Damage in Sandwich Composites, Composites Science and Technology, Vol. 68, pp. 1348-1356.

Foroutan, K., Ahmadi, H., and Carrera, E. (2019), Nonlinear Vibration of Imperfect FG-CNTRC Cylindrical Panels under External Pressure in the Thermal Environment, Composite Structures, Vol. 227,111310.

Garnet, H., and Kemper, J. (1964), Axisymmetric free vibrations of conical shells, Journal of Applied Mechanics, Vol.31, No. 3, pp. 458-466.

Goldsmith, W. (1960), Impact: The Theory and Physical Behavior of Colliding Solids, Edward Arnold (Publishers) Ltd., London.

Guo, H., Ouyang, X., Yang, T., Zur, K.K., and Reddy, J.N. (2021), On the Dynamics of Rotating Cracked Functionally Graded Blades Reinforced with Graphene Nanoplatelets. Engineering Structures, Vol. 249, 113286.

Guo, H., Ouyang, X., Żur, K.K., Wu, X., Yang, T., and Ferreira, A.J.M. (2022), On the Large-Amplitude Vibration of Rotating Pre-Twisted Graphene Nanocomposite Blades In A Thermal Environment, Composite Structures, Vol. 282, 115129.

Hajlaoui, A., Chebbi, E., and Dammak, F. (2019), Buckling Analysis of Carbon Nanotube Reinforced FG Shells using An Efficient Solid-shell Element Based on a Modified FSDT, Thin-Walled Structures, Vol. 144, 106254.

Han, Y, and Elliott, J. (2007), Molecular Dynamics Simulations of the Elastic Properties of Polymer/Carbon Nanotube Composites, Computational Materials Science, Vol. 39, pp. 315-323.

Hasrati, E., Ansari, R., and Torabi, J. (2017), Nonlinear Forced Vibration Analysis of FG-CNTRC Cylindrical Shells under Thermal Loading using a Numerical Strategy, International Journal of Applied Mechanics, Vol. 09, No. 08, 1750108.

Heidari, M., and Arvin, H. (2019), Nonlinear Free Vibration Analysis of Functionally Graded Rotating Composite Timoshenko Beams Reinforced by Carbon Nanotubes, Journal of Vibration and Control, Vol. 25, No.14, pp. 2063-2078.

Hertz, H. (1881), Über Die Berührung Fester Elastischer Körper (On the Contact of Rigid Elastic Solids), J. reine und angewandte Mathematik, Vol. 92, pp. 156-171.

Heydarpour, Y., Aghdam, M.M., and Malekzadeh, P. (2014), Free Vibration Analysis of Rotating Functionally Graded Carbon Nanotube-Reinforced Composite Truncated Conical Shells, Composite Structures, Vol. 117, pp.187-200.

Heydarpour, Y., Malekzadeha, P., and Gholipour, F. (2019), Thermoelastic Analysis of FG-GPLRC Spherical Shells under Thermo-Mechanical Loadings Based on Lord-Shulman Theory, Composites Part B: Engineering, Vol. 164, pp. 400-424.

Hieu, P.T., and Tung, H.V. (2020a), Thermomechanical Postbuckling of Pressure-Loaded CNT-Reinforced Composite Cylindrical Shells Under Tangential Edge Constraints and Various Temperature Conditions, Vol. 41, No.1, pp. 244-257.

Hieu, P.T., and Tung, H.V. (2020b), Thermal and Thermomechanical Buckling of Shear Deformable FG-CNTRC Cylindrical Shells and Toroidal Shell Segments with Tangentially Restrained Edges, Archive of Applied Mechanics, Vol. 90, DOI: 10.1007/s00419-020-01682-7.

Hu, H., Belouettar, S., Potier-Ferry, M., and Daya, E.M. (2008), Review and Assessment of Various Theories for Modeling Sandwich Composites, Composite Structures, Vol. 84, pp. 282–292.

Hu, X.X., Sakiyama, T., Matsuda H., and Morita, C. (2002), Vibration of Twisted Laminated Composite Conical Shells, International Journal of Mechanical Sciences, Vol. 44, pp. 1521-1541.

Icardi, U., and Ferrero, L. (2009), Impact Analysis of Sandwich Composites Based on A Refined Plate Element with Strain Energy Updating, Composite Structures, Vol. 89, pp. 35-51.

Irie, T., Yamada, G., and Muramoto, Y., (1984), Free Vibration of Joined Conical-Cylindrical Shells, Journal of Sound and Vibration, Vol. 95, No. 1, pp. 31-39.

Ji, X-Y., Cao, Y-P., and Feng X-Q. (2010), Micromechanics Prediction of the Effective Elastic Moduli of Graphene Sheet-Reinforced Polymer Nanocomposites, Modelling and Simulation in Materials Science and Engineering, Vol. 18, No. 4, 045005.

Jones, R.M. (1975), Mechanics of Composite Materials, McGraw Hill Kogakusha Limited.

Kamarian, S., Salim, M., Dimitri, R., and Tornabene, F. (2016), Free Vibration Analysis of Conical Shells Reinforced with Agglomerated Carbon Nanotubes, International Journal of Mechanical Sciences, Vol.108–109, pp.157-165.

Kant, T., and Pandya, B.N. (1988), A Simple Finite Element Formulation of a Higher-order Theory for Unsymmetrically Laminated Composite Plates, Composite Structures, Vol. 9, pp. 215-246.*in*.

Kardomateas, G. A. (2001), Elasticity Solutions for a Sandwich Orthotropic Cylindrical Shell under External Pressure, Internal Pressure and Axial Force, AIAA Journal, Vol. 39, No. 4, pp. 713–719.

Karmakar, A., and Kishimoto, K. (2006), Free Vibration Analysis of Delaminated Composite Pretwisted Rotating Shells─ A Finite Element Approach, JSME International Journal Series A Solid Mechanics and Material Engineering, Vol. 49, No. 4, pp. 492-502.

Karmakar, A., and Sinha, P.K. (1997), Finite Element Free Vibration Analysis of Rotating Laminated Composite Pretwisted Cantilever Plates, Journal of Reinforced Plastics and Composites, Vol. 16, pp. 1461-1491.

Karmakar, A., and Sinha, P.K. (1998), Finite Element Transient Dynamic Analysis of Laminated Composite Pretwisted Rotating Plates Subjected to Impact, International Journal of Crashworthiness, Vol. 3, No. 4, pp. 379-392.

Karmakar, A., and Sinha, P.K. (2001), Failure Analysis of Laminated Composite Pretwisted Rotating Plates, Journal of Reinforced Plastics and Composites, Vo. 20, No.14-15, pp. 1326-1357.

Karmakar, A., Roy, H. and Kishimoto, K. (2005), Free Vibration Analysis of Delaminated Composite Pretwisted Shells, Aircraft Engineering and Aerospace Technology, Vol. 77, pp. 486-490.

Kee, Y-J., and Kim, J-H. (2004), Vibration Characteristics of Initially Twisted Rotating Shell Type Composite Blades, Composite Structures, Vol. 64, pp. 151-159.

Khalili, S.M.R., Rahmani, O., Fard, K.M., and Thomsen, O.T. (2014), High-order Modelling of Circular Cylindrical Composite Sandwich Shells with a Transversely Compliant Core Subjected to Low Velocity Impact, Mechanics of Advanced Materials and Structures, Vol. 21, No. 8, pp. 680-695.

Khalkhali, A., Malek, N.G., and Nejad, M.B. (2020), Effects of the Impactor Geometrical Shape on the Non-Linear Low-Velocity Impact Response of Sandwich Plate With CNTRC Face Sheets, Journal of Sandwich Structures and Materials, Vol. 22, No. 4, pp. 962-990.

Khatri, K.N. (1995), Vibrations of Arbitrarily Laminated Fiber Reinforced Composite Material Truncated Conical Shell, Journal of Reinforced Plastics and Composites, Vol. 14, No. 9, pp. 923-948.

Khatua, T.P., and Cheung, Y.K., (1973), Bending and Vibration of Multilayer Sandwich Beams and Plates, International Journal for Numerical Methods in Engineering, Vol. 6, No. 1, pp. 11-24.

Kiani, F., Hekmatifar, M., and Toghraie, D. (2020), Analysis of Forced and Free Vibrations of Composite Porous Core Sandwich Cylindrical Shells and FG-CNTs Reinforced Face Sheets Resting on Visco-Pasternak Foundation under Uniform Thermal Field, Journal of the Brazilian Society of Mechanical Sciences and Engineering, Vol. 42, No. 10, 504.

Kiani, Y. (2017), Thermal post-Buckling of FG-CNT Reinforced Composite Plates, Composite Structures, Vol. 159, pp. 299-306.

Kiani, Y. (2018), Thermal Post-buckling of temperature Dependent Sandwich Plates with FG-CNTRC Face Sheets, Journal of Thermal Stresses, Vol. 41, No.7, pp. 866-882.

Kiani, Y. (2018), Isogeometric Large Amplitude Free Vibration of Graphene Reinforced Laminated Plates in Thermal Environment using NURBS Formulation, Computer Methods in Applied Mechanics and Engineering, Vol. 332, pp. 86–101.

Kiani, Y. (2019), Buckling of Functionally Graded Graphene Reinforced Conical Shells Under External Pressure in Thermal Environment, Composites Part B: Engineering, Vol. 156, pp. 128-137.

Kirchoff, G. (1850), Uber Das Gleichgewicht und Die Bewegung Einer Elastischen Scheibe, Journal Fur Die Reine und Angewandte Mathematik (Crelle's Journal), Vol. 40, pp. 51-88.

Kolář, V., and Němec, I. (1973), The Efficient Finite Element Analysis of Rectangular And Skew Laminated Plates, International Journal for Numerical Methods in Engineering, Vol. 7, pp. 309-323.

Kuilla, T., Bhadra, S., Yao, D., Kim, N.H., Bose, S., and Lee, J.H. (2010), Recent Advances in Graphene Based Polymer Composites, Progress in Polymer Science, Vol. 35, pp. 1350–1375.

Kwon, H., Bradbury, C.R., and Leparoux, M. (2011), Fabrication of Functionally Graded Carbon Nanotube-Reinforced Aluminum Matrix Composite, Advanced Engineering Materials, Vol. 13, No. 4, pp. 325-329.

Lam, K.Y., and Loy, C.T. (1998), Influence of Boundary Conditions for a Thin Laminated Rotating Cylindrical Shell, Composite Structures, Vol. 41, No. 215–228.

Laurenzi, S., Pastore, R., Giannini, G., and Marchetti, M. (2013), Experimental Study of Impact Resistance in Multi-Walled Carbon Nanotube Reinforced Epoxy, Composite Structures, Vol. 99, pp. 62-68.

Lee, J.D., Du, S., and Liebowitz, H. (1984), Three-dimensional Finite Element and Dynamic Analysis of Composite Laminate Subjected to Impact, Computers and Structures, Vol. 19, No. 5-6, pp. 807-813.

Lei, Z., Su, Q., Zeng, H., Zhang, Y., and Yu, C. (2018), Parametric Studies on Buckling Behavior of Functionally Graded Graphene-Reinforced Composites Laminated Plates in Thermal Environment, Composite Structures, Vol. 202, pp. 695-709.

Lei, Z.X., and Tong, L.H. (2019), Analytical solution of low-velocity impact of graphene-reinforced composite functionally graded cylindrical shells, Journal of the Brazilian Society of Mechanical Sciences and Engineering, Vol. 41, 486.

Lei, Z.X., Liew, K.M., and Yu, J.L. (2013), Free Vibration Analysis of Functionally Graded Carbon Nanotube-Reinforced Composite Plates using the Element-free kp-Ritz Method in Thermal Environment, Composite Structures, 106, 128-138.

Leissa, A.W., Lee, J.K., and Huang, A.J. (1983), Vibrations of Cantilevered Doubly-curved Shallow Shells, International Journal of Solids and Structures, Vol. 19, No. 5, pp. 411-424.

Leissa, A.W., Lee, J.K., and Huang, A.J. (1984), Vibrations of Twisted Rotating Blades, Journal of Vibration, Acoustics, Stress, and Reliability in Design, Vol. 106, No. 2, pp. 251–257.

Leissa, A.W., Lee, J.K., and Wang, .A.J. (1982), Rotating Blade Vibration Analysis Using Shells, Journal of Engineering for Gas Turbine and Power, Vol. 104, No. 2, pp. 296–302.

Leissa, A.W., Lee, J.K., Huang, A.J. (1981), Vibrations of Cantilevered Cylindrical Shallow Shells Having Rectangular Planform, Journal of Sound and Vibration, Vol. 78, No. 3, pp. 311–328.

Li, C., Shen, H.S., Yang, J., and Wang, H. (2021), Low-velocity Impact Response of Sandwich Plates with GRC Face Sheets and FG Auxetic 3D Lattice Cores, Engineering Analysis with Boundary Elements, Vol.132, pp. 335-344.

Librescu, L., and Hause, T. (2000), Recent Developments in the Modeling and Behavior of Advanced Sandwich Constructions: A Survey, Composite Structures, Vol. 48, pp. 1–17.

Liew, K.M., Lei, Z.X., and Zhang, L.W. (2015), Mechanical Analysis of Functionally Graded Carbon Nanotube Reinforced Composites: A Review, Composite Structures, Vol. 120, pp. 90-97.

Liew, K.M., Lim, C.W., and Kitipornchai, S. (1997), Vibration of Shallow Shells: A Review with Bibliography, Applied Mechanics Reviews, Vol. 50, No. 8, pp. 431-444.

Liew, K.M., Lim, C.W., and Ong, L.S. (1994), Vibration of Pretwisted Cantilever Shallow Conical Shells, International Journal of Solids and Structures, Vol. 31, No. 18, pp. 2463-2476.

Liew, K.M., Lim, M.K., Lim, C.W., Li, D.B., and Zhang, Y.R. (1995), Effects of Initial Twist and Thickness Variation on the Vibration Behaviour of Shallow Conical Shells, Journal of Sound and Vibration, Vol. 180, No. 2, pp. 271-296.

Liew, K.M., Pan, Z., and Zhang, L.W. (2020), The Recent Progress of Functionally Graded CNT Reinforced Composites and Structures, Science China Physics Mechanics and Astronomy, Vol. 63, No. 3, pp. 234601 (1-17).

Lim, C.W., Liew, K.M., and Kitipornchai, S. (1997), Free Vibration of Pretwisted, Cantilevered Composite Shallow Conical Shells, AIAA Journal, Vol. 35, pp. 327-333.

Lin, J.H., Lin, Z.I., Pan, Y.J., Huang, C.L., Chen, C.K., Lou, and C.W. (2016), Polymer Composites Made of Multi-Walled Carbon Nanotubes and Graphene Nano-Sheets:

Effects of Sandwich Structures on their Electromagnetic Interference Shielding Effectiveness, Composites Part B: Engineering, Vol. 89, pp. 424-431.

Liu, D., and Zhou, Y., and Zhu, J. (2021), On the Free Vibration and Bending Analysis of Functionally Graded Nanocomposite Spherical Shells Reinforced with Graphene Nanoplatelets: Three-Dimensional Elasticity Solutions, Engineering Structures, Vol. 226, 111376.

Liu, D., Kitipornchai, S., Chen, W., and Yang, J. (2018), Three-dimensional Buckling and Free Vibration Analyses of Initially Stressed Functionally Graded Graphene Reinforced Composite Cylindrical Shell, Composite Structures, Vol. 189, pp. 560-569.

Liu, F., Hu, N., Ning, H., Liu, Y., Li, Y., and Wu, L. (2015), Molecular Dynamics Simulation on Interfacial Mechanical Properties of Polymer Nanocomposites with Wrinkled Graphene, Computational Materials Science, Vol. 108, pp. 160-167.

Liu, T., Phang, I.Y., Shen, L., Chow, S.Y., and Zhang, W.D. (2004), Morphology and Mechanical Properties of Multiwalled Carbon Nanotubes Reinforced Nylon-6 Composites, Macromolecules, Vol. 37, pp. 7214-7222.

Liu, Y.J., and Chen, X.L. (2003), Evaluations of the Effective Material Properties of Carbon Nanotube-based Composites using a Nanoscale Representative Volume Element, Mechanics of Materials, Vol. 35, pp. 69-81.

Lo, K. H., Christensen, R. M., and Wu, E. M. (1977a), A High-Order Theory of Plate Deformation, Part-1: Homogeneous Plates, Journal of Applied Mechanics, Vol. 44, No. 4, pp. 663-668.

Lo, K. H., Christensen, R.M., and Wu, E. M. (1977b), A Higher Order Theory of Plate Deformation, Part 2: Laminated Plates, ASME Journal of Applied Mechanics, Vol. 44, No. 4, pp. 669-676.

Mahani, R.B., Eyvazian, A., Musharavati, F., Sebaey, T.A., and Talebizadehsardari, P. (2020), Thermal Buckling of Laminated Nano-Composite Conical Shell Reinforced with Graphene Platelets, Thin–Walled Structures, Vol. 155, 106913.

Maiti, D.K., and Sinha, P.K. (1996), Low Velocity Impact Analysis of Composite Sandwich Shells Using Higher-Order Shear Deformation Theories, Sadhana, Vol. 21, pp.597-622.

Maji, P., and Singh, B.N. (2021), Free Vibration Responses of 3D Braided Rotating Cylindrical Shells Based on Third-Order Shear Deformation, Composite Structures, 260, 113255.

Maji, P., Rout, M., and Karmakar, A. (2020), Free Vibration Response of Carbon Nanotube Reinforced Pretwisted Conical Shell under Thermal Environment, Proceedings of the Institution of Mechanical Engineers, Part C: Journal of Mechanical Engineering Science, Vol. 234, No.3, pp.770-783.

Maji, P., Rout, M., and Karmakar, A. (2021), The Thermo-Elastic Vibration of Graphene Reinforced Composite Stiffened Plate with General Boundary Conditions, Structures, Vol. 33, pp. 99-112.

Malekzadeh, K., Khalili, M.R., and Mittal, R.K. (2006), Analytical Prediction of Low-velocity Impact Response of Composite Sandwich Panels using New TDOF Spring–mass–damper Model, Journal of Composite Materials, Vol. 40, No. 18, pp. 1671-1689,

Malekzadeh, P., and Dehbozorgi, M. (2016), Low Velocity Impact Analysis of Functionally Graded Carbon Nanotubes Reinforced Composite Skew Plates, Composite Structures, Vol. 140, pp. 728-748.

Manh, D.T., Anh, V.T.T., Nguyen, P.D., and Duc, N.D. (2020), Nonlinear Post-Buckling of CNTs Reinforced Sandwich Structured Composite Annular Spherical Shells, International Journal of Structural Stability and Dynamics, Vol. 20, No. 02, 2050018.

Mawenya, A.S., and Davies, J.D. (1974), Finite Element Bending Analysis of Multilayer Plates, International Journal for Numerical Methods in Engineering, Vol. 8, pp. 215-225.

McGee, O. G. and Chu, H. R. (1994), Three-Dimensional Vibration Analysis of Rotating Laminated Composite Blades, Journal of Engineering Gas Turbines and Power, Vol. 116, No. 3, pp. 663-671.

Medwadowski, S.J. (1958), A Refined Theory of Elastic Orthotropic Plates, Journal of Applied Mechanics, Vol. 25, No. 4, pp. 437-443.

Meguid, S.A., and Sun, Y. (2004), On the Tensile and Shear Strength of Nano Reinforced Composite Interfaces, Materials and Design, Vol. 25, No. 4, pp. 289-296.

Mehar, K., and Panda, S.K. (2018), Thermal Free Vibration Behavior of FG-CNT Reinforced Sandwich Curved Panel using Finite Element Method, Polymer Composites, Vol. 39, No. 8, pp. 2751-2764.

Mehar, K., Panda, S.K., and Mahapatra, T.R. (2018), Nonlinear Frequency Responses of Functionally Graded Carbon Nanotube-Reinforced Sandwich Curved Panel Under Uniform Temperature Field, International Journal of Applied Mechanics, Vol. 10, No. 03, 1850028.

Mehar, K., Panda, S.K., and Sharma, N. (2020), Numerical Investigation and Experimental Verification of Thermal Frequency of Carbon Nanotube-Reinforced Sandwich Structure, Engineering Structures, Vol. 211, 110444.

Mehar, K., Panda, S.K., Devarajana, Y., and Choubey, G. (2019), Numerical Buckling Analysis of Graded CNT-reinforced Composite Sandwich Shell Structure under Thermal Loading, Composite Structures, Vol. 216, pp. 406–414.

Mehri, M., Asadi, H., and Wang, Q. (2016), Buckling and Vibration analysis of a Pressurized CNT Reinforced Functionally Graded Truncated Conical Shell under an Axial Compression Using HDQ Method, Computer Methods in Applied Mechanics and Engineering Volume, Vol. 303, pp. 75-100.

Meunier, M., and Shenoi, R.A. (1999), Free Vibration Analysis of Composite Sandwich Plates, Proceedings of the IMechE, Part C: Journal of Mechanical Engineering Science, Vol. 213, No. 7, pp. 715–727.

Milani, M.A., Gonza´lez, D., Quijada, R., et al. (2013), Polypropylene/Graphene Nanosheet Nanocomposites by in Situ Polymerization: Synthesis, Characterization and Fundamental Properties, Composite Science and Technology, Vol. 84, pp. 1–7.

Mindlin, R.D. (1951), Influence of Rotatory Inertia and Shear in Flexural Motions of Isotropic Elastic Plates. Journal of Applied Mechanics, Vol. 18, No. 1, pp. 31-38.

Mirzaei, M., and Kiani, Y. (2016), Free Vibration of Functionally Graded Carbon Nanotube Reinforced Composite Cylindrical Panels, Composite Structures, Vol. 142, pp. 45-56.

Mohseni, A., and Shakour, M. (2020), Natural Frequency, Damping and Forced Responses of Sandwich Plates with Viscoelastic Core and Graphene Nanoplatelets Reinforced Face Sheets, Journal of Vibration and Control, Vol. 26 , No. 15-16, pp. 1165-1177.

Moita, J.S., Araújo, A.L., Martins, P., Soares, C.M.M., and Soares, C.A. M. (2011), A Finite Element Model for the Analysis of Viscoelastic Sandwich Structures, Computers and Structures, Vol. 89, No. 21-22, pp. 1874-1881.

Moon, F.C. (1972), Wave Surfaces Due to Impact on Anisotropic Plates, Journal Composite Materials, Vol. 6, pp. 62-79.

Moon, F.C. (1973), Stress Wave Calculations in Composite Plates using the Fast Fourier Transform, Computers and Structures, Vol. 3, pp. 1195-1204.

Moradi-Dastjerdi, R., and Momeni-Khabisi, H. (2018), Vibrational Behavior of Sandwich Plates with Functionally Graded Wavy Carbon Nanotube-Reinforced Face Sheets Resting on Pasternak Elastic Foundation, Journal of Vibration and Control, Vol. 24, No. 11, pp. 2327-2343.

Naghdi, P. M., and Kalnins, A. (1962), On Vibrations of Elastic Spherical Shells, Journal of Applied Mechanics, Vol. 29, No. 1, pp. 65-72.

Ninh, D.G., Minh, V.T., Tuan, N.V., Hung, N.C., and Phong, D.G. (2021), Novel Numerical Approach for Free Vibration of Nanocomposite Joined Conical-Cylindrical-Conical Shells, AIAA Journal, Vol. 59, https://doi.org/10.2514/1.J059518.

Niu, N., Zhang, W., and Guo. X.Y. (2019), Free Vibration of Rotating Pretwisted Functionally Graded Composite Cylindrical Panel Reinforced with Graphene Platelets, European Journal of Mechanics - A/Solids, Vol. 77, 103798.

Noor, A.K., Burton, W.S., and Bert, C.W. (1996), Computational Models for Sandwich Panels and Shells, Applied Mechanics Reviews, Vol. 49, No. 3, pp. 155-199.

Pagano, N.J. (1970), Exact Solutions for Rectangular Bidirectional Composites and Sandwich Plates, Journal of Composite Materials, Vol. 4, pp. 20-34.

Palazotto, A.N., Herup, E.J., and Gummadim, L.N.B. (2000), Finite element Analysis of Low-Velocity Impact on Composite Sandwich Plates, Composite Structures, Vol. 49, pp. 209-227.

Pan, Z-Z, Chen, X., and Zhang, L.W. (2020), Modeling Large Amplitude Vibration of Pretwisted Hybrid Composite Blades Containing CNTRC Layers and Matrix Cracked FRC Layers, Applied Mathematical Modelling , Vol. 83, pp. 640–659.

Pan, Z-Z., and Liew, K.M. (2020), Predicting Vibration Characteristics of Rotating Composite Blades Containing CNT-Reinforced Composite Laminae and Damaged Fiber-Reinforced Composite Laminae, Composite Structures, Vol. 250, 112580.

Panda, S.K., and Singh, B.N. (2011), Large Amplitude Free Vibration Analysis of Thermally Post-Buckled Composite Doubly Curved Panel using Nonlinear FEM, Finite Elements in Analysis and Design, Vol. 47, No. 4, pp. 378-386.

Pandit, M.K., Sheikh, A.H., and Singh, B.N. (2008), An Improved Higher Order Zigzag Theory for the Static Analysis of Laminated Sandwich Plate with Soft Core, Finite Elements in Analysis and Design, Vol. 44, pp. 602-610.

Pandya, B.N., and Kant, T. (1988a), Flexure Analysis of Laminated Composites using Refined Higher-order C^0 Plate Bending Elements, Computer Methods in Applied Mechanics and Engineering, Vol. 66, No. 2, pp. 173-198.

Pandya, B.N., and Kant, T. (1988b), A Refined Higher-Order Generally Orthotropic C^0 Plate Bending Element, Computers and Structures, Vol. 28, pp. 119-133.

Pandya, B.N., and Kant, T. (1988c), Finite Element Analysis of Laminated Composite Plates using a Higher-Order Displacement Model, Composites Science and Technology, Vol. 32, pp. 137-155.

Patra, A.K., and Mitra, N. (2018), Mixed-mode Fracture of Sandwich Composites: Performance Improvement with Multiwalled Carbon Nanotube Sonicated Resin, Journal of Sandwich Structures and Materials, Vol. 20, No. 3, pp. 379-395.

Phuong, N.T., Nam, V.H., Trung, N.T., Duc, V.M., Loi, N.V., Thinh, N.D., and Tu, P.T. (2021), Thermomechanical Postbuckling of Functionally Graded Graphene-reinforced Composite Laminated Toroidal Shell Segments Surrounded by Pasternak's Elastic Foundation, Journal of Thermoplastic Composite Materials, Vol. 34, No. 10, pp. 1380-1407.

Pryor Jr., C.W., and Barker, R.M. (1971), A Finite Element Analysis including Transverse Shear Effects for Application to Laminated Plates, AIAA Journal, Vol. 9, No. 5, pp. 912-917.

Punera, D., and Kant, T. (2021), Two Dimensional Kinematic Models for CNT Reinforced Sandwich Cylindrical Panels with Accurate Transverse Interlaminar Shear Stress Estimation, Thin-Walled Structures, Vol. 164, 107881.

Putter, S., and Manor, H. (1978), Natural Frequencies of Radial Rotating Beams, Journal of Sound and Vibration, Vol. 56, pp. 175-185.

Putz, K.W., Compton, O.C., Palmeri, M.J., Nguyen, S.T., and Brinson, L.C. (2010), High-nanofiller-content Graphene Oxide-Polymer Nanocomposites via Vacuum-Assisted Self-Assembly, Advanced Functional Materials, Vol. 20, pp. 3322-3329.

Qaderi, S., and Ebrahimi, F. (2022), Vibration Analysis of Polymer Composite Plates Reinforced with Graphene Platelets Resting on Two-Parameter Viscoelastic Foundation, Engineering with Computers, Vol. 38, pp. 419-435.

Qaderi, S., Ebrahimi, F., and Mahesh, V. (2019), Free Vibration Analysis of Graphene Platelets–reinforced Composites Plates in Thermal Environment Based on Higher-order Shear Deformation Plate Theory, International Journal of Aeronautical and Space Sciences, Vol. 20, No. 4, pp. 902-912.

Qatu, M.S. (1992), Review of Shallow Shell Vibration Research, The Shock and Vibration Digest, Vol. 24, pp. 3-15.

Qatu, M.S., and Leissa, A.W. (1991), Natural Frequencies for Cantilevered Doubly-Curved Laminated Composite Shallow Shells, Composite Structures, Vol.17, No. 3, pp. 227-255.

Qatu, M.S., and Leissa, A.W. (1991), Vibration Studies for Laminated Composite Twisted Cantilever Plates, International Journal of Mechanical Sciences, Vol. 33, pp. 927–940.

Qian, D., Dickey, E.C., Andrews R., and Rantell, T. (2000), Load Transfer and Deformation Mechanisms in Carbon Nanotube-Polystyrene Composites, Applied Physics Letter, Vol. 76, pp. 2868-2870.

Qian, H., Greenhalgh, E.S., Shaffer, M.S.P., and Bismarck, A. (2010), Carbon Nanotube-Based Hierarchical Composites: A Review, Journal of Material Chemistry, Vol. 20, pp. 4751–4762.

Qin, Z., Shengnan, Z., Xuejia, P., Safaei, B., Chu, F. (2020), A Unified Solution for Vibration Analysis of Laminated Functionally Graded Shallow Shells Reinforced by Graphene with General Boundary Conditions, International Journal of Mechanical Sciences, Vol. 170, 105341.

Rafiee, M., Nitzsche, F., and Labrosse, M. (2017), Dynamics, Vibration and Control of Rotating Composite Beams and Blades: A Critical Review. Thin-Walled Structures, Vol. 119, pp. 795–819.

Rafiee, M.A., Rafiee, J., Wang, Z., Song, H., Yu, Z.Z., and Koratkar, N. (2009), Enhanced Mechanical Properties of Nanocomposites at Low Graphene Content, ACS Nano, Vol. 3, No. 12, pp. 3884-3890.

Rahman, R., and Haque, A. (2013), Molecular modeling of Crosslinked Graphene-Epoxy Nanocomposites for Characterization of Elastic Constants and Interfacial Properties, Composites Part B: Engineering, Vol. 54, pp. 353-364.

Ramezani, M., Rezaiee-Pajand, M., and Tornabene, F. (2022), Linear and Nonlinear Mechanical Responses of FG-GPLRC Plates using A Novel Strain-Based Formulation of Modified FSDT Theory, International Journal of Non-Linear Mechanics, Vol. 140, 103923.

Rao J.S. (1977), Turbine Blading Excitation and Vibration, The Shock and Vibration Digest, Vol. 9, No. 3, pp. 15-22.

Rao J.S. (1980), Turbomachine Blade Vibration, The Shock and Vibration Digest, Vol. 12, No. 2, pp.19-26.

Rao J.S. (1983), Turbomachine Blade Vibration, The Shock and Vibration Digest, Vol. 15, No. 5, pp. 3-9.

Rao, J.S. (1973), Natural Frequencies of Turbine Blading - A survey, The Shock and Vibration Digest, Vol. 5, No. 10, pp. 1-10.

Rasoolpoor, M., Ansari, R., and Hassanzadeh-Aghdam, M. K. (2020), Influences of carbon nanotubes on low velocity impact performance of metallic nanocomposite plates – A coupled numerical approach, Mechanics Based Design of Structures and Machines, https://doi.org/10.1080/15397734.2020.1840392.

Rasoolpoor, M., Ansari, R., and Hassanzadeh-Aghdam, M.K.A. (2021), A Numerical Investigation on Low Velocity Impact Response of polymer-Based Nanocomposite Plates Containing Multiscale Reinforcements, Journal of the Brazilian Society of Mechanical Sciences and Engineering, Vol. 43(2), DOI: 10.1007/s40430-021-02824-w.

Ray, M.C., and Batra, R.C. (2007), A single-walled Carbon Nanotube Reinforced 1–3 Piezoelectric Composite for Active Control Of Smart Structures, Smart Materials and Structures, Vol. 16, pp. 1936-1947.

Reddy, J.N. (1980), A Penalty Plate Bending Element for the Analysis of Laminated Anisotropic Composite Plates, International Journal for Numerical Methods in Engineering, Vol. 15, pp. 1187-1206.

Reddy, J.N. (1984), A Simple Higher-order Theory for Laminated Composite Plates, ASME Journal of Applied Mechanics, Vol. 51, No. 4, pp. 745-752.

Reddy, J.N. (1987), A Generalization of Two-Dimensional Theories of Laminated Composite Plates, Communications in Applied Numerical Methods, Vol. 3, No. 3, pp. 173 180.

Reddy, R.M.R., Karunasena, W., and Lokuge, W. (2018), Free Vibration of Functionally Graded-GPL Reinforced Composite Plates with Different Boundary Conditions, Aerospace Science and Technology, Vol. 78, pp. 147-156.

Reissner, E. (1944), On the Theory of Bending of Elastic Plates, Journal of Mathematics and Physics, Vol. 23, pp. 184-191.

Reissner, E. (1945), The Effect of Transverse Shear Deformation on the Bending of Elastic Plates, Journal of Applied Mechanics, Vol. 12, No. 2, pp. 69-76.

Reissner, E., and Stavsky, Y. (1961), Bending and Stretching of Certain Types of Heterogeneous Aerolotropic Elastic Plates, Transactions of ASME, Journal of Applied Mechanics, Vol. 28, pp. 402-408.

Rostami, R., and Mohammadimehr, M. (2022), Vibration Control of Rotating Sandwich Cylindrical Shell-reinforced Nanocomposite Face Sheet and Porous Core Integrated with Functionally Graded Magneto-electro-elastic Layers, Engineering with Computers, Vol. 38, No. 9, pp. 87-100.

Rout, M., and Karmakar, A. (2019), Free Vibration of Rotating Pretwisted CNTs-Reinforced Shallow Shells in Thermal Environment. Mechanics of Advanced Material and Structures, Vol. 2, pp. 1808-1820.

Rout, M., Hota, S.S., Karmakar, A. (2019), Thermoelastic Free Vibration Response of Graphene Reinforced Laminated Composite Shells, Engineering Structures, Vol. 178, pp. 179-190.

Safaei, B., Moradi-Dastjerdi, R., and Chu, F. (2018), Effect of Thermal Gradient Load on Thermo-Elastic Vibrational Behavior of Sandwich Plates Reinforced by Carbon Nanotube Agglomerations, Composite Structure, Vol. 192, pp. 28-37.

Sankar, A., Natarajan, S., Merzouki, T. and Ganapathi, M. (2017), Nonlinear Dynamic Thermal Buckling of Sandwich Spherical and Conical Shells with CNT Reinforced Facesheets, International Journal of Structural Stability and Dynamics, Vol. 17, No. 9, 1750100.

Sayyad, A.S., and Ghugal, Y.M. (2015), On the Free Vibration Analysis of Laminated Composite and Sandwich Plates: A Review of Recent Literature with Some Numerical Results, Composite Structures, Vol. 129, pp. 177-201.

Schapery, R. (1968), Thermal Expansion Coefficients of Composite Materials based on Energy Principles, Journal of Composite Materials, Vol. 2, No. 3, pp. 380-404.

Seidel, G.D., and Lagoudas, D.C. (2006), Micromechanical Analysis of the Effective Elastic Properties of Carbon Nanotube Reinforced Composites, Mechanics of Materials, Vol. 38, pp. 884-907.

Selim, B.A., Zhang, L.W., Liew, K.M. (2017), Impact Analysis of CNT-reinforced Composite Plates Based on Reddy's Higher-order Shear Deformation Theory using an Element-Free Approach, Composite Structures, Vol. 170, pp. 228-242.

Serdoun, S.M.N., and Cherif, S.M.H. (2016), Free Vibration Analysis of Composite and Sandwich Plates by Alternative Hierarchical Finite Element Method Based on Reddy's C^1 HSDT, Journal of Sandwich Structures and Materials, Vol. 18, No. 4, pp. 501-528.

Setoodeh, A.R., Shojaee, M., and Malekzadeh, P. (2019), Vibrational Behavior of Doubly Curved Smart Sandwich Shells with FGCNTRC Face Sheets and FG Porous Core, Composites Part B, Vol. 165, pp. 798-822.

Shadmehri, F., Hoa, S.V., and Hojjati, M. (2012), Buckling of Conical Composite Shells, Composite Structures, Vol. 94, pp. 787–792.

Shahedi, S., and Mohammadimehr, M. (2020), Vibration Analysis of Rotating Fully-Bonded And Delaminated Sandwich Beam with CNTRC Face Sheets and AL-foam Flexible Core in Thermal And Moisture Environments, Mechanics Based Design of Structures and Machines, Vol. 48, 2020, 584-614.

Shao, Z.S., and Ma, G.W. (2007), Free Vibration Analysis of Laminated Cylindrical Shells by Using Fourier Series Expansion Method, Journal of Thermoplastic Composite Materials, Vol. 20, No. 6, pp.551-573.

Shariyat, M., and Hosseini, S.H. (2014), Eccentric Impact Analysis of Pre-Stressed Composite Sandwich Plates with Viscoelastic Cores: A Novel Global–Local Theory and a Refined Contact Law, Composite Structures, Vol. 117, pp. 333-345.

Shen, H.S. (2009), Nonlinear Bending of Functionally Graded Carbon Nanotube-Reinforced Composite Plates in Thermal Environments, Composite Structures, Vol. 91, No. 1, pp. 9-19.

Shen, H.S., and Xiang, Y. (2018), Postbuckling of Functionally Graded Graphene-reinforced Composite Laminated Cylindrical Shells Subjected to External Pressure in Thermal Environments, Thin-Walled Structures, Vol. 124, pp. 151-160.

Shen, H.S., and Zhang, C.H. (2010), Thermal Buckling and Postbuckling Behavior of Functionally Graded Carbon Nanotube-Reinforced Composite Plates, Materials and Design, Vol. 31, pp. 3403-3411.

Shen, H.S., and Zhu, Z.H. (2012), Postbuckling of Sandwich Plates with Nanotube-Reinforced Composite Face Sheets Resting on Elastic Foundations, European Journal of Mechanics - A/Solids, Vol. 35, pp. 10-21.

Shen, H.S., Xiang, Y., and Fan, Y. (2017), Nonlinear Vibration of Functionally Graded Graphene-reinforced Composite Laminated Cylindrical Shells in Thermal Environments, Composite Structures, Vol. 182, pp. 447-456.

Shen, H.S., Xiang, Y., Fan, Yin, and Hui, D. (2018), Nonlinear Vibration of functionally Graded Graphene-reinforced Composite Laminated Cylindrical Panels Resting on Elastic Foundations in Thermal Environments, Composites Part B: Engineering, Vol. 136, pp. 177-186.

Shen, H-S., Xiang, Y., and Lin, F. (2017), Nonlinear Vibration of Functionally Graded Graphene-Reinforced Composite Laminated Plates in Thermal Environments, Computer Methods in Applied Mechanics and Engineering, Vol. 319, pp. 175-193.

Shenas, A.G., Malekzadeh, P., and Ziaee, S. (2017), Vibration Analysis of Pre-Twisted Functionally Graded Carbon Nanotube Reinforced Composite Beams in Thermal Environment, Composite Structures, Vol. 162, pp. 325-340.

Shivakumar, K. N., Elber, W., and Illg, W. (1985), Prediction of Impact Force and Duration due to Low-Velocity Impact on Circular Composite Laminates, ASME Journal of Applied Mechanics, Vol. 52, No. 3, pp. 674-680.

Shokri-Oojghaz, R., Moradi-Dastjerdi, R., Mohammadi, H., and Behdinan, K. (2019), Stress Distributions in Nanocomposite Sandwich Cylinders Reinforced by Aggregated Carbon Nanotube, Polymer Composites, Vol. 40, No. S2, pp. 1918-1927.

Sinha, S.K., and Turner, K.E. (2011), Natural Frequencies of A Pre-Twisted Blade in A Centrifugal Force Field, Journal of Sound and Vibration, Vol. 330, pp. 2655–2681.

Sobhy, M., and Zenkour, A.M. (2019), Vibration Analysis of Functionally Graded Graphene Platelet-Reinforced Composite Doubly-Curved Shallow Shells on Elastic Foundations, Steel and Composite Structures, Vol. 33, No. 2, pp. 195-208.

Sofiyev, A.H. (2018), Application of The First Order Shear Deformation Theory to the Solution of Free Vibration Problem for Laminated Conical Shells, Composite Structures, Vol. 188, pp. 340–346.

Sofiyev, A.H., Bayramov, R.P., and Heydarov, S.H. (2020), The Stability of Composite Conical Shells Covered by Carbon Nanotube-Reinforced Coatings under External Pressures, Acta Mechanica, Vol. 231, pp. 4547-4562.

Song, M., Kitipornchai, S., and Yang. J. (2017), Free and Forced Vibrations of Functionally Graded Polymer Composite Plates Reinforced with Graphene Nanoplatelets, Composite Structures, Vol. 159, pp. 579-588.

Song, M., Li, X., Kitipornchai, S,, Bi, Q., and Yang, J. (2019), Low-velocity Impact Response of Geometrically Nonlinear Functionally Graded Graphene Platelet-reinforced Nanocomposite Plates, Nonlinear Dynamics, Vol. 95, No. 12, pp. 2333-2352.

Song, M., Yang, J., Kitipornchai, S., and Zhu, W. (2017), Buckling and Postbuckling of Biaxially Compressed Functionally Graded Multilayer Graphene Nanoplatelet-reinforced Polymer Composite Plates, International Journal of Mechanical Sciences, Vol. 131–132, pp. 345-355.

Song, P., Cao, Z., Cai, Y., Zhao, Y., Fang, Z., and Fu, S. (2011), Fabrication of Exfoliated Graphene-Based Polypropylene Nanocomposites with Enhanced Mechanical and Thermal Properties, Polymer, Vol. 52, pp. 4001-4010.

Song, Z.G., Zhang, L.W., and Liew, K.M. (2016), Dynamic Responses of CNT Reinforced Composite Plates Subjected to Impact Loading, Composite Part B: Engineering, Vol. 99, pp. 154-161.

Song, Z.G., Zhang, L.W., and Liew, K.M. (2016), Vibration Analysis of CNT-reinforced Functionally Graded Composite Cylindrical Shells in Thermal Environments, International Journal of Mechanical Sciences, Vol. 115–116, pp. 339-347.

Spanos, K.N., Georgantzinos, S.K., and Anifantis, N.K. (2015), Mechanical Properties of Graphene Nanocomposites: A Multiscale Finite Element Prediction, Composite Structures, Vol. 132, pp. 536-544.

Sreenivasamurthy, S., and V. Ramamurthi (1981b). Coriolis effect on the vibration of flat rotating low aspect ratio cantilever plates, The Journal of Strain Analysis for Engineering Design, Vol. 16, pp. 97-106.

Sreenivasamurthy, S., and V. Ramamurti. (1981a), A parametric study of vibration of rotating pre-twisted and tapered low aspect ratio cantilever plates, Journal of Sound and Vibration, Vol. 76, No.3, pp. 311-328.

Srinivas, S. (1973), A Refined Analysis of Composite Laminates, Journal of Sound and Vibration, Vol. 30, No. 4, pp. 495-507.

Stavsky, Y. (1961), Bending and Stretching of Laminated Aeolotropic Plates, Proceedings of the American Society of Civil Engineers, Journal of Engineering Mechanics Division, Vol. 8, pp. 31-56.

Sun, C.T. (1973), Propagation of Shock Waves in Anisotropic Composite Plates, Journal of Composite Materials, Vol.7, No. 3, pp. 366-382.

Sun, C.T., and Chattopadhyay, S. (1975), Dynamic Response of Anisotropic Laminated Plates under Initial Stress to Impact of a Mass, Journal of Applied Mechanics, Vol. 42, No. 3, pp. 693-698.

Sun, C.T., and Chen, J.K. (1985), On the Impact of Initially Stressed Composite Laminates, Journal of Composite Material, Vol. 19, No. 6, pp. 490-504.

Tan, T.M., and Sun, C.T. (1985), Use of Statical Indentation Laws in the Impact Analysis of Laminated Composite Plates, Journal of Applied Mechanics, Vol. 52, No. 1, pp. 6-12.

Thai, C.H., Ferreira, A.J.M., Tran, T.D., and Phung-Van, P. (2019), Free vibration, Buckling and Bending Analyses of multilayer Functionally Graded Graphene Nanoplatelets Reinforced Composite Plates using the NURBS Formulation, Composite Structures, Vol. 220, pp. 749-759.

Thanh, N.V., Quang, V.D., Khoa, N.D., Seung-Eock, K., and Duc, N.D. (2019), Nonlinear Dynamic Response and Vibration of FG CNTRC Shear Deformable Circular Cylindrical Shell with Temperature-dependent Material Properties and surrounded on Elastic Foundations, Journal of Sandwich Structures & Materials, Vol. 21, No. 7, pp. 2456-2483.

Thomsen, O.T. (2009), Sandwich Materials for Wind Turbine Blades – Present and Future, Journal of sandwich structures and materials, Vol. 11, No. 1, pp.7-26.

Tong, L. (1993), Free Vibration of Composite Laminated Conical Shells, International Journal of Mechanical Sciences, Vol. 35, No. 1, pp. 47-61.

Torabi, J., and Ansari, R. (2017), Nonlinear Free Vibration Analysis of Thermally Induced FG-CNTRC Annular Plates: Asymmetric Versus Axisymmetric Study, Computer Methods in Applied Mechanics and Engineering, Vol. 324, pp. 327-347.

Tran, T.T., Tran, V.K., Le, P.B., Phung, V.M., Do, V.T., and Nguyen, H.N. (2020), Forced Vibration Analysis of Laminated Composite Shells Reinforced with Graphene Nanoplatelets using Finite Element Method, Advances in Civil Engineering, Vol. 2020, 1471037, https://doi.org/10.1155/2020/1471037.

Tripathi, V., Singh, B.N., and Shukla, K.K. (2007), Free Vibration of Laminated Composite Conical Shells with Random Material Properties, Composite Structures, Vol. 81, pp. 96–104.

Vadiraja, D.N., and Sahasrabudhe, A.D.(2009), Vibration Analysis and Optimal Control of Rotating Pre-Twisted Thin-Walled Beams using MFC Actuators and Sensors, Thin-Walled Structures, Vol. 47, No. 5, pp. 555-567.

Vaziri, R., Quan, X., and Olson, M.D., (1996), Impact Analysis of Laminated Composite Plates and Shells By Super Finite Elements, International Journal of Impact Engineering, Vol.18, Nos 7-8, pp. 765-782.

Vinson, J.R. (2001), Sandwich structures, Applied Mechanics Reviews, Vol. 54, No. 3, pp. 201-214.

Viswanathan, K.K., Javed, S., Prabakar, K., Aziz, Z.A., and Bakar, I.A. (2015), Free Vibration of Anti-symmetric Angle-ply Laminated Conical Shells, Composite Structures, Vol. 122, pp. 488–495.

Vlachoutsis, S. (1992), Shear Correction Factors for Plates and Shells, International Journal for Numerical Methods in Engineering, Vol. 33, No. 7, pp. 1537–1552.

Vu, H.N., Nguyen, T.P., Ho, S.L., Vu, M.D., and Cao, V.D. (2021). Nonlinear Buckling Analysis of Stiffened FG-GRC Laminated Cylindrical Shells Subjected to Axial Compressive Load in Thermal Environment, Mechanics Based Design of Structures and Machines, https://doi.org/10.1080/15397734.2021.1932522.

Wang, A., Chen, H., and Zhang, W. (2019), Nonlinear Transient Response of Doubly Curved Shallow Shells Reinforced with Graphene Nanoplatelets subjected to Blast Loads Considering Thermal Effects, Composite Structures, Vol. 225, 111063.

Wang, H., Long, S., Yao, X., Lu, G., Zhang, X., Han, Q. (2021), Analytical Study on the low-Velocity Impact Penetration of the Fully-Clamped Foam-Core Composite Sandwich Panels, Composites Part B: Engineering, Vol. 224, 109214.

Wang, M., Li, Z.M., and Qiao, P. (2018), Vibration Analysis of Sandwich Plates with Carbon Nanotube-Reinforced Composite Face-Sheets, Composite Structures, Vol. 200, pp. 799-809.

Wang, Q., Cui, X., Qin, B., and Liang, Q. (2017), Vibration Analysis of the functionally Graded Carbon Nanotube Reinforced Composite Shallow Shells with Arbitrary Boundary Conditions, Composite Structures, Vol.182, pp. 364-379.

Wang, Z.X., and Shen, H.S. (2012), Nonlinear Vibration and Bending of Sandwich Plates with Nanotube-reinforced Composite Face Sheets, Composites Part B: Engineeering, Vol. 43, pp. 411-421.

Wang, Z.X., and Shen, H-S. (2018), Nonlinear Vibration Of Sandwich Plates with FG-GRC Face Sheets In Thermal Environments, Composite Structures, Vol. 192, pp. 642-653.

Wang, Z.X., Xu, J., and Qiao, P. (2014), Nonlinear Low-Velocity Impact Analysis of Temperature-Dependent Nanotube-Reinforced Composite Plates, Composite Structures, Vol. 108, pp. 423-434.

Wilkins Jr., D.J., Bert, C.W., and Egle, D.M. (1970), Free Vibrations of Orthotropic Sandwich Conical Shells with Various Boundary Conditions. Journal of Sound and Vibration, Vol. 13, No. 2, pp. 211-228.

Wu, H.Y., and Fu-Kuo, C. (1989), Transient Dynamic Analysis of Laminated Composite Plates Subjected to Transverse Impact, Computers and Structures, Vol. 31, No. 3, pp. 453-466.

Xiang, P., Xia, Q., Jiang, L.Z., Peng, L., Yan, J.W., and Liu, X. (2021), Free Vibration Analysis of FG-CNTRC Conical Shell Panels Using The Kernel Particle Ritz Element-Free Method, Composite Structures, Vol. 255, 112987.

Xiang, R., Pan, Z-Z, Ouyang, H., and Zhang, L.W. (2020), A Study of the Vibration and Lay-Up Optimization of Rotating, Cross-Ply Laminated Nanocomposite Blades, Composite Structures, Vol. 235,111775.

Yadav, A., Amabili, M., Panda, S.K., and Dey, T. (2021), Nonlinear Analysis of Cylindrical Sandwich Shells with Porous Core and CNT Reinforced Face-sheets by Higher-order Thickness and Shear Deformation Theory, European Journal of Mechanics - A/Solids, Vol. 90, 104366.

Yang, B. Kitipornchai, S., Yang, Y-F., and Yang, J. (2017), 3D thermos-mechanical Bending Solution of Functionally Graded Graphene Reinforced Circular and Annular Plates, Applied Mathematical Modelling, Vol. 49, pp. 69-86.

Yang, C.C. (1974), On Vibrations of Orthotropic Conical Shells. Journal of Sound and Vibration, Vol. 34, No. 4, pp. 552-555.

Yang, C.H., Ma, W.N., Ma, D.W., He, Q., and Zhong, J.L. (2018), Analysis of the Low Velocity Impact Response of Functionally Graded Carbon Nanotubes Reinforced Composite Spherical Shells, Journal of Mechanical Science and Technology, Vol. 32, No.6, pp. 2681-2691.

Yang, P.C., Norris, C.H., and Stavsky, Y. (1966), Elastic Wave Propagation in Heterogeneous Plates, International Journal of Solids and Structures, Vol. 2, pp. 665-684.

Yang, S., Hao, Y., Zhang, W., Yang, L., and Liu, L. (2021), Nonlinear Vibration of Functionally Graded Graphene Platelet Reinforced Composite Truncated Conical Shell using First-order Shear Deformation Theory, Applied Mathematics and Mechanic, Vol. 42, No. 7, pp. 981–998.

Yang, S.H., and Sun, C.T. (1982) Indentation Law for Composite Laminates, Composite Materials: Testing and Design (6th Conference), ASTM International: 425–449.

Yengejeh, S.I., Kazemi, S.A., and Öchsner, A. (2017), Carbon Nanotubes as Reinforcement in Composites: A Review of the Analytical, Numerical and Experimental Approaches, Computational Materials Science, Vol. 136, pp. 85–101.

Yokoyama, T. (1988), Free Vibration Characteristics of Rotating Timoshenko Beams, International Journal of Mechanical Science, Vol. 30, pp.743-755.

Yu, Y., Shen, H-S., Wang, H., and Hui, D. (2018), Postbuckling of Sandwich Plates with Graphene-Reinforced Composite Face sheets in Thermal Environments, Composites Part B: Engineering, Vol. 135, pp. 72-83.

Zamani, H.A. (2021), Free Vibration of Rotating Graphene-Reinforced Laminated Composite Conical Shells, Composites Part C, Vol. 5, 100153.

Zarei, H., Fallah, M., Bisadi, H., Daneshmehr, A.R. and Minak, G. (2017), Multiple Impact Response of Temperature-Dependent Carbon Nanotube -Reinforced Composite (CNTRC) Plates with General Boundary Conditions, Composites Part B: Engineering, Volume 113. pp. 206-217.

Zghal, S., Frikha, A., and Dammak, F. (2018), Free Vibration Analysis of Carbon Nanotube-Reinforced Functionally Graded Composite Shell Structures, Applied Mathematical Modelling, Vol. 53, pp. 132-155.

Zhang, L.W., Pan, Z-Z., and Chen, X. (2020), Vibration Characteristics of Matrix Cracked Pretwisted Hybrid, Composite Blades Containing CNTRC Layers, Journal of Sound and Vibration 2020, Vol. 473, 115242.

Zhang, L.W., Song, Z.G., Qiao, P., and Liew, K.M. (2017), Modeling of Dynamic Responses of CNT Reinforced Composite Cylindrical Shells Under Impact Loads, Computer Methods in Applied Mechanics and Engineering, Vol. 313, pp. 889–903.

Zhang, W., Niu, Y., and Behdinan, K. (2020), Vibration Characteristics of Rotating Pretwisted Composite Tapered Blade with Graphene Coating Layers, Aerospace Science and Technology, Vol. 98, 105644.

Zhao, J., Choe, K., Shuai, C., Wang, A., and Wang, Q. (2019), Free Vibration Analysis of Functionally Graded Carbon Nanotube Reinforced Composite Truncated Conical Panels with General Boundary Conditions, Composites Part B: Engineering, Vol. 160, pp. 225-240.

Zhao, S., Zhao, Z., Yang, Z., Ke, L.L., Kitipornchai, S., and Yang, J. (2020) Functionally Graded Graphene Reinforced Composite Structures: A review, Engineering Structures 210, 110339.

Zhao, T.Y., Jiang, Z.Y., Zhao, Z., Xie, L.Y., and Yuan, H.Q. (2021a), Modeling and Free Vibration Analysis of Rotating Hub-Blade Assemblies Reinforced with Graphene Nanoplatelets, The Journal of Strain Analysis for Engineering Design, Vol. 56 , No. 8, pp. 563-573.

Zhao, T.Y., Maa, Y., Zhang, H.Y., Pane, H.G., and Cai. Y. (2021b), Free Vibration Analysis of A Rotating Graphene Nanoplatelet Reinforced Pre-Twist Blade-Disk Assembly with a Setting Angle, Applied Mathematical Modelling, Vol. 93, pp. 578-596.

Zhu, P., Lei, Z.X., and Liew, K.M. (2012), Static and Free Vibration Analyses of Carbon Nanotube-Reinforced Composite Plates using Finite Element Method with first Order Shear Deformation Plate Theory, Composite Structures, Vol. 94, No. 4, pp. 1450-1460.

Zhu, S., and Chai, G.B. (2016), Low-velocity Impact Response of Composite Sandwich Panels, Proceedings of the IMechE, Part L: Journal of Materials: Design and Applications, Vol. 230, No. 2, pp. 388-399.

Appendix

Elements of the matrices $[S]$ matrix

$$=\begin{bmatrix}
S_{11} & & & & & & & & & & & & & & & & \\
S_{21} & S_{22} & & & & & & & & & & & & & & & \\
0 & 0 & S_{33} & & & & & & & & & & & & & & \\
0 & 0 & S_{43} & S_{44} & & & & & & & & & & & & & \\
0 & 0 & 0 & 0 & S_{55} & & & & & & & & & & & & \\
0 & 0 & 0 & 0 & S_{65} & S_{66} & & & & & & & & & & & \\
S_{71} & S_{72} & 0 & 0 & 0 & 0 & S_{77} & & & & & & & & & & \\
S_{81} & S_{82} & 0 & 0 & 0 & 0 & S_{87} & S_{88} & & & & & & & & & \\
0 & 0 & S_{93} & S_{94} & 0 & 0 & 0 & 0 & S_{99} & & & & & & & & \\
0 & 0 & S_{103} & S_{104} & 0 & 0 & 0 & 0 & S_{109} & S_{1010} & & & & & & & \\
0 & 0 & 0 & 0 & S_{115} & S_{116} & 0 & 0 & 0 & 0 & S_{1111} & & & & & & \\
0 & 0 & 0 & 0 & S_{125} & S_{126} & 0 & 0 & 0 & 0 & S_{1211} & S_{1212} & & & & & \\
S_{131} & S_{132} & 0 & 0 & 0 & 0 & S_{137} & S_{138} & 0 & 0 & 0 & 0 & S_{1313} & & & & \\
S_{141} & S_{142} & 0 & 0 & 0 & 0 & S_{147} & S_{148} & 0 & 0 & 0 & 0 & S_{1413} & S_{1414} & & & \\
0 & 0 & S_{153} & S_{154} & 0 & 0 & 0 & 0 & S_{159} & S_{1510} & 0 & 0 & 0 & 0 & S_{1515} & & \\
0 & 0 & S_{163} & S_{164} & 0 & 0 & 0 & 0 & S_{169} & S_{1610} & 0 & 0 & 0 & 0 & S_{1615} & S_{1616} & \\
0 & 0 & 0 & 0 & S_{175} & S_{176} & 0 & 0 & 0 & 0 & S_{1711} & S_{1712} & 0 & 0 & 0 & 0 & S_{1717} \\
0 & 0 & 0 & 0 & S_{185} & S_{186} & 0 & 0 & 0 & 0 & S_{1811} & S_{1812} & 0 & 0 & 0 & 0 & S_{1817} & S_{1818}
\end{bmatrix}$$

$Symmetric$

in which

$$S_{11} = S_{33} = S_{55} = N_x, \quad S_{22} = S_{44} = S_{66} = N_y\,, \quad S_{21} = S_{43} = S_{65} = N_{xy}\,,$$

$$S_{77} = S_{99} = S_{1111} = N_x h^2/12, \quad S_{88} = S_{1010} = S_{1212} = N_y h^2/12,$$

$$S_{87} = S_{109} = S_{1211} = N_{xy} h^2/12,$$

$$S_{1313} = S_{1515} = S_{1717} = N_x h^6/448, \quad S_{1414} = S_{1616} = S_{1818} = N_y h^6/448,$$

$$S_{1413} = S_{1615} = S_{1817} = N_{xy} h^6/448\,, \quad S_{71} = S_{93} = S_{115} = M_x,$$

$$S_{82} = S_{104} = S_{126} = M_y, \quad S_{81} = S_{103} = S_{125} = M_{xy}\,, \quad S_{137} = S_{159} = S_{1711} = N_x h^4/80,$$

$$S_{148} = S_{1610} = S_{1812} = N_y h^4/80, \quad S_{147} = S_{169} = S_{1811} = N_{xy} h^4/80,$$

$$S_{131} = S_{153} = S_{175} = M_x^*, \quad S_{142} = S_{164} = S_{186} = M_y^*, \quad S_{141} = S_{163} = S_{185} = M_{xy}^*$$